Collège Doctoral du Languedoc-Roussillon

THÈSE

Pour obtenir le grade de

Docteur

Délivré par l'**UNIVERSITÉ MONTPELLIER 2**

Préparée au sein de l'école doctorale **SIBAGHE**
Et de l'unité de recherche **IRD, UMR 212 EME**

Spécialité: **Ecosystèmes et sciences agronomiques**

Présentée par **Emmanuelle Dortel**

Croissance de l'albacore (*Thunnus albacares*) de l'océan Indien : de la modélisation statistique à la modélisation bio-énergetique

Soutenue le 11 juin 2014 devant le jury composé de

M. Roger Pradel	DR	Univ. Montpellier 2	Président du jury
M. Etienne Prévost	CR	AgroParisTech	Rapporteur
M. Jean-Christophe Poggiale	Pr	Univ. Aix-Marseille	Rapporteur
M. Ronan Fablet	CR	Telecom Bretagne	Examinateur
M. Daniel Gaertner	CR	Univ. Montpellier 2	Directeur
M. Emmanuel Chassot	IR	Univ. Montpellier 2	Co-directeur

UNIVERSITÉ MONTPELLIER 2
SCIENCES ET TECHNIQUES

Remerciements

Je tiens tout d'abord à remercier Emmanuel Chassot qui m'a offert l'opportunité de réaliser cette thèse. Tu m'as permis de découvrir le monde passionnant de l'halieutique et j'ai beaucoup appris grâce à toi. Je te suis sincèrement reconnaissante pour ton soutient, pour avoir toujours tout fait pour que ces trois années se déroulent dans les meilleures conditions et pour avoir supporter mon humeur pas toujours très agréable. Même si c'était parfois difficile, je suis contente d'avoir pu travailler avec toi. Merci aussi pour m'avoir impliquée dans les activités de la CTOI et pour tous ces voyages dans l'océan Indien.

Je souhaite remercier Daniel Gaertner, directeur officiel de la thèse, pour ses conseils avisés et sa disponibilité et pour tout le temps qu'il a accordé à la relecture du manuscrit et aux obligations administratives liées à sa fonction.

Bien qu'elle ne fasse pas officiellement partie de l'équipe encadrante, le chapitre DEB n'aurait probablement jamais vu le jour sans la participation de Laure Pecquerie. Merci Laure pour ton implication active dans l'encadrement de mon travail. Merci aussi pour ta générosité et ta patience, j'ai réellement apprécié les moments passés à Brest.

Je tiens également à remercier chaleureusement Nicolas Bousquet qui m'a énormément aidée en modélisation Bayésienne. Merci pour tes précieux conseils, pour ta gentillesse et pour t'être montré disponible quand j'en avais besoin malgré ta charge de travail.

Je remercie tous ceux qui m'ont apporté leur aide et sans qui cette thèse ne serait pas ce qu'elle est. En particulier Etienne Rivot pour ses conseils en modélisation et pour m'avoir accueillie au sein de son laboratoire, Alain Fonteneau qui m'a fait partager ses précieuses connaissances sur les thons et les pêcheries thonières, Jean-Pierre Hallier pour ses explications concernant le programme marquage, Olivier Gimenez et Martin Huret pour leurs conseils, Fany Sardenne qui m'a fait bénéficier de son expertise pour la lecture d'otolithe, Monin Justin Amandè qui m'a si souvent aidée à résoudre mes problèmes, David Kaplan pour ses indispensables coups de pouce, Céline Rodriguez, Laurent Floch, Pascal Cauquil et Laurent Dubroca pour toutes les fois où je les ai sollicités pour problèmes en tout genre, Pierre Chavance pour la gestion de mes contrats et de mes missions, Michel Potier et Frédéric Ménard pour les analyses de contenu stomacaux.

Je tiens aussi à remercier tous ceux qui ont participé à la collecte, à la gestion et à l'analyse des données, Julien Million, Miguel Herrera, Patrice Dewals, Gaël Le Croizier, Fany Sardenne, Eric Morize, Jean-Marie Munaron, Carys Davies, Claire Geffroy, Eric Dabas et les techniciens de la SFA.

Ces trois années au sein de l'UMR se sont déroulées dans de bonnes conditions grâce à l'ensemble du personnel. Je remercie particulièrement Isabelle Vidal-Ayouba et Laurence Vicens que j'ai fréquemment sollicité et qui ont été très réactives afin de résoudre mes soucis administratifs. Je souhaite aussi saluer mes collègues sétois pour les bons moments passés ensemble. En particulier Victoria et Marion qui m'ont accompagné et soutenu durant ce périlleux parcours et Alex pour sa fabuleuse idée du gâteau du mardi.

Dans le cadre de ce travail, j'ai été amené à effectué plusieurs séjours et je remercie l'équipe du LEMAR et les membres du Pôle Halieutique de l'Agrocampus Ouest pour leur accueil ainsi que les personne que je n'ai pas cité mais avec qui j'ai pris plaisir à échanger et à partager les déjeuners. Je remercie également la SFA pour m'avoir accueilli dans ses locaux lors de mon séjour aux Seychelles.

J'adresse mes remerciements à Jean-Christophe Poggiale, Etienne Prévost, Ronan Fablet et Roger Pradel qui ont accepté d'évaluer ce travail.

Enfin je remercie mes parents qui m'ont soutenu et encouragé durant ces trois années et qui ont mis leur soucis de côté pour consacré du temps à la correction de ce manuscrit.

UNIVERSITY MONTPELLIER 2

Graduate School SIBAGHE - Systèmes intégrés en biologie, agronomie, géosciences, hydrosciences et environnement

Growth of Indian Ocean yellowfin tuna (*Thunnus albacares*) : from statistical to bioenergetic modelling

by

Emmanuelle Dortel

Thesis submitted of the requirements for the degree of
DOCTOR OF UNIVERSITY MONTPELLIER 2

in

Ecosystems and agricultural sciences specialty

Defended the June 11 2014 before the jury :

M. Roger Pradel, *CEFE, CNRS*	Chair
M. Etienne Prévost, *ECOBIOP, INRA*	Examiner
M. Jean-Christophe Poggiale, *Univ. Aix-Marseille*	Examiner
M. Ronan Fablet, *LabSTICC, Telecom Bretagne*	Examiner
M. Daniel Gaertner, *EME, IRD*	Supervisor
M. Emmanuel Chassot, *EME, IRD*	Co-supervisor

IRD, UMR 212 Exploited Marine Ecosystems
Avenue Jean Monnet BP 171 34 203 Sète cedex

Preface

This thesis has been proposed as part of the The Regional Tuna Tagging Project (RTTP), a large scale mark-recapture program of tuna conducted in the Indian Ocean from May 2005 to September 2012. It was funded by the Direction des Pêches Maritimes et de l'Aquaculture (DPMA) of the French Ministry of Ecology, Sustainable Development and Energy (www.developpement-durable.gouv.fr), by the Organisation of producers of frozen and deep-frozen tropical tuna (ORTHONGEL, orthongel.fr/) and by the Institut de Recherche pour le Dévelopement (IRD, www.ird.fr).

This thesis was carried out under the scientific direction of Emmanuel Chassot and supervised by Daniel Gaertner within the Observatoire Thonier team (www.ot.ird.fr/) in the UMR 212 "Exploited Marine Ecosystems" (EME, IRD, Sète). It was carried out in collaboration with the Indian Ocean Tuna Commission (IOTC, www.iotc.org/) and supported by the ANR EMOTION project (ANR 11 JSV7 007 01). The development work of the bioenergetics model has benefited from the collaboration of Laure Pecquerie and involved several stays in the Laboratoire des sciences de l'Environnement Marin (LEMAR, Brest).

The thesis work benefited from technical support of Nicolas Bousquet, Fany Sardenne, Monin Justin Amandè, David Kaplan and from helpful discussions with Etienne Rivot, Alain Fonteneau, Olivier Gimenez, Michel Potier. We are grateful to all the people that have been involved in the Regional Tuna Tagging Project of the Indian Ocean (RTTP), particularly Jean-Pierre Hallier for its explanations, Julien Million, Miguel Herrera for data management, P. Dewals and his team for their work on biological data and Eric Morize, Jean-Marie Munaron, Carys Davies, Claire Geffroy, Gaël Le Croizier, Fany Sardenne, Eric Dabas for their contribution to otolith analyses. We are also grateful to Laurent Floch and Céline Rodriguez for their help with the Balbaya database.

This PhD project aims to exploit the data collected during the RTTP program to improve current knowledge on the growth of Indian Ocean yellowfin in order to enhance the stock assessment.
The first chapter provides an overview of data used.
The second chapter is devoted to the development of a model for estimating individual ages from repeated otolith readings. Developed within a Bayesian framework, this model explicitly represents the sources of uncertainty associated with age estimation and includes knowledge from expertise.
In the third chapter, this ageing error model is coupled with a two-stanzas growth model. Also developed in a hierarchical Bayesian framework, the growth model combines aging data derived from otolith readings, length-frequency data sampled

from the European purse seine fishery over the last decade and mark-recapture data and accounts for the uncertainties associated with each dataset.
The fourth chapter is devoted to the formulation of a Dynamic Energy Budget model for yellowfin. This model still requires developments, however it could be subsequently used to better understand the factors behind the observed growth pattern.
Finally, in the conclusion, the interest and limitations of results obtained from chapters 2 to 4 are discussed and put into perspective and methodological improvements are proposed.

The chapters 2 and 3 of the thesis manuscript are based on scientific publications :

Dortel E., Massiot-Granierr F., Rivot E., Million J., Hallier J.P., Morize E., Munaron J.M., Bousquet N., Chassot E. (2013) Accounting for Age Uncertainty in Growth Modeling, the Case Study of Yellowfin Tuna (*Thunnus albacares*) of the Indian Ocean, *PLoS ONE* **8**(4) : 12p.

Dortel E., Sardenne F., Bousquet N., Rivot E., Million J., Le Croizier G., Chassot E. (*in press*) An integrated Bayesian modeling approach for the growth of Indian Ocean yellowfin tuna, *Fisheries Research*

Table of contents

Introduction

1 Exploitation et gestion des stocks de thonidés

Il convient en premier lieu de définir quelques termes utilisés en halieutique.
La ***population*** désigne l'ensemble des individus d'une même espèce vivant dans un écosystème spécifique ou sur une étendue géographique déterminée, généralement inférieure à l'aire de répartition totale de l'espèce.
Le ***stock*** est la fraction de la population exploitable par la pêche (Laurec and Le Guen, 1981). L'expression de *stock halieutique* sous-entend généralement que la population à laquelle il se réfère est plus ou moins isolée des autres populations de la même espèce (Majkowski, 2007).
Une ***cohorte*** désigne un ensemble d'individus d'un stock donné nés durant une même période de ponte.
Le ***recrutement*** est le processus par lequel les plus jeunes individus intègrent pour la première fois la phase exploitable. Ce processus est généralement lié à une ***taille de recrutement***, taille seuil à partir de laquelle un individu devient accessible à la pêcherie. Cette taille varie en fonction de l'engin de pêche considéré. Tout individu franchissant cette taille seuil est une ***recrue***.

1.1 Les thonidés, une ressource économique importante

Les thons sont des espèces épipélagiques largement répandues dans les écosystèmes océaniques hauturiers et côtiers de la planète. En raison de leur forte valeur marchande, ils font l'objet d'un commerce international intensif. Depuis la seconde moitié du XX$^{\text{ème}}$ siècle, l'exploitation des thonidés s'est considérablement accrue, avec une hausse des prises annuelles mondiales de moins de 500 000 tonnes en 1950 à près de 6,5 millions de tonnes en 2009 (Figure 1 ; FAO Fisheries Departement (FAO-FI), 2013). Six espèces sont particulièrement prisées par la pêche industrielle, le listao (*Katsuwonus pelamis*, 50.7% des captures mondiales), l'albacore (*Thunnus albacares*, 31.7%), le patudo (*T.obesus*, 10.8%), le germon (*T.alalunga*), le thon rouge de l'Atlantique (*T.thynnus*) et le thon rouge du Sud (*T.maccoyii*) (Miyake et al., 2010; Pillai and Satheeshkumar, 2012).
Les retombées socio-économiques de l'industrie thonière sont très importantes, notamment pour les états côtiers dont les revenus proviennent en grande partie des accords de pêche, des activités liées aux processus de transformation, de conservation et d'exportation des thons et des activités de pêche proprement dites (Sweenarain et al., 1998). De plus, les thonidés mineurs, à moins forte valeur marchandes, constituent une des principales sources de protéines animales dans beaucoup de ces pays. Le déclin ou l'effondrement des pêcheries thonières pourrait donc avoir des conséquences dramatiques tant au plan économique qu'au plan de la sécurité sanitaire et alimentaire.

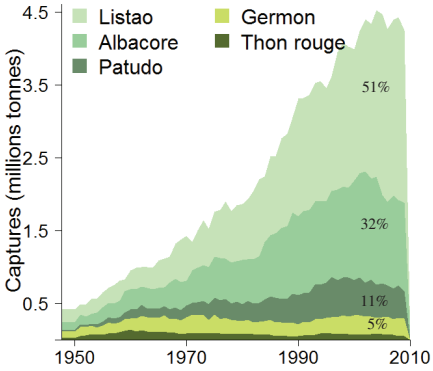

FIGURE 1 – Evolution des captures mondiales cumulées par espèces en milliers de tonnes (source : FAO, 2010)

1.2 Les pêcheries thonnières

La pêche à la senne est le mode de pêche le plus largement répandu et correspond à 60% des captures mondiales. Elle est suivie par la pêche à la palangre et à la canne qui correspondent respectivement à 15% et 11% des captures mondiales (Miyake et al., 2004; Majkowski, 2007). La pêche à la senne tournante consiste à encercler un banc de poissons avec un filet, puis à refermer le filet par le bas pour éviter la fuite des poissons par le fond. La palangre est constituée de longues lignes munies de nombreux hameçons et maintenues soit sur le fond à l'aide d'ancrages, soit à la surface à l'aide de flotteurs. Pour la pêche à la canne, les thons sont attirés à proximité du bateau en lançant des appâts puis sont pris à l'aide de cannes tenues à la main ne disposant que d'une seule ligne (Figure 2).

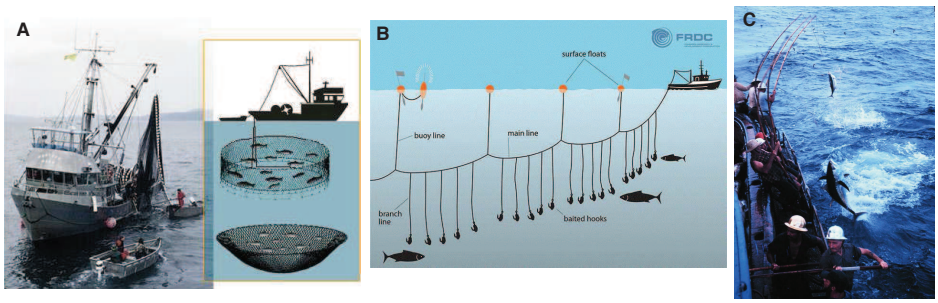

FIGURE 2 – Les principaux modes de pêches ; A : senne, B : palangre, C : canne

L'océan Pacifique constitue la principale zone productrice et représente 64% des captures mondiales, puis viennent l'océan Indien et l'océan Atlantique avec respectivement 25% et 11 % des captures (Miyake et al., 2010; Herpandi et al., 2011).

1.3 Gestion des stocks de thonidés

Le suivi et la gestion des stocks de thonidés sont sous la juridiction d'Organisations Régionales de Gestion des Pêches (ORGPs) au nombre de cinq (Figure 3). Ces organisations réunissent les pays côtiers et les pays impliqués dans les pêcheries de la zone concernée. Ces ORGPs organisent des groupes de travail réunissant des experts scientifiques, des gestionnaires des pêches et des politiques des différents pays concernés. Les experts examinent les informations disponibles sur les pêcheries et s'appuient sur l'évaluation des stocks pour rendre des avis sur l'état des ressources et les mesures de gestion nécessaires à leur exploitation durable.
L'*évaluation des stocks* est une estimation quantitative de l'état des ressources et de l'intensité de la pêche exercée sur ces dernières. Elle s'appuie sur des indicateurs des pêcheries (structures de tailles des captures, quantification des captures en nombre ou masse de poissons, effort de pêche) et sur des points de référence biologique dont le plus utilisé est le *Rendement Maximal Soutenable* (MSY ; Majkowski, 2007; Chen et al., 2003). Le MSY correspond à la capture maximale en terme de biomasse pouvant être prélevé chaque année sans épuiser la ressource. Cette évaluation intègre généralement l'estimation des principaux taux démographiques (croissance, mortalité naturelle ; Fournier et al., 1998; Langley et al., 2012), principalement basée sur des données collectées à partir de la pêche commerciale ou des informations issues des programmes scientifiques de marquage-recapture.

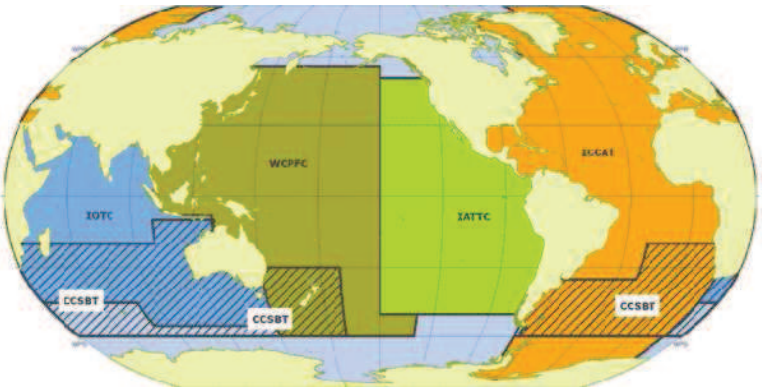

FIGURE 3 – Les différentes ORGPs impliquées dans la gestion des stocks de thonidés (source : FAO Fisheries Departement (FAO-FI), 2013) : Commission des Thons de l'Océan Indien (IOTC), Commission Inter-Americaine des Thons Tropicaux (IATTC), Commission Internationale pour la Conservation des Thonidés de l'Atlantique (ICCAT), Commission pour la Conservation du Thon rouge du Sud (CCSBT), Commission des pêches pour le Pacifique occidental et central (WCPFC)

1.4 Croissance et évaluation des stocks

La dynamique d'un stock est sous-jacente à celle de la population exploitée qui est tributaire de quatre taux démographiques dits *vitaux* : natalité, fécondité, croissance et mortalité. Ces taux varient en fonction des capacités intrinsèques de chaque individu à faire face aux conditions hydro-climatiques et trophiques de l'environnement et à diverses pressions telles que la prédation et la pêche. La taille d'un stock dépend de l'équilibre entre la mortalité naturelle (parasitisme, vieillesse et surtout prédation), celle résultant de la pêche et le recrutement. Ce dernier varie en fonction de la qualité et de la quantité d'œufs pondus et donc du nombre de reproducteurs de la population exploitée, de leur fécondité ainsi que de la survie larvaire. La biomasse du stock évolue en fonction du nombre de nouvelles recrues et de la croissance propre de l'ensemble des individus. Des phénomènes de densité-dépendance peuvent également entrer en jeu, par exemple la croissance peut être altérée par un nombre élevé d'individus engendrant une forte compétition trophique.
L'état de santé d'un stock est donc conditionné par quatre processus biologiques majeurs : le recrutement, la croissance, la mortalité naturelle et la pêche. La croissance est particulièrement importante dans le sens où elle influe sur les autres processus. Par exemple, le taux de mortalité par prédation dépend de la taille des individus et diminue d'autant plus vite pour ceux dont la croissance est rapide. De plus, la croissance permet de percevoir l'adaptabilité des espèces et d'évaluer leur capacité de résilience à la pêche. Exposées à de fortes pressions de pêche, certaines espèces peuvent répondre par une accélération de leurs taux de croissance et une réduction de la taille à maturité sexuelle (Jennings et al., 1999; Law, 2000; King and McFarlane, 2003).

D'autre part, la plupart des évaluations des stocks reposent sur l'estimation de la structure en âge des captures de pêche. Cette estimation s'appuie sur la conversion de la structure en taille des captures, elle-même estimée à partir d'échantillonnages effectués lors du débarquement des flottilles commerciales. Dans les modèles de production agrégés par âge (ASPM), cette conversion est réalisée *a priori* au moyen d'une clé taille-âge déterminée à partir des paramètres de croissance (Gascuel, 1994; Gerritsen et al., 2006). Dans les modèles dynamiques structurés en âge (Multifan-CL, SS3), cette conversion est intégrée au modèle. Elle s'appuie sur le suivie trimestriel des cohortes à partir des fréquences de tailles des captures et des paramètres de croissances qui sont soit fixés *a priori*, soit estimés (Hampton and Fournier, 2001; Shono et al., 2009). Par suite, une estimation biaisée de la croissance affectera l'estimation des prises par âge qui en découle et par conséquent les avis scientifique sur l'état des stocks.

2 Modélisation de la croissance

La croissance des poissons est un phénomène plus ou moins continu qui se poursuit tout au long de la vie de l'individu. Elle est contrôlée par des facteurs endocriniens endogènes (stéroïdes, hormones thyroïdiennes et hypophysaires) et régulée par divers facteurs exogènes dont les principaux sont la température et la disponibilité en nourriture, mais aussi la salinité et la concentration en oxygène. Le statut sexuel, l'âge ou la taille, la compétition entre les individus et la pêche peuvent également influencer cette croissance.
La connaissance de la croissance est capitale pour apprécier la productivité des stocks et mettre en place une gestion adaptée à leur exploitation durable. Son estimation est donc un enjeu majeur pour la recherche halieutique. Deux approches d'estimation de la croissance individuelle peuvent être distinguée, la modélisation statistique et la modélisation dynamique de type bio-énergétique.

2.1 Modèles statistiques

Conventionnellement, un modèle de croissance est une relation empirique qui décrit l'évolution en poids ou en taille d'un individu en fonction de son âge. Il existe de nombreuses formes fonctionnelles de croissance, certaines reposant sur des hypothèses d'équilibre énergétique entre différents processus physiologiques, tandis que d'autres sont purement empiriques (Ricker, 1975; Schnute, 1981; Katsanevakis, 2006). Dans cette section, seuls les modèles les plus couramment utilisés pour décrire la croissance des thonidés sont traités.

2.1.1 Modèles classiques

Le modèle de Von Bertalanffy (1938) est sans conteste le plus classiquement utilisé en halieutique (Fabens, 1965; Longhurst and Pauly, 1987; Katsanevakis, 2006). Celui-ci décrit l'évolution du poids W de l'individu comme la résultante des processus physiologiques de synthèse (anabolisme) et de dégradation (catabolisme) qui s'équilibrent lorsque les conditions de température et de disponibilité en nourriture sont constantes :

$$\frac{dW}{dt} = aW^m - cW^n \tag{1}$$

Selon Von Bertalanffy (1957), le processus d'anabolisme aW^m, lié à la respiration, est proportionnel à la surface, elle-même proportionnelle à la masse élevée à la puissance $2/3$ ($m = 2/3$), tandis que le processus de catabolisme cW^n est proportionnel à la masse ($n = 1$) :

$$\frac{dW}{dt} = aW^{2/3} - cW \tag{2}$$

En posant $W_\infty = {}^{a}/_{cW^3}$, poids asymptotique de l'individu atteint lorsque que ${}^{dW}/_{dt} = 0$, et $k = {}^{c}/_{3}$, coefficient de vitesse de croissance, l'intégration de l'Eq.2 fournit la croissance en poids de Von Bertalanffy :

$$W(t) = W_\infty[1 - exp(-k(t - t_0))]^3 \tag{3}$$

La relation entre le poids et la longueur des poissons est communément décrite selon l'équation $W = \alpha L^{\beta}$. La valeur de β est souvent très proche de 3, ce qui indique une croissance isométrique. Ainsi, le modèle de Von Bertalanffy considère le poids des poissons proportionnel au cube de la longueur (Von Bertalanffy, 1957; Essington et al., 2001). La croissance en taille est alors :

$$L(t) = L_{\infty}[1 - exp(-k(t - t_0))] \tag{4}$$

L_{∞} est la longueur asymptotique qui est généralement interprétée comme la longueur moyenne qu'atteindrait un individu à croissance infinie (Longhurst and Pauly, 1987). Le coefficient de vitesse de croissance k caractérise la rapidité avec laquelle le poisson croît vers la taille asymptotique. t_0 est l'âge correspondant à une longueur nulle. Il s'agit d'un âge théorique, le modèle de Von Bertalanffy n'étant pas adapté à la croissance larvaire. Ce modèle prédit une croissance continue, d'abord rapide qui diminue progressivement chez l'adulte à l'approche de la taille asymptotique (Von Bertalanffy, 1957).

Le modèle de Von Bertalanffy Généralisé ne fait pas d'hypothèse particulière sur la valeur de β, cette valeur pouvant être affectée par la nourriture disponible ou le statut reproducteur (Essington et al., 2001) :

$$L(t) = L_{\infty}[1 - exp(-k(1 - m)(t - t_0))]^{\frac{1}{1-m}} \tag{5}$$

Ce modèle décrit une croissance continue de forme sigmoïdale présentant une légère inflexion à l'âge $t = t_0 + \dfrac{ln(1 - m)}{k}$ (Katsanevakis, 2006).

Le modèle de Gompertz (1825) décrit une croissance continue de type sigmoïdale qui décroit de façon exponentielle avec la taille (Ricker, 1975) :

$$L(t) = L_0 exp(G(1 - exp(-gt))) \tag{6}$$

L_0 est la taille à l'âge $t = 0$, G le taux instantané de croissance à l'âge 0 et g le taux de décroissance de G.

Le modèle de Richards (1959) décrit une croissance continue de type logistique (Katsanevakis, 2006) :

$$L(t) = L_{\infty}[1 + rexp(-k(t - t_0))]^{\frac{-1}{r}} \tag{7}$$

Ce modèle présente une inflexion au point $L(t) = L_{\infty}(1 + r)^{\frac{-1}{r}}$. C'est un modèle flexible dont la forme dépend de la valeur du paramètre r ; il correspond à un modèle de Von Bertalanffy pour $r = -1$, à un modèle logistique pour $r = 1$, à un modèle de Von Bertalanffy généralisé pour $r = -(1 - m)$ et à un modèle de Gompertz lorsque r tend vers 0.

Le modèle de Schnute-Richards (1981) est un modèle générique basé sur l'interprétation biologique d'une accélération de croissance chez les juvéniles, incluant les différentes formes de croissance mentionnées ci-dessus (Schnute, 1981) :

$$L(t) = [\alpha + \beta exp(\gamma t)]^{\delta} \tag{8}$$

α, β, γ et δ sont des constantes sans dimension. Leurs valeurs déterminent la forme du modèle : Von Bertalanffy, Richards, Gompertz, logistique, exponentiel, quadratique ou linéaire.

2.1.2 Modèles multi-stances

Certaines espèces de thons, en particulier l'albacore, le patudo et le thon rouge, peuvent présenter des phases distinctes d'accélération et de ralentissement de croissance appelées *stances de croissance*. Les modèles classiques ne considèrent qu'un coefficient de vitesse de croissance constant tout au long de la vie du poisson et de ce fait ne permettent pas une représentation satisfaisante de ces stances. Aussi, des modèles multi stances, considérant différents coefficients de vitesse de croissance, ont été élaborés.
Le premier modèle dont nous avons connaissance est celui de Gascuel (1992) développé pour l'albacore de l'Atlantique. Cette espèce présente une croissance en deux stances caractérisée par une accélération brutale lorsque la taille atteint 60-65 cm (Fonteneau, 1980; Gascuel et al., 1992; Gaertner and Pagavino, 1992). Afin de reproduire cette accélération, Gascuel et al. (1992) a élaboré un modèle composite combinant une fonction linéaire (croissance lente des juvéniles) et l'équation de Von Bertalanffy Généralisé (croissance rapide des adultes) :

$$L(t) = L_0 + bt + (L_\infty - (L_0 + bt))[1 - exp(-kt)]^m \tag{9}$$

L_0 est la longueur à l'âge $t = 0$, b le taux de croissance initial, L_∞ la longueur asymptotique, k le coefficient de vitesse de croissance de Von Bertalanffy et m un paramètre de forme. Le modèle de Gascuel a été choisi comme référence pour l'évaluation du stock d'albacore de l'Atlantique (ICCAT, 2013).

L'albacore du Pacifique présenterait vraisemblablement une croissance en trois stances (Yamanaka, 1990; Lehodey and Leroy, 1999), caractérisée par la succession d'une phase de ralentissement autour de 40-45 cm puis d'une phase d'accélération autour de 70 cm. Lehodey and Leroy (1999) ont alors proposé d'introduire, dans un modèle de Von Bertalanffy, une fonction de contrôle de la décélération du taux de croissance en corrigeant le coefficient de vitesse de croissance k par $k - \mathcal{N}(t_m, \sigma^2)$:

$$L(t) = L_\infty \left[1 - exp\left(\frac{-ka}{\sigma\sqrt{2\pi}} exp\left(\frac{-(t-t_m)^2}{4\sigma^2}\right)(t - t_0)\right)\right] \tag{10}$$

t_m est l'âge moyen correspond à la décélération maximale de k, σ représente l'incertitude autour de l'âge t_m et a un paramètre proportionnel à la décélération maximale de k.

Hearn and Polacheck (2003) ont noté un important changement dans la croissance du thon rouge du Sud, lié à un ralentissement du taux de croissance au cours du stade juvénile. Ils ont alors modélisé ce changement de façon discontinue en associant deux modèles de Von Bertalanffy :

$$L(t) = \begin{cases} L_{\infty_1}[1 - exp(-k_1(t - t_0))] & \text{pour} \quad t \leqslant t^* \\ L^* + (L_{\infty_2} - L^*)[1 - exp(-k_2(t - t_0))] & \text{pour} \quad t > t^* \end{cases} \tag{11}$$

Les ensembles de paramètres (L_{∞_1}, k_1) et (L_{∞_2}, k_2) correspondent respectivement au premier et au second modèles de Von Bertalanffy, t^* est l'âge moyen auquel le changement de croissance se produit et L^* la longueur correspondant à l'âge t^*.

L'ajustement d'un modèle discontinu, tel que celui décrit par Hearn and Polacheck (2003), est souvent malaisé et peu satisfaisant. De plus, une variation de croissance aussi abrupte paraît peu plausible. Ainsi, s'appuyant sur les travaux de Wang (1998b) et Hearn and Polacheck (2003), Laslett et al. (2002) ont proposé une extension continue du modèle de Von Bertalanffy. Le coefficient de vitesse de croissance de Von Bertalanffy k est alors remplacé par une fonction logistique dépendant du temps $k(t)$, afin d'obtenir une transition lisse entre les deux coefficients de vitesse de croissance, k_1 et k_2 :

$$k(t) = k_1 + \frac{k_2 - k_1}{1 + exp(-\beta(t - t_0 - \alpha))} \begin{cases} k_1 & \text{pour} \quad t \ll t_0 + \alpha \\ k_2 & \text{pour} \quad t \gg t_0 + \alpha \end{cases} \tag{12}$$

α est l'âge moyen relatif à t_0 et correspond au point d'inflexion de la courbe, β un paramètre régulant la vitesse de transition entre k_1 et k_2 (une valeur élevée de β induisant une transition abrupte). L'équation différentielle de Von Bertalanffy s'écrit alors $L(t)' = k(t)(L_\infty - L(t))$ et sa solution analytique est la suivante (Laslett et al., 2002; Eveson et al., 2004) :

$$L(t) = L_\infty \left[1 - exp(-k_2(t - t_0)) \left(\frac{1 + exp(-\beta(t - t_0 - \alpha))}{1 + exp(\beta\alpha)} \right)^{k_1 - k_2/\beta} \right] \tag{13}$$

Ce modèle initialement développé pour le thon rouge du Sud est baptisé *VB log-K*. Il est actuellement utilisé dans les évaluations des stocks d'albacore et de patudo de l'océan Indien (Nishida and Rademeyer, 2011; Dortel et al., 2012; Eveson et al., 2012).

2.2 Modèles bio-énergétiques

D'un point de vue bio-énergétique, la croissance en poids d'un organisme résulte d'un bilan d'énergie ou de masse entre d'une part, l'acquisition d'énergie via la consommation de nourriture (C), et d'autre part, les pertes énergétiques liées à la respiration (R), à l'excrétion d'urée (U), à la production de fèces (F) et à l'énergie dépensée pour le maintient du métabolisme basal (M_s) et secondaire (M_a) (Hansen et al., 1993; Nisbet et al., 2012). En d'autres termes, un individu ne peut croître que si la quantité

d'énergie fournie par la nourriture est en excès une fois les pertes énergétiques prises en compte et les besoins du métabolisme satisfaits, la reproduction (G) entrant en compétition avec la croissance (Kitchell et al., 1977; Ney, 1993; Kooijman, 2010) :

$$\frac{dW}{dt} = C - [(M_s + M_a) + (R + U + F) + G] \tag{14}$$

Toutes les approches de modélisation bio-énergétique reposent sur ce principe. Les flux d'énergie entre les différentes fonctions de l'organisme sont définis par des règles qui dépendent de la température et de la disponibilité en nourriture et peuvent s'adapter à différents forçages tels que la compétition, la prédation ou la pression de pêche.

Deux approches de modélisation bio-énergétiques sont considérées, les modèles traditionnels et les modèles de bilans dynamiques d'énergie (Dynamic Energy Budget, DEB). Le terme de modèles traditionnels fait ici référence à plusieurs théories bio-énergétiques fondées sur le même principe. Dans ces modèles, l'organisme est assimilé à une "boîte" où les flux d'énergie sont modélisés par des fonctions allométriques du poids. L'énergie provenant de la nourriture consommée est d'abord allouée au maintien du métabolisme, le reste étant utilisé pour la croissance et la reproduction, une fois les pertes énergétiques prises en compte (Kitchell et al., 1977; Ney, 1993).
Ces modèles bio-énergétiques sont appliqués aux études halieutiques depuis les années 1970. Ils sont essentiellement utilisés pour simuler les patrons de croissance et de reproduction de différentes espèces en fonction des conditions environnementales, perchaude et dorée jaune (Kitchell et al., 1977), plie canadienne (Roff, 1983), thon rouge de l'Atlantique (Chapman et al., 2011).

La théorie DEB, développée à la fin des années 1970, partitionne l'organisme en trois compartiments. L'énergie provenant de la nourriture intègre un premier compartiment nommé "réserve". À partir de ce dernier, une part fixe de l'énergie est allouée à un second compartiment correspondant à la maintenance somatique et à la croissance, avec priorité pour la maintenance. La partie restante est allouée à un troisième compartiment constitué de la maturation et de sa maintenance qui est prioritaire. La maturation fait référence au développement physiologique de l'organisme et inclue les fonctions qui ne sont pas nécessaires à la survie immédiate, comme le système immunitaire ou le développement de l'appareil reproducteur. Au stade adulte, l'organisme est pleinement développé, l'énergie est alors redirigée vers la reproduction (Kooijman, 2010).
Depuis une dizaine d'années, La théorie DEB est largement utilisée pour étudier l'influence des conditions du milieu sur la croissance et la fertilité des espèces aquacoles, en vue d'optimiser les méthodes d'élevage (huître et moule ; Ren and Schiel, 2008; Bourlès et al., 2009; Sarà et al., 2012). Elle est plus récemment utilisée pour mieux comprendre l'influence des facteurs environnementaux sur la croissance des populations sauvages, telles que l'anchois (Pecquerie et al., 2009) ou le thon rouge du Pacifique (Jusup et al., 2011).

2.3 Sources de données

Trois principales sources de données peuvent être utilisées pour l'estimation de la croissance : (i) les estimations d'âge à partir des marques périodiques enregistrées dans les tissus calcifiés, (ii) les distributions des fréquences de tailles des captures commerciales, (iii) les expériences de marquage-recapture. Ces différentes sources de données présentent des caractéristiques spécifiques et fournissent des informations complémentaires sur la croissance. Aussi, il peut être difficile d'obtenir un patron global de croissance à partir d'une seule source (Eveson et al., 2004; Santiago and Arrizabalaga, 2005; Restrepo et al., 2010).

2.3.1 Estimations individuelles d'âge à partir des tissus calcifiés

L'idée d'estimer l'âge des vertébrés à partir des marques naturelles périodiques inscrites dans leurs tissus osseux a fait son apparition au XVII siècle. Cependant, ce n'est que dans les années 1970 que se développe la sclérochronologie, science visant à reconstituer l'histoire de vie des organismes à partir des marques de croissance de leur tissus durs (Castanet et al., 1992; Bagliniére et al., 1992). Chez les poissons osseux, plusieurs pièces anatomiques peuvent être utilisées : otolithes, écailles, vertèbres et épines dorsales. Ces pièces présentent des marques d'accroissement annuelles ou journalières dont le dénombrement fournit une estimation directe de l'âge.
Pour les thons, les otolithes sont les plus utilisés (Pannella, 1971; Wild and Foreman, 1980; Williams et al., 2013). Ils sont métaboliquement inertes et s'accroissent de façon continue tout au long de la vie du poisson (Mugiya and Tanaka, 1992; Panfili et al., 2009). Les marques d'accroissement journalières constituent alors un critère d'âge individuel fiable. Des plus, ces marques ont la capacité d'apporter des renseignements sur certains événements du cycle de vie des organismes, tels que l'acquisition de la maturité sexuelle, les périodes de migrations ou l'état nutritionnel (Panfili et al., 2002).

A l'heure actuelle, les données estimations d'âge sont considérés comme la source d'information la plus utile pour l'estimation de la croissance individuelle. Cependant, la préparation des otolithes est longue et délicate et leur lecture peut s'avérer fastidieuse (Sardenne et al., ress). Elles ne sont donc généralement effectuées que pour un nombre limité d'individus. De plus, les estimations d'âges sont associées à des biais et incertitudes, notamment pour les plus vieux individus chez lesquels les marques journalières peuvent être indiscernables en raison de chevauchement ou d'une formation intermittente de ces marques. Ces incertitudes influencent les estimations des paramètres biologiques qui en découlent (Campana, 2001; Punt et al., 2008).

2.3.2 Distributions des fréquences de longueurs et progression modale

Bien que moins précises que les estimations d'âge à partir des tissus calcifiés, les distributions de fréquences de longueurs peuvent être obtenues facilement pour un grand nombre d'individus. Elles sont utiles pour les espèces présentant des périodes de reproduction bien définies, permettant alors l'estimation indirecte de l'âge et de la croissance moyenne de la population (Schnute and Fournier, 1980; Andrade and Kinas, 2004; Morton and Bravington, 2008).

La progression modale consiste à des identifier des modes de taille dans les histogrammes de fréquences de longueurs, chaque mode étant supposé correspondre à une cohorte. Le suivi de ces modes dans le temps permet d'obtenir une estimation de la croissance (Pauly and Morgan, 1987). Mensuellement, ce suivi fournit un aperçu des fluctuations saisonnières de la croissance (Laslett et al., 2004). Sur plusieurs années, il permet d'apprécier l'impact de la pêche sur les populations exploitées (Hampton and Fournier, 2001; Gilman et al., 2012).
L'analyse de ces histogrammes pour l'étude de la croissance des espèces halieutiques a été initiée par Petersen (1892). La méthode de Petersen repose sur l'identification visuelle des modes de longueur et n'implique qu'un seul histogramme. Celui-ci est répété le long d'un axe de temps, une courbe de croissance reliant les différents modes successifs est alors ajustée (Longhurst and Pauly, 1987; Pauly and Morgan, 1987). Cette méthode manque de fiabilité car l'intervalle de temps séparant deux modes successifs de l'histogramme est purement subjectif.
Les analyses de progressions modales (MPA) impliquent l'identification visuelle des modes de longueur à partir de différents histogrammes correspondant à des périodes de temps successives (mensuelles ou trimestrielles). En supposant une faible variation de la relation taille-âge entre les individus et en considérant une même période de reproduction pour l'ensemble de la population, les modes plus petits peuvent alors être considérés comme représentatifs de pics de recrutement. Lorsque la période de ponte est connue, il est alors possible d'attribuer à ces pics un âge moyen ou un groupe d'âge (groupe 0 pour les poissons de moins d'un an, groupe 1 pour ceux de un à deux ans et ainsi de suite ; Longhurst and Pauly, 1987; Pauly and Morgan, 1987). Cependant, les espèces tropicales présentent couramment plusieurs périodes de pontes par an qui peuvent s'étaler sur plusieurs mois. Par convention, le premier groupe d'âge est alors défini par rapport au 1^{er} janvier (Laurec and Le Guen, 1981; Pauly and Morgan, 1987). Par suite, les modes d'histogrammes successifs sont reliés, ce qui permet l'estimation d'une courbe de croissance.
L'identification visuelle des modes peut se révéler fastidieuse en cas de chevauchement des cohortes résultant d'une augmentation de la variabilité individuelle de la croissance avec l'âge ou de l'étalement des périodes de reproduction (Morton and Bravington, 2008). Face à ces difficultés, des méthodes analytiques d'identification des modes ont été développées. Celles-ci considèrent que les longueurs au sein d'une même cohorte se distribuent autour d'une valeur moyenne selon une certaine loi de probabilité et décrivent ainsi les histogrammes de fréquences de longueurs comme des mélanges de distributions de probabilités (Hasselblad, 1966; Pauly, 1985).

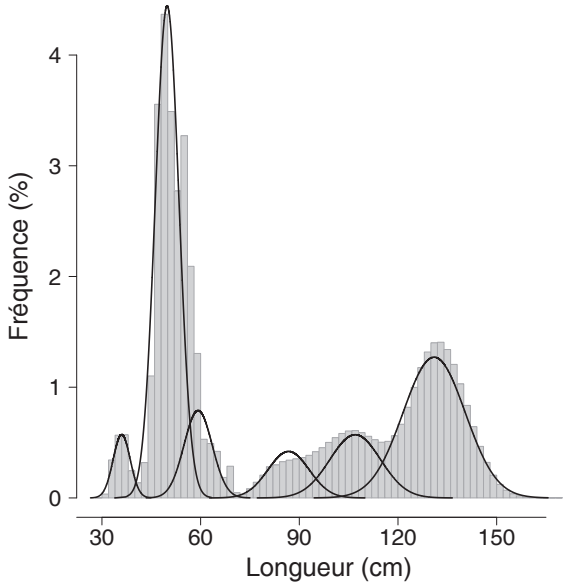

FIGURE 4 – Histogramme des fréquences de taille et lois de distribution des longueurs au sein d'une cohorte (lignes continues)

Les fréquences de longueurs sont depuis longtemps utilisées pour l'étude de la croissance des thonidés (Kume and Joseph, 1966; Marsac and Lablache, 1985; Gascuel et al., 1992; Laslett et al., 2004; Morton and Bravington, 2008). Elle sont le plus souvent échantillonnées à partir des prises de la pêche commerciale et elle dépendent de la sélectivité de l'engin de pêche pour certaines tailles, du choix des zones de pêche et du comportement des poissons, les poissons d'un même banc présentant des tailles similaires (Longhurst and Pauly, 1987; Morton and Bravington, 2008). Elles ne peuvent donc être considérées comme un échantillon représentatif de la population. De plus, les estimations des paramètres de croissance peuvent être biaisées par la sélectivité des engins de pêche qui ciblent les jeunes poissons à croissance rapide et les poissons âgés à croissance lente (Lucena and O'Brien, 2001; Taylor et al., 2005).

2.3.3 Expériences de marquage-recapture

Les expériences de marquage-recapture consistent à capturer et marquer individuellement une fraction de la population souhaitée représentative. Après une série de mesures (taille et poids), les individus sont relâchés et certains d'entre eux seront ultérieurement recapturés. Les opérations de marquage sont généralement effectuées lors de campagnes scientifiques tandis que les recaptures nécessitent la collaboration des professionnels de la pêche.
Ces expériences apportent de l'information sur différents paramètres démographiques (croissance, mortalité naturelle et par pêche). Elles permettent ainsi une vision plus précise de la dynamiques des populations. En particulier, elles fournissent une information sur le taux de croissance moyen de la population et sur sa variabilité

inter-individuelle (Amstrup et al., 2005). Toutefois, l'âge des poissons n'étant pas connu, il est difficile d'estimer la relation taille-âge.
La méthode de Fabens permet d'obtenir la forme de la courbe de croissance sans connaissance préalable de l'âge. Cette méthode, s'appuyant l'équation de Von Bertalanffy, permet d'exprimer le gain de taille en fonction de l'intervalle de temps entre le marquage et la recapture (Fabens, 1965). Elle est critiquée car, utilisant la méthode d'estimation des moindres carrés, elle ne tient pas compte de la variabilité individuelle de croissance, ce qui peut biaiser les estimations (Wang, 1998a). Il existe des alternatives à cette méthode plus robustes, telles que la méthode proposée par (Wang et al., 1995) où l'estimation des paramètres de Von Bertalanffy est basée sur la méthode du maximum de vraisemblance.

Dans certaines expériences de marquage-recapture, le marquage chimique des individus est utilisé. Ils consiste à injecter un composé chimique qui dépose un signal permanent dans les structures calcifiées. A la recapture, un examen de ces structures permet une estimation directe de l'âge de chaque individu. Dans le milieu marin, le composé le plus utilisé est la tétracycline, un antibiotique visible sous lumière fluorescente qui s'incorpore dans les liaisons calcium.

D'autres expériences font intervenir le marquage électronique. Des balises pop-up ou des marques archives sont insérées dans la cavité abdominale ou dans la musculature dorsale des poissons. Elles permettent d'enregistrer des informations sur l'environnement, telles que la température, la salinité, et la profondeur, ainsi que des caractéristiques intrinsèques, comme la température corporelle (Dagorn et al., 2006).

3 L'albacore de l'océan Indien

3.1 Description

L'albacore ou thon à nageoires jaunes (*Thunnus albacares*, Bonnaterre 1788), en anglais "yellowfin", est une espèce cosmopolite largement répandue dans les eaux tropicales et sub-tropicales des océans Indien, Atlantique et Pacifique. Il peut mesurer plus de 2 m et peser jusqu'à 160 kg. Sa longévité est estimée à 8 ans (ICCAT, 2014). Sa taille à maturité sexuelle est comprise entre 70 à 110 cm, soit entre 2 et 3 ans (Zhu et al., 2008; Rohit and Rammohan, 2009; Zudaire et al., 2013a). Les pêcheries ciblent principalement des individus de 30 à 170 cm.
Son corps est allongé et fusiforme. Son dos va du noir au bleu foncé, ses flancs sont argentés avec la présence d'une bande médiane jaune et ses nageoires sont jaune vif à jaunâtre. Chez les spécimens de grande taille, la deuxième nageoire dorsale et la nageoire annale sont très longues et en forme de faucille.

L'albacore possède des caractéristiques anatomiques, physiologiques et fonctionnelles exceptionnelles, ce qui en fait une espèce clé sur le plan évolutif. Il présente (i) un mode de locomotion particulièrement efficace qualifié de "nage thunniforme" (Shadwick and Syme, 2008), (ii) un rythme cardiaque modulable en fonction de l'effort fournie (Korsmeyer et al., 1997), (iii) un métabolisme élevé (Bushnell and Jones, 1994) et (iv) la capacité à maintenir une température interne supérieure à celle du milieu ambiant grâce à des systèmes vasculaires échangeurs de chaleur. Ces systèmes sont constitués d'un enchevêtrement de fins vaisseaux capillaires où la circulation du sang veineux à contre-courant du sang artériel permet la conservation de la chaleur produite par le métabolisme (Cayré, 1989; Shadwick et al., 2013).

Les individus inférieurs à 70 cm se rencontrent dans les eaux chaudes de surface, principalement côtières. Ils se rassemblent en bancs sous des objets flottants naturels (bois, débris) ou artificiels (Dispositifs de Concentration de Poissons) avec d'autres espèces de thons (jeunes patudos et listaos ; Stéquert and Marsac, 1986; Fonteneau and Gascuel, 2008). Les adultes présentent un comportement hautement migrateur et se répartissent sur de larges zones géographiques incluant les eaux hauturières. Ils se déplacent en bancs en s'associant parfois à d'autres espèces (thon, dauphin, requin-baleine ; Stéquert and Marsac, 1986; Fréon and Dagorn, 2000). Ils évoluent habituellement dans les cent premiers mètres de profondeur, les adultes pouvant effectuer de courtes immersions sous la thermocline jusqu'à 500 m de profondeur et plus rarement jusqu'à 1000 m (Dagorn et al., 2006; Schaefer et al., 2011).

Dans l'océan Indien, l'albacore présente un cycle sexuel saisonnier avec deux saisons de pontes coïncidant avec les périodes de moussons : une saison principale de novembre à mars (mousson nord-ouest) et une saison secondaire en juin-juillet (mousson sud-est ; Stéquert et al., 2001; Zudaire et al., 2013a). La zone équatoriale située entre 0° Nord et 10° Sud constitue la principale zone de ponte. Des zones secondaires ont été identifiées au large du Sri Lanka, dans le Canal du Mozambique et au large de l'Australie (IOTC, 2013).
L'albacore est une espèce ovipare à fécondité indéterminée qui se caractérise par un développement folliculaire asynchrone, c'est-à-dire que les ovaires présentent des ovocytes de différents stades de maturité. De plus, les femelles ont la possibilité de frayer plusieurs fois au cours d'une même saison de reproduction (Timochina and Romanov, 1991; Zudaire et al., 2013b). Lors d'une ponte, une femelle peut expulser de 0,32 à 6,91 millions d'œufs (Zudaire et al., 2013a). Ce nombre varie en fonction de la taille des femelles (il étant d'autant plus élevé que la femelle est grande), de leur condition physiologique et des facteurs environnementaux dont les principaux

sont la température et la disponibilité en nourriture (Margulies et al., 2007). En particulier, la température semble être un facteur important régulant l'activité de ponte (observée dans le Pacifique entre 24 et 28°C ; Itano, 2000; Margulies et al., 2007).

3.2 Exploitation et évaluation du stock

Dans l'océan Indien, l'albacore est exploité depuis le début des années 1950 par les flottilles semi-industrielles et artisanales des Maldives, de l'Iran, du Sri-Lanka et d'Inde et par les flottilles industrielles dominées par les senneurs européens et les palangriers asiatiques qui représentent respectivement 36% et 15% des captures (Herrera and Pierre, 2010). Depuis le début de son exploitation, les captures ont augmenter de manière constante, dépassant les 500 000 tonnes par an au cours de la période 2004-2005, puis elles ont diminués, atteignant en 2010 une moyenne annuelle de 291 356 tonnes (Pillai and Satheeshkumar, 2012).
Les senneurs opèrent essentiellement dans l'ouest de l'océan Indien (Canal du Mozambique, région entourant les Seychelles jusqu'à 70° Est et 10° Nord) et suivent les migrations saisonnières de l'albacore. De décembre à mars, la pêche à la senne est principalement pratiquée sur bancs libres et cible les grands individus matures (90-130 cm). Le reste de l'année, elle est pratiquée sur bancs objets, un banc objet étant le regroupement de poissons sous objets flottants naturels ou artificiels. Les prises sont alors essentiellement composées de juvéniles (40-60 cm). Le plus souvent, des objets flottants artificiels, appelés dispositifs de concentration de poissons (DCP), sont utilisés. Généralement constitués de bambou, ces dispositifs sont équipés de balises indiquant la position et la présence éventuelle de poissons.
Les palangriers opèrent au nord et au sud-ouest de l'océan Indien et ciblent essentiellement les grands individus ($>$ 90 cm).

Le suivi et la gestion du stock d'albacore de l'océan Indien sont sous la responsabilité de la Commission des Thons de l'Océan Indien (CTOI[1]). Ce suivi s'appuie sur des modèles de dynamique de population structurés en âge. Il intègrent des connaissances sur la croissance et la mortalité naturelle et des informations sur l'intensité de pêche (Langley et al., 2012). Ce suivi est complexe car cette espèce hautement migratrice occupe une large distribution géographique et présente une période de reproduction s'étendant sur plusieurs mois. De plus, les pêcheries industrielles hauturières sont capables de ré-allouer très vite leur effort de pêche en fonction des concentrations locales de thon ou de changer d'espèce cible et d'océans en quelques jours.
Les dernières évaluations suggèrent que le stock d'albacore de l'océan Indien n'est actuellement pas en surexploitation. Toutefois, la biomasse de reproducteurs a connu une forte baisse au cours de la dernière décennie et le stock pourrait ne peut plus être en mesure de faire face à la pression de pêche si le niveau des captures des flottilles industrielles venait à s'intensifier (IOTC, 2011). L'étude des processus

1. www.iotc.org/

biologiques élémentaires, tels que la croissance et la mortalité, a été largement négligée. En effet, il existe de nombreuses incertitudes sur la courbe de croissance actuellement considérée dans les évaluations du stock, celles-ci conduisant à un affaiblissement des avis scientifiques sur l'état de la ressource.

3.3 Croissance de l'albacore

Depuis le début des années 1960, la croissance de l'albacore a fait l'objet de nombreuses études basées sur (i) des estimations d'âge (otolithes, écailles et épines ; Yang et al., 1969; Le Guen and Sakagawa, 1973; Stéquert et al., 1996), (ii) des fréquences de tailles (Marsac and Lablache, 1985; Gascuel et al., 1992; Gaertner and Pagavino, 1992) et (iii) des expériences de marquage-recapture (Fonteneau, 1980; Bard, 1984). Traditionnellement, la croissance de l'albacore est supposée suivre un modèle de Von Bertalanffy où le taux de croissance diminue de façon continue tout au long de la vie du poisson. Cependant, les études menées depuis les années 1980 dans les trois océans mettent en évidence la succession de deux stances de croissance différentes, une croissance lente des juvéniles et une croissance rapide des adultes (Fonteneau, 1980; Bard, 1984; Gascuel et al., 1992; Gaertner and Pagavino, 1992; Lehodey and Leroy, 1999). Cette croissance en stances est très particulière parmi les thonidés, à l'exception du patudo de l'océan Indien pour lequel un patron de croissance similaire a récemment été mis en évidence (Fonteneau and Gascuel, 2008; Eveson et al., ress). Les mécanismes biologiques et écologiques à l'origine de ces stances demeurent encore très mal compris.
Bien que cette croissance en stances constitue actuellement la courbe de référence pour les évaluations des stocks des océans Indien et Atlantique, elle est encore controversée, certains auteurs préconisant le maintient du modèle de Von Bertalanffy (Stéquert et al., 1996; Driggers et al., 1999; Shuford et al., 2007; Kolody, 2011). Une meilleure compréhension du patron de croissance de l'albacore et de ses mécanismes sous-jacents permettrait une évaluation plus fiable du stock, une perception plus réaliste des conséquences potentielles de la pêche et une prédiction des capacités d'adaptation de l'espèce. En effet, celle-ci est actuellement confronté à des changements océanographiques liés au réchauffement climatique globale qui modifie les communautés pélagiques dont il dépend de manière substantielle.

Afin d'améliorer les estimations des paramètres biologiques nécessaires à l'évaluation des stocks, en particulier la croissance, un vaste programme de marquage de thons, Regional Tuna Tagging Project (RTTP) a été conduit dans l'océan Indien, de mai 2005 à septembre 2007 (Hallier, 2008). Ce programme, mené par la Commission de l'Océan Indien (COI) et supervisé par la CTOI a permis de marquer plus de 64 000 albacores. En septembre 2012, plus de 10 000 albacores marqués ont été recapturés, dont 256 marqué à l'oxytétracycline (OTC).

S'appuyant sur les données collectées au cours du programme RTTP ainsi que sur les distributions des fréquences de longueurs échantillonnées à partir de la pêche à la senne, cette étude se propose d'améliorer les connaissances actuelles sur

la croissance de la population d'albacore de l'océan Indien.
Dans un premier temps, des modèles d'état stochastique bayésiens visant à une meilleure estimation du patron de croissance ont été mis en œuvre. Le premier objectif était d'appréhender et de quantifier les différentes sources d'incertitudes autour des estimations d'âge issues de la lecture d'otolithes et leur influence sur les estimations de croissance. Le second objectif était de proposer un modèle exploitant les différentes sources d'informations actuellement disponibles pour l'étude de la croissance. Ce modèle intégrait explicitement des connaissances issues de l'expertise et des études historiques et tenait compte des incertitudes associées à chaque source de données ainsi qu'au processus de modélisation.
Dans un deuxième temps, un modèle bio-énergétique s'appuyant sur les principes de la théorie DEB a été développé afin de tester différentes hypothèses susceptibles d'expliquer le patron de croissance observé pour l'albacore.

4 L'approche Bayésienne

Depuis une vingtaine d'années, les approches de modélisation Bayésienne suscitent un vif intérêt dans les domaines de l'écologie et des sciences halieutiques. Ces approches représentent un outil prometteur pour l'évaluation des stocks halieutiques et l'analyse des risques liés aux décisions de gestion des pêches (Punt and Hilborn, 1997; Meyer and Millar, 1999; Chen et al., 2003).

4.1 Philosophie de l'approche Bayésienne

Soit un phénomène X décrit par un ensemble de paramètres θ et lié à une série d'observations x. L'objectif de l'inférence Bayésienne est de déduire de façon logique et explicite les probabilités des différentes valeurs possibles des paramètres θ, à partir de connaissances initiales dites *a priori* d'une part, et des observations x d'autre part. Les paramètres θ sont traités comme des variables aléatoires pour lesquelles nous disposons d'une connaissance préalable plus ou moins exacte. Cette connaissance est modélisée par une distribution de probabilités dite *loi a priori* et notée $\pi(\theta)$. L'inférence Bayésienne consiste alors à mettre à jour la connaissance $\pi(\theta)$ à partir des observations x en appliquant la formule de Bayes et de la fonction de vraisemblance $f(x/\theta)$:

$$\pi(\theta/x) = \frac{f(x/\theta).\pi(\theta)}{\int f(x/\theta).\pi(\theta).d\theta}$$

Cette actualisation de la connaissance conduit à une nouvelle distribution de probabilités dite *loi a posteriori* et notée $\pi(\theta/x)$. À titre de comparaison, les statistiques classiques, dites fréquentistes, considèrent les paramètres θ comme des quantités fixes dont les estimations sont basées uniquement sur les observations x.
Le plus souvent, l'estimation analytique de la *loi a posteriori* $\pi(\theta/x)$ est difficile. Elle repose alors sur la simulation de $\pi(\theta/x)$ par des méthodes d'échantillonnages de type MCMC (Monte Carlo par Chaîne de Markov) ou SIR (Sampling Importance Resampling). L'outil utilisé dans cette étude s'appuie sur un échantillonnage de type

MCMC qui consiste à tirer aléatoirement des valeurs dans $\pi(\theta)$ afin de constituer une suite de variables aléatoires θ_t où l'état à un temps t est contraint par l'état au temps précédent.

4.2 Intérêts de l'approche Bayésienne

L'utilisation du cadre Bayésien permet d'inclure, d'une manière simple et rigoureuse, des connaissances supplémentaires issue de l'expertises et de l'analyse de données externes dans les estimations statistiques (Gelman et al., 2004; Cressie et al., 2009), les estimations étant alors plus cohérentes. De plus, l'approche Bayésienne quantifie explicitement les incertitudes associées à l'estimation de chaque paramètre (Punt and Hilborn, 1997; Clark, 2005). Cette approche s'avère donc appropriée pour les sciences halieutiques du fait du caractère limité des données concernant la biologie et l'écologie des espèces exploitées et de la fiabilité incertaine des données collectées à partir de la pêche.

4.3 Modélisation hiérarchique Bayésienne

La modélisation hiérarchique Bayésienne est particulièrement adapté à l'inférence d'un grand nombre de variables latentes et de paramètres décrivant des relations complexes à partir de nombreuses sources d'information. Le phénomène à modéliser est alors décomposé en une série de sous modèles plus simples (Clark, 2005; Eaton and Link, 2011). Les modèles hiérarchiques permettent aussi de prendre en compte séparément les différentes sources d'incertitudes associées aux processus d'observation et de modélisation et fournissent ainsi des inférences puissantes (Cressie et al., 2009).

Chapter 1

Data presentation

1 Regional Tuna Tagging Project - Indian Ocean

The Regional Tuna Tagging Project (RTTP) is a large scale mark-recapture program of tuna conducted in the Indian Ocean from May 2005 to September 2012. Funded by the European Union, this program was carried out by the Indian Ocean Commission (IOC [1]) and supervised by the Commission of the Indian Ocean Tuna (IOTC [2]). The overall objective of this program was acquiring independent data of commercial fisheries in order to strengthen knowledge on tuna's population dynamics, particularly on growth and mortality, and thus improve the regional stock management for the principal market tropical tuna species : skipjack (*Katsuwonus pelamis*, Linnaeus 1758), bigeye (*Thunnus obesus*, Lowe 1839) and yellowfin (*T. albacares*, Bonnaterre 1788).

The tagging operations of RTTP were conducted between 2005-2007 on two pole-and-line vessels that were chartered to operate in the Western Indian Ocean. Field operations consisted in catching tunas for a short time, tagging them on a vinyl-covered cradle, measuring their fork length F_L, i.e. fish length from the front to the fork in the center of the tail (Figure 1.2) through marks printed directly on the cradle, weighing and finally releasing them alive at sea (Hallier, 2008). The fish were tagged with plastic dart tags of *spaghetti* type (Figure 1.1) inserted into the musculature, below the second dorsal fin. The information associated with the whole school ; i.e. date and geographic location, were recorded or each tag event (Hallier et al., 2010). In addition, from 2002 to 2009, the IOTC released 31,455 tunas during tagging operations in the Western (Maldives, Laccadive, Andaman, Indonesia, Mayotte) and Eastern Indian Ocean. A total of 100,578 skipjack, 34,960 bigeye and 64,323 yellowfin were tagged (Figure 1.3). Among them, 2,443 bigeye and 2,741 yellowfin received an oxytetracycline (OTC) injection, an antibiotic that is rapidly incorporated into calcified parts such as bones, scales, and otoliths and leaves a permanent fluorescent mark in the growth increment being formed at the time of tagging. Depending on fish size, between 1.5-3 mL of OTC were injected with a syringe in the intramuscular region of the back (Hallier, 2008).

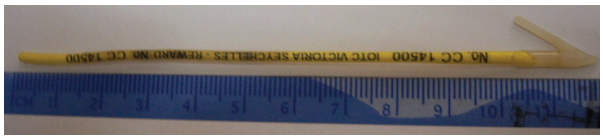

FIGURE 1.1 – Hallprint^{TM} dart tags, the most common tag used

Recovery operations took place across the entire Indian Ocean basin between 2005-2012. The majority of recoveries came from fish caught by the European purse seiners and reported during landings in Seychelles (IOTC 2011). The recovered fish were weighed and different length measurements were made, fork length F_L,

1. www.coi-ioc.org/
2. www.iotc.org/

pre-dorsal length F_{DL} and curved length C_L (Figure 1.2) with calipers or a tape measure to the nearest 0.5 cm. As fish are dead, their handling is easier and allows the use of more precise measurement tools. However, some length measurements were made on frozen fish, that may include a bias due to shrinkage, i.e. frozen fish in brine are often severely compressed. The tag could be recovered in various places (fishing boat, cannery, fish store, fish market) and in various processing stages in the fishing industry (fishing, transferring, unloading, sorting ranking, fishmonger ; Hallier et al., 2010). The accuracy in the date and location of recaptures is dependent on the place and the process in which the tag is recovered. About 20% of the recoveries were made during purse seine fishing operations, which resulted in the recovered fish being associated with only one position and date. In contrast, tunas recovered during the unloading of purse seiners could be associated with several dates and catch locations due to the process of storing tunas in refrigerated wells that contain up to 5 sets collected over an entire fishing trip. The recovery can also occur downstream of the unloading process or in the canneries. The range of dates associated with each recapture was derived from logbook data and well maps and conducted in close collaboration with the IOTC and the purse seine fishing industry (Figure 1.3). In September 2012, 15,387 skipjack, 5,639 bigeye and 10,395 yellowfin had been recovered, including 192 bigeye and 256 yellowfin chemically tagged with OTC. These latter were beheaded with a hacksaw and their sagittal otoliths were extracted with forceps. Otoliths were rinsed in water and ultrasound to remove adhering tissues and stored dry in plastic micro-tubes for subsequent analyses.

FL : Fork length
FDL : Pre-dorsal length
CL : Curved length

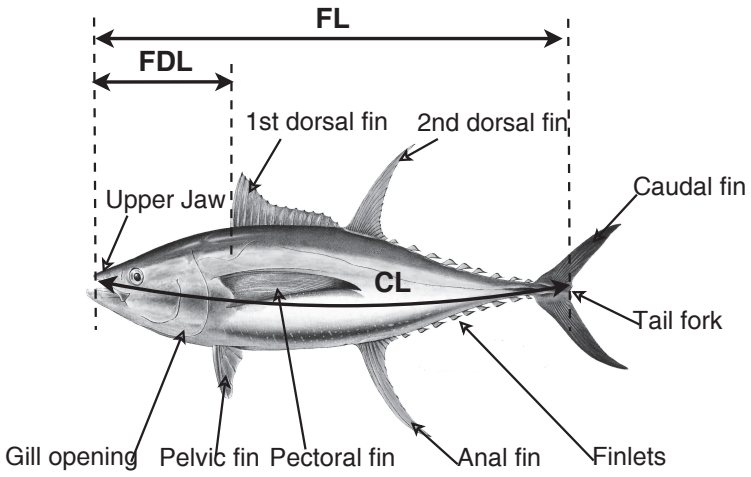

FIGURE 1.2 – The various fish length measurements

All the otoliths collected were read by the technicians of the "Laboratoire de Sclérochronologie des Animaux Aquatiques" (LASAA) in Brest, France. Otoliths were prepared for age analysis using the following method (Secor et al., 1991; Stéquert, 1995; Panfili et al., 2002). They were cleaned in sodium hypochlorite and rinsed with distilled water before being embedded in resin blocks and transversally cut on both sides of the nucleus. The sections containing the nucleus were then fixed

to a glass slide using thermoplastic glue and sanded to the level of the nucleus using different alumina grains (0.3 to 3 μm). The operation was performed on each side of the section until a slice of about 100 μm thickness was decalcified with EDTA (tri-sodium-ethylene-diamine-tetra-acetic acid) to increase the contrast between increments. The thin slides were examined under a microscope (1000x magnification) to count increments along the counting path on the sagitta, i.e. from the primordium, original point of growth, to the last increment deposited on the maximal growth axis.

The RTTP data include various sources of uncertainty and variability in the quality of the data collected. Based on information available and expert opinion gathered from the personnel participating to the program, some selection criteria were applied to produce a reliable and consistent dataset. Thus, all tunas described by the following characteristics were excluded from analysis :

- Fish whose species recorded at tagging differs from that recorded at recovery.
- Fish measured in pre-dorsal length and curved length because the conversion into fork length is considered imprecise.
- Fish whose length measurement at tagging and/or at recapture were reported as unreliable by the RTTP team.
- The OTC-tagged fish that spent less than 30 days.
- Tunas collected prior to 2007 that were considered unreliable due to logistical issues in the tag-recovery system in place at Victoria, Seychelles (Hallier, *pers. com*)

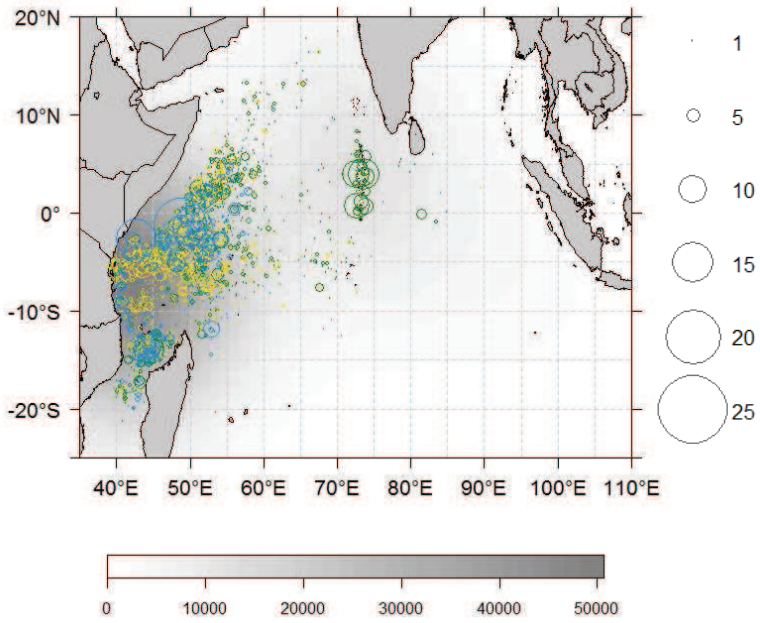

FIGURE 1.3 – Tagging area (gray-colored) and points of tag recovery (circles) of RTTP program for skipjack (○), bigeye (○) and yellowfin (○)

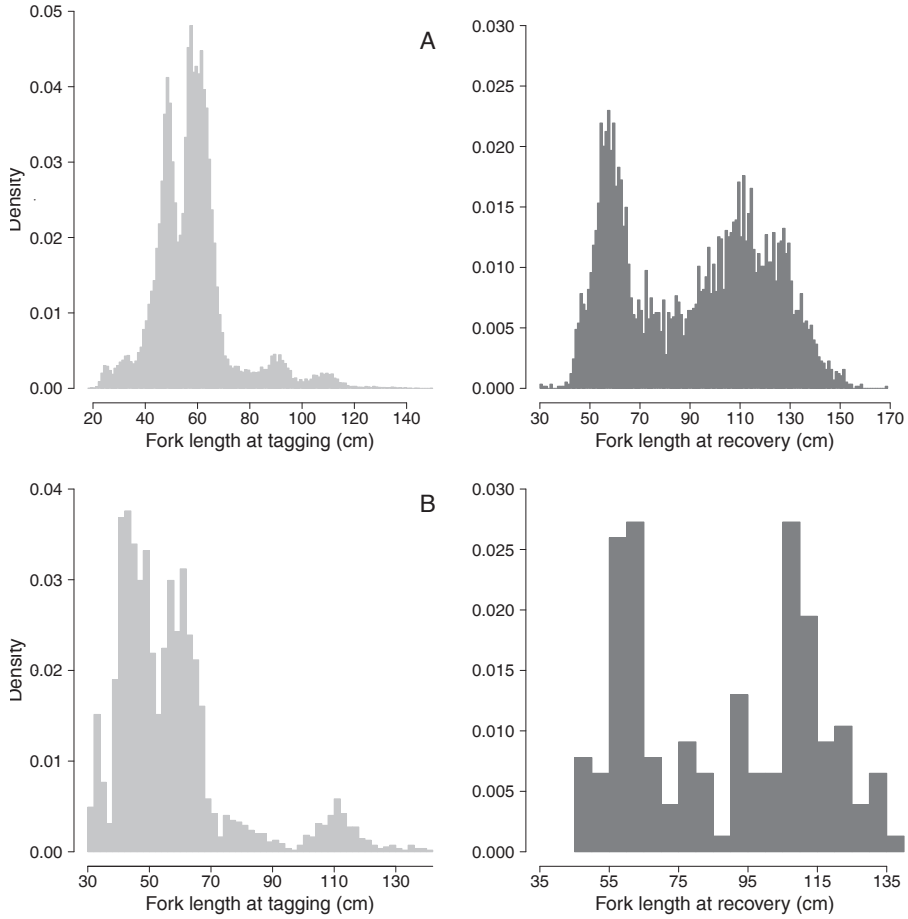

FIGURE 1.4 – Distributions of sizes-at-tagging and sizes-at-recovery for tagged yellowfin during the RTTP program (A) and those chemically tagged (B)

2 West Sumatra Tuna Tagging Project

The West Sumatra Tuna Tagging Project (WSTTP) was a simple capture program conducted off the western Indonesian coast in August 2007 (Figure 1.5). Funded by the government of Japan, this program was carried out by the IOTC on a pole-and-line vessel. 18 yellowfin were caught, weighed and their fork length were measured using a graduated cradle or a caliper and the accurate date and geographic location were recorded for each fish caught (Anonymous, 2008). Their otoliths were extracted with forceps, rinsed in water to remove adhering tissues and stored dry. The WSTTP data provide complementary information to the RTTP data size commonly caught because they include small fish of size comprised between 19-29 cm F_L.

FIGURE 1.5 – Sampling area of WSTTP tunas capture program

3 Length-frequency data

Length-frequency data were extracted from the *Balbaya* database managed by the Institut de Recherche pour le Développement (IRD, Sète). These data have been collected by IRD in cooperation with the Instituto Español de Oceanografia (Spain) and the Seychelles Fishing Authority (Seychelles) since the early 1980s (Pianet, 1999). The sampling is made during the unloading of the purse seiners at the fishing ports of Victoria (Seychelles), Diego Suarez (Madagascar) and Port-Louis (Mauritius). Some wells are selected from among those containing homogeneous strata, a stratum is defined by a spatial area, a quarter fishing and a fishing mode, i.e. free swimming school or FAD-associated school. From these wells, a number of fish are randomly collected, their species are identified and then they are measured. The fish sampling in each selected well is considered as representative of the whole fishing hauls, a well can match several fishing hauls. Knowing the tonnage of the fishing hauls, the representativeness of each hauls in the sampled well and the weight of fish sampling, it is possible to estimate both size structure and species composition of catches. From a technical point of view, the sampling is made in 2 rounds separated from a few hours and supposed to be a simple random sampling within each selected well. The number of fishes counted and measured depends both on the fish size category within the well and on the fish species. Typically, a sample is composed of about 200 measurements for a well containing large tunas (> 70 cm) and of about 500 counts and measurements otherwise.

The data set selected for this study encompassed 566,394 length measurements of yellowfin collected from commercial catches of European, Seychelles, Iranian and Mayotte purse-seiners between December 2000 and March 2010. The catches came from both FAD-associated schools and free swimming schools in three fishing areas, Southeast and Northwest Seychelles and South Somali (Figure 1.6).

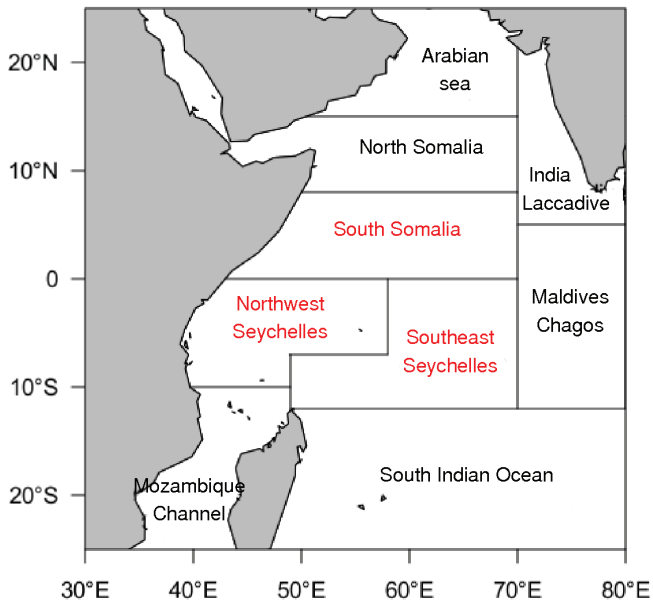

FIGURE 1.6 – Fishnig areas of Indian Ocean

4 EMOTION project

EMOTION (Estimation of Maternal effects On the sustainability of large pelagic populaTIONs) is a scientist project aimed at strengthen knowledge on the processes governing the growth and the reproduction of the three main species of tropical tunas of the Indian Ocean, yellowfin (*Thunnus albacares*), bigeye (*T. obesus*) and skipjack (*Katsuwonus pelamis*). Funded by the Agence National de la Recherche (ANR), this project is currently carried out in the Western Indian Ocean by the Institut de Recherche pour le Développement (IRD, UMR 212 Exploited Marine Ecosystems [3]) in collaboration with the Seychelles Fishing Authority (SFA [4]), the Fundacion AZTI-Tecnalia (AZTI [5]), the Agrocampus Ouest [6], the Institut français de recherche pour l'exploitation de la mer (Ifremer [7]) and the Institut National de la Recherche Agronomique (INRA [8]) (Chassot, 2011).
In 2012 and 2013, a number of yellowfin, bigeye and skipjack was sampled during the unloading of the purse seiners at the fishing ports of Victoria (Seychelles). These fish were weighed, different length measurements were made (Figure 1.2) and their sex as well as their maturity stage were identified. Then, the red and white muscles, the liver, and the gonads were collected for further analysis (characterisation of the tissues composition, particularly lipid profile).

3. http://www.umr-eme.org/
4. www.sfa.sc/
5. www.azti.es/
6. www.agrocampus-ouest.fr
7. www.ifremer.fr/delst/
8. www.inra.fr

Chapter 2

Accounting for age uncertainty in growth modelling

1 Introduction

Estimating individual age of living beings is fundamental in ecological studies. For some time, growth, survival and reproductive characteristics have been shown to be age-dependent as ageing generally conducts to decreasing fertility and increasing mortality with advancing age (Kirkwood and Austad, 2000). Age information currently forms the basis of most population dynamics models used for the management of natural populations (Cailliet et al., 2006; Booth et al., 2011). For example, quantitative stock assessment models use age information to relate distinct demographic rates to age classes (Cotter et al., 2004). Although some stock assessment models may link demographic processes to size or stage classes rather than to age, the transition rates between such classes are generally based on estimates of age-dependent growth.

1.1 Ageing fish from hard parts

Sclerochronology is the study of the growth increments deposited in the hard and skeletal tissues of vertebrates that are capable of recording some biological phenomena. The field of sclerochronology is interested in both chemical composition to reconstruct environmental conditions experienced by organisms and periodicity of incremental deposits so as to for ageing and reconstruct the life history of living organisms (Bagliniére et al., 1992; Panfili et al., 2002). Age estimates can be derived from counting periodic growth increments of mammalian teeth (Dabin, 2006), tortoise shell (Bertolero et al., 2005), bird feather (Saether et al., 1994), insect cuticle (Hayes and Wall, 1999), bivalve shell (Moura et al., 2009) and coral skeleton (Mitchell et al., 1993). For bony fishes, different calcified structures can be used for age determination, i.e. scales (scalimetry), vertebrae (skeletochronology), otoliths (otolithometry) and spines (Figure 2.1 ; Natanson et al., 2006; Buratti and Santos, 2010; Williams et al., 2013).

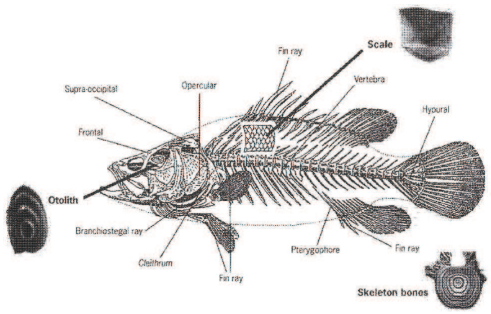

FIGURE 2.1 – The main calcified structures used to ageing fish (source : Panfili et al., 2002)

Over the last decades, otoliths have become an invaluable tool for ageing fish. This is because the otoliths of many temperate and tropical fish species exhibit seasonal and daily growth marks and continue to grow even when somatic growth is slowed or naturally stopped (Pannella, 1971; Mugiya and Tanaka, 1992; Panfili et al., 2009). Consequently, counts of otolith increments provide a direct estimation of fish age.

1.2 Otolithometry

1.2.1 What is an otolith ?

The otoliths are small extracellular structures mostly composed of aragonite, crystallised form of calcium carbonate ($CaCO_3$), precipitated in a protein matrix composed of otoline, keratin-like protein, and rich in aspartate and glutamate (Degens et al., 1969; Campana, 1999).
Otoliths are located in the otic sacs of membranous labyrinth of the inner ear and work an important role in hydrostatic equilibrium. The Osteichthyan have three otic sacs, the *sacculus*, *lagena* and *utriculus*, each containing a pair of otolith that differs in size and shape, the *sagitta*, *lapillus* and *astericus* respectively (Panfili et al., 2002; Popper et al., 2005). In most teleosts, such as tunas, the sagittae are the largest and therefore the most commonly used for age estimation (Stéquert, 1995; Panfili et al., 2002). The sagittal otolith have three orientation plans, sagittal, frontal and transverse and all have been used for otolith preparation (Stéquert, 1995). It is laterally compressed with a convex proximal side (inside) and a concave distal side (outer) and a dorso-ventral asymmetry. Its main growth axis is oriented in the antero-posterior direction (Panfili et al., 2002).

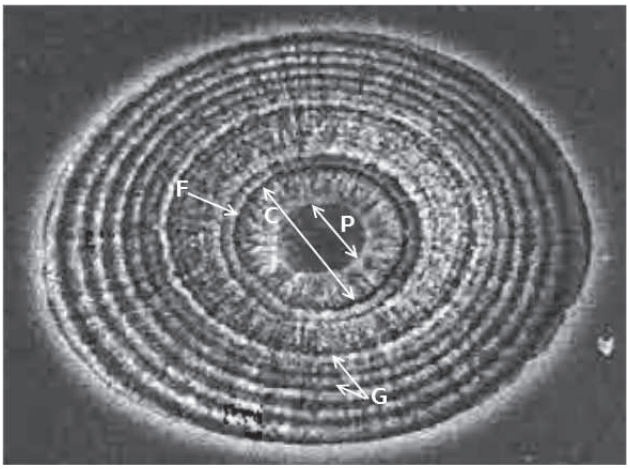

FIGURE 2.2 – Otolith of oceanic lightfish (*Vinciguerria nimbaria*) viewed with a compound microscope (photo L.Marec and E.Dabas from Panfili et al. (2002))
P : Primordium, C : Core (nucleus), F : First increment, G : Growth increments

Otolith formation begins in the later part of embryogenesis with the aggregation of protein granules through the action of ciliated cells that line the inner ear epithelium. These protein, partially calcified, form the primordium and appearing as an optically opaque disk (Campana and Neilson, 1985; Panfili et al., 2002). The first increment, formed at hatching, appears like a discontinuity surrounding this disk, forming the otolith core, also called nucleus (Figure 2.2). Then, otolith grows continuously throughout the life of the fish by successive deposits of rich layers in calcium carbonate and rich layers in proteins arround the nucleus (Campana and Thorrold, 2001; Panfili et al., 2002, 2009).
Otolith growth is a periodic phenomenon that occurs daily in most fish. This phenomenon leads to growth increments formation composed of two zones : (i) a discontinuous zone, narrow, opaque and rich in organic material and (ii) a accretion zone which defines the increment width, translucent and rich in calcium carbonate crystals (Figure 2.2 ; Campana and Neilson, 1985; Panfili et al., 2009). The formation of the discontinuous zone is controlled by endogenous endocrine rhythms and continues even when the somatic has ceased. In contrast, the formation of the accretion zone is related to physico-chemical processes and the growth of this latter is proportionnal to somatic growth (Mugiya and Tanaka, 1992; Morales-Nin, 2000).
The total width of an increment varies between 0.4 and 12 μm (Panfili et al., 2002) and depends on the metabolism of the fish and environmental conditions, such as temperature and feeding frequency.

1.2.2 Sources of uncertainty in otolith reading

Otolith reading involves some interpretation by the reader which can lead to imprecision and bias in age estimation (Marriott and Mapstone, 2006; Punt et al., 2008). This may subsequently affect estimates of demographic and biological parameters of populations and eventually modify the perception of stock status and the associated management advice (Bertignac and De Pontual, 2007).
Errors in interpreting and counting daily increments can initially be related to otolith preparation for reading. In particular, some increments may be "lost" at the otolith nucleus, i.e. the core, and edge due to an oversanding (Neilson, 1992). The identification of the first increment, which appears as a discontinuity surrounding the nucleus, is a particularly important step. The nucleus disappearance is reflected by the absence of a correctly defined starting point and the age estimates will be invariably biased (Campana, 2001). In addition, some increments can be more or less apparent, especially because of the over-decalcification that can blacken the otolith preparation. The position and the number of lost increments have then been estimated. A poor decalcification or a non perpendicular cutting section to the axis from the nucleus to the last increment deposited require frequent changes in the microscope focus and counts made on different reading axis and therefore some increments can be omitted or counted more than once (Sardenne et al. *in press*).
Otoliths can also exhibit discontinuities and zones of overlap which can also result in errors in increment counts. Reading errors are generally higher for older fish because they have more increments to count and increments tend to get narrower with the

distance from the nucleus (Uchiyama and Struhsaker, 1981; Stéquert, 1995).
In addition, the growth increments may not always have consistent daily deposition, i.e., sub-daily increments and discontinuities in the accretion rate may occur due to stress, reproduction, and environmental conditions (Radtke and Fey, 1996; Panfili et al., 2009). Finally, some factors such as temperature of feeding frequency have also been shown to affect the endogenous rhythm that controls otolith growth (Morales-Nin, 2000).

Multiple independent readings of the same otolith have often been used to estimate the consistency and reproducibility of reading method, to compare the readers skill and to assess the imprecision in age estimates (Eltink et al., 2000; Marriott and Mapstone, 2006). The two main measures of reading precision are the coefficient of variation (CV) and the average percent error (APE) :

$$CV = 100 \times \frac{\sqrt{\frac{\sum_{l=1}^{R}(I_{i,l}-\bar{I}_i)^2}{R-1}}}{\bar{I}_i} \quad APE = 100 \times \frac{\sum_{l=1}^{R}|I_{i,l}-\bar{I}_i|}{R \times \bar{I}_i} \tag{2.1}$$

where $I_{i,l}$ is the increments number at the reading l of the otolith i, $\bar{I}_i$ is the mean increments number for otolith i and R is the readings number for otolith i. Both metrics measure the reproducibility of repeated otolith readings, but not the accuracy of the reading method (Campana, 2001).

Validating the frequency of increment formation is also crucial to obtain an accurate fish age. Various approaches exists, such as release of tagged fish of known age, nuclear or radiochemical dating, modal progression of catch-at-size over time, captive rearing or mark-recapture experiments of fish that have been chemically tagged with oxytetracycline (OTC) or strontium ($SrCl_2$). Mark-recapture experiments are considered to be one of the best methods for validating age interpretation (Caillart and Morize, 1989; Campana, 2001). After injection, the OTC is rapidly incorporated into the otolith and results in a permanent mark at the increment that formed at the time of tagging. This mark is visible under fluorescent light. The number of growth increments formed after the mark can then be compared to the time between tagging and recapture, i.e. time-at-liberty, to test the periodicity of the increment formation.

1.2.3 Accounting for age uncertainty in growth modelling

Using yellowfin (*Thunnus albacares*) as a case study, we describe an approach for estimating the individual ages of fish from multiple readings of otoliths that takes into account the uncertainties associated with the observation process. We apply our model to an original age-length dataset collected through large-scale mark-recapture experiments conducted in the Indian Ocean between 2005 and 2012 (chapter 1, section 1).
Firstly, an ageing error model was developed to explicitly represent the sources of uncertainty associated with age estimation. Developed in a hierarchical Bayesian framework, expert judgment was included in the model through the choice of stochastic

error structure and informative prior density functions. A simulation framework was developed to evaluate the accuracy of the model, its limitations and its relevance to the traditional ageing method that estimates age based on average increment counts. Secondly, the ageing error model was coupled to a two-stanza somatic growth model to propagate age uncertainty into growth parameter estimates. Through this growth model, we evaluated the impact of the age estimation method on the catch age composition of the commercial fisheries targeting yellowfin in the Indian Ocean.
Finally, we used the ageing-growth coupled model to test the influence of reading method on growth estimates. With this case study, we provide a flexible statistical framework that accounts for age-related uncertainty in growth modeling and addresses an applied ecology problem of immediate concern for the Indian Ocean Tuna Commission.

2 Materials and methods

2.1 Development of an ageing error model

2.1.1 Otolith sampling, preparation and reading

Sagittal otoliths were collected from 128 yellowfin recovered in the Western Indian Ocean through the RTTP measuring between 43 to 85 cm F_L at tagging and 47.9 to 146.5 cm F_L at recapture (chapter 1, section 1). These ones including 124 fish chemically tagged with oxytetracycline (OTC). Otoliths were also collected from (i) 18 yellowfin captured during the WSTTP measuring between 19 to 46.6 cm F_L (chapter 1, section 2) and (ii) 28 fish collected from 2008-2009 from the Indian Ocean Tuna Ltd (IOT) cannery measuring between 31-128.7 cm F_L.

All the otoliths collected were read by the technicians of the "Laboratoire de Sclérochronologie des Animaux Aquatiques" (LASAA) in Brest, France. Otoliths were prepared for age analysis using the method described by Secor et al. (1991); Stéquert (1995); Panfili et al. (2002) (chapter 1, section 1). For otoliths collected from OTC-tagged fishes, an increment count was made for different otolith sections : (i) between the nucleus and the OTC mark (It), (ii) between the OTC mark and the edge (Im) and (iii) between the nucleus and the edge (Ir) (Figure 2.3). Fish that were not chemically tagged were read in full (Ir). All otolith readings were performed by the same reader. Each otolith was read two to five times without prior knowledge on length or time-at-liberty of the individuals sampled so as to maintain certain independence between the multiple readings.

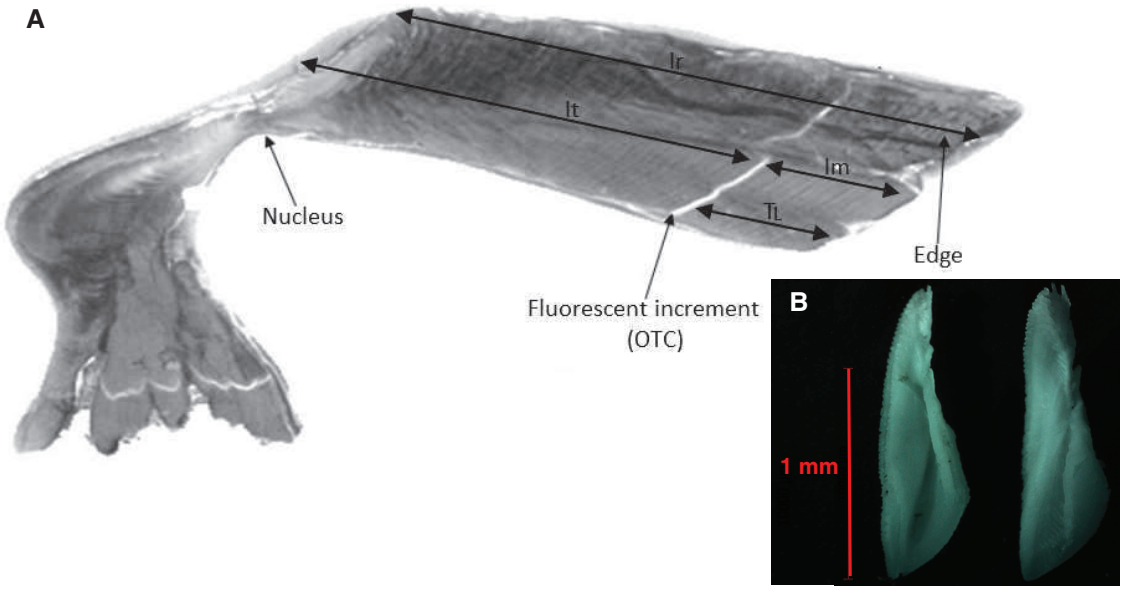

FIGURE 2.3 – Saggital otoliths of yellowfin tuna (external right and internal left, B) and (a) the different sections used for reading the number of increments (A)
OTC : Oxytetracycline ; It : section from the nucleus to the OTC mark ; Im : section from the OTC mark to the edge ; Ir : section from the nucleus to the edge ; T_L : Time-at-Liberty

2.1.2 Ageing error model

In this section, a hierarchical model was developed to estimate the age of each fish. The stochastic processes associated with otolith preparation and reading were modeled with the choice of an error structure and informative prior density functions based on expert judgment (Table 2.1). In a first step, the hypothesis of daily increment deposition in otoliths, that has been observed in eastern Pacific yellowfin tuna (Wild and Foreman, 1980; Wild et al., 1995), was tested using a subset of OTC-tagged otolith data. Information on the increment deposition process was subsequently used for estimating yellowfin age based on counts of otolith increments (Appendix B).

A. Modeling observation errors

We assumed that the discrepancies between repeated readings of the same otolith mainly resulted from errors in interpreting missing increments and, to a lesser extent, from errors in counting, i.e. increment omission or multiple counts. These counting errors were considered to be equiprobable.
Each increment has the same independent probability of misinterpretation, so errors tend to increase with age. In addition, the identification and interpretation of increments become increasingly difficult with increasing distance from the nucleus. Therefore, the relative reading error was considered to be dependent on the true fish age and a multiplicative error was used. The relative percentage of misread incre-

ments, p, was assumed to be a constant factor uniformly distributed between 0 and 0.5 (Table 2.2, Eq. 2.21).
For each reading of the same otolith, the reader was assumed to have the same probability of underestimating or overestimating the number of increments. The number of increments counted for reading l of otolith i ($I^*_{i,l}$) was assumed to be distributed around the expected number of increments (I_i) according to a Poisson process. However a normal distribution, closely approximates the Poisson distribution for large values to provide more flexibility in modeling uncertainty in readings, was used (Table 2.2, Eqns. 2.13-2.15) :

$$I^*_{i,l} \sim \mathcal{N}(I_i, (p \times I_i)^2) \tag{2.2}$$

Identifying the first growth increment is an important step in defining the starting point of ageing and accurately estimating fish age. During preparation, excessive sanding of the otolith can result in the disappearance of the nucleus as well as the removal of some increments. Similar difficulties can be associated with distinguishing the marginal increment at the edge of the otolith. In this region, increments are often more difficult to read because they are narrower and can appear laterally compressed (Neilson, 1992). In addition, the otolith must be cut perpendicularly to the daily growth axis passing by the nucleus, otherwise some increments can disappear.
Technical experts considered that up to 15 of the first otolith increments and up to 20 increments at the otolith edge may be lost during preparation. The lost increments are then estimated with a bias of 2-3 increments near the nucleus (ψ_n, Table 2.2, Eq. 2.19) and a bias of 3-4 increments at the otolith edge (ψ_e, Table 2.2, Eq. 2.20).

B. Determining of the deposition periodicity

In a first step, the number of counted increments between the nucleus and the edge (Im) were modeled as a function of the days-at-liberty (T_L), to determine the periodicity of increment deposition estimated by the reader. For this step, a subsample of 27 OTC-tagged fishes of 49.7-131 cm F_L was selected for its reliability, i.e. individuals for which the accurate date of recapture was known and for which the coefficient of variation (CV) of the repeat readings of a given otolith was less than or equal to 10% (Marriott and Mapstone, 2006).
A Bayesian linear regression model was fitted to the data to estimate the rate of increment deposition (R) and the error at the otolith edge (ψ_e). For the fish otolith i, under the assumption of a daily increment deposition (Wild and Foreman, 1980; Wild et al., 1995), the expected number of increments Im could be related to T_L according to the following equation :

$$Im_i = R \times T_{Li} - \psi_e \tag{2.3}$$

Im_i was estimated for multiple counts according to Eq.2.2 (Table 2.2, Eq. 2.13). We used a dilated beta distribution as prior for R so as to provide information on the limit values without a particular trend in the distribution shape. This distribution was equivalent to a uniform distribution, but allowed more flexibility (Table 2.2,

Eq. 2.18). Based on expert knowledge, an informative prior was considered for the marginal error ψ_e (Table 2.2, Eq. 2.20).

C. Estimating age from multiple readings

In a second step, the uncertainty associated with multiple otolith readings was modeled to estimate the true number of increments for each fish otolith. This number was then converted to age by taking into account R. When the date of recapture was known with precision (CV $\leqslant 5\%$), the age-at-tagging (At) was derived from It (Eq.2.4) and the age-at-recapture (Ar) was deduced from It and the time-at-liberty so as to decrease the reading-associated uncertainty (Eq.2.5)

$$It_i = R \times At_i - \psi_n \tag{2.4}$$
$$Ar_i = At_i + T_{Li} \tag{2.5}$$

When the number of increments at tagging was unknown, the age-at-recapture was derived from Ir (Eq.2.6) and the age-at-tagging was derived by subtracting the time-at-liberty to this number of increments (Table Eq.2.7).

$$Ir_i = R \times Ar_i - \psi_n - \psi_e \tag{2.6}$$
$$At_i = Ar_i - T_{Li} \tag{2.7}$$

For yellowfin collected through the RTTP with low accuracy in time-at-liberty (CV $> 5\%$) and for those from WSTTP, only the age-at-recapture was estimated from It. To account for uncertainty associated with the recapture dates (see section 2.1.1), the time-at-liberty was considered to be a random variable with a uniform distribution between its minimal and maximal value. The posterior distributions of R and ψ_e, that were estimated in the previous step, were used to estimate fish age. An informative prior was considered for the nucleus bias ψ_n. In the absence of information in the data, these distributions were not updated during the estimation process.

2.1.3 Evaluating model performance through simulations

Different simulations were performed to test and validate the ageing error model (Figure 2.4). The first simulation aimed to assess the accuracy of the model in estimating R. For this simulation, two alternative runs with and without individual variability in increment formation were considered, i.e. R fixed to 0.95 and R varying according to a normal distribution around 0.95. This simulation was repeated three times using datasets of 25 individuals whose time-at-liberty was generated according to a uniform distribution between 30 and 970 days. Four noisy readings of the number of Im increments were then generated according to Eqns.2.3 and 2.13 (Table 2.2).
A second set of simulations was performed using 2 to 5 readings of the same otolith to evaluate the model's ability to accurately estimate fish age and its relevance relative to the traditional method which is based on averaging individual-specific increment counts. An intermediate method based on averaging individual increment

counts, but also accounting for potential bias in the increment deposition, was also considered. For these simulations, R was fixed to 0.95. The approach consisted of simulating realistic ages-at-recapture from which increment counts were derived with respect to R, ψ_e, and ψ_n (Table 2.2 Eq. D4). Noise was then added to the increment counts by randomly generating repeated readings (Eq. S3). Five age classes were considered, from 6 months to 5 years. Three simulations were performed using datasets composed of 500 individuals, i.e. 100 individuals for each age class whose ages were generated according to a uniform distribution between the minimum and the maximum values of the class. The accuracy of age estimates was assessed with the relative root mean square error (RMSE), a normalized indicator that measures the discrepancy between simulated and estimated ages. For each individual, the RMSE was calculated as follows :

$$RMSE = \frac{\sqrt{(A^* - A_s)^2}}{A^*}$$

where A^* is the estimated age and A_s is the simulated age.

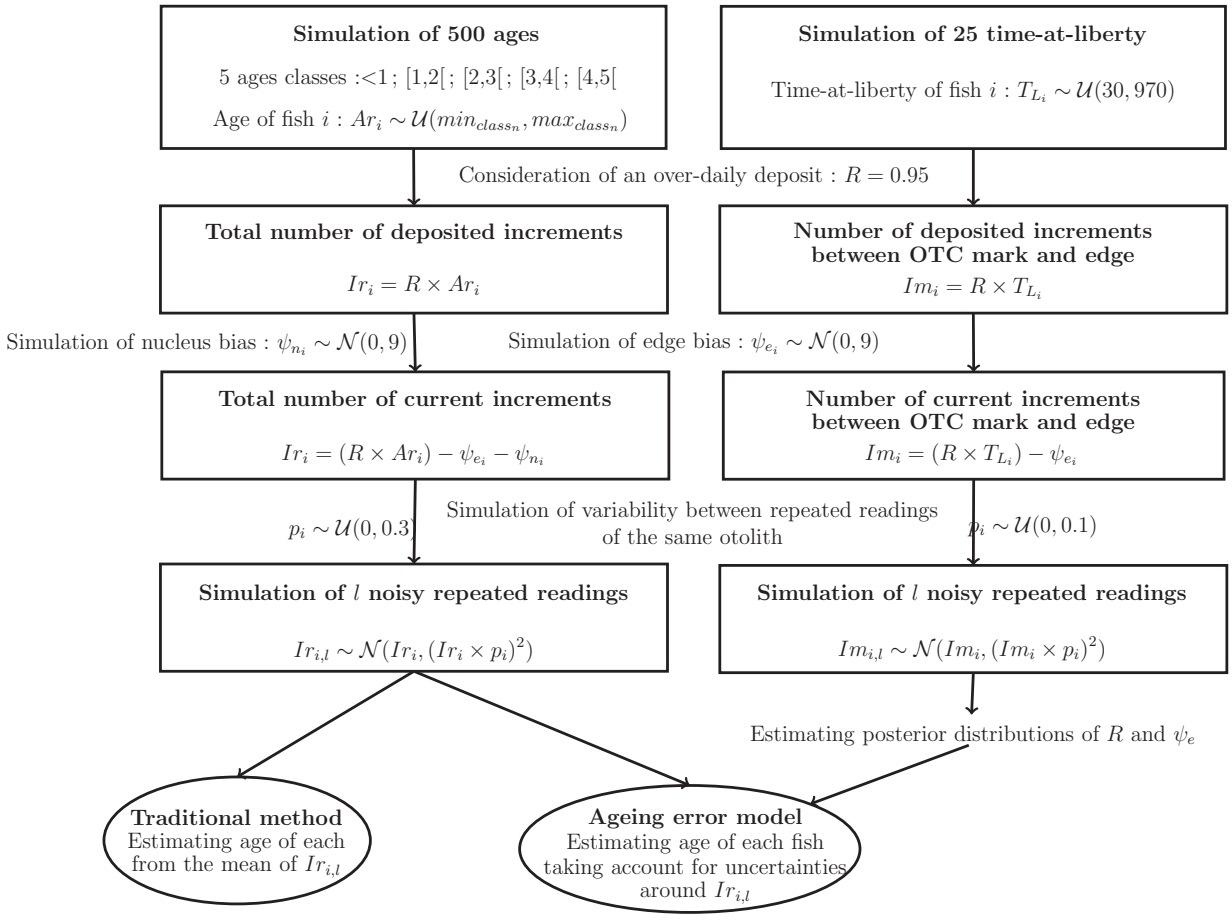

FIGURE 2.4 – Simulation framework for testing the ageing error model

TABLE 2.1 – Parameters and variables used in the ageing error and somatic growth models

Variable	Definition	Equations
Ageing error model		
L_i^*	Observed fork length, i.e. length from the front to the fork in the center of the tail, for fish i (cm)	
$L(A_i)$	Expected fork length for fish i (cm)	
T_{Li}	Number of days between tagging and recapture for fish i (d)	2.3, 2.5, 2.7
At_i	Age-at-tagging for fish i (day)	2.4, 2.7
Ar_i	Age-at-recapture for fish i (day)	2.5, 2.6
Im_i	Number of increments between OTC mark and edge for otolith of fish i	2.3,2.13
$Im_{i,l}^*$	Number of increments counted between OTC mark and edge for reading l of otolith for fish i	2.13
It_i	Number of increments between nucleus and OTC mark for otolith of fish i	2.4, 2.14
$It_{i,l}^*$	Number of increments counted between nucleus and OTC mark for reading l of otolith for fish i	2.14
Ir_i	Total number of increments for otolith of fish i	2.6, 2.15
$Ir_{i,l}^*$	Total number of increments counted for reading l of otolith for fish i	2.15
R	Ratio between number of increments after OTC mark and time-at-liberty	2.3, 2.4, 2.6
ψ_n	Bias at the nucleus	2.3, 2.6
ψ_e	Bias at otolith edge	2.4, 2.6
p	Relative percentage of misread otolith increments	2.13, 2.14, 2.15
Somatic growth model		
t_0	Theoretical age at fork length 0 (year)	2.11, 2.12
k_1	Juvenile growth rate coefficient (year^{-1})	2.11, 2.12
k_2	Adult growth rate coefficient (year^{-1})	2.11, 2.12
α	Inflection point between the 2 stanzas (year)	2.11, 2.12
β	Transition rate between k_1 and k_2 (year^{-1})	2.11, 2.12
L_∞	Asymptotic fork length (cm)	2.12
ε	Length measurement error (cm)	2.16, 2.17

2.1.4 Coupling the ageing error and the growth models

In this section, we implemented a hierarchical model that allows for growth variations according to an individual's specific stochastic process. For Indian Ocean yellowfin, modal progression analysis (Marsac and Lablache, 1985; Lumineau, 2002; Viera, 2005) and the preliminary analysis of the RTTP data (Eveson and Million, 2008) indicated a succession of phases of growth deceleration and acceleration, supporting the use of a two-stanza growth model. Accordingly, we used the Von Bertalanffy logK model (VB log-K) developed for southern bluefin tuna (*Thunnus maccoyii*), which allows for a smooth transition between two different growth rate coefficients (k_1 and k_2) by modeling changes in growth using a logistic function (Laslett et al., 2002; Eveson et al., 2004). The fork length of fish i at the opportunity of capture j, $j = t$ at tagging and $j = r$ at recapture, was then modeled as :

$$L^*_{i,j} = L_\infty(1 - exp(-k_2(A_{i,j} - t_0)) \times \left(\frac{1 + exp(-\beta(A_{i,j} - t_0 - \alpha))}{1 + exp(\beta\alpha)}\right)^{\frac{(k_1 - k_2)}{\beta}} + \varepsilon_{i,j} \quad (2.8)$$

where errors in length measurements, $\varepsilon_{i,j}$, were assumed to be independent and normally distributed around zero with a common variance σ^2_ε.
The somatic VB log-K growth model was coupled to the ageing error model and fitted to the data using Bayesian inference (Table 2.2, Eq. 2.11 and 2.12). Consider the vector of growth parameters, $\theta_g = \{L_\infty,\ k_1,\ k_2,\ t_0,\ \alpha,\ \beta,\ \sigma_\varepsilon\}$, the vector of ageing parameters $\theta_a = \{R,\ \psi_e,\ \psi_n\}$, and the relative percentage of misread otolith increments, p. $\pi[\theta_g|Lj^*_i, Aj_i]$, $\pi[\theta_a|Ij_i]$, $\pi[p, Ij_i|Ij^*_{i,l}]$ denote the posterior distributions of these parameters and $\pi[\theta_g]$, $\pi[\theta_a]$, $\pi[p]$ denote their prior distributions. Here, Aj_i and Ij_i are not directly observable latent variables. The full model corresponds to the joint distribution of parameters and latent variables. As Lj^*_i and $Ij^*_{i,l}$ are independent, this joint posterior distribution can be written as :

$$\begin{aligned}\pi[\theta_g, \theta_a, p|Lj^*_i, Ij^*_{i,l}] \propto\ & \pi[Lj^*_i, Aj_i|\theta_g] \times \pi[Ij_i|Aj_i, \theta_a] \times \pi[Ij^*_{i,l}|Ij_i, p] \\ & \times \pi[\theta_g] \times \pi[\theta_a] \times \pi[p]\end{aligned} \quad (2.9)$$

where $\pi[Lj^*_i, Aj_i|\theta_g]$ represents the conditional Gaussian likelihood of the observed lengths. Thus, the length values were predicted from the marginal posterior distribution :

$$f(Lj^*_i|Ij^*_{i,l}, \theta_g, \theta_a) = \int \pi[Lj^*_i|Aj_i, \theta_g] \times \pi[Aj_i|Ij_i, \theta_a] \times \pi[Ij_i|Ij^*_{i,l}, p]\ .dAj_i\ .dIj_i \quad (2.10)$$

The growth rate coefficients k_1 and k_2 are partly model-specific, thus weakly informative priors were assigned to them. k_1 was assumed to vary according to a gamma prior distribution with a mean and coefficient of variation determined from the literature. k_2 was set equal to $k_1 + \kappa$ with κ following a uniform distribution (Table 2.2 Eq. 2.23 and 2.24).
The transition rate between k_1 and k_2, β, which is specific to the VB-logK model, and the theoretical age of zero length, t_0, which depends on the data, were assigned uniform distributions (Eq. 2.26 and 2.27).

The parameter α is the mean age relative to t_0 at which the change in growth occurs. This was assigned a weakly informative prior gamma distribution with a mean defined from the literature (Eq. 2.25 ; Gascuel et al., 1992; Lehodey and Leroy, 1999; Lumineau, 2002; Viera, 2005).
The standard deviation of size measurement errors, σ_ε, was determined from the differences in the fork length of RTTP-IO fish released and recaptured several times with time-at-liberty less than or equal to seven days. These individuals were not included in subsequent analyses and therefore constitute an independent data set (Eq. 2.28).
The asymptotic length, L_∞, is a particularly important parameter because it determines the shape of the second part of the growth curve. As the dataset included limited information on the asymptotic part of the growth curve, auxiliary information was provided for this parameter consistently with the available knowledge on the biology of the species. An informative prior distribution was defined for L_∞ using a generalized extreme value distribution (GEV). This allows for the extrapolation of the behavior of distribution tails from the greatest values of a sample and thus estimates the probability of the occurrence of extreme events (Borchani, 2010). The choice of this distribution is motivated by the fact that yellowfin grow throughout their life, such that the largest observed sizes should correspond to the oldest fish. The distribution was fit based on size measurement data from fresh fish that were collected during 1952-2011 from the European and Seychelles purse seine fisheries, Maldivian pole and line vessels, and Taiwanese and Japanese longliners. The observed maximum fork length from each measurement platform, i.e. either on vessels board or in cannery, fishery, and year was considered to represent n independent random variables (L_1,...,L_n) with common continuous distribution function F. Asymptotic length L_∞ was then estimated from the approximation of the upper tail of $F(\ell)$ by using the $GEV_(\mu, \sigma, \xi)$ distribution :

$$GEV_{(\mu,\sigma,\xi)}(\ell) = exp\left(-\left(1+\xi\left(\frac{\ell-\mu}{\sigma}\right)\right)^{\frac{-1}{\xi}}\right)$$

where μ is a location parameter, σ is the scale parameter ($\sigma > 0$) and ξ is a tail index (shape parameter). These parameters were estimated using the maximum likelihood method (Hosking, 1985).

The estimates of ages and growth parameters were evaluated based on 350,000 samples, thinned to one draw every 1000^{th} sample, from Markov Chain Monte Carlo (MCMC) simulations of the joint posterior distribution. A burn-in period of 5,000 iterations was rejected. Three MCMC chains were produced using a Gibbs sampler as implemented in OpenBugs version 3.2.1 (Spiegelhalter et al., 2011). The convergence of the MCMC to a stationary posterior distribution was visually evaluated from the Gelman-Rubin diagnostic, which was based on the ratio of inter-chain variance on intra-chain variance, i.e. it must be close to 1 in order to converge (Gelman and Rubin, 1992).

TABLE 2.2 – Deterministic and stochastic processes used in the ageing error and growth models. All variables are defined in table 2.1

Process functions

$$Im_i = R \times T_{Li} - \psi_e \tag{2.3}$$
$$It_i = R \times At_i - \psi_n \tag{2.4}$$
$$Ar_i = At_i + T_{Li} \tag{2.5}$$
$$Ir_i = R \times Ar_i - \psi_n - \psi_e \tag{2.6}$$
$$At_i = Ar_i - T_{Li} \tag{2.7}$$

$$L(At_i) = L_\infty(1 - exp(-k_2(At_i - t_0)) \times \left(\frac{1 + exp(-\beta(At_i - t_0 - \alpha))}{1 + exp(\beta\alpha)}\right)^{\frac{(k_1 - k_2)}{\beta}} \tag{2.11}$$

$$L(Ar_i) = L_\infty(1 - exp(-k_2(Ar_i - t_0)) \times \left(\frac{1 + exp(-\beta(Ar_i - t_0 - \alpha))}{1 + exp(\beta\alpha)}\right)^{\frac{(k_1 - k_2)}{\beta}} \tag{2.12}$$

Observation functions

$$Im^*_{i,l} \sim \mathcal{N}(Im_i, (p \times Im_i)^2) \tag{2.13}$$
$$It^*_{i,l} \sim \mathcal{N}(It_i, (p \times It_i)^2) \tag{2.14}$$
$$Ir^*_{i,l} \sim \mathcal{N}(Ir_i, (p \times Ir_i)^2 \tag{2.15}$$
$$Lt^*_i \sim \mathcal{N}(L(At_i)), \sigma^2_\varepsilon) \tag{2.16}$$
$$Lr^*_i \sim \mathcal{N}(L(Ar_i)), \sigma^2_\varepsilon) \tag{2.17}$$

Prior probability distributions

$$R = 2 \times R' \,;\, R' \sim \mathcal{B}eta(1, 1) \tag{2.18}$$
$$\psi_n \sim \mathcal{N}(0, 3^2) \tag{2.19}$$
$$\psi_e \sim \mathcal{N}(0, 4^2) \tag{2.20}$$
$$p \sim \mathcal{U}(0, 0.5) \tag{2.21}$$
$$L_\infty \sim GEV(173.141, 11.067, -0.3474) \tag{2.22}$$
$$k_1 \sim \Gamma(2.778, 0.211) \tag{2.23}$$
$$k_2 = k_1 + \kappa \text{ with } \kappa \sim \mathcal{U}(0, 3) \tag{2.24}$$
$$\alpha \sim \Gamma(4, 0.725) \tag{2.25}$$
$$\beta \sim \mathcal{U}(0, 20) \tag{2.26}$$
$$t_0 \sim \mathcal{U}(-2, 0) \tag{2.27}$$
$$\varepsilon \sim \mathcal{N}(0, \sigma^2_\varepsilon) \,;\, \sigma_\varepsilon \sim \mathcal{U}(1.7, 3) \tag{2.28}$$

2.1.5 Testing the influence of the ageing technique on growth modeling

Simulations were performed to evaluate the contribution of the error model on growth parameter estimates and resulting age classification of commercial catches. For illustration purpose, a simple tagging dataset was simulated. The relationship specified from posterior marginal mode that was obtained with the growth model coupled with the ageing error model was used as reference growth curve (section 2.1.4 and Table 2.5).
In this approach, four fork lengths for each 2 cm class, from 20 to 146 cm, were simulated to obtain a data set of 252 fishes. As age cannot be estimated by the inversion of the VB log-K curve, corresponding ages were deduced by minimizing the difference between the simulated and expected length (2.29).

$$\arg\min \left(L^* - L_\infty(1 - exp(-k_2(A - t_0)) \times \left(\frac{1 + exp(-\beta(A - t_0 - \alpha))}{1 + exp(\beta\alpha)} \right)^{\frac{(k_1 - k_2)}{\beta}} \right)^2 \tag{2.29}$$

These ages were then converted into numbers of increments from which noisy repeated readings were generated as per the approach previously developed (section 2.1.3). The growth parameters were then re-estimated using a VB log-K model coupled with the ageing error model and a classical VB log-K model which estimates age using the traditional method. As the parameter β is difficult to estimate from a tagging dataset, its value was fixed using the value obtained by fitting the otolith data to the coupled growth model.

The mean squared error (MSE) was used to compare the marginal posterior distributions of each parameter with its actual value and evaluate the accuracy of models fits. Accuracy is related to the similarity between the marginal modes and the true values, while precision refers to the uncertainty around the modal value, i.e. the discrepancies between the samples generated by the MCMC simulation. The MSE is a measure of the average of the square of errors and was calculated as follows :

$$MSE(\theta) = \frac{1}{N} \sum_{i=1}^{N} (\theta_i^* - \theta_a)^2$$

where N is the size of the MCMC sample, θ_i^* is the parameter estimate at iteration i and θ_a is the actual value of the parameter.
In addition, the mean relative error (MRE) was used to give information on the bias in parameter estimates :

$$MRE(\theta) = \frac{1}{N} \sum_{i=1}^{N} \frac{\theta_i^* - \theta_a}{\theta_a} \begin{cases} \text{parameter underestimate if } MRE(\theta) < 0 \\ \text{parameter overestimate if } MRE(\theta) > 0 \end{cases}$$

Finally, an age-length key was derived from both the coupled model and the classical model and used to convert the catch-at-size into catch-at-age. The two conversions were then compared. For this example, we used the catches of the French purse seiners having operated in the Western Indian Ocean in 2010.

2.2 Differences between readers and effects on the growth estimate

In this section, the efficiency of different reading methods for otoliths of yellowfin and bigeye was assessed using the ageing error model previously developed (section A.). Then, the influence of these reading methods on the estimation of growth was evaluated using the coupled ageing-growth model (section 2.1.4).

2.2.1 Otolith and length data

Sagittal otoliths were collected from 163 yellowfin and 91 bigeye throughout the RTTP. Otoliths were prepared and read using the same method as previously (chapter 1, section 1). Then, otolith readings were performed by two readers teams for each species, teams 1 and 2 for yellowfin and teams 2 and 3 for bigeye respectively. As otoliths of yellowfin and bigeye have the same morphology, the reading method were similar across species (Sardenne et al. *in press*). Each otolith was read two to five times without prior knowledge on length or time-at-liberty of the individuals and the counts were made for different otolith sections (Figure 2.3 and Table 2.3).

TABLE 2.3 – Summarize of otolith data used in coupled ageing-growth error model for yellowfin and bigeye

	Yellowfin				Bigeye			
	Team 1		Team 2		Team 2		Team 3	
Otolith section	Im	It	Im	It	Im	It	Im	It
Number of fish	39	89	20	74	9	40	37	72
Fork length at tagging (cm)	47-81	43-85	48-85	47-89	45-65	44-69	44-71.5	45-71.5
Fork length at recapture (cm)	49.7-131	47.9-119	47.9-120	51.4-152	50-108.5	46-141.6	46-117.3	47.7-141.6
Time-at-liberty (days)	37-969	32-720	49-815	49-1948	54-589	37-1369	37-748	43-1167

2.2.2 Assessing the accuracy of readers teams

The three readers teams differed by the reading method applied. Although quite close from one team to another, the reading methods may result in some differences in interpreting otolith microstructures.

A daily increment deposition rate in sagittal otoliths was validated for yellowfin (Wild and Foreman, 1980; Wild et al., 1995) and more recently, for bigeye (Stéquert and Conand, 2004; Farley et al., 2006). Thus, in order to estimate the reading accuracy of the different teams, a specific linear regression model between the number of otolith increments from the OTC mark to the edge (Im) and the time-at-liberty (T_L) was adjusted for each team. These models were fitted from a subsample of OTC-tagged fishes whose the date of recapture was known accurately (Table 2.3). The same Bayesian procedure as described in the section A. was used to estimate the rate of increment deposition (R) and the error at the otolith edge (ψ_e). The same distributions of R and ψ_e were considered for both species (Table 2.2, Eqns.2.18 and 2.20)

2.2.3 Effect of the readers team on the growth estimate

To assess the influence of the different reading methods on growth estimates, a growth curve was estimated for each readers team by coupling the ageing error model with the somatic VB log-K growth model (section 2.1.4).
The ages-at-recapture (Ar) were estimated form the total number of increments (Ir) using the ageing error model (section A., paragraph C.). The ages-at-tagging (At) were then deduced from Ar and the times-at-liberty. The VB log-K growth model was then fitted to these age estimates using Bayesian inference.
The technical details on the modeling process, the elicitation of prior distributions and the posterior estimations are described in sections A. and 2.1.4. With the exception of the parameters L_∞ and k_1, the same priors were used for yellowfin and bigeye (Tables 2.2 and 2.4)

Table 2.4 – Prior distributions on growth parameters used for bigeye

Parameter	Unit	Prior distribution
Asymptotic length	cm	$L_\infty \sim GEV(187.622, 9.189, -0.3313)$
Juvenile growth rate coefficient	year^{-1}	$k_1 \sim \Gamma(4, 0.058)$

3 Results

3.1 Ageing error model

3.1.1 Simulation evaluation

The fit of the ageing model to the simulated data showed good agreement between the estimated and simulated age, as well as a strong ability to estimate the increment deposition rate R. From the simulations conducted in the first model step, the marginal posterior distributions of R, derived from MCMC outputs, followed symetric distributions around a mean value of 0.95 to 0.96 according to simulation. In cases where a fixed value of R was simulated, this value was well within the 95% credibility interval of the posterior distributions (Figure 2.5, a1, b1 and c1). For the simulations performed from a variable values for R, the model predicted posterior marginal distributions with a mean and variance very close to the simulated distributions (Figure 2.5, a2, b2 and c2). As against, the model showed difficulties in estimating the edge bias ψ_e by systematically underestimating its variability.

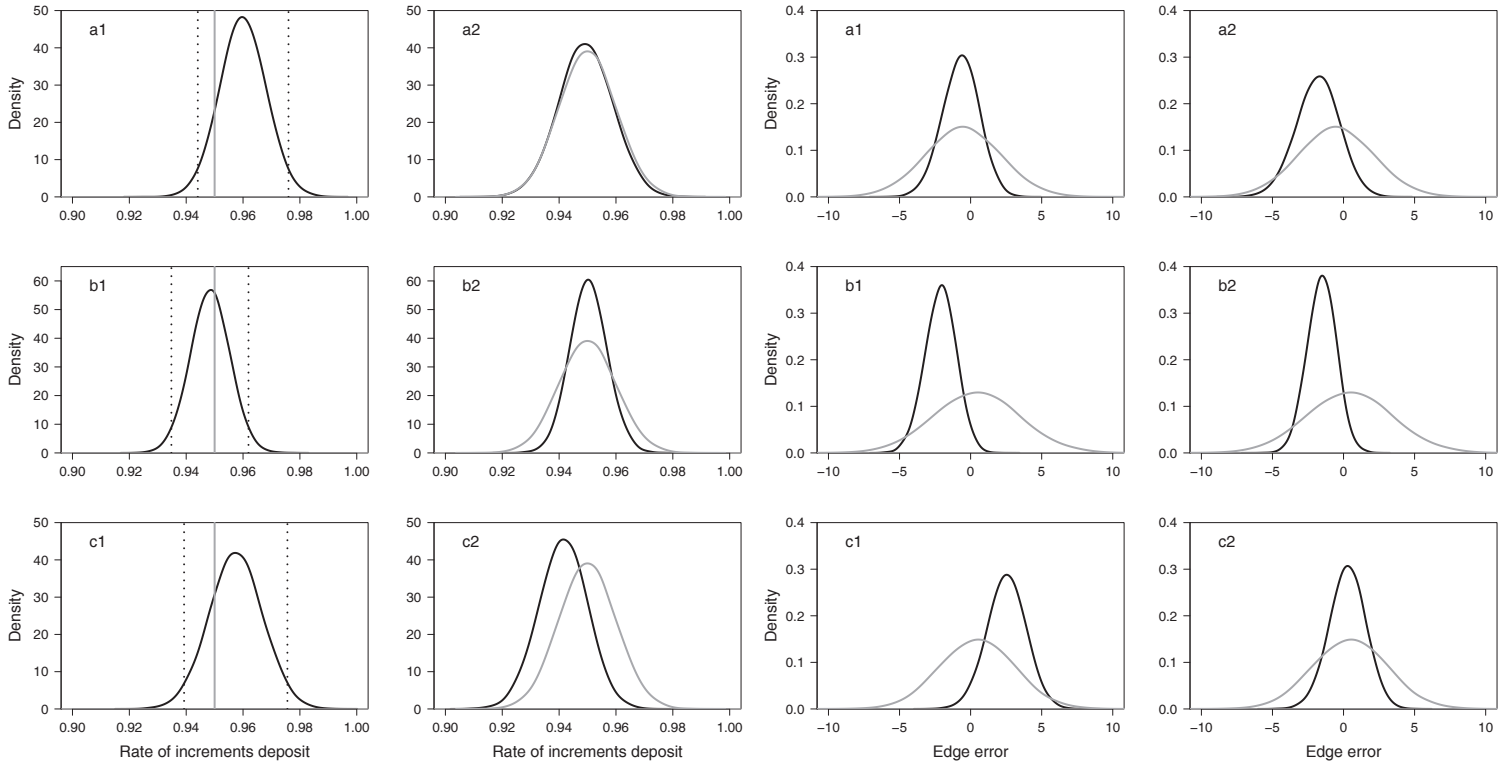

FIGURE 2.5 – Marginal posterior distributions as estimated from the ageing error model parameters (black) compared with the simulated values (grey). Two alternatives were considered, (1) without and (2) with individual variability in increment formation ; a, b and c represents the first, second and third simulated data set respectively.

Simulations that focued on the number of readings showed that the ageing error model provided accurate age estimates, with accuracy increasing with the number of readings (Figure 2.6). The RMSE values were significantly lower when the number of readings for a same otolith increased (Wilcoxon : p-value < 0.05). From five to three readings, the loss of accuracy was generally low, i.e. an average loss of 1%. However, the loss of accuracy became more important between three to two readings, suggesting that three readings was a good compromise between accuracy of estimates and reading cost.

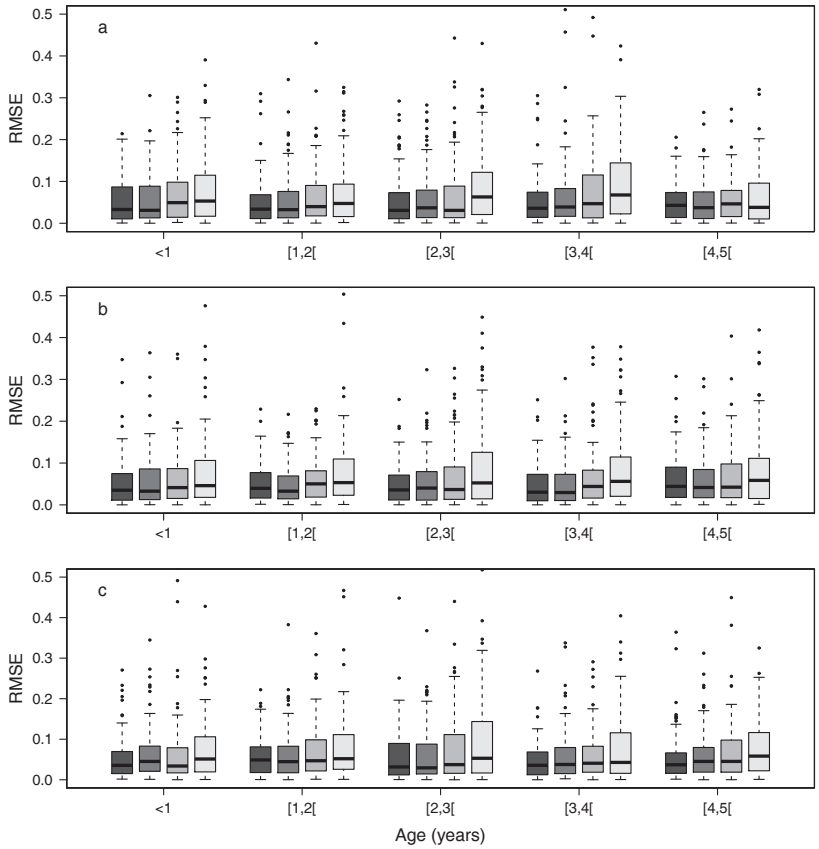

FIGURE 2.6 – Boxplot of the RMSE values obtained with the ageing error model for 5 (■), 4 (■), 3 (■) or 2 (■) readings of the same otolith. a, b and c represents the first, second and third simulated dataset respectively

Regardless of the number of readings, the ageing error model estimated age more accurately than the traditional method. The RMSE values obtained with the ageing error model were significantly lower than those obtained with the traditional method (Wilcoxon : p-value < 0.01 ; Figure 2.7). The ageing error model and the intermediate ageing method provided age estimates as accurate. The RMSE values obtained with the ageing error model and the intermediate method did not differ significantly, with the exception of second simulation dataset where the RMSE values were significantly lower with the ageing error model (Wilcoxon : p-value < 0.01).

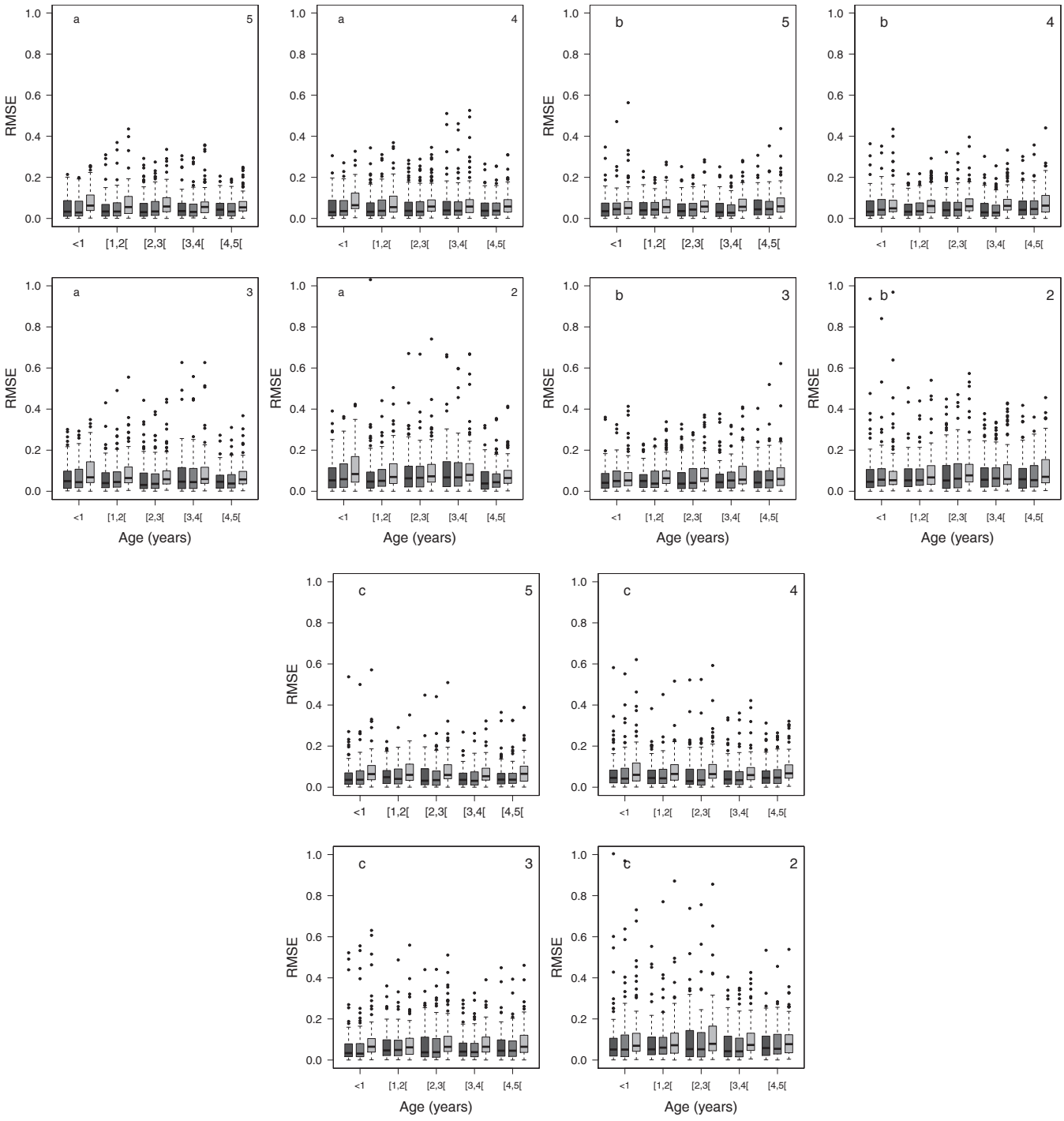

FIGURE 2.7 – Boxplot of RMSE values obtained with the ageing error model (■), the traditional method (■) and the intermediate method (■) for different number of otolith readings. a, b and c represents the first, second and third simulated data set respectively

3.1.2 Testing the hypothesis of daily increment deposition

The ratio R and the mean edge bias ψ_e were precisely estimated in the regression model. R was normally distributed around 0.94 with little variability (Table 2.5). The value of one was not included in the Bayesian 95% credibility interval which resulted in a significant failure of the hypothesis of daily increment deposition. The reader tended to underestimate the fish ages. The edge bias was close to zero, with a lower variability than expected from the prior distribution, resulting in error values ranging from 1.6% for a six month-old fish to 0.16% for a five year-old fish (Table 2.5).

3.1.3 Yellowfin tuna growth

The fit of the coupled growth model revealed strong correlations among some parameters. A positive correlation was found between k_1 and k_2 (0.8) and a negative correlation was found between these growth rate coefficients and the asymptotic length (-0.93 and -0.8 with k_1 and k_2 respectively). These correlations resulted in some model instability and difficulty fitting the posterior distributions of the parameters, particularly in the absence of information from the prior distribution. The expected asymptotic length was estimated at 151.8 cm F_L, which was close to the maximum fork length of the data, 146.5 cm F_L, but comparatively low to the mean asymptotic fork length estimated at about 173 cm from the catch of the purse seiners and longliners and to the maximum lengths of 200 cm historically reported for yellowfin in the Indian Ocean. In contrast, the data provided more information for the first part of the growth curve (< 3 years), where the model fit was good. The uncertainty associated with the mean growth curve that was derived from marginal posterior modes increased as the fish aged.

Table 2.5 – Attributes of marginal posterior distributions from VB log-K growth model coupled with ageing error model fit to yellowfin otolith data. Std.dev : Standard deviation

Parameters	Mode	Mean	Std.dev	Posterior quantiles	
				2.5%	97.5%
R (days)	0.939	0.94	0.029	0.8834	0.9983
ψ_e	-0.54	-0.549	2.469	-5.404	4.263
L_∞ (cm)	146.243	151.809	15.963	126.6	188.4
k_1	0.246	0.249	0.04	0.1745	0.3283
k_2	0.664	0.878	0.434	0.371	2.114
α (years)	2.61	2.625	0.162	2.353	2.951
β	12.583	11.663	4.807	3.718	19.58
t_0 (years)	-0.43	-0.446	0.088	-0.642	-0.3022
σ_ε (cm)	8.809	8.876	0.557	7.864	10.05

The model supported a two-stanza growth for the Indian Ocean yellowfin with two distinct phases over the fish lifespan of the fish (Figure 2.8). The first stanza was characterized by relatively slow growth, which decreased gradually to a minimum of 1.75 cm.month^{-1} for fish up to 1.85 years of age (63 cm F_L). In the second stanza, growth accelerated up to a maximum of 3.54 cm.month^{-1} for fish up to 2.38 years of age (79 cm F_L) and then progressively decreased with size, becoming very slow when the size approached the asymptotic length.

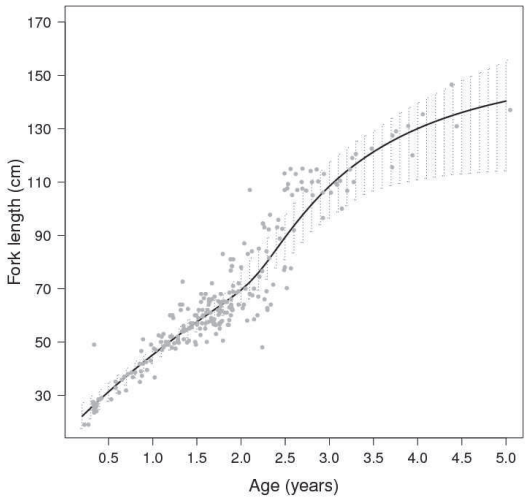

FIGURE 2.8 – Yellowfin growth curbe as estimated from the VB log-K model coupled with the ageing error model. The solid line correspond to the mean growth curve the dashed lines to the uncertainty around the mean curve and the points to observation data

3.1.4 Sensitivity of growth parameters to biased age estimates

Except for k_2, the MRE values derived from the simulations indicated that estimates were more accurate for the growth model coupled with the ageing error model than for the growth model in which the age estimates derived from the classical ageing method (Tables 2.6 and 2.7). For both models, k_2 was estimated with a negative bias of an average value of 19% and 10% for the coupled and classical models respectively. t_0 was estimated with a positive bias for the classical model. For the other parameters, the mean biases were less than 10%. The MSE values were high for the asymptotic length L_∞ resulted in a significant discrepancies between the simulated and estimated values. The values of MRE indicated an overestimation of the asymptotic lengths. For the other parameters, the MSE values were low (Tables 2.6 and 2.7). The MSE values for the estimates of k_1, k_2 and t_0 were higher for the coupled model than for the classical model indicating a greater variability in the estimates of the coupled model. These results suggested that the coupled model provided more accurate, but less precise, estimates than the classical model because it accounted for uncertainties associated with age estimates while the ages were fixed in the classical model.

The growth curve obtained from the coupled model fit coincided with the simulated data in the first stanza but tended to underestimate the growth between 3.5 and 6.5 years. The growth curve of the classical model consistently overestimated the simulated growth (Figure 2.9). Such deviations in growth patterns led to a significant divergence in the age-length key that was derived from both models. This divergence resulted in potentially major differences when converting catch-at-size into catch-at-age. As illustrated by the 2010 yellowfin catch data, the proportions-at-age by 10 cm class lengths were significantly different according to the age-length key, particularly for lengths of less than 100 cm (Figure 2.9).

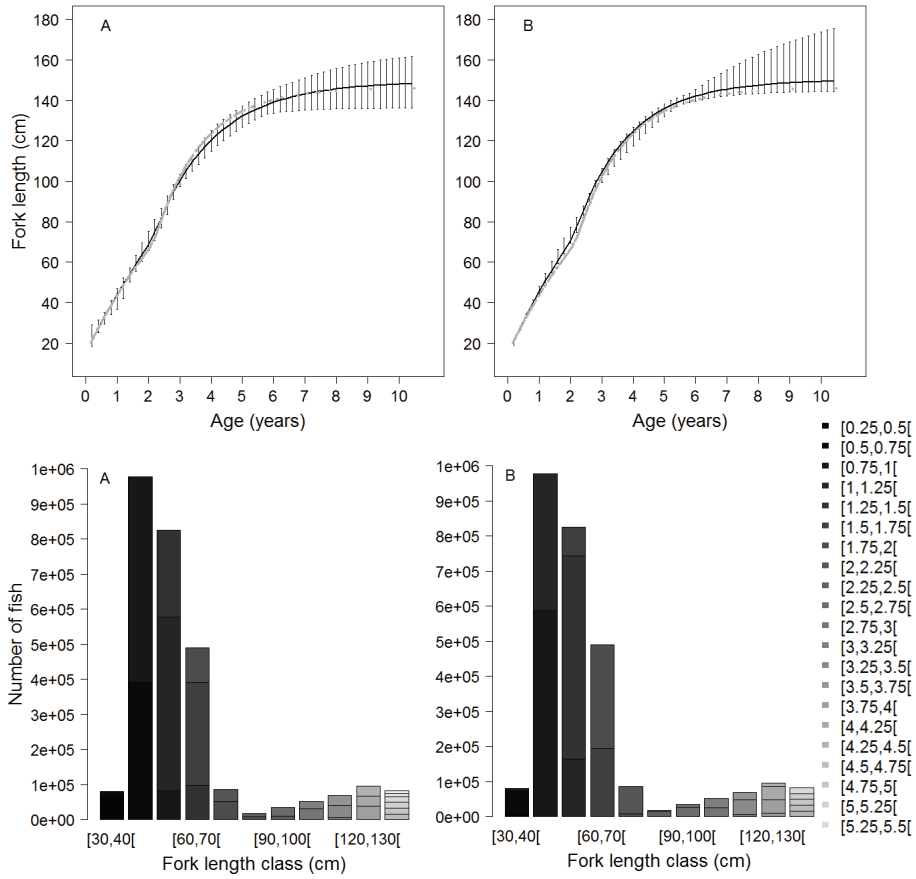

FIGURE 2.9 – Growth curves obtained from the fit to simulated data (•) with the coupled growth model (A) and the classical growth model (B, up) and their use to convert the size frequencies from fishing catches into age frequencies (down). The gray levels correspond to the age classes (quarter), the black solid lines correspond to modal curves and the thin lines correspond to the 95% Bayesian credibility interval.

TABLE 2.6 – Features of coupled growth model fit to simulated data. Std.dev : Standard deviation

Parameters	Mode	Mean	Std.dev	Posterior quantiles 2.5%	Posterior quantiles 97.5%	MSE	MRE
L_∞ (cm)	148.288	149.433	4.940	141.3	160.9	35.517	0.022
k_1	0.252	0.247	0.029	0.2042	0.2831	0.0008	0.005
k_2	0.535	0.539	0.084	0.3815	0.7136	0.023	-0.190
α (years)	2.482	2.481	0.153	2.161	2.774	0.040	-0.051
t_0 (years)	-0.398	-0.438	0.223	-0.5863	-0.3146	0.0461	0.015

TABLE 2.7 – Features of classical growth model fit to simulated data. Std.dev : Standard deviation

Parameters	Mode	Mean	Std.dev	Posterior quantiles 2.5%	Posterior quantiles 97.5%	MSE	MRE
L_∞ (cm)	149.15	150.465	6.952	146	185.3	64.900	0.029
k_1	0.264	0.262	0.009	0.2374	0.2777	0.0003	0.065
k_2	0.604	0.596	0.072	0.2463	0.6827	0.009	-0.101
α (years)	2.438	2.538	0.579	2.338	5.228	0.308	-0.029
t_0 (years)	-0.376	-0.374	0.028	-0.4183	-0.2746	0.004	-0.127

3.2 Influence of readers teams

3.2.1 Respect of daily increment deposition

For both tuna species, the relationship between the increment counts after the OTC mark (Im) and the time-at-liberty (T_L) depended on the readers team considered (Figure 2.10). For yellowfin, the increment deposit was underestimated for the team 1 with a mean value of 0.852, while it was overestimated for the team 2 with a mean value of 1.025. For team 1, the value of 1 was not included in the 95% Bayesian credibility interval which resulted in a significant failure of the hypothesis of daily increment deposition (Table 2.8). For bigeye, the increment deposit was understimated by the two teams with mean values of 0.98 and 0.955 for the team 2 and 3 respectively. According to the 95% Bayesian credibility interval, the periodicity of the deposit was significantly different from one day for the team 3 but not for the team 2 (Table 2.9).

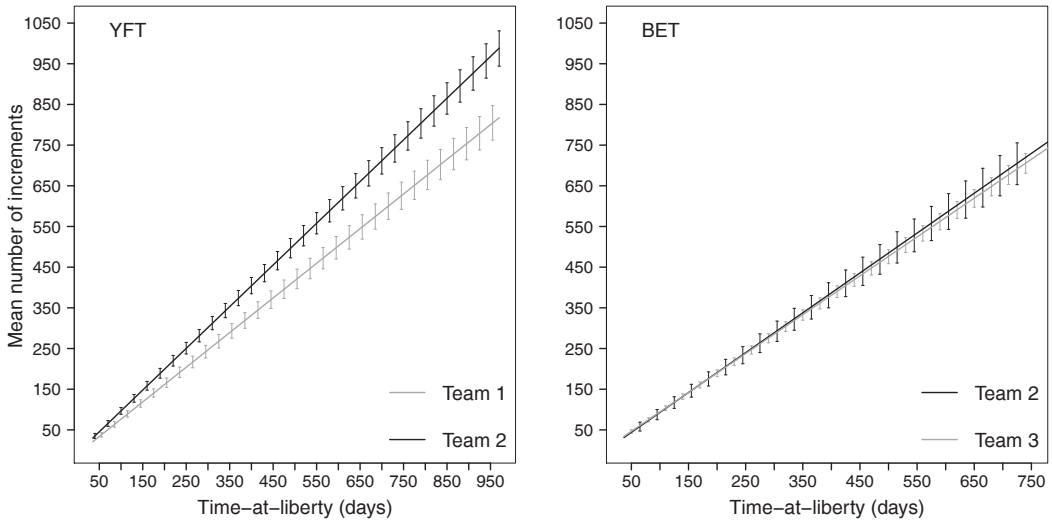

FIGURE 2.10 – Relationship between the number of increments counts after the OTC mark and the time-at-liberty as estimated by the ageing error model for the different readers teams for yellowfin (YFT) and bigeye (BET). The solid lines represent the mean linear regressions and the thin vertical lines represent the 95% Bayesian credibility intervals.

3.2.2 Influence of reading method on growth estimate

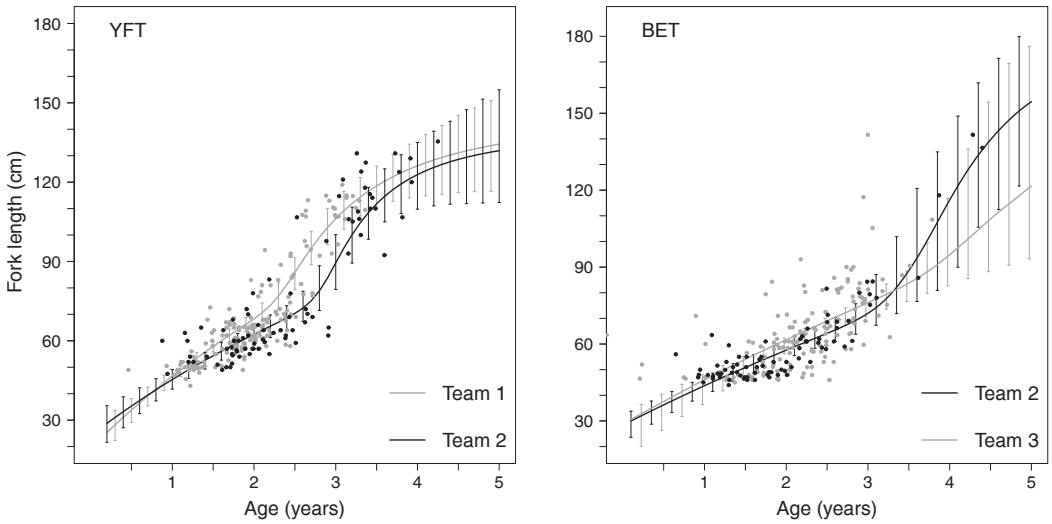

FIGURE 2.11 – Growth curves as estimated by the coupled ageing-growth model for each readers teams for yellowfin (YFT) and bigeye (BET). The solid lines represent the mean curves and the thin vertical lines represent the 95% Bayesian credibility intervals.

The divergences in age estimates between the readers teams had sgnificant repercussions on the estimates of growth parameters (Figure 2.11). Thus, for yellowfin, the team 2 tended to overestimate fish ages comparatively to the team 1 and led to a much slower growth than this estimated by the team 1 (Table 2.8). For bigeye, age estimates close for the two teams led to similar growth curve up to 80 cm F_L, then the growth estimated by the team 2 was faster than this of team 3. However, there were very few data in this part of curve (Table 2.9).

TABLE 2.8 – Attributes of marginal posterior distributions for yellowfin models
Std.dev : Standard deviation, icr. :increments

Parameters	Team 1				Team 2			
	Mean	Std. dev.	Posterior quantiles 2.5%	97.5%	Mean	Std. dev.	Posterior quantiles 2.5%	97.5%
R (day)	0.852	0.023	0.808	0.895	1.025	0.021	0.983	1.066
ψ_e (icr.)	-8.985	1.953	-12.831	-5.211	-5.908	2.375	-11.015	-0.807
p	0.178	0.007	0.165	0.194	0.128	0.006	0.116	0.14
L_∞ (cm)	170.931	17.811	136.495	199.515	153.763	10.54	136.692	175.422
α (year)	5.142	2.459	2.183	11.128	4.357	0.193	3.98	4.701
β (year^{-1})	15.062	8.774	1.247	29.651	17.582	6.646	5.869	28.64
k_1 (year^{-1})	0.202	0.051	0.118	0.307	0.146	0.016	0.115	0.176
k_2 (year^{-1})	1.265	0.901	0.229	3.085	0.894	0.341	0.43	1.638
t_0 (year)	-0.64	0.453	-1.769	-0.05	-1.898	0.109	-1.998	-1.624

TABLE 2.9 – Attributes of marginal posterior distributions for bigeye models
Std.dev : Standard deviation, icr. :increments

Parameters	Team 2				Team 3			
	Mean	Std. dev.	Posterior quantiles 2.5%	97.5%	Mean	Std. dev.	Posterior quantiles 2.5%	97.5%
R (day)	0.98	0.034	0.915	1.043	0.955	0.015	0.925	0.986
ψ_e (icr.)	-5.105	3.466	-12.584	1.375	-1.264	1.582	-4.314	1.742
p	0.144	0.01	0.126	0.166	0.089	0.005	0.08	0.101
L_∞ (cm)	182.192	13.982	149.673	208.615	188.031	11.539	166.992	207.93
α (year)	5.059	0.476	4.155	5.963	6.537	2.191	2.518	11.121
β (year^{-1})	14.401	8.054	2.893	28.541	15.255	8.406	1.726	29.162
k_1 (year^{-1})	0.106	0.017	0.083	0.139	0.115	0.017	0.088	0.158
k_2 (year^{-1})	1.153	0.714	0.335	2.841	1.308	0.88	0.127	2.991
t_0 (year)	-1.637	0.295	-1.992	-1.004	-1.485	0.344	-1.98	-0.651

4 Discussion

Otoliths have been widely used to study fish species that consistently deposit growth increments over time (Mugiya and Tanaka, 1992; Stéquert et al., 1996; Norbis et al., 1999; Buratti and Santos, 2010). However, estimating fish age by counting of otolith increments can result in large biases and uncertainties due to the combination of processing and interpretation errors (Neilson, 1992). Both error types can affect the estimates of age with potential consequences on growth or other demographic rates required for population dynamics models, such as mortality. However, to our knowledge, only a few studies have previously attempted to quantify errors in age estimates.

In this study, we have developed an ageing error model that explicitly accounts for these potential biases and uncertainties, thus improving age estimation. Coupling this ageing model with a growth model allowed propagating the uncertainty that arises from otolith reading into the estimation of fish growth. We applied our model to Indian Ocean yellowfin tuna, drawing on a dataset of repeated otolith readings that were collected during a large mark-recapture experiment. To illustrate the interest of our method and assess the potential consequences of uncertainties in the input data used in fish stock assessment models, we completed a series of simulations. Through Bayesian analysis, the uncertainty associated with age estimates derived from hard structures can be combined with supplementary information, e.g., observations of the maximum size, or growth estimates in other areas, and expert knowledge to estimate growth.

4.1 Age estimation method

The traditional ageing method, which converts an average count of increments into age, depends on the assumption that each increment corresponds to one day (Wild, 1986). Otherwise, the use of this method will lead to systematically biased age estimates. In the case of the European hake (*Merlucccius merluccius*), although internationally accepted, it has recently been demonstrated that the assumption of a daily deposition rate is not met. As such, the use of the traditional ageing method for this species has resulted in a significant overestimation of fish age with important implications for estimates of key biological parameters (De Pontual et al., 2006). This example highlights that validation of the increment deposition rate for the entire age range of interest should be major prerequisite for any ageing study.

Various age validation techniques exist including the release of tagged fish of a known age, nuclear or radiochemical dating, modal progression of catch-at-size data over time, and captive rearing (Campana, 2001). For yellowfin, the assumption of daily deposition was tested through a mark-recapture experiment of wild fish with oxytetracycline (OTC) in the length interval from 49.7-131 cm F_L. The result of this experiment suggested that the deposition rate estimated by the reader within this length interval is significantly different than the assumed single increment per day, with an increment-over-day ratio of 1 :0.939. The marginal posterior distribution revealed little variation in this ratio, suggesting that the reading method tended

to systematically underestimate the actual fish ages. However, additional readings performed by new readers for some of the otolith data used in the present study however indicate a 1 :1.025.

Assessing the precision of the ageing technique is necessary (Campana, 2001). The main uncertainty in age estimates arises from discrepancies between repeated readings. For some otoliths, the interpretations of the first and marginal growth increments can generate further uncertainty, particularly as these rings may obliterate during a poor otolith preparation. These additional uncertainties were reflected in the model through the choice of stochastic error structures and informative prior distributions based on the expertise to compensate for the lack of information in the data. In this context, Bayesian analysis appears particularly adapted to include such information into the statistical inference procedure.
The model evaluation by simulation suggested that it was capable of estimating both the ageing biases and an accurate age regardless of the age of the fish. The mean and variance of the deposit bias were consistently well-estimated. The model performed less well in estimating the bias linked to the misinterpretation of the marginal rings. However, edge level errors are partly estimated by the overall reading error.
For yellowfin, expert judgement suggests that the nucleus and edge biases could be very low, i.e. less than five increments, resulting in error ranging from 4% for a six month-old fish to 0.4% for a five year-old fish. As such, these biases would become negligible when the age in days values are converted to age in year values. Thus, the intermediate method in which the average number of increments is corrected for the actual deposit frequency provided age estimates as accurately as the ageing error model. However, the range of uncertainty is fully ignored which may have serious implications on the final outcome of the analysis (Punt and Hilborn, 1997).

4.2 Growth of Indian Ocean yellowfin

The method developed in this study appears suitable for modeling the growth of Indian Ocean yellowfin. The fit of the growth model appeared to be adequate in the first stanza. In this first phase, the expected first growth rate, 2.11 cm.month^{-1} for fish from 22 to 63 cm F_L, and length from which growth accelerates, 63 cm F_L, were consistent with several growth studies for the same population. Growth rates of small yellowfin have been estimated to be between 1.3 and 2.9 cm.month^{-1} (Marsac and Lablache, 1985; Anderson, 1988; Marsac, 1991; Firoozi and Carrara, 1992; Lumineau, 2002) with growth acceleration occurring around 62 to 66 cm F_L (Marsac, 1991), 70 cm F_L (Firoozi and Carrara, 1992), 56 to 66 cm F_L (Lumineau, 2002) and from 60 cm F_L (Viera, 2005). The low growth rate for pre-adult yellowfin and the apparent acceleration of growth was also observed for yellowfin in the other oceans. The growth acceleration was observed between 63-66 cm in Atlantic (Bard, 1984; Gaertner and Pagavino, 1992; Gascuel et al., 1992) and around 70 cm in Pacific (Lehodey and Leroy, 1999; Hampton and Fournier, 2001). However, in the absence of older fish, the model seemed to underestimate the expected asymptotic

length leading to an apparent underestimation of yellowfin growth over 2.7 years of age (95.72 cm F_L).

Increasing the uncertainty in the second stanza reflected greater individual variability in growth. A primary source of variability in growth rates may arise from sexual dimorphism, characterized by faster growth and a larger asymptotic length for males than females (Yamanaka, 1990; Gascuel et al., 1992). According to Wild (Wild, 1986), in the eastern Pacific, yellowfin females grow faster than males until 94.9 cm F_L, i.e. at about 2 years old, and then the trend reverses. Several authors have also shown that in Indian Ocean yellowfin, males are largely dominant above 145 cm F_L (Nootmorn et al., 2005; Zhu et al., 2008) which is close to the modal value of the asymptotic length estimated in this study at 146.5 cm F_L.

4.3 Sensitivity of growth estimates to ageing method

Estimating the growth parameters with the growth model coupled with the ageing error model was more accurate, but less precise, than with the growth model which used the traditional ageing method. This latter underestimated the actual age of fish and resulted in a consistent overestimation in the growth curve. In contrast, taking into account uncertainties associated with age estimates led to a growth curve that fitted very closely to the simulated data in the first stanza. Such differences greatly influenced the age distributions of the fisheries catches.
In addition, by disregarding the ageing errors, the classical model was overconfident in determining uncertainties of growth estimates. It is critical to represent the full range of uncertainty to adequately evaluate management alternatives and the expected consequences of decision-making (Ludwig et al., 1993; Hilborn and Mangel, 1997), especially with little accurate estimates. Developed within a hierarchical Bayesian framework, our method appears particularly suited to quantifying the uncertainties resulting from otolith reading or observational errors and their propagating in the estimates of biological parameters.

However, there are some technical difficulties associated with the use of Bayesian inferences. One of the main criticisms is the need to specify prior distributions, which can have some influence on the parameter posterior distributions (Meyer and Millar, 1999; Clark, 2005). In addition, when some parameters are highly correlated, the prior for each parameter can affect the estimates of all other correlated parameters. Commonly, sensitivity analyses are performed to evaluate the effect of prior change on the posterior. As increasing data quality and quantity reduces the prior influence. Therefore, these sensitivity analyses are above all an assessment tool for appreciate the amount of information in the data (Cressie et al., 2009). In this study, extensive work was undertaken on prior specification and weakly informative distributions were assigned to the parameters for which there was no established scientific understanding. This was done to obtain estimates that were more consistent with the biology of yellowfin.

4.4 Reading method effect

Validating the accuracy of different reading methods or various readers teams is fundamental when converting the counted increments into age. For both tuna species, the estimates of increment deposition rate, and therefore the reading accuracy, varied according to the considered readers team. These differences have led to contradictory outcomes. Regarding yellowfin, Team 1 led to the conclusion of an over-daily deposit while the daily deposit was verified with Team 2, although this latter team has tended to overestimate the number of increments deposited. This highlights the need for inter-comparison exercises between research institutes, using reference otolith collections, so as to harmonise reading methods (Eltink et al., 2000).

Despite the use of an ageing method which explicitly takes into account the bias in the daily increments deposit, the age estimates for yellowfin and bigeye differed according to reader team. The differences in age have subsequently led to significant differences in growth curves. Thus, for yellowfin from 50 to 110 cm F_L, the ranges of uncertainty of the growth curves obtained with the two teams did not overlap. The underestimation of the fish ages by Team 1 led to estimate growth rates significantly higher than those obtained by Team 2. For bigeye, the growth curves estimated for both teams were very close with an apparent discrepancy for fish above 80 cm F_L, in relation with the lack of data available for larger tunas. Such divergence in growth estimates will invariably lead to differences in the determination of the age composition of commercial fisheries with serious repercussion on scientific advice on stock status.

As tuna otoliths are structurally complex, a high degree of interpretation is required is when reading them. In such cases, the accurate of age estimates is strongly dependent on the proficiency of the reader (Punt et al., 2008). Thus, when a calcified structure is read by various readers, the precision of each reader and the variability between readers within a team should be examined. As tuna otoliths are structurally complex, a high degree of interpretation is required is required when reading them. In such cases, the accurate of age estimates is strongly dependent on the proficiency of the reader (Punt et al., 2008). Thus, when a calcified structure is read by various readers, the precision of each reader and the variability between readers of a same team should be examined. This was not done in this study because it has not always been possible to determine the identity of each readers within a team.

The general approach developed in this study for ageing fish can be applied to other species and can be adapted to any structure that produces periodic growth increments in response to various ecological issues. The ageing error model has proven effective in improving age estimation, in particular with the correction for a failure to daily deposit by the reader, and in propagating the uncertainty that arises from otolith reading into growth estimation processes. Nevertheless, in the absence of additional informations, random reading errors can not be corrected and the resulting estimates of biological parameters can be strongly biased. In view of this, the use of integrated modeling approaches that combine ageing data from several methods as well as other data sources on growth seems to be preferable (Dortel et al. *in submission* ; Eveson et al. *in press*).

Chapter 3

An integrated Bayesian growth model

1 Introduction

The knowledge of growth variability between individuals is essential to understanding the biology of fish populations, their productivity, and their response to environmental changes and fishing pressure. Indeed, growth rates are an integral part of stock assessments, a process which aims to supply scientific advice on the health of a fishery (Cotter et al., 2004). Consequently, biased growth estimates can affect our understanding of a stock's status and lead to poor fisheries management decisions (Punt and Hilborn, 1997; Fournier et al., 1998).

There are three principal data sources available for studying wild fish growth rates : (i) direct ageing of a fish of a known size from periodic deposits in hard tissues, (ii) modal progression in length-frequency distributions obtained from commercial fisheries catches or scientific monitoring, and (iii) the increase in fish length over time-at-liberty from mark-recapture experiments.
Direct ageing data have been widely used to study growth in fish species that consistently deposit growth increments in calcified tissues, such as otoliths (Campana, 2001; Panfili et al., 2002). For example, counting the microstructural features deposited daily in otoliths has been shown to be a useful ageing technique for many species of tropical fishes (Pannella, 1971; Williams et al., 2013). However, the preparation and analysis of otoliths is time consuming, requires considerable care, and can involve some biases and uncertainties (e.g., miscounting increments can lead to errors in age estimations ; Sardenne et al. *in press*).
Although considered less accurate than direct ageing methods, the analysis of length-frequency data obtained from fisheries catches can provide indirect age estimates for species that exhibit well defined spawning periods (Pauly and Morgan, 1987). In this method, modes (assumed to represent fish cohorts) are identified in the length-frequency distributions of catches and their length progression is tracked over time.
Finally, mark-recapture data have been widely used since the first tagging experiments were conducted in the early 1950s on tropical tunas in the Pacific Ocean (Anonymous, 1955). With this method, the change in fish length during the time between release and recovery provides valuable information on how each individual grows over time (Amstrup et al., 2005). However, tagging data do not provide information on the age of a fish and complementary data or expert knowledge are required to anchor the growth curve.
It can be difficult to obtain an overall growth pattern from a single data source, and using all three data sources provides complementary information on the different growth phases experienced over the lifespan of a fish. Although considerable research effort is invested in determining age and growth patterns of fish, to our knowledge, with the notable exception of Eveson et al. (2004), only a few studies have previously attempted to combine the three different data sources into an integrated growth model. Assimilating different growth data sets within a statistical framework is challenging because to do so effectively, we must address : (i) the multiple observation errors in the data, (ii) potential contradictions between data sets, and

(iii) the variability in growth among individuals, which is typically modeled by a process error term. The hierarchical Bayesian approach appears particularly well suited for modeling growth because it can integrate several different data sources and allows for stochasticity at multiple levels (Clark, 2005). Bayesian models can draw inferences from large numbers of parameters and latent variables that describe complex relationships. In addition, the Bayesian framework allows for the inclusion of expert judgment and supplementary information.

Yellowfin tuna (*Thunnus albacares*, Bonnaterre 1788) is an epipelagic species that is widely distributed in the tropical and subtropical waters of the world's major oceans (Fonteneau, 2010). In the Indian Ocean (IO), yellowfin has been commercially exploited since the early 1950s and over the last decade, annual catches have exceeded 350,000 t (Herrera and Pierre, 2010). There is considerable diversity in the fleets that target this species ; whilst industrial purse seiners and longliners dominate, small-scale fishing fleets were responsible for more than 35% of total catch estimates in the last decade (Herrera and Pierre, 2010). The management of the IO yellowfin is under the jurisdiction of the Indian Ocean Tuna Commission (IOTC). Currently, their management approach relies on temporal trends in fish abundance and fishing mortality-at-age data derived from a spatially-explicit population model (Langley et al., 2012). The most recent stock assessment from 2011 determined that current fishing pressure on the yellowfin stock was at a safe level (IOTC, 2012). Nevertheless, there are uncertainties associated with the current approach to the IO yellowfin stock assessment, in particular with regards to the growth curve that is used (IOTC, 2012).

Using data collected through the Indian Ocean Tuna Tagging Program of the Indian Ocean (RTTP-IO), this study describes a hierarchical growth model for IO yellowfin that combines ageing data derived from otolith readings, length-frequency data sampled from the European purse seine fishery over the last decade, and mark-recapture data. The influence of each data source on growth estimates was assessed by gradually increasing the model's complexity. Developed in a hierarchical Bayesian framework, our model explicitly accounts for the uncertainties associated with age estimates and length measurements. In addition, the model reflects expert opinion on two key areas : otolith reading and historical length and growth observations for yellowfin. In this study, we provide a flexible statistical framework that accounts for uncertainty in growth modeling and addresses a current concern of the IOTC.

2 Materials and methods

2.1 Mark-recapture data

Mark-recapture data were collected in the Western Indian Ocean during the Regional Tuna Tagging Program (RTTP-IO, section 1). In the growth model, we only used data from fish for which an accurate recovery date was known and having a length at recapture greater than or equal to 120 cm F_L. In total, 373 fish were considered, measuring between 44-113 cm F_L at tagging and 120-159 cm F_L at recapture (Figure 3.1). Time-at-liberty values for this group ranged between eight month and five years at sea.

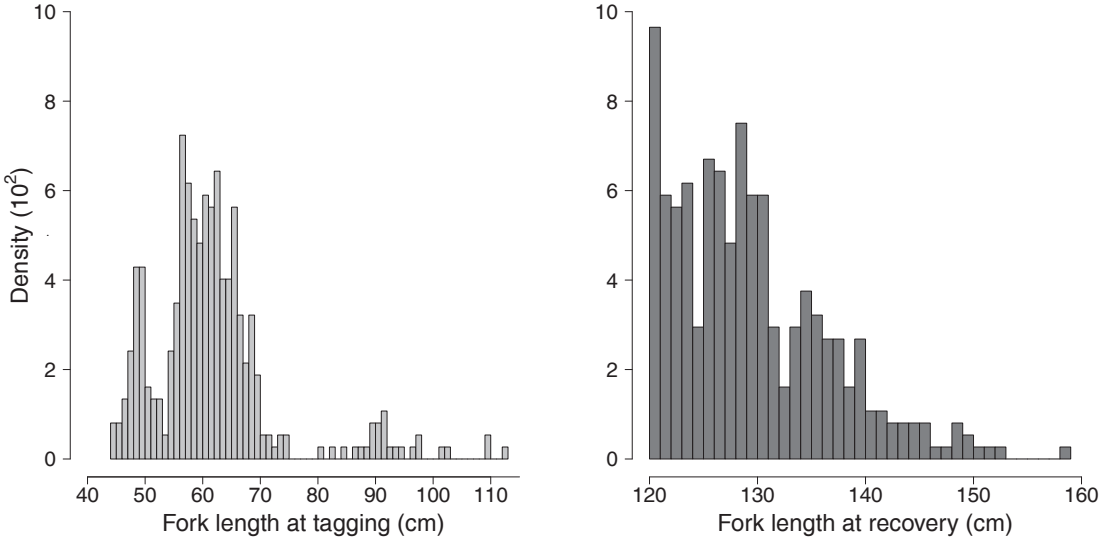

FIGURE 3.1 – Distributions of sizes-at-tagging and sizes-at-recovery

2.2 Ageing data from otolith readings

A total of 174 saggital otoliths were prepared and analyzed for ageing purposes, comprised of (i) 128 fish, of which 124 were OTC-tagged, collected through the RTTP-IO program measuring between 43-72 cm F_L at tagging and 47.9-135.4 cm F_L at recapture, (ii) 28 fish collected from 2008-2009 from the Indian Ocean Tuna Ltd (IOT) cannery measuring between 31-128.7 cm F_L and (iii) 18 fish caught in 2007 through the West Sumatra Tuna Tagging Project (WSTTP) measuring between 19-29 cm F_L (section 2).

Otoliths were prepared for age analysis following the method as described by Secor et al. (1991); Stéquert (1995); Panfili et al. (2002). Transverse sections of saggital otoliths were examined by two teams of readers under a microscope (1000x magnification). Each team counted the daily growth increments along the counting path, definied as the distance between the primordium, original point of growth, to the last increment deposited (Morize et al., 2008, Sardenne et al. *in press*). For

the OTC-tagged fish, the number of increments was counted for different otolith sections : (i) between the nucleus, i.e. the otolith core, and OTC mark (It), (ii) between the OTC mark and otolith edge (Im) and (iii) between the nucleus and otolith edge (Ir). In the remaining fish, otoliths were read in full, i.e., between the nucleus and otolith edge, (I_r). Each otolith was read between 2-5 times, giving a total of 521 otolith readings. Readers did not have prior knowledge of the size or time-at-liberty of the sampled individuals,thus ensuring that independence was maintained between the multiple readings (Morize et al., 2008, Sardenne et al. *in press*).

Otolith ageing techniques of fish are associated with counting errors and subjective interpretations by the reader. Both factors can lead to imprecision and bias in the age estimates generated (Neilson, 1992; Panfili et al., 2009). A hierarchical Bayesian model that accounted for process and interpretation errors was applied to estimate the age of each fish (Table 3.1). Initially,, the number of increments counted from the OTC mark to the otolith edge (Im) was related to the time-at-liberty (T_L) to estimate the deposition rate accounting for the reading method and reader skills. This relationship was estimated for each readers team r following :

$$Im_{ri} = R_r * T_{Li} + \psi_{e_r} \tag{3.1}$$

The subscript i corresponds to fish. ψ_{e_r} represents an additional error related to the counting increment of the otolith edge by the readers team r. Indeed, some of these increments may disappear during otolith preparation for ageing. Im_{ri} was assessed from the multiple readings k for the same fish i by the readers team r according the following relationship :

$$Im^*_{rik} \sim \mathcal{N}(Im_{ri}, (p_r.Im_{ri})^2) \tag{3.2}$$

p_r corresponds to the relative percentage of misread otolith increments for readers team r.
The reader-specific deposition rate was then subsequently used to estimate fish age using the multiple readings made for each otolith. Age estimates were preferentially derived from the number of increments at tagging It according to the same procedure as previously described. Thus, the fish age at tagging At_{ri}, expressed in days, was assessed as follows :

$$\begin{aligned} It_{ri} &= R_r * At_{ri} + \psi_n \\ It^*_{rik} &\sim \mathcal{N}(It_{ri}, (p_r.It_{ri})^2) \end{aligned} \tag{3.3}$$

ψ_n is an additional error related to counting increments near the nucleus, which may disappear further to an excessive sanding of the otolith during its preparation for ageing.
When It was unknown and for all fish collected through the WSTTP and the IOT cannery, the fish age at recovery Ar_{ri}, in days, were derived from Ir following :

$$\begin{aligned} Ir_{ri} &= R_r * Ar_{ri} + \psi_n + \psi_e \\ Ir^*_{rik} &\sim \mathcal{N}(Ir_{ri}, (p_r.Ir_{ri})^2) \end{aligned} \tag{3.4}$$

The stochastic processes associated with the preparation of the otoliths and their resulting reading errors, ψ_e and ψ_n, were modeled by choosing an error structure

and eliciting informative prior density functions that were based on expert judgment (Table 3.1). The technical details of the ageing model and the elicitation of prior distributions are described in chapter 2, section A. (Dortel et al., 2013).

Table 3.1 – Parameters and variables used in the ageing error model

Parameter	Definition
T_{L_i}	Time-at-liberty between tagging and recapture for fish i (days)
At_{ri}	Age-at-tagging of fish i estimated with readers team r (days)
Ar_{ri}	Age-at-recapture of fish i estimated with readers team r (days)
Im_{rk}	Number of increments between OTC mark and edge estimated for fish i by readers team r
It_{ri}	Number of increments between nucleus and OTC mark for otolith estimated for fish i by readers team r
Ir_{ri}	Total number of increments estimated for fish i by readers team r
I^*_{rik}	Number of increments counted by readers team r for the reading k of fish otolith i
R_r	Deposition periodicity estimated for readers team r
ψ_n	Error in counting increments near the nucleus
ψ_e	Error in counting increments of the otolith edge for readers team r
p_r	Relative percentage of misread otolith increments of readers team r

2.3 Modal progression from length-frequency data

Length-frequency data were collected from commercial catches of European, Seychelles, Iranian and Mayotte purse seiners between December 2000 and March 2010 (Floch et al., 2012). The monthly length-frequency distributions exhibited various modes which assumed to correspond to different cohorts. The length progression of each mode was then monthly tracked to provide both mean age and length estimates of Indian Ocean yellowfin population (Pauly and Morgan, 1987). To optimize the identification of the modes, the length distributions of the various cohorts in a given month were considered as a set of overlapping normal distributions (Hasselblad, 1966; Schnute and Fournier, 1980). A mixture of normal distributions was fitted with the mix function applied in the mixdist package of the statistical software R version 2.12.1 (R Development Core Team, 2010), using an Expectation-Maximization algorithm (Macdonald and Green, 1988). The normalmixEM function of the mixtools package was used to define the initial values for the means and standard deviations of each of the length distributions. The standard deviation was constrained to increase with the mean length. This was done to account for overlaps between two successive length-at-age distributions which are exacerbated by a slower growth and an increased individual variability with increasing age.
The smallest length modes were identified as the recruitment peak of each cohort of the Indian Ocean yellowfin. An age with an uncertainty of 3-4 months was given to these modes, as yellowfin has a seasonal sexual activity characterized by two distinct periods in Indian Ocean, a main spawning season from November to February with a peak in January and a second minor spawning period from June to August (Stéquert et al., 2001; Zhu et al., 2008; Zudaire et al., 2013a).

2.4 Modelling somatic growth using Bayesian inference

2.4.1 Growth model

A hierarchical Bayesian model was implemented to estimate yellowfin growth by gradually adding data from the three different sources. The VB log-K model, currently used for Indian Ocean yellowfin stock assessment (IOTC, 2013), was considered. This model can account for two growth phases through a logistic function that linked the two distinct growth rates coefficient k_1 and k_2 (Laslett et al., 2002; Eveson et al., 2004). The fork length of a fish at an age A, $F_L(A)$, was described as :

$$F_L(A) = L_\infty \left(1 - exp(-k_2(A - t_0)) \left(\frac{1 + exp(-\beta(A - t_0 - \alpha))}{1 + exp(\beta\alpha)}\right)^{\frac{k_1 - k_2}{\beta}}\right) \quad (3.5)$$

L_∞ is the asymptotic length, i.e. the maximum length that a fish can reach, t_0 is the age of zero fork length, α is the inflection point, i.e the age relative to t_0 at which the change in growth rate occurs and β is the parameter that controls the transition rate between k_1 and k_2 (Table 3.2).
The growth model takes into account both length measurement errors (ε) and process errors (ψ). Indeed, the asymptotic length, the growth rate as well as the age at which the change in growth occurs depend on environmental conditions, food availability and the intrinsic characteristics of fish, which likely to vary from one fish to another. In addition, the different datasets included measurements errors and other uncertainties, resulting in individual growth curves that do not conform exactly to the pattern described by Eq.3.5.

2.4.2 Model fit to ageing data

The observed fork length $F^*_{L_{ij}}$ of fish i at capture event j was modeled according Eq.(3.5) as :

$$F^*_{L_{ij}} = L_\infty \left(1 - exp(-k_2(A_{ij} - t_0)) \left(\frac{1 + exp(-\beta(A_{ij} - t_0 - \alpha))}{1 + exp(\beta\alpha)}\right)^{\frac{k_1 - k_2}{\beta}}\right) \times \psi_{ij} + \varepsilon_{ij} \quad (3.6)$$

A_{ij}, the age of fish, was estimated from otolith readings using the ageing error model (Eqns.(3.3) and (3.4)). This model was used to propagate age uncertainty into growth parameter estimates. The process errors, ψ_{ij}, followed a log-normal distribution with mean 0 and a common variance, σ^2_ψ. The length measurement errors, ε_{ij}, were assumed to be independent and normally distributed around 0 with a common variance, σ^2_j.
The length measurement errors at tagging, ε_{i1}, were assessed from RTTP-IO fish released and recaptured several times with time-at-liberty less than or equal to 7 days. These individuals were not included in the subsequent analyses and therefore constitute an independent dataset. The fork length differences between two successive measurements of the same fish, ΔL, were assumed to follow the same distribution as ε_1, i.e. a normal distribution around 0 with a standard deviation σ_1. Thus for each fish i, $\Delta L^*_i \sim \mathcal{N}(0, \sigma^2_1)$.

At recovery, the fork lengths were often measured on frozen fish in brine, which could add an additional error. This error was assumed to be normally distributed around 0 with a standard deviation σ_f. The standard deviation was estimated using fish that were measured frozen and then thawed and re-measured with excellent precision. Let ΔS, the fork length differences between frozen and fresh measurements of the same fish, for each fish i, $\Delta S_i^* \sim \mathcal{N}(0, \sigma_f^2)$. The length measurement errors at recovery ε_{i2} were calculated as the sum of the classical measurement errors and measurement errors associated with freezing.
Consider the vector of growth parameters $\theta_{G1} = \{L_\infty, k_1, k_2, t_0, \alpha, \beta\}$, the vector of ageing parameters θ_A and the standard deviations of measurement and process errors, σ_1 and σ_ψ respectively. For fish caught once, all observation variables are considered independent and as such, the likelihood was written as :

$$\mathcal{L}_1(\theta_{G1}, \theta_A, \sigma_1, \sigma_\psi) = \int f(F^*_{L_{i1}} | A_{i1}, \sigma_1, \theta_{G1}) \times f(A_{i1} | It^*_{ijk}, \theta_A) \times f(\sigma_1 | \Delta L_i^*).dA_{i1} \quad (3.7)$$

For fish from RTTP-IO that were observed twice, the A_{i1} was estimated from At_i (Eq.3.3) and A_{i2} was calculated as the sum of $A_{i1} + T^*_{L_i}$, where $T^*_{L_i}$ is the time-at-liberty recorded for fish i. Otherwise A_{i2} was assessed from Ar_i (Eq.3.4) and A_{i1} was calculated as the difference $A_{i2} - T^*_{L_i}$. The likelihood was then written as :

$$\mathcal{L}_2(\theta_{G1}, \theta_A, \sigma_1, \sigma_f, \sigma_\psi) = \int\int \begin{array}{l} f(F^*_{L_{i1}} | A_{i1}, \sigma_1, \theta_{G1}) \times f(A_{i1} | It^*_{ijk}, \theta_A) \times f(\sigma_1 | \Delta L_i^*) \\ \times f(F^*_{L_{i2}} | A_{i1} + T^*_{L_i}, \sigma_1 + \sigma_f, \theta_A) \times f(\sigma_f | \Delta S_i^*).dA_{i1}.dT^*_{L_i} \end{array} \quad (3.8)$$

Tunas associated with several fishing sets can be linked to a range of potential recapture dates, a factor which results in some uncertainty in time-at-liberty. In this case, T_{L_i} was a variable assumed to follow an uniform distribution on the interval $[T^*_{L_{1i}}, T^*_{L_{2i}}]$. $T^*_{L_{1i}}$ and $T^*_{L_{2i}}$ were the minimal and the maximal time-at-liberty respectively. The likelihood was then written as :

$$\mathcal{L}_3(\theta_{G1}, \theta_A, \sigma_1, \sigma_f, \sigma_\psi) = \int\int \begin{array}{l} f(F^*_{L_{i1}} | A_{i1}, \sigma_1, \theta_{G1}) \times f(A_{i1} | I^*_{ijk}, \theta_A) \times f(\sigma_1 | \Delta L_i^*) \\ \times f(F^*_{L_{i2}} | A_{i1} + T_{L_i}, \sigma_1 + \sigma_f, \theta_{G1}) \times f(T_{L_i} | T^*_{L_{1i}}, T^*_{L_{2i}}) \\ \times f(\sigma_f | \Delta S_i^*).dA_{i1}.dT_{L_i} \end{array} \quad (3.9)$$

2.4.3 Model fit to modal progression

The modal progressions estimated from the length-frequency distributions can be treated as multiple mark-recapture events where the initial age is known. Let μ_{cd} the value of the modal length for cohort c at the month d, and a_{c1} the age associated with the smallest modal length. As the time interval between two successive length modes was one month, the corresponding age for the modal length μ_{ck} was $a_{ck} = a_{c1} + (d-1)$. Thus, from Eq.3.5 :

$$\mu^*_{cd} = L_\infty(1 - exp(-k_2(\frac{a_{c1} + (d-1)}{12} - t_0)) \left(\frac{1 + exp(-\beta(\frac{a_{c1}+(d-1)}{12} - t_0 - \alpha))}{1 + exp(\beta\alpha)} \right)^{\frac{(k_1 - k_2)}{\beta}} \times \psi_{\mu_{cd}} \quad (3.10)$$

The uncertainty around the value of the modal length, associated with the identification of mode, was assumed to increase with the length value. Thus $\psi_{\mu_c d}$ combines both the process error and the uncertainty around the value of the modal length of cohort c at the month d. The errors $\psi_{\mu_c k}$ were assumed to follow a log-normal distribution with mean 0 and a common variance σ^2_μ. The likelihood for the length-frequency data can be written as :

$$\mathcal{L}_4(\theta_{G1}, \sigma_\mu, a_{c1}) = \int f(\mu^*_{cd} | a_{c1} + (d-1), \theta_{G1}, \sigma_\mu).da_{c1} \tag{3.11}$$

where $\theta_{G1} = \{L_\infty, k_1, k_2, t_0, \alpha, \beta\}$ is the vector of growth parameters.

2.4.4 Model fit to mark-recapture data

The change in fish length over the time interval between tagging and recapture $[t_1 ; t_2]$ is given by the following differential equation :

$$\frac{\Delta F_L(t)}{\Delta t} = \int_{t_1}^{t_2} (L_\infty - F_L(t)) \left(k_1 + \frac{k_2 - k_1}{1 + exp(-\beta(t - t_0 - \alpha))} \right) \tag{3.12}$$

The solution of this differential equation allowed to express the length at recapture $F^*_{L_{i2}}$ as a function of the length at tagging $F^*_{L_{i1}}$, the age at tagging t_{1_i} and the time-at-liberty $T^*_{L_i}$ for each fish i (Wang, 1998b) :

$$F^*_{L_{i2}} = L_\infty - (L_\infty - F^*_{i1}) \left(exp(-k_2 \times T^*_{L_i}) \left(\frac{1 + exp(-\beta(t_{1_i} + T^*_{L_i} - t_0 - \alpha))}{1 + exp(-\beta(t_{1_i} - t_0 - \alpha))} \right)^{\frac{k_1 - k_2}{\beta}} \right) \times \psi_{r_i} + \varepsilon_{i2} \tag{3.13}$$

ε_{i2} are the length measurements errors at recovery. ψ_{r_i} are the process errors for the mark-recapture data. These errors were assumed to follow a log-normal distribution with mean 0 and a common variance σ^2_r. The age at tagging t_{1_i} of each fish i was considered to be a random variable because the fish were not the same length when tagged and corresponded to different cohorts. In addition, the yellowfin spawning period extends over several months and the larvae and juveniles can exhibit some variability in growth. These ages were assumed to follow gamma distributions whose the mean t^*_1 sourced from the literature, in particular from studies considered a two-stanza growth curve (Gaertner and Pagavino, 1992; Gascuel et al., 1992; Lehodey and Leroy, 1999; Lumineau, 2002; Viera, 2005), with a coefficient of variation of 0.5. Yellowfin were grouped according to their length at tagging into size classes which progressed in 10 cm increments. The ages-at-tagging in a same size-class could be regarded as random values from the same overall prior distribution. Yellowfin measuring less than 50 cm were considered to be younger than one year in age and the mean age was definied to 0.5 years. For fish in the 50-60 cm size range, the mean age was 1.75 years. Then, for each increasing size class, the mean age progressed of 0.5 years. To assess the sensitivity of the prior distribution for the ages-at-tagging, normal and log-normal distributions were also considered.
The mark-recapture data were not used to update the posteriors of the age-dependent parameters, i.e. α and t_0, since they do not provide any information on the fish age.

Considering the vector of growth parameters $\theta_{G2} = \{L_\infty, k_1, k_2, \beta, t_{1_i}\}$, the likelihood for the mark-recapture data can be written as :

$$\mathcal{L}_5(\theta_{G2}, \sigma_1, \sigma_f, \sigma_r) = \int f(F^*_{L_{i2}} | F^*_{L_{i1}}, t_{1_i} + T^*_{L_i}, \theta_{G2}, \sigma_1 + \sigma_f, \sigma_r) \times f(\sigma_1 | \Delta L^*_i) \times f(\sigma_f | \Delta S^*_i) . dt_{1i} . dT^*_{L_i} \tag{3.14}$$

TABLE 3.2 – Variables and parameters used in the somatic growth models

Parameters	Unit	Description
L_∞	cm	Asymptotic fork length
t_0	$years$	Age of zero fork length
α	$years$	Relative age to t_0 at which the change in growth occurs (inflexion point)
k_1	$years^{-1}$	Growth rate coefficient of the first stanza
k_2	$years^{-1}$	Growth rate coefficient of the second stanza
β	$years^{-1}$	Transition rate between k_1 and k_2
F_{Lij}	cm	Fork length of fish i at capture event j
T_{L_i}	$years$	Time-at-liberty of fish i
A_{ij}	$years$	Age of fish i at capture event j estimated by otolith reading
μ_{cd}	cm	Modal length value for cohort c at month d
a_{cd}	$years$	Age related to μ_{cd}
a_{c1}	$years$	Age associated with the smallest modal length of cohort c
t_{1_i}	$years$	Age at tagging of fish i for mark-recapture data
ε_1	cm	Length measurement error at tagging
σ_1	cm	Standard deviation related to ε_1
ε_2	cm	Length measurement error at recovery
σ_2	cm	Standard deviation related to ε_2
ψ	cm	Process error used with ageing data
σ_ψ	cm	Standard deviation related to ψ
ψ_μ	cm	Process error used with modal progression data
σ_μ	cm	Standard deviation related to ψ_μ
ψ_r	cm	Process error used with mark-recapture data
σ_r	cm	Standard deviation related to ψ_r
ΔL	cm	Fork length differences between two successive measurements of the same fish
ΔS	cm	Fork length differences between frozen and fresh measurements of the same fish
σ_f	cm	Standard deviation related to measurements errors associated with freezing

2.4.5 Bayesian inference

The prior distributions of the growth model parameters were assumed to be independent and were specified as being weakly informative or uninformative (Table 3.3). An exception to this was the asymptotic length, L_∞, which was assigned an informative prior using a generalized extreme value (GEV) distribution. The GEV distribution allows the extrapolation of the behavior of the distribution tails from the greatest values of a sample, and thus estimates the occurrence probability of extreme events (Borchani, 2010). L_∞ can be interpreted as the maximal length reached by the oldest fishes. As tunas grow throughout their lives, the largest observed sizes were assumed to correspond to the oldest fishes, which motivated the choice of using the GEV distribution. The GEV distribution was fitted to a

data set containing records of the largest fish collected between 1952-2011 from the European and Seychelles purse seiners, Maldivian pole and liners, and Taiwanese and Japanese longliners (Dortel et al., 2013).
The growth rate coefficients, k_1 and k_2, are, in part, model-specific. For k_1, a weakly informative gamma distribution was assigned from values published in the literature (Table 3.4). k_2 was set equal to $k_1 + \kappa$ with κ following a uniform distribution. The age α, which is relative to t_0, was assigned a weakly informative gamma distribution defined from results of studies considered a two-stanza growth curve (Gaertner and Pagavino, 1992; Gascuel et al., 1992; Lehodey and Leroy, 1999; Lumineau, 2002; Viera, 2005). The parameters β, which is specific to the VB log-K model, and t_0, which depends on the data, were assigned uniform distributions. The standard deviations of the length measurement errors at tagging, σ_1, the errors associated with freezing, σ_f, and the process errors σ_ψ, σ_μ, σ_r, were assigned uninformative priors through using inverse gamma distributions (Table 3.3).

The growth parameters, fish ages and associated error estimations were evaluated by Markov Chain Monte Carlo (MCMC) simulations using a the Metropolis-within-Gibbs sampling algorithm as implemented in OpenBUGS version 3.2.1 (Spiegelhalter et al., 2011). Three chains starting at contrasting initial values were considered to check for the convergence of the algorithm. First, the growth model was fitted to the otolith age estimations and fish length (Model 1). The length-frequency data were then added to the growth model as a second likelihood component (Model 2). Finally, the mark-recapture data were included as a third likelihood component (Model 3). For each model, the convergence of the MCMC to the stationary posterior distribution was evaluated by the Gelman-Rubin diagnostic, based on the ratio of inter-chain variance to intra-chain variance. A ratio close to 1 indicates convergence (Gelman and Rubin, 1992). This ratio was computed from second half of MCMC simulation sample. The code of the integrated model is given in Appendix B.

TABLE 3.3 – Prior probability distribution used in both ageing and growth models

Parameter	Prior distribution
Somatic growth model	
L_∞	$G_{ev}(173.141, 11.067, -0.3474)$
k_1	$\Gamma(2.778, 0.211)$
k_2	$k_1 + \kappa$ with $\kappa \sim \mathcal{U}(0, 3)$
α	$\Gamma(4, 0.725)$
β	$\mathcal{U}(0, 30)$
t_0	$\mathcal{U}(-2, 0)$
a_{c1}	$\Gamma\left(\frac{a_{c1}^{*2}}{9}, \frac{a_{c1}^{*}}{9}\right)$
t_1	$\Gamma\left(\frac{1}{0.25}, \frac{1}{0.25 t_1^{*}}\right)$
ε_{i1}	$\mathcal{N}(0, \sigma_1^2)$ with $\sigma_1 \sim$Inv$\Gamma(0.01, 0.01)$
ε_{i2}	$\mathcal{N}(0, \sigma_2^2)$ with $\sigma_2 = \sigma_1 + \sigma_f$
σ_f	Inv$\Gamma(0.01, 0.01)$
ψ_{ij}	$\ln\mathcal{N}(0, \sigma_\psi^2)$ with $\sigma_\psi \sim$Inv.$\Gamma(0.01, 0.01)$
$\psi_{\mu_{cd}}$	$\ln\mathcal{N}(0, \sigma_\mu^2)$ with $\sigma_\mu \sim$Inv.$\Gamma(0.01, 0.01)$
$\psi_{r_{ij}}$	$\ln\mathcal{N}(0, \sigma_r^2)$ with $\sigma_r \sim$Inv.$\Gamma(0.01, 0.01)$
Ageing model	
R_r	$2 \times R'_r$ with $R'_r \sim \mathcal{B}eta(1, 1)$
ψ_n	$\mathcal{N}(0, 3^2)$
ψ_e	$\mathcal{N}(0, 4^2)$
p_r	$\mathcal{U}(0, 0.5)$

TABLE 3.4 – Growth parameters of yellowfin for the three main oceans ; F : female, M : male

Region	Data type	Method	FL range	k	L_∞	t_0	Reference
Indian	Otoliths	Von Bertalanffy		0.176	245.541	0.266	Stéquert et al. (1996)
	Length-frequency	Gascuel Model	30 to 135	0.86	162.7		Viera (2005)
				0.828	163.411		
Western Indian	Otoliths	Von Bertalanffy	60 to 20	0.176	272.7	-0.266	Stéquert (1995)
	Length-frequency	Von Bertalanffy	60 to 144	0.88	154.77	1.16	Lumineau (2002)
				0.8	150.9	1.7	
		Gascuel model	30 to 144	2.25	136.34		
				0.84	152.07		
Minicoy	Length-frequency	Von Bertalanffy	27 to 137	0.32	145	-0.34	Mohan and Kunhikoya (1985)
Atlantic	Scales	Von Bertalanffy		0.278	222.8		Yang et al. (1969)
	Dorsal spines	Von Bertalanffy		0.37	192.4	-0.003	Draganik and Pelczarski (1984)
	Length-frequency	Von Bertalanffy		0.72	166.4		Fon
				0.5		189	
	Tagging	Von Bertalanffy		0.56	183.9		Miyabe (1984)
		Von Bertalanffy		0.411	198.08		Bard et al. (1991)
				0.485	152.59		
Western Atlantic	Dorsale spines	Von Bertalanffy		0.267	230.7	-0.081	Lessa and Duarte-Neto (2004)
Eastern Atlantic	Length-frequency	Von Bertalanffy		0.42	194.8		Le Guen and Sakagawa (1972)
		Von Bertalanffy	63 to 170	0.42	194.8	-0.748	Gascuel et al. (1992)
		Gascuel model	40 to 150	1.195	158.5		
			41.4 to 147.4	1.495	152.6		
Gulf of Guinea	Tagging	Von Bertalanffy	65 to 180	0.474	196.55	0.847	Bard (1984)
Gulf of Guinea	Tagging and Length-frequency	Von Bertalanffy		0.864	166.4	1.292	Fonteneau (1980)
				0.936	161.02		
Dakar and Senegal				0.6	189		
Venezuela	Length-frequency	Von Bertalanffy	65.88 to 160	0.884	155.069	0.957	Gaertner and Pagavino (1992)
Brasil			65 to 155	0.43	184.12	-0.079	
Africa			63.07 to 180	0.566	189.04	1.193	
Gulf of Guinea and North Carolina	Otoliths	Von Bertalanffy	30 to 179	0.281	245.541	0.0423	Shuford et al. (2007)
Pacific			70 to 148	1.72	148	2	Hennemuth (1961)
			72 to 149	1.888	149	2.294	Davidoff (1963)
Western Pacific	Scales			0.333	192.8		Huang and Yang (1974)
				0.386	174.9		Huang et al. (1973)
				0.129	178.6		Li et al. (1995)
		Von Bertalanffy	M : 58 to 119	0.276	202.1	0	Le Guen and Sakagawa (1973)
			F : 57 to 119	0.372	174.9	0	
		Von Bertalanffy	70 to 140	0.33	190.1	0	Yabuta et al. (1960)
		Von Bertalanffy	60 to 139	0.36	195.2		Yang et al. (1969)
	Otoliths	Von Bertalanffy	45 to 70	0.39	199.6	-0.177	Lehodey and Leroy (1999)
		Modified Von Bertalanffy		0.728	151.7	-0.085	
				M : 0.805	146.7	-0.049	
				F : 0.511	177.1	-0.167	
	Length-frequency		0.25	166			Hampton (2000)
		Von Bertalanffy	50.8 to 164.4	0.392	175	0.00306	Sun et al. (2003)
			80 to 150	0.66	150	0.4	Yabuta and Yukinawa (1959)
		Von Bertalanffy	30 to 96	0.292	180.9	0	Wankowski (1981)
Eastern Central Pacific	Length-frequency	Von Bertalanffy	93 to 167	0.52	175.9	0.19	Zhu et al. (2011)
Western coast of America	Increment technic	Von Bertalanffy	80 to 140	0.45	180		Diaz (1963)
				0.66	167		
				0.36	214		
				0.7	166		
Hawaii	Weight modes	Von Bertalanffy	70 to 120	0.44	192	0.22	Moore (1951)
Japanese	Length-frequency	Von Bertalanffy	30 to 150	0.55	168	0.35	Yabuta and Yukinawa (1957)
Philippine waters	Length-frequency	Von Bertalanffy	20 to 60	0.29	179		White (1982)
				0.25	189		
			20 to 60 and 90 to 150	0.43	182		
			20 to 70	0.2	169		
		Von Bertalanffy	20 to 60 and 120 to 160	F : 0.32	173		Yesaki (1983)
				M : 0.3	175		

3 Results

3.1 Modal progression analysis

Twenty one yellowfin cohorts ranging in size from 35-130 cm F_L were identified by tracking the montly progression of length modes (Figure 3.2) in length-frequency histograms for the period 2000-2010. Recruitment to the purse seine fishery peaks occured at approximately 35.8 cm F_L (SD = 1.7 cm) from February to August. A clear pattern in the month of recruitment was not apparent from the data of the studied period. Linkages between successive modes assumed as belonging to the same cohort proved to be difficult to establish above 70 cm F_L. This was due to the lack of intermediate-sized fish caught, between 70-90 cm F_L, and the general absence of clearly identifiable modes in the length distributions of large tunas, i.e. > 90 cm F_L. The increase in modal length across cohorts over time showed strong inter-annual variability (Figure 3.2). Some cohorts showed an apparent decrease in growth rates at around 50 cm F_L, followed by a faster growth above 60 cm F_L (e.g. cohort 9), while the growth rates appeared more linear for other cohorts (e.g. cohorts 7).

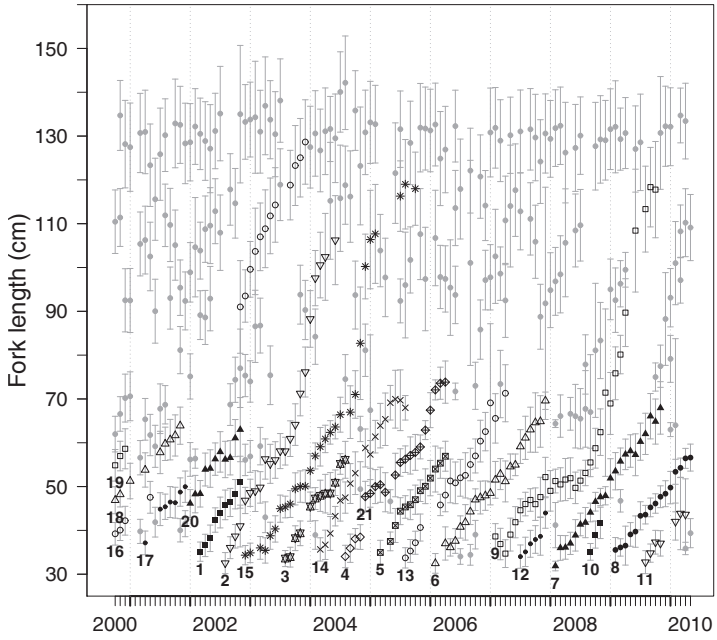

FIGURE 3.2 – Monthly length modes and cohorts identified from length-frequency purse seine data. Each cohort is distinguished by a different symbol and is numbered. Filled grey circles represent identified modes which did not belong to a complete cohort. The symbols and the circles represent the mode values estimated from fitting a mixture of normal distributions to the length-frequency data. Vertical lines indicate standard deviations.

TABLE 3.5 – Main features for the marginal posterior distributions of the growth parameters as estimated from the three combinations of the datasets ; Std.dev. : Standard deviation

Parameters	Otolith data					Otolith and length-frequency data					Otolith, length-frequency and mark-recapture data				
	Mode	Mean	Std.dev.	Posterior quantiles 2.5%	97.5%	Mode	Mean	Std.dev.	Posterior quantiles 2.5%	97.5%	Mode	Mean	Std.dev.	Posterior quantiles 2.5%	97.5%
L_∞	167.907	165.07	14.135	136.697	190.21	151.327	155.703	11.941	135.095	181.107	137.555	137.908	2.182	135.9	
t_0	-0.483	-0.489	0.091	-0.691	-0.338	-0.845	-0.851	0.069	-0.987	-0.72	-0.863	-0.864	0.094	-1.002	-0.74
α	2.75	2.776	0.307	2.382	3.557	2.861	2.865	0.068	2.749	3.009	2.859	2.882	0.085	2.774	3.015
β	15.56	16.463	8.027	2.27	29.331	20.791	19.821	5.883	9.534	29.56	18.038	19.552	5.388	9.984	29.003
k_1	0.211	0.217	0.03	0.171	0.288	0.182	0.184	0.021	0.147	0.228	0.214	0.214	0.01	0.199	0.228
k_2	0.513	0.668	0.353	0.359	1.589	0.732	0.78	0.195	0.498	1.181	1.358	1.365	0.105	1.197	1.556
σ_ψ	0.136	0.138	0.009	0.122	0.157	0.145	0.146	0.009	0.129	0.165	0.153	0.155	0.011	0.137	0.176
σ_μ	-	-	-	-	-	0.069	0.069	0.003	0.064	0.076	0.067	0.068	0.003	0.062	0.074
σ_r	-	-	-	-	-	-	-	-	-	-	0.029	0.029	0.003	0.024	0.034
σ_1	3.168	3.168	0.066	3.045	3.301	3.163	3.167	0.067	3.039	3.303	3.173	3.166	0.067	3.043	3.299
σ_2	5.575	5.578	0.201	5.213	5.968	5.498	5.584	0.207	5.201	6.026	5.536	5.566	0.21	5.203	6.021
σ_f	2.378	2.41	0.192	2.06	2.794	2.371	2.417	0.196	2.089	2.858	2.343	2.4	0.198	2.047	2.837

TABLE 3.6 – Matrice of correlation and covariance between growth parameters ; the numbers in bold correspond to the correlations

	Otolith data						Otolith and length-frequency data						Otolith, length-frequency and mark-recapture data					
	L_∞	α	β	k_1	k_2	$t0$	L_∞	α	β	k_1	k_2	$t0$	L_∞	α	β	k_1	k_2	$t0$
L_∞	234.184	**0.042**	**0.052**	**-0.886**	**-0.600**	**-0.268**	147.225	**0.156**	**0.138**	**-0.941**	**-0.849**	**-0.415**	5.351	**-0.167**	**0.047**	**-0.377**	**-0.73**	**-0.017**
α	0.235	0.131	**-0.352**	**-0.144**	**0.478**	**-0.210**	0.139	0.005	**-0.232**	**-0.362**	**0.053**	**-0.702**	-0.035	0.008	**-0.407**	**-0.746**	**0.216**	**-0.920**
β	6.400	-1.021	64.119	**0.040**	**-0.291**	**0.127**	9.844	-0.100	34.320	**-0.094**	**-0.219**	**0.079**	0.594	-0.200	30.084	**0.288**	**-0.108**	**0.326**
k_1	-0.451	-0.002	0.011	0.001	**0.534**	**0.612**	-0.240	-0.001	-0.012	0.000	**0.847**	**0.643**	-0.009	-0.001	0.016	0.000	**0.308**	**0.846**
k_2	-3.321	0.063	-0.842	0.006	0.131	**0.128**	-2.102	0.001	-0.262	0.004	0.042	**0.369**	-0.199	0.002	-0.069	0.000	0.014	**0.030**
t_0	-0.391	-0.007	0.097	0.002	0.004	0.009	-0.362	-0.004	0.033	0.001	0.005	0.004	-0.004	-0.008	0.173	0.001	0.000	0.009

3.2 Statistical inference

The performance of each model was checked based on 1,500,000 samples from the joint posterior distribution generated from MCMC simulation. The joint posterior distribution was considered to be stationary as indicated by a Gelman-Rubin diagnostic of convergence which approached a value of 1, and by the three MCMC chains that mixed well for each parameter of the three models. For each model, the data provided information on most of the parameters, i.e. the posterior distributions were narrower than the prior distributions, with the exception of β (Figure 3.3). The precision in the parameter estimates increased as each dataset provided an increasing amount of information. The marginal posterior distributions became increasingly narrow as the level of input information increased from model 1, based on otolith data only to model 3 which used all three data types (otolith, length-frequency, and mark-recapture). However, although the addition of data beyond improved by the information added to the otolith data was beneficial, the transition rate, β, in model 3 was poorly estimated. This was indicated by its posterior distribution which was irregular and characterized by a large variance. (Figure 3.3). The main marginal posterior distribution statistics (mean, mode, standard deviation, and 95% Bayesian posterior credibility interval) were computed after rejecting a burn-in period of 5,000 samples and and a thinning by drawing every $2{,}500^{th}$ sample (Table 3.5).

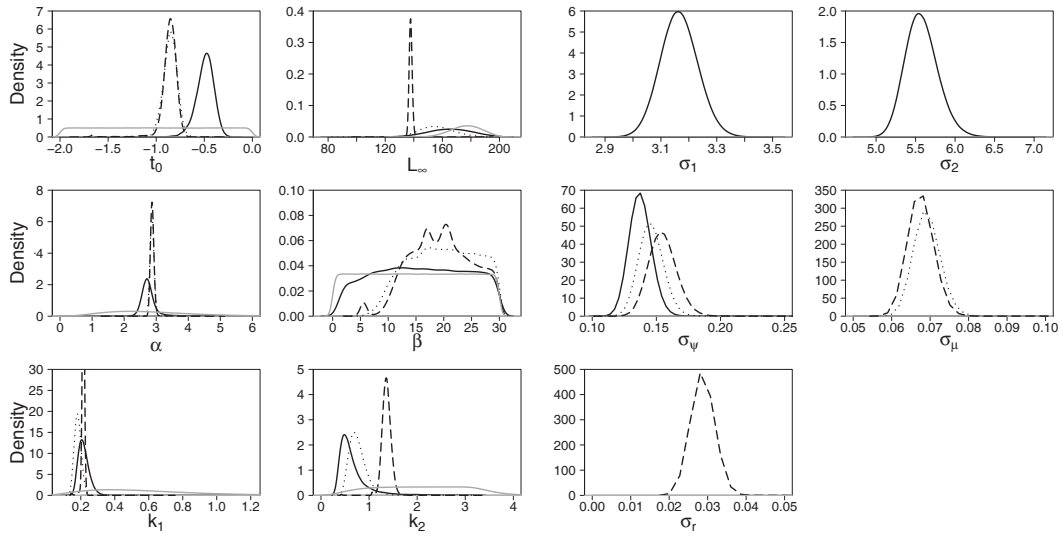

FIGURE 3.3 – Comparison of the prior distributions (grey solid line) with the marginal posterior distributions of the three growth parameters sets (described in Table 3.1) as estimated from the model 1, which was fitted to the otolith data (solid black line), model 2, which was fitted to both the otolith and length-frequency data (dotted black line), and model 3, which was fitted to the otolith, length-frequency, and mark-recapture data (dashed black line).

While the models 2 and 3 proved effective in estimating the initial age of each cohort identified from length-frequency dataset, the model 3 was unable to accurately estimate the ages of the 373 yellowfin from the mark-recapture dataset. Thus, the

posterior estimates of the ages-at-tagging for fish of 70 cm F_L and over were very similar (Figure 3.5). The poor age-at-tagging estimates indicate that model 3 was overparameterized due to the absence of age information in the tagging data. The gradually increasing of the number of observations from model 1 to 3 led to an overall decrease in the process error and uncertainty around the mean curve (Figure 3.4).

3.3 Indian Ocean yellowfin growth

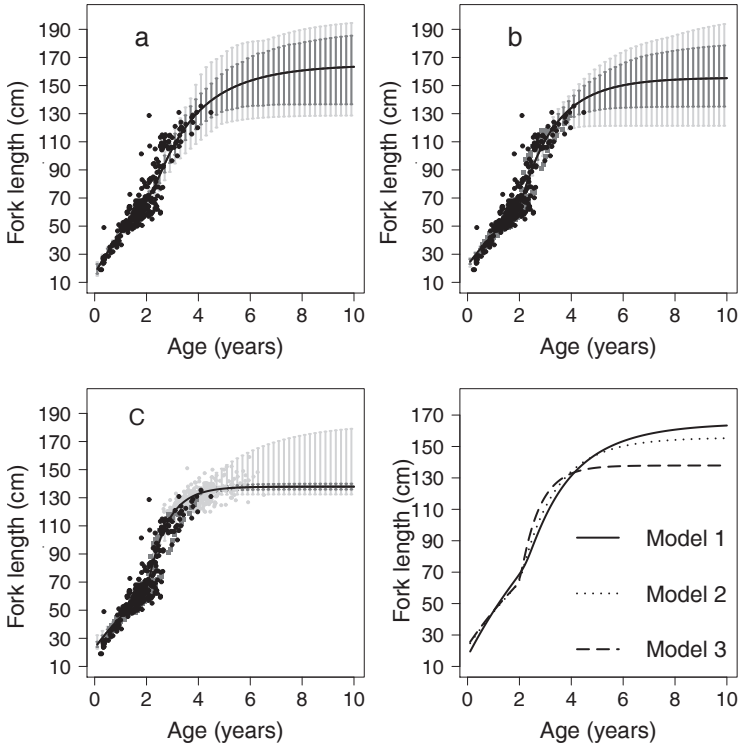

FIGURE 3.4 – Growth curves of Indian Ocean yellowfin as estimated from (a) model 1 fitted to otolith data (•), (b) model 2 fitted to otolith and length-frequency data (▲) and (c) model 3 fitted to otolith, length-frequency and mark-recapture data (•). The dark grey vertical lines correspond to the 95% Bayesian credibility interval and the light grey vertical lines to the overall uncertainty defining the minimal and maximal length related to each age.

Growth parameter estimates for Indian Ocean yellowfin were found to vary according to the amount of information input into each model. For each of the three models, two distinct growth phases were observed over the yellowfin lifespan (Figure 3.4). The growth rate coefficients, k_1 and k_2 were significantly differed according to the Bayesian 95% credibility interval (Table 3.5). The first phase was characterized by a relatively slow growth rate that gradually decreased to a minimum rate of 1.87 cm.month^{-1} at 1.9 years (65.5 cm F_L), 1.57 cm.month^{-1} at 1.7 years (58.2 cm F_L) and 1.47 cm.month^{-1} at 1.64 years (57.2 cm F_L) for models 1 to 3 respectively. In the second phase, the growth rate accelerated, reaching maximum rates of 3.52

cm.month^{-1} at 2.51 years (86.4 cm F_L), 4.83 cm.month^{-1} at 2.19 years (74.8 cm F_L) and of 6.4 cm.month^{-1} at 2.15 years (76.1 cm F_L) for models 1 to 3 respectively. Thereafter, the growth rate progressively decreased with increasing size and approached 0 close to asymptotic length.
The different datasets provided little information on the β parameter which was found to be > 15.3 in each of the three models, suggesting that the transition between the growth stanzas occured rapidly, less than six months (Table 3.5). The age α at which this transition occurred varied between 1.8 and 2.3 years, which corresponded to 75, 63 and 66 cm F_L for models 1 to 3 respectively. The asymptotic length L_∞ described by a mean prior value of 173 cm F_L decreased from model 1 to model 3 (Figure 3.4)

3.4 Sensibility to the prior distribution for the ages-at-tagging

The distribution law used for the ages-at-tagging did not have a major impact on the growth parameters estimates (Table 3.7 and Figure 3.5). With the exception of parameter *beta*, the sets of growth parameters forecasted by the gamma and normal distibutions were similar and resulted in identical mean growth curves (Figure 3.6). The use of the log-normal distribution led to a smaller asymptotic length with a growth rate coefficient higher in the first stanza and lower in the second stanza. However, these differences in relation to the estimates provided by the gamma and normal distributions according to the 95% Bayesian credibility interval, resulting in a similar mean growth curve.

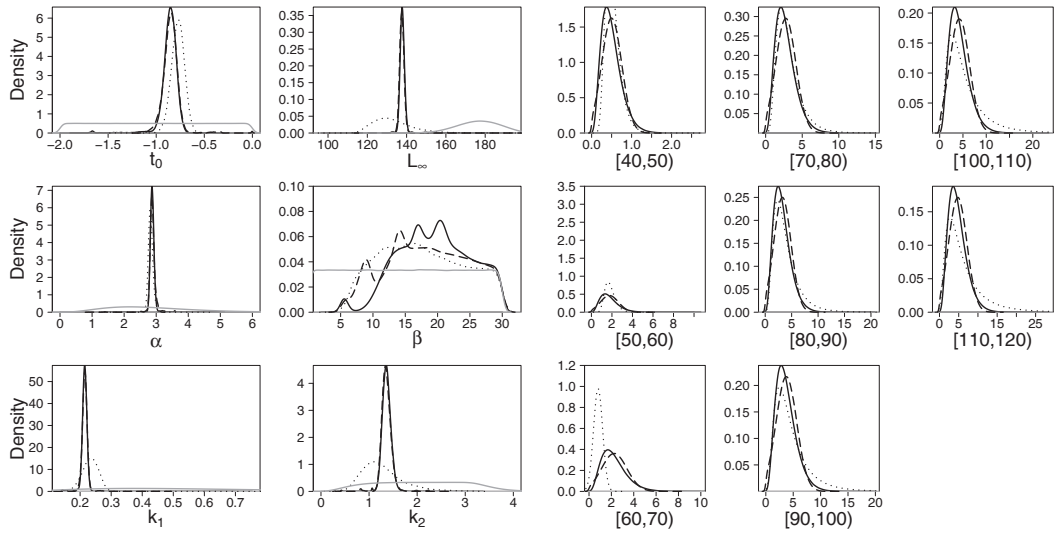

FIGURE 3.5 – Comparison of the prior distributions (grey solid line) with the marginal posterior distributions of the growth parameters sets as estimated from model 3 with different prior distributions on ages-at-tagging : gamma (solid black line), log-normal (dotted black line) and normal (dashed black line) and marginal hyper-posterior distributions of ages-at-tagging

As against, the distribution used had an impact on the model ability as showed by an increasing uncertainty around the mean growth curve from normal to gamma distributions and from gamma to log-normal distributions (Figure 3.6).

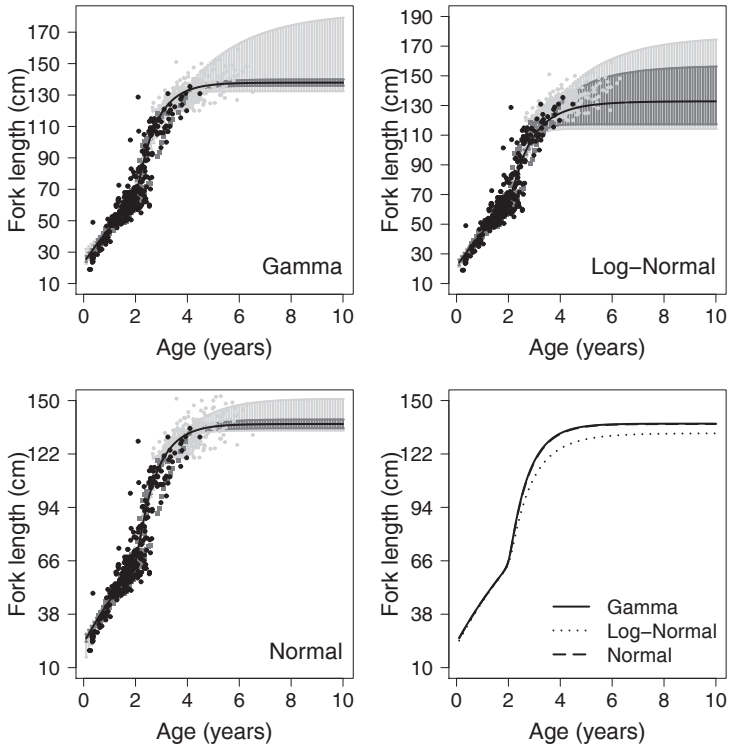

FIGURE 3.6 – Growth curves of Indian Ocean yellowfin as estimated from model 3 fitted to otolith (•), length-frequency (▲) and mark-recapture (•) data with different prior distributions on ages-at-tagging. The dark grey vertical lines correspond to the 95% Bayesian credibility interval and the light grey vertical lines to the overall uncertainty defining the minimal and maximal length related to each age.

TABLE 3.7 – Main features for the marginal posterior distributions of the growth parameters as estimated from the model 3 with the log-normal and normal prior distributions for ages-at-tagging ; Std.dev. : Standard deviation

Parameters	Log-normal distribution					Normal distribution				
	Mode	Mean	Std.dev.	Posterior quantiles 2.5%	97.5%	Mode	Mean	Std.dev.	Posterior quantiles 2.5%	97.5%
L_∞	128.638	132.866	10.175	117.28	156.83	137.579	137.712	1.477	135.5	140.1
t_0	-0.761	-0.77	0.068	-0.923	-0.636	-0.852	-0.85	0.077	-1.01	-0.729
α	2.809	2.823	0.074	2.696	2.99	2.865	2.875	0.072	2.76	3.032
β	15.21	18.006	6.434	7.16	29.312	18.321	18.631	6.298	7.495	29.331
k_1	0.24	0.233	0.026	0.181	0.281	0.216	0.215	0.009	0.198	0.23
k_2	1.158	1.289	0.445	0.63	2.501	1.335	1.353	0.099	1.198	1.543
σ_ψ	0.144	0.146	0.009	0.129	0.166	0.153	0.155	0.01	0.135	0.175
σ_μ	0.069	0.069	0.003	0.063	0.075	0.067	0.068	0.004	0.062	0.078
σ_r	1.877	1.906	0.098	1.737	2.113	0.028	0.029	0.003	0.024	0.034

With the exception of fish in size class 60-70 cm, for which the log-normal law predicted younger fish about 1 year, the posterior distributions for the ages-at-tagging obtained with the three laws were very similar (Figure 3.5).

4 Discussion

To our knowledge, this study presents the most comprehensive analysis of yellowfin growth in the Indian Ocean by combining the best information currently available from a variety of data sources collected at both the population and individual levels. These data encompassed about 600,000 length measurements of yellowfin caught by purse seiners over a 10-years period, which we used to track monthly changes in the modal length of age classes. In addition, to inform our analysis, we drew on nearly 373 individual growth rate values which were based on accurate times-at-liberty and more than 500 otolith readings. To take advantage of these varied data sources, we developed an integrated model that exploited all the available information and took explicitely into account the various observation and process errors associated with the growth estimation. Despite estimation difficulties encountered with the mark-recapture dataset, we argue that the resulting growth curves are an improvement of the one currently used in the Indian Ocean yellowfin stock assessments.

4.1 Gradual integration of the three datasets

Most previous studies on Indian Ocean yellowfin growth used a single data source, especially length-frequency data (Mohan and Kunhikoya, 1985; Marsac, 1991; Viera, 2005) or direct age estimates from vertebrae or otoliths (Romanov and Korotkova, 1988; Stéquert et al., 1996) and sometimes mark-recapture data (Fonteneau and Gascuel, 2008). The collection processes for each of the data sources are very different and associated with inherent uncertainties that can make comparisons between growth curves difficult. Sampling differences, i.e. size-range, gear selectivity and spatio-temporal coverage, observation errors and the process that is being observed itself, e.g. variability in the deposition rates of growth rings in fish otoliths, are all factors that can give rise to these uncertainties. However, the use of an integrated approach enables the different data sources to complement each other, thus providing a more robust estimation of growth (Eveson et al., 2004; Restrepo et al., 2010).
In this study, growth was estimated by gradually adding data from the three different sources into the statistical model, allowing to appraise their individual contribution to the final estimations. At first, the model was fitted to ageing data derived from otolith readings. Our model explicitly accounts for the uncertainties and biases associated with estimating fish growth from otolith readings, especially uncertainties related to age estimates. In a previous study, Dortel et al. (2013) showed, through simulation, that the modeled ages were reliable.

In a second step, the most comprehensive length-frequency dataset available for Indian Ocean yellowfin was added to the growth model. The addition of the likelihood component improved the overall parameters estimation and resulted in a smaller asymptotic length, L_∞, a larger second-stanza growth rate coefficient, k_2, and a more pronounced transition between the two growth stanzas.
Growth studies conducted over the last few decades on Indian Ocean yellowfin growth using length-frequency data generally support a two-stanza growth rate pattern (Marcille and Stéquert, 1976; Marsac and Lablache, 1985; Anderson, 1988; Marsac, 1991; Firoozi and Carrara, 1992; Lumineau, 2002; Viera, 2005). However, the length frequency data sampled from commercial fisheries catches dependent on size-selectivity of fishing gear, fishing areas and fish schooling behavior. Therefore, these data can not be considered as a representative random sample of the population (Longhurst and Pauly, 1987). In particular, the size-selectivity fishing has been shown to produce bias in the length-at-age samples. The bimodal size-selectivity associated with purse seine sets may result in the over-representation of young fast-growing fish and old slow-growing fish in size-age samples. This in turn may entail bias in growth estimations resulting in an apparent growth deceleration and unrealistic estimates of asymptotic length (Lucena and O'Brien, 2001; Taylor et al., 2005).
In addition, the identification of modes increasingly difficult with increasing size may affect the growth parameter estimates. In this analysis, proportions of length-at-age were derived using a mixture of normal distributions fitted to the length-frequency data. This is to optimize the identification of modes and accounted for uncertainties associated with yellowfin age. Nevertheless, some subjectivity remains in the assignment of a mode to a particular cohort.

Finally, mark-recapture data were introduced to the growth model. These data provides valuable information on the growth variability between individuals, however the ignorance of fish age, which forms the basis in any length-age relationship, weakens the growth estimations using mark-recapture data. The majority of fish growth studies that use mark-recapture data are based on the von Bertalanffy model, which assumes a linear decrease in growth rate over the lifespan of a fish (Von Bertalanffy, 1957). The shape of the growth curve can then be estimated without prior knowledge of age using the Fabens method (Fabens, 1965) or alternative Fabens-type approachs (Wang, 1998a). These methods expresse the change in length of a fish as a function of its time-at-liberty. However, these methods can not applied to more complicated multi-stanzas growth models, such as the VB log-K model where the transition between the various growth phases is related to age parameters (Laslett et al., 2002; Eveson et al., 2004).
In this study, as the ages-at-tagging were assumed to vary from one fish to another, they were modeled as random variables. Ideally, the ages of the various individuals should be considered as independent random variables, but this would lead to a model overparametrization. To reduce the overparametrization, yellowfin were classified according their length at tagging and the ages-at-tagging of fish in the same size-class were considered as random values from the same overall prior distribution.

Thus, the growth estimations were based on the joint estimating of the parameters and the ages-at-tagging. To use this approach, it was essential to have information on fish age at a given length, which was provided by ageing data. Nonetheless, the ageing data were insufficient to compensate the lack of information on age in mark-recapture observations. Hence, our results showed that ages estimated for the fishes tagged and recaptured with such a complex growth curve are poorly estimated whatever the prior distribution used. Indeed, for the three distributions used, the marginal hyperposterior distributions for fish from 70 to 120 cm F_L were very similar, which implied a very rapid growth. However, such growth rates seems implausibles. In addition, the model 3 forecasted a mean asymptotic length of 137.9 cm F_L, which was comparatively low to the maximum lengths historically reported for yellowfin in the Indian Ocean.

The increasing uncertainty around the mean curve in the second stanza (Figure 3.4) and the strong correlations obtained between the asymptotic length L_∞ and the growth rate coefficients k_1 and k_2 (Table 3.6) were related to a lack of information for the asymptotic part of the curve. Ageing and length-frequency data provide information on the length of a given age and growth rates which depend on both L_∞ and k_2 or k_1, but no information on larger fish. When the data are not enough informative, several parameters sets can lead to the same maximum likelihood due to the correlation between some parameters, which results in identifiability problems. This may bring about some model instability and difficulty to estimate the posterior distributions with incredible parameter values. This may bring about some model instability and difficulty to estimate the posterior distributions with potentially the obtaining of incredible parameter values. In this study, information was provided through the prior distribution of Linf to get more consistent values.

Based on a frequentist approach, Eveson et al. (*in press*) encountered similar estimation problems due to the imbalance between the likelihoods components of the model including the three data sources, as these authors used a larger number of mark-recapture data. In this study, only the larger fish of mark-recapture dataset were considered, in order to compensate the lack of information of ageing and length-frequency datasets for the asymptotic part of the curve, without for all noised the accurate information provided by these datasets. In their study, Eveson et al. (*in press*) assumed that the ages-at-tagging of each individual fish can be considered as a same random parameter modeled through a normal distribution (Laslett et al., 2002). We have considered this method unsuitable, in particular because the tagged fish corresponded to different cohorts spawned at various times as evidenced by the bimodal length-frequency distribution from RTTP-IO tagging data (Figure 3.1). Thus, we have considered an alternative approach.
Our modeling approach differs in several key points to the statistical model of Eveson et al. (*in press*). Firstly, we considered the uncertainty in age estimations derived from otolith counts using an ageing error model. This error model has been shown to outperform methods that use an average age derived from multiple otolith counts (Dortel et al., 2013). However, we only selected fish with accurate

time-at-liberty values in the likelihood component of the mark-recapture data to ensure that the sources of variability in the model were decreased. Secondly, we used length-frequency data while Eveson et al. (*in press*) only used otolith and mark-recapture data. Thirdly, we included process error in our model to account for individual variability in the whole growth term, whilst (Eveson et al. *in press*) considered that individual variability was mainly driven by differences in individual L_∞. Finally, we used Bayesian inference to account for historical observations of the largest yellowfin caught in Indian Ocean fisheries to provide information on L_∞. Indeed, little information was provided to the asymptotic length, L_∞ due to the small number of large individuals (>130 cm F_L) in the dataset.

4.2 Growth of Indian Ocean yellowfin

Overall, the resulting growth curves of both our approache and that of Eveson et al. (*in press*) demonstrate that Indian Ocean yellowfin tuna exhibits a more complex growth pattern than expected by the classical von Bertalanffy growth model, characterised by a sharp acceleration of growth. In this study, the growth acceleration was forecasted between 65.5 and 58.5 cm F_L according to models 1 and 2 respectively. The addition of length-frequency data led to an earlier acceleration of greater intensity, with instantaneous growth rates between 3.43 and 4.84 cm.month^{-1} for larger fish, against 2.7 to 3.517 cm.month^{-1} with ageing data only. In return, the addition of these data resulted in a slower juvenile growth, with growth rates between 1.52 and 1.9 cm.month^{-1} against 1.87 and 2.42 cm.month^{-1} with ageing data only. Such results were consistent with previous studies on growth of Indian Ocean yellowfin. These studies brought to light an acceleration occuring around 56-70 cm F_L (Marsac, 1991; Firoozi and Carrara, 1992; Lumineau, 2002; Viera, 2005) with growth rates comprised between 1.3-2.9 cm.month^{-1} and 2.5-4.8 cm.month^{-1} for smaller and larger fish respectively (Marsac and Lablache, 1985; Anderson, 1988; Marsac, 1991; Firoozi and Carrara, 1992; Lumineau, 2002). The inflection points of the growth curves corresponded to a fork lengths of 76.4 cm (2.3 years) and 65.7 cm (2 years) for the models 1 and 2 respectively.

Several assumptions have been put forward to explain the growth acceleration, however the underlying growth mechanisms were little studied and were not yet well understood. To our opinion, the acceleration would be related to the transition from a sedentary schooling fish in shallow and warm waters to a more mobile state in offshore waters. According to fisheries observations, the fish leave the associated school with Fish Aggregating Devices at sizes close to forecasted length for the growth acceleration (Stéquert and Marsac, 1986; Fonteneau and Gascuel, 2008). This fact is notably causing difficulty to identify length modes for fish > 70 cm from the length-frequency data.

Integrated statistical models appear to be a useful approach to combine all available information within a unifying framework and allow for the functional form of growth to be described in a holistic manner. However, statistical models exhibit limitations when dealing with complex growth patterns when ageing data are only provided through time-consuming and expensive methods (e.g., otolith analysis). Furthermore, they do not provide insights into the biological and ecological mechanisms that lie behind the growth stanzas. Future modeling work could focus on alternative approaches aimed at expressing age as a function of fish length and to understanding kinetic energy transfers in fish over time. Bioenergetic models that explicitly represent the allocation of metabolic energy between growth, maintenance, and reproduction might provide a way forward (Nisbet et al., 2000; Walters and Essington, 2010; Jusup et al., 2011).

Chapter 4

A bioenergetic modelling approach for yellowfin growth pattern

1 Introduction

Yellowfin tuna (*Thunnus albacares*, Scombridae, Bonnaterre 1788) is an epipelagic species that is widely distributed in the tropical and subtropical waters of the three world's major oceans where it is a valuable resource for commercial fisheries (Stéquert and Marsac, 1986; Fonteneau, 2010). In terms of catch, yellowfin ranks second among the most intensively exploited tuna species (Miyake et al., 2010; Pillai and Satheeshkumar, 2012). Yellowfin features special functional traits have received considerable research interest for evolutionary and physiological purposes, such as thermo-conservation abilities, which allows for a wide range of habitats, and efficient swimming, which allows to migrate over long distances (Graham and Dickson, 2004; Shadwick et al., 2013). More recently, yellowfin has been the focus of a particular attention as a potential species for tuna farming (Kaji et al., 1999; Wexler et al., 2003).

In the past 50 years, growth of yellowfin tuna has been subject of considerable research efforts leading to obvious evidences supporting a really specific two-stanza growth pattern, characterised by a sharp acceleration of growth around 60-65 cm F_L (Fonteneau, 1980; Gascuel et al., 1992; Gaertner and Pagavino, 1992; Lehodey and Leroy, 1999, Dortel et al. *in submission*). Currently, this growth pattern is commonly used in the Indian Ocean yellowfin stocks assessments, a process based on age-structured population dynamics models incorporating explicitly the growth rates, which aims to supply scientific advice for the sustainable exploitation of fish stocks (Langley et al., 2012; Cotter et al., 2004). Despite this, the growth stanza is still controversial, which weakened the proposed management measures.
Several assumptions likely to explain the acceleration in yellowfin growth have been put forward. Changes in growth rates with size might result from a combination of physiological, ecological and behavioral factors, but the role and contribution of each of them have not been addressed yet. Most studies are based on a statistical modelling of growth, which reveals useful for describing the functional form of growth, but does not provide any explanation as to these factors. Besides, some authors have attributed the growth stanza to an artefact related to size selectivity of the purse seine fisheries from which most of the growth data for yellowfin are available (Kolody, 2011).

It has been recognized for some time that growth rates are related to metabolic processes and vary in response to changes in temperature and food conditions (Roff, 1983; Walters and Essington, 2010). An organism acquires energy from food, assimilates it and converts it, and then allocates it according to its needs, i.e. survival, growth, development and reproduction. A modelling growth approach that explicitly represents energy transfers resulting of catabolism and anabolism processes in relation to organism requirements and environmental conditions would allow for a better understanding of the mechanisms regulating growth and therefore provide insights into the determinants of yellowfin growth. Improving our understanding of such processes is key for predicting the effects of global warming on tuna populations

by explicitly modelling the functional linkage between environmental features and demographic parameters. Bioenergetic modelling which describes energy fluxes between maintenance, growth, development and reproduction offers a particularly suitable framework to study yellowfin growth (Nisbet et al., 2000; Jusup et al., 2011).

1.1 Tunas physiology, ecology and growth

Tunas are part of the Scombridae family which includes 51 epipelagic species divided into 15 genus (Figure 4.1). With bonitos and mackerels, they form a commercially important group throughout world's oceans (Collette et al., 2001). Tunas are of major interest for physiologists and evolutionary biologists because of their particular anatomical, physiological and functional adaptations. The adaptations that distinguish them from other fish species are mainly related to their thermoregulation ability, their exceptional swimming capacities, their high metabolic rate and their notably different cardiovascular system (Brill and Bushnell, 2001; Graham and Dickson, 2004; Shadwick et al., 2013).

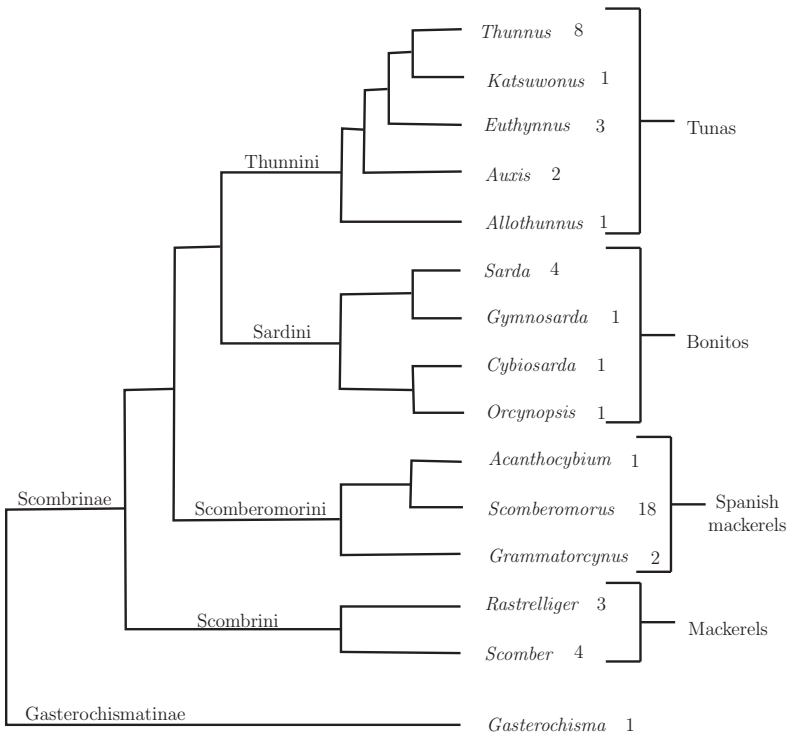

FIGURE 4.1 – Phylogenetic tree of Scombridae family according to Wegner et al. (2012). The number of species in each genus is given to the left

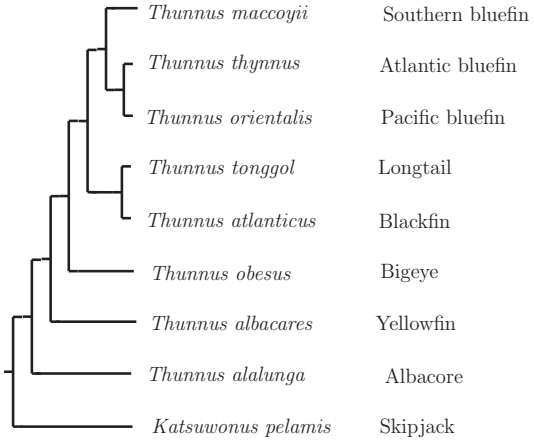

FIGURE 4.2 – Classification of main tunas according to cytochrome b phylogeny from Collette et al. (2001)

1.1.1 Thermoregulation physiology in tunas

Fish are mostly ectothermic species, which means that their body temperature is set by that of ambient environment and therefore varies with the ambient temperature. In contrast, tunas are able to maintain an internal temperature above the ambient temperature in some parts of their body and then, they are classified as regional endothermic species (Shadwick et al., 2013). Indeed, some authors pointed out an excess of temperature in red muscle comparatively to seawater temperature, up to 21°C for Atlantic Bluefin (Carey et al., 1971), 12°C for bigeye (Carey and Teal, 1966) and more than 5°C for yellowfin (Dizon and Brill, 1979). The tunas ability to maintain a body temperature above the ambient temperature is due to the presence of vascular heat exchanger systems, also known as *retia mirabilia*, based on a countercurrent blood flow to keep the heat produced by metabolism (Dizon and Brill, 1979; Cayré, 1989).
In all fish species, the warm venous blood carrying the metabolic heat goes towards the gills where the heat excess is dissipated (Cayré, 1989; Brill et al., 1994). In tunas, the vascular countercurrent heat exchanger systems recover the metabolic heat from warm venous blood before it reaches the gills. These systems consist of a dense tangle of fine venous and arterial capillaries where the excess of temperature of warm venous blood, transported from the tissues to the gills, is transferred to the cold arterial blood transported from the gills to the tissues. The blood flow in these tangles is slow in order to increase the heat exchanges (Graham and Dickson, 2001; Shadwick et al., 2013). The result is an effective warming of red and white muscles, viscera, brain and eyes (Graham and Dickson, 2004).

Three types of heat exchanger systems can be distinguished according to their location : (i) a central system located under the spinal column in the hemal arch, (ii) a lateral system in each side of the body (Figure 4.4) and (iii) a visceral system located on the ventral side of the liver (Cayré, 1989). All tunas of the genera *Katsuwonus*, *Euthynnus*, and *Thunnus* possess a lateral retia. Tunas of the genera

Auxis, *Euthynnus*, *Katsuwonus* and the species *Thunnus tonggol*, *T.atlanticus* and *T.albacares* possess a central retia assumed to correspond to an ancestral trait (Shadwick et al., 2013). The three bluefin species, bigeye and albacore have lost the central retia, but their lateral retia are highly developed and their ability to kept the metabolic heat is enhanced. Both retia are adjacent to the red muscles where the heat is the product of the continously lipidic oxydation due to the tunas requirement for a constantly swimming (Graham and Dickson, 2001). However the heat exchange is more effective within lateral retia than central retia (Shadwick et al., 2013).
Five tuna species of genera *Thunnus*, *T.albacares*, *T.obesus*, *T.maccoyii*, *T.thynnus* and *T.alalunga* also have a visceral retia. In this case, the source of heat are the digestion, absorption and anabolic processes within the stomach (Carey et al., 1984; Graham and Dickson, 2001).

1.1.2 Swimming adaptations

Tunas possess morphological, anatomical and biomechanical specialisations giving them increased swimming performances compared to others teleosts. Indeed, among teleosts, tunas are the only ones to practice the "thunniform swimming" (Graham and Dickson, 2004). The main locomotor features include a highly streamlined body, a high-aspect-ratio lunate tail with a narrow caudal peduncle, finlets along the trailing edges of the body, anterior and median aerobic red muscles and elevated core temperatures (Altringham and Shadwick, 2001; Shadwick and Syme, 2008). Some of these thunniform locomotor systems are also found in lamnid sharks by a phenomenon of evolutionary convergence (Syme and Shadwick, 2011).

A. Body shape features

Tunas have a thick but highly streamlined body and the resulting ratio of body thickness to length close to optimum for minimum drag (Shadwick et al., 2013). Thus, the water flow on the body could be laminar, even at high speeds, up to the point when the body begins to taper towards the tail (Figure 4.3 ; Altringham and Shadwick, 2001). The caudal peduncle of tunas ends with a stiff hydrofoil-like tail fin that generates thrust by forward directed hydrodynamic lift (Syme and Shadwick, 2011; Shadwick et al., 2013). The tapering body shape in the caudal region associated with a rather ellipsoidal profile in the middle part of the body allows to minimize the effect of lateral recoil forces from the tail, indicating that the tuna are designed to swim in a straight line (Shadwick et al., 2013). Vertical lift is provided by the large area of the pectoral fins. These fins have a role in the maintenance of hydrostatic equilibrium, thus tunas with largest area lifting due to pectoral fins, as bigeye and yellowfin, have a lower density (Magnuson, 1973).
The first dorsal and pelvic fins are retractables and are used for maneuvering. The second dorsal and anal fins allow to reduce lateral body movements (Altringham and Shadwick, 2001).

Another unusual tuna feature is the presence of finlets, small non-retractable fins located in pairs along the dorsal and ventral sides of the caudal region (Figure 4.3). Tunas have 6 to 10 finlet pairs, likely contribute to the maintenance of flow over the body toward the tail and may provide a less turbulent environment for oscillation of the tail (Nauen and Lauder, 2000).

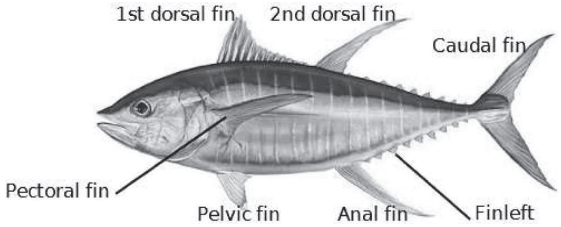

FIGURE 4.3 – Fin positions in yellowfin

B. Thunniform swimming

Most fish swim using undulatory movements of their body from head to tail. These movements are powered by both myotomal muscles on either side of the body, red muscles (aerobic) and white muscles (glycolytic). A sequential contraction of these myotomes generates a wave of bending that travels backward, the body and caudal fin push against the water, generating forward thrust (Wardle et al., 1995; Altringham and Ellerby, 1999).

Generally, the red muscles are confined just beneath the skin, along the horizontal midline near the lateral edge of the body. In tunas, the red muscles are located more anteriorly, near to the vertebral column and are completely surrounded by the white muscles (Figure 4.4 ; Altringham and Ellerby, 1999; Graham and Dickson, 2001). In addition, tunas have a high proportion of red muscles comparatively to most fish. While most fish have a relatively uniform quantity of red muscles throughout the body, in tunas these muscles are concentrated deep in the middle of the body (Shadwick et al., 2013). This specific anatomy provides the basis for the thunniform swimming.

The thunniform swimming mode is characterized by a reducing lateral mid-body undulation, the thrust mainly comes from rapid oscillations of caudal fin (Syme and Shadwick, 2002; Graham and Dickson, 2004). The red muscle fibers are elongated and connected to the skin and axial skeletion by robust myosepta and tendons, thus the force generated by red muscles is transmitted to the caudal fin (Shadwick et al., 1999; Syme and Shadwick, 2011). Thus, the reducing undulation body is accompanied by an increase of the tailbeat frequency. The thunniform mode is a highly efficient swimming mode, allowing tunas to reach high cruise speeds and migrate over long distances.

The power output of swimming muscles is highly temperature-dependent ; at higher temperatures, the muscles contract faster and more forcefully resulting in an increasing swimming speed. Thus, tunas ability to conserve muscle heat through their heat

exchanger systems is an advantage for fast sustained swimming (Altringham and Block, 1997; Shadwick et al., 2013).

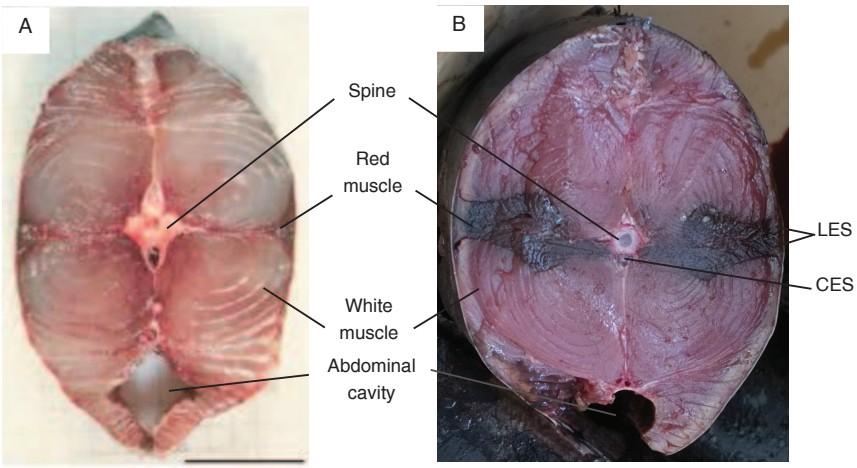

FIGURE 4.4 – Cross-section of a mackerel (A, *Scomberomorus cavalla* photograph from Westneat and Wainwright, 2001) and a yellowfin tuna (B, *Thunnus albacares* photograph taken by E.Chassot) showing red and white muscles positions and the location of central (CES) and lateral (LES) heat exchanger systems

C. Swimming speed and hydrostatic equilibrium

Scombroid fish have a density greater than seawater and thus they must swim continuously to maintain their position in the water column and, to a lesser extent, for gill ventilation (Magnuson, 1973; Dotson, 1976), the swimming providing the force required to drive water into the mouth and through the branchial chamber (Wegner et al., 2012). To compensate for their negative buoyancy, these fish swim with the pectoral fins extended ; this behavior ensure lift that balances their weight in water. Tunas with the largest pectoral lifting area, as bigeye and yellowfin, require lower swimming speed to maintain their hydrostatic equilibrium (Magnuson, 1973).

Additionally to the lift generated by the pectoral fins, with the exception of skipjack and kawakawa, tunas, bonitos and mackerels can counter the high densities of their skeleton and their muscles through the swim-bladder (Magnuson, 1973; Fänge, 1983). This bladder, located in the viscera, is filled with oxygen, carbon dioxide, and nitrogen (Fänge, 1983). In juvenile tunas the swim-bladder is little developed and does not contain gas, e.g. for albacore less than 55 cm in fork length (F_L ; Dotson, 1976) or for yellowfin less than 2 kg (50-60 cm F_L ; Magnuson, 1973). Then, the bladder grows rapidly and allometrically and, in adults, it occupies a large volume of the gut cavity. The swim-bladder is fully developed and functional for an albacore of 80 cm F_L (Dotson, 1976) and for a yellowfin of 8 kg (70-75 cm F_L ; Magnuson, 1973).
Tunas can adjust their buoyancy by secreting gases from the blood into the swim-bladder (Taylor et al., 2010). When the gases are secreted into the swim-bladder,

it expands and imparts a positive buoyancy to the fish, which becomes less dense than the water and tends to rise to the surface. Conversely, when the bladder volume decreases, the fish has a negative buoyancy and tends to sink (Jones, 1951). Absorption rates are relatively fast, which prevents swim-bladder burst, while the gas secretion is a slow process. During fast divings, the volume of the swim-bladder can not be correctly adjusted and the fish must compensate its buoyancy by action of its fins (Jones, 1951; Bertrand et al., 1999), which implies additional energy costs. However, the swim-bladder allows lower speeds for maintaining the hydrostatic equilibrium (Dotson, 1976). For example, skipjack have no gas bladder and pectoral fins much narrower than yellowfin, thus its minimum speed needed to maintain hydrodynamic equilibrium is higher than that of yellowfin (Shadwick and Syme, 2008). In addition, a wider swim-bladder can compensate for small pectoral fins (Magnuson, 1973)
Besides, tunas can use their negative buoyancy to practice the "gliding" swimming allowing to conserve energy. The gliding phase is characterized by the absence of propulsive movements, the fish slides downward and then goes back to the surface by active swimming (Fish, 2010).

1.1.3 Maintenance of a high metabolism

Although regional endothermy gives an obvious selective advantage to tunas (Shadwick et al., 2013), it is associated with a substantial metabolic cost. Indeed, as highlighted by several authors, tunas have significantly higher metabolic rates than other ectothermic teleosts (Graham and Laurs, 1982; Korsmeyer and Dewar, 2001; Blank et al., 2007). Standard metabolic rate (SMR) of tunas, i.e. the metabolic rate at the resting state for zero velocity, is 2 to 10 times greater than those for most other active fish and close to those of mammals (Bushnell and Jones, 1994; Korsmeyer and Dewar, 2001; Fitzgibbon et al., 2008).
In addition, related to their necessity of continuous swimming activity for ram-ventilation and maintaining sufficient lift, tunas can not suspend their aerobic activity in the red muscle which needs to be oxygenated. Thus, they have swimming rates of oxygen uptake 2-10 times higher than other swimmers species at comparable speeds (Dewar and Graham, 1994; Graham and Dickson, 2004). For instance, Sepulveda and Dickson (2000) observed, for fish of similar size at a temperature of 24°C, higher metabolic rates in juvenile kawakawa than in ectothermic mackerel due to an higher oxygen consumption.

The high metabolic rates of tunas are supported by physiological adaptations of a cardiorespiratory system allowing for a rapid oxygen delivery in tissues (Korsmeyer and Dewar, 2001). These adaptations included a large gill surface areas and a thin blood-water epithelia promoting high oxygen transfer rates (Bushnell and Jones, 1994). Tunas have a large heart with an extensive coronary circulation, a relatively high proportion of compact myocardium (Farrell and Jones, 1992) and myocardial fibers maximizing pumping efficiency (Korsmeyer et al., 1997; Brill and Bushnell, 2001). Moreover, the heart is characterizd by high levels of myoglobin

and aerobic enzyme activities (Swimmer et al., 2004) and rapid cardiac contraction frequencies (Korsmeyer et al., 1997).
Metabolic rates vary according to the species depending on the relative proportion and the operating mechanism of red muscles, its lift pectoral area and its endothermic capacities. For example, at 20°C, Pacific bluefin have metabolic rates about 37% higher than those of yellowfin for identical swimming speeds (Blank et al., 2007). Pacific bluefin have smaller pectoral fins, generating less lift than yellowfin, accordingly it swims with greater tailbeat frequency to maintain higher speeds (Blank et al., 2007). Higher tailbeat frequencies are likely to increase the oxygen demand for muscle activity and contribute directly to high metabolic rates (Blank et al., 2007).
As all species, the mass-specific metabolism of tunas decreases with increasing mass and therefore size (Fitzgibbon et al., 2008). In tunas, this decrease could be exacerbated because the caudal and pectoral fins are not fully developed in juveniles (Tamura and Takagi, 2009), which constrains them to more moves to maintain vertical position.

1.1.4 Distribution and movements

The endothermic lifestyle allows the exploitation of an extensive thermal niche (Block et al., 1993; Dickson and Graham, 2004) and access to food resources in colder waters than an ectothermic fish can tolerate. The "thermal niche expansion" results in the extension of their vertical habitat, i.e. diving below the thermocline, and geographical ranges (Brill et al., 1999).

A. Geographic distribution

With the exception of genus *Allothunnus*, the tunas are widely spread throughout the tropical and sub-tropical oceans and in oceanic and coastal ecosystems as far as 45°C North and South latitudes (Graham and Dickson, 2004). Small coastal tunas of genera *Auxis* and *Euthynnus* are strictly tropicals (Cayré, 1989). Blackfin and longtail are mainly tropical whereas yellowfin, bigeye and skipjack are circumtropicals, with a temperate affinity for bigeye. All three bluefin tunas and albacore have warmer tissues due to higher heat production and they are more frequently encountered in more temperate areas. Pacific bluefin have an elevated heart rate and high tailbeat frequencies resulting in an elevation of red muscles temperature, which allows a more extensive thermal-niche than tropical species (Blank et al., 2007).
As juvenile tunas have the vascular counter-current heat exchangers still poorly developed (section 1.1.1), they require warmer waters. Thus, yellowfin and bigeye less than 70 cm are almost exclusively tropical (Cayré, 1989).

B. Migration

Thanks to their highly efficient swimming mode, nine tuna species, albacore, Atlantic bluefin, bigeye, skipjack, yellowfin, blackfin, Southern bluefin and two species of

the genus Euthynnus, are considered as highly migratory species (United Nations Convention on the Law of the Sea [1]). Horizontal movements of tunas can be affected by geographic and bathymetric factor and dynamic oceanographic processes (Schaefer et al., 2011) and involve the need to reach either best foraging areas or more favorable waters for reproduction and offspring success (Bard et al., 1998; Shadwick et al., 2013).

C. Vertical movements

As demonstrated by several studies based on ultrasonic telemetry or archival tags (Brill et al., 1999; Dagorn et al., 2000; Schaefer et al., 2011), tunas routinely dive and reach the thermocline and sometimes much deeper waters. Vertical movements of tunas are limited by the cooling rate of body temperature and their tolerances to reduced oxygen concentrations occuring with depth (Brill, 1994).
In tunas, vascular heat exchanger systems slow the body temperature variations following abrupt reductions of water temperature consecutive to transitions from the surface layer to deeper and colder waters (Brill et al., 1998). Associated with high physiological tolerances at low dissolved oxygen concentrations (Brill, 1994; Fitzgibbon et al., 2010), tunas can then spend more time below the mixed layer. Generally, tunas dive to maximum depths during daytime whereas they remain in or closely the surface-layer during the nighttime (Dagorn et al., 2000; Schaefer et al., 2011). These deep divings are considered as alternative foraging strategies to access richer food sources.
Yellowfin spend most of their time above or immediately below the mixed surface-layer, at depths not exceeding 100 m, in water temperatures around 18°C (Block et al., 1997; Brill et al., 1999). They can make short divings below the thermocline up to 300-350 m (5-7°C) and the larger yellowfin occasionally descend over 500 m (Schaefer et al., 2011). The diving depths are limited by temperatures and by an ambient oxygen concentration of 3.5 ml $O_2.L^{-1}$ (Graham and Dickson, 2004). By contrast, bigeye are mainly encountered at depths from 100 to 500 m and frequently dive to greater than 500 m depth (Dagorn et al., 2000; Schaefer and Fuller, 2010). They can experiment prolonged exposure to temperatures up to 20°C colder than surface-layer and oxygen concentrations less than 1.5 ml $O_2.L^{-1}$ (Brill et al., 2005). With greater thermoregulatory capacity, Atlantic bluefin can experiment water temperatures up to 1°C. Adults and juveniles reside most of their time in surface-layer at depths not exceeding 50 m, they frequently dive to depth of 500–1000 m with short maximum depth exceeding 1,200 m depth (Block et al., 2001; Walli et al., 2009).

For most tuna species, adults have higher physiological tolerance to low temperatures, due to more efficient vascular heat exchanger systems, and to low dissolved oxygen concentrations than juveniles, which allows them to more extensive vertical movements, reach greater depths and spend more time below the thermocline (Brill et al., 1999). Thus, adult bigeye can reach maximum depths greater than 500

1. www.un.org/depts/los/convention_agreements/convention_overview_convention.htm

m whereas juveniles reach maximum depths less than 300 m (Brill and Lutcavage, 2001). Schaefer et al. (2011) evaluated that the yellowfin less than 60 cm F_L were not doing deep diving. As against, adult skipjack have higher oxygen requirements than juveniles and they are restricted to more limited vertical habitats.

1.1.5 Schooling behavior

Most tuna form schools which, depending on species or lifecycle stage, can be free or associated with floating objects, animals, topographic structures, or other tuna species. The principal hypothesis that has been put forward to explain the schooling behavior in tropical tunas is that of the meeting point.
Tuna would take several advantages of schooling including (i) reducing predation through a better predator detection and a decrease of individual capture probability, (ii) increasing the encounter rate for finding a mate and (iii) improving the foraging by increasing the research area or the hunting success (Fréon and Dagorn, 2000; Marsac et al., 2000). By contrast, schooling behavior might also result in increased intra and interspecies competition as well as enhanced detectability by predators.
Although the reasons for schooling behavior remain unclear, skipjack and juvenile yellowfin and bigeye ($<$ 60-70 cm) form mixed associated schools with natural or artificial floating objects, such as fish aggregating devices (FADs) which are artificial bamboo rafts equipped with radio buoys indicating their position and the presence of fish (Fonteneau et al., 2000; Ohta and Kakuma, 2005; Schaefer and Fuller, 2005). Larger yellowfin and bigeye can also be encountered around FADs, with shorter residence times, but generally form monospecific free-swimming schools in offshore areas. Adults bigeye, skipjack, black skipjack, frigate tuna and especially yellowfin can also be associated with dolphins (Fréon and Dagorn, 2000). Young Atlantic bluefin also form schools in areas of abundant food (Royer et al., 2004). Longtail, kawakawa and frigate tunas joined together in school near the coastal waters (Yesaki, 1987).

1.2 Tunas comparative growth

Tunas, as most of fish, grow throughout their life with rates highly variable between individuals. Their growth are controlled by endogenous endocrine factors (steroids, thyroid and hypophyseal hormones) and by various exogenous factors, whose the main are the temperature and the food availability. Sexual status, age or size, competition between individuals and fishing can also influence growth.

Historical studies on tunas growth, based on the most commonly used Von Bertalanffy model, surmised a rapid growth of juveniles and pre-adults that gradually decreasing through adulthood as asymptotic size approache, maximum size reached by the older fish (Mohan and Kunhikoya, 1985; Thorogood, 1987; Yesaki, 1987; Santiago and Arrizabalaga, 2005; Restrepo et al., 2010). However, for some species, the Von Bertalanffy model is not able to represent the complexity of

growth process, especially because of the succession of phases of acceleration and deceleration.
For yellowfin, more and more studies conducted in the three major oceans over the last fifteen years indicated a two-stanza growth characterized by a relatively slow growth during juvenile stage that accelerates at adulthood and then gradually decreasing as asymptotic size approache (Fonteneau, 1980; Gascuel et al., 1992; Gaertner and Pagavino, 1992; Lehodey and Leroy, 1999; Viera, 2005). More recently, this two-stanza growth pattern has been pointed out for Indian Ocean bigeye (Fonteneau and Gascuel, 2008; Nishida and Rademeyer, 2011) and skipjack (Eveson and Million, 2008).
Yellowfin could have a third stanza characterised by a fast growth of early juveniles followed by a slowdown from 35-45 cm. This third stanza was highlighted by some studies conducted in the Pacific Ocean (Yamanaka, 1990; Lehodey and Leroy, 1999) and it is suspected to occur in the Indian Ocean (Fonteneau, *com.pers.*). The faster growth in early juvenile stage was also found for the Southern bluefin (Hearn and Polacheck, 2003; Eveson et al., 2004), Bayliff (1991) observed that the growth of the Pacifc northern bluefin (*T.orientalis*) was best described by a two-stage model. To our knowledge, for other tuna species, no study has attempted to challenge the classical von Bertalanffy growth described by a unique stanza growth.

1.3 Which mechanisms behind the two-stanzas growth of yellowfin ?

Some authors ascribe the growth slowdown observed in the first stanza to the acquisition of sexual maturity (Gascuel et al., 1992; Lehodey and Leroy, 1999). These authors assume that gonad development and maturation processes require a great energy amount which might result in a deficit for the somatic growth. Indeed, the inflexion point between the two stanzas appears to correspond at the length at first maturity, defined as the length at which 50% of fish start to mature (L_{50}) , i.e. between 75 and 90 cm for Indian Ocean yellowfin (Rohit and Rammohan, 2009; Zudaire et al., 2013a).
In most species with determinate growth, such as mammals, growth accelerates with the onset of puberty due to some hormones produced by the gonads, this acceleration being usually more pronounced in males. When individuals acquire the reproduction ability, the growth slows dramatically and then stops (Karkach, 2006; Mcfee et al., 2009). In fish species, such a speeding growth consecutive to the onset of puberty has never been demonstrated. In addition, in many farmed fish, the spawning season goes with a slowdown in somatic growth (Norberg et al., 2001; Taranger et al., 2010). Therefore, there is currently no evidence that the observed slower growth might be due to sexual maturity acquisition.

Growth acceleration has also been assumed to be related to the development of the swim-bladder (Lehodey and Leroy, 1999; Lumineau, 2002). The bladder of yellowfin begins to grow at about 60 cm, which is close to the observed size of the growth acceleration. The gradual development of this bladder associated with fins

developement reduces the energy costs required for sustain the position in water column. Thus, a lower swimming metabolism would lead to an energy surplus for growth. However, other tuna species with a bigger swim-bladder than yellowfin, such as bluefin, do not show any growth acceleration in relation with the swim-bladder developement. Hence, the growth acceleration is unlikely to be directly associated with the development of swim-bladder or pectoral fins.

The developments of swim-bladder and pectoral fins contribute to the improvement of swimming abilities. Associated with other physiological changes, such as a better ability to maintain metabolic heat and higher physiological tolerances at dissolved oxygen concentrations, they can lead in behavioral and ecological changes resulting in an extension of the habitat and variations in food diet with potential impacts on growth. The sexual maturation and the transition to a sexually active state may also lead to behavioral changes.
The change in growth pattern could also result from the transition from a schooling behavior in shallow and warm waters to a more mobile behavior allowing for the spread in deeper and colder offshore waters. Juveniles yellowfin, less than 70 cm, have a rather sedentary behavior. They are usually located in shallow and warm equatorial waters between 10°N and 10°S (Stéquert and Marsac, 1986; Fonteneau and Gascuel, 2008) where most of them are gathered with skipjack and young bigeye associated with drifting objects. In such multi-species associations, the intra and inter-specific competition for food resource is probably strong (Bromhead et al., 2003). Indeed, studies on stomach contents indicate a lower feed intake for yellowfin in multispecies schools associated with FADs than those in monospecies free schools, suggesting that yellowfin in mixed associations are in poor health conditions (Potier et al., 2001; Hallier and Gaertner, 2008).
The enhancement of swimming performances and higher tolerances to low temperatures, due to the full development of vascular counter-current heat exchangers, lead to increasing migration trends. Thus, yellowfin between 70 and 100 cm become more mobile and are dispersed over a wider geographical area covering deeper and colder waters. These tunas, called *chicaneurs*, are weakly represented in the purse seine fishery catch (Fonteneau and Gascuel, 2008). They would have a rather solitary behavior and could migrate outside the fishing areas toward higher primary productivity waters in the nothern Indian Ocean, which could explain the growth acceleration observed for this size range.
Adults yellowfin, larger than 100 cm, are widely spread throughout the Indian Ocean, with the exception of South Australia because of the influence of Antarctic waters (Stéquert and Marsac, 1986). Although, they usually live in the first 100-150 m deep, they can dive below the thermocline contrary to juveniles (Schaefer et al., 2011). These divings are observed for individuals larger than 60-70 cm, which is close to the size of growth acceleration. Carried out during daylight, they are likely foraging strategies to access more energetic preys in deep waters. Indeed, in Indian Ocean, yellowfin feed on a wide variety of epipelagic and mesopelagic fish, crustaceans and cephalopods (Potier et al., 2007) and their diet varies according to size and foraging depth (Maldeniya, 1996; Potier et al., 2004).

1.4 Arguments against the growth stanza

The stanza could be an artefact resulting from a sexual dimorphism in growth. The existence of such sexual dimorphism is a commonly accepted assumption that has however been very little studied. It has been highlighted for the eastern Pacific yellowfin where Wild (1986) showed a significant divergence between males and females from 95 cm F_L, characterized by a faster growth for males which can reach larger asymptotic lengths. In the Atlantic and Indian Oceans, some authors showed an increasing proportion of males in the purse seine catch above 145 cm, with an accumulation of females in the size range 125-145 cm, suggesting a lower asymptotic length for females than for males (Albaret, 1977; Zhu et al., 2008). Thus, in case where the size-selective fishing would go along with a differential sex-specific selectivity, it could result in an "artificial" growth acceleration. However, sex-ratio is balanced up to 125 cm F_L, which is larger than size of growth acceleration (Figure 4.5).

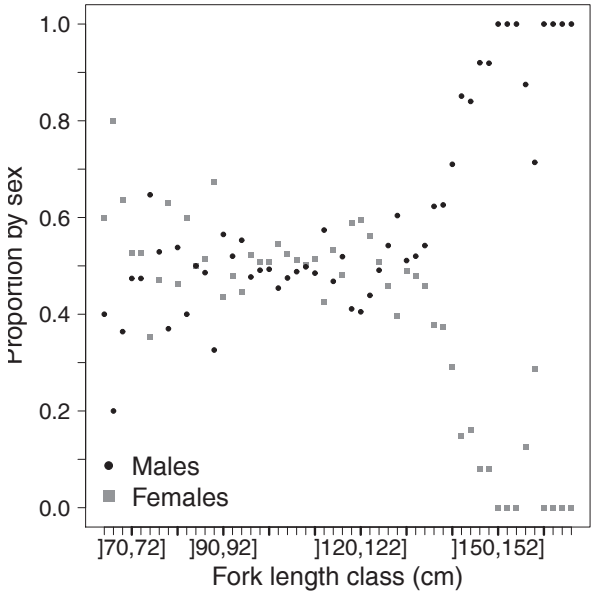

FIGURE 4.5 – Proportions of male and female yellowfin according to fish sizes in commercial fishing catches of Indian Ocean

According to some authors, the apparent two-stanzas growth would represent the effect of size-based fishing selectivity (Driggers et al., 1999; Kolody, 2011). In particular, purse seine fishing vessels target large mature individuals (90-130 cm F_L) in free swimming schools during the spawning season while catches of schools associated with FADs are mainly composed of small juveniles of yellowfin (40-60 cm F_L) for the rest of the year. The substantial difference in size structure of the catch between fishing modes and spatio-temporal area has been put forward to explain the apparent two-stanzas growth of yellowfin. The slow growing fish would spend more time under FAD and therefore they would be more vulnerable and for a longer period to a selective fishing for smaller sizes (Kolody, 2011). Conversely, the fast growing fish

may happen sooner in free schools and therefore they would be more vulnerable to a selective fishing for larger sizes. Thus the gear selectivity and the size-specific fishing pressure which, in addition to a high individual variability in growth, would lead to biased length-at-age samples (Taylor et al., 2005; Kolody, 2011). However, there is little evidence to support this assumption simulation studies showed that fishing selectivity had no influence on the yellowfin growth functional form (Hampton, 2008; Chassot et al., 2012).

1.5 Yellowfin life cycle

The yellowfin life cycle includes five different stages, embryo, larva, early juvenile, juvenile, pre-adult and adult (Figure 4.6).

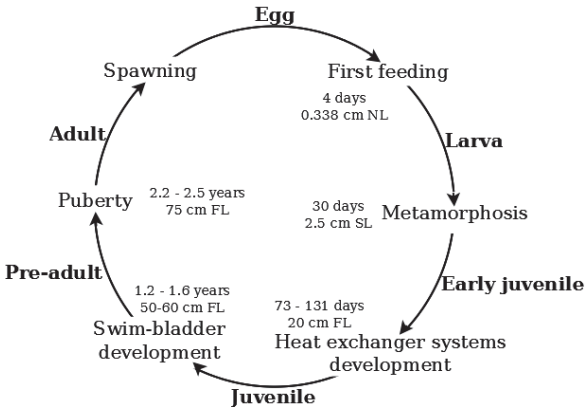

FIGURE 4.6 – Yellowfin life cycle recounts the stages (bold) and the transition events (normal) included in DEB model

The embryo stage includes the egg development and the first larva stages called *yolk-sac larva* and corresponds to individuals which do not feed but use the yolk reserves from the egg. In the yolk-sac larva, the digestive system begins to develop ; 4 days after hatching its structure is sufficiently developed and enables the larvae to ingest and digest exogenous nutrients. Concurrently, the upper and lower jaws are differentiated and the mouth is open and fully functional (Kaji et al., 1999). The first feeding gives the beginning of the larva stage. The larva then measures about 0.338 cm in notochordal length (N_L), i.e. length from the tip of the snout to the end of the notochord (Wexler et al., 2001; Margulies et al., 2007). During the larva stage, yellowfin undergoes significant transformations in both physiologically and morphologically, such as the development of spines and rays, vascular heat exchanger systems and a more efficiency digestive system. The larva grows exponentially.
The metamorphosis, marking the end of the larval phase, occurs 30 days after hatching and leads to an early juvenile. At this stage, the fish is about 1.3 cm in standard length (S_L), i.e. length from the tip of the snout to the posterior end of the last vertebra (Kaji et al., 1999). The early juvenile shows almost the same morphology as an adult, the most visible differences relating mainly to the fins that are much smaller and it maintains a relatively high growth rate. The early juveniles have not yet the

thermoregulation ability and they are, as the larvae, strongly vulnerable to surrounding temperature fluctuations.
The ability to maintain an elevated internal temperature in relation to the seawater temperature appears in yellowfin of approximately 20 cm F_L (Wexler et al., 2011). This ability is related to the presence of vascular heat exchanger systems based on a flow of blood against the current to keep the heat produced by metabolism (Graham and Dickson, 2001; Shadwick et al., 2013). The appearance of the ability to maintain metabolic heat marks the end of the early juvenile stage and the beginning of the juvenile stage itself. This ability will then progressively enhance through to adulthood (Cayré, 1989). In tunas, the end of the early juvenile stage would be associated with a decline in growth rate (Jusup et al., 2011).
The beginning of pre-adult stage, is marked by anatomical and physiological changes likely to lead behavioral changes and ultimately to expected growth acceleration. The swim-bladder, located in the viscera, becomes functional around 2 kg, i.e. 50-60 cm F_L, and then grows allometrically until the adulthood (Magnuson, 1973). Concurrently, yellowfin gain higher physiological tolerances to colder temperatures and lower oxygen concentrations and they start to dive below the thermocline (Schaefer et al., 2011).
The transition from pre-adult to adult stage is determined by the sexual maturity acquisition, a swim-bladder fully developed and optimal thermoregulation abilities and it is assumed to occur at about 75 cm F_L. Indeed, this size correspond to the length at which 50% of females reached sexual maturity estimated for Indian Ocean yellowfin (Rohit and Rammohan, 2009; Zudaire et al., 2013a). Moreover, the swim-bladder is entirely developed around 8 kg (Magnuson, 1973), i.e. between 70-75 cm F_L. According to Cayré (1989), heat exchanger systems are fully effective for fish larger than 70 cm.

1.6 Choice of a bioenergetic modelling approach

A bioenergetic model describes the energy balance relationship of an organism, at individual or population level, between the energy acquisition from feeding, its use for maintenance, growth, reproduction and activity and its losses by respiration, excretion or heat production (Brown et al., 2004; Nisbet et al., 2012). Bioenergetic modelling has been mostly used in fisheries research for growth studies (Kitchell et al., 1977; Hansen et al., 1993; Pecquerie et al., 2009). As an example, the Von Bertalanffy model, the most commonly used to describe fish growth, was originaly built to express the growth in weight as a function of the balance between the anabolism (synthesis) and the catabolism (degradation) in constant environmental conditions, i.e. constant temperature and food availability (Von Bertalanffy, 1957; Essington et al., 2001).

Two major bioenergetic approaches can be distinguished, the traditional approaches as opposed to the approach of Dynamic Energy Budget (Figure 4.7). The first are based on mass-balance equations in which the energy comes from consumed food, some part is lost through excretion or respiration and the rest

is allocated to metabolism, growth and reproduction (Hansen et al., 1993; Ney, 1993; Kitchell et al., 1977). The energy allocation rules can be readily modified to adjust at different organization levels or to take account for various biological or physical conditions (Hansen et al., 1993; Ney, 1993) and the parameter values can be directly estimated from measurements of growth, reproduction and respiration rates (Essington, 2003; Roff, 1983). Consequently, these approaches have been mostly used as powerful simulating tools for assessing fish growth or their reproduction pattern under various scenarios of temperature and food availability (Kitchell et al., 1977; Ney, 1993). However, the traditional bioenergetic models are often specific to a particular life cycle stage and are generally unsuitable for modelling the transitions between distinct stages of life, e.g. between larva and juvenile.

The Dynamic Energy Budget (DEB) theory considers that energy from food integrates a first compartment from which a fixed part is allocated to maintenance and growth and the rest is allocated to development or reproduction (Kooijman, 2010). The DEB theory has been successfully applied to describe jointly growth and reproduction under various food and temperature conditions of many species (Pecquerie et al., 2009; Freitas et al., 2010), to evaluate the effect of various contaminants on the organism performances (Nisbet et al., 1997) and, more recently, to study the evolution of populations and ecosystems (Nisbet et al., 2000; Maury and Poggiale, 2013). This theory provides a powerful conceptual framework to describe the full life cycle of an organism in a variable environment (Nisbet et al., 2012), which is, in our opinion, its greatest asset. But in return, a DEB model relies on many parameters difficult to estimate and the state variables of the model are directly neither observable nor measurable (van der Veer et al., 2006; Kooijman et al., 2008).

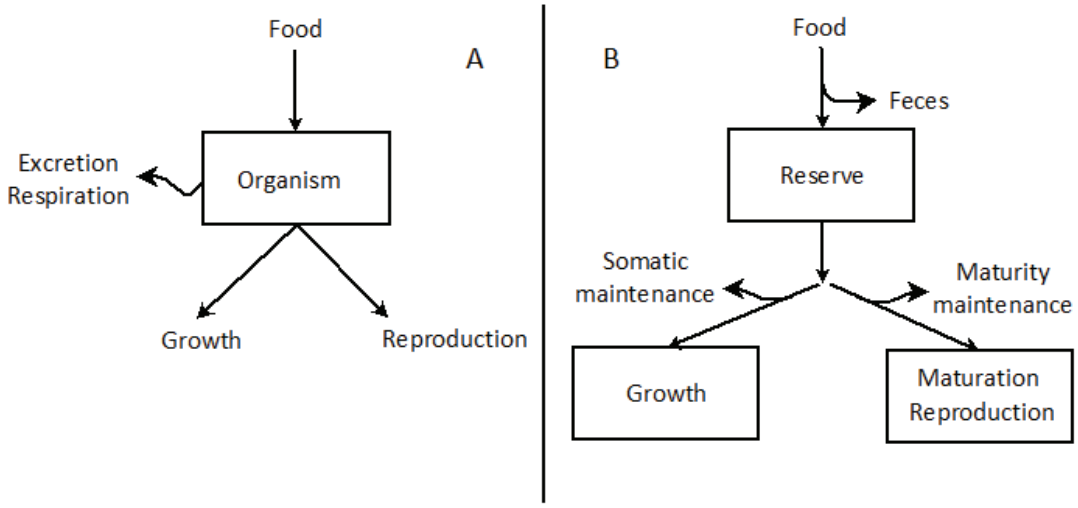

FIGURE 4.7 – Schematic representation of a traditional bioenergetic model (A) and a Dynamic Energy Budget model (B)

In the present study, we investigated, through the Dynamic Energy Budget (DEB) theory, two assumptions that we have considered as the most relevant to explain the growth acceleration observed for the wild population of Indian Ocean yellowfin. Both assumptions were related to changes in yellowfin behavior : (i) an improved nutrition due to a decrease in inter and intra-species competition for food resulting from the dispersion of yellowfin to offshore waters after a phase of associated schooling in warm surface and generally more coastal waters and (ii) a food diet change characterized by the consumption of more caloric prey due to the vertical and horizontal expansion of habitat. We also looked for the effect of increasing thermoregulation abilities.

2 Materials and methods

2.1 Design of a Dynamic Energy Budget model for yellowfin

2.1.1 Dynamic Energy Budget theory

Conceptually, the DEB theory partitions the fish in two main compartments, reserve and structure which are distinguished by their dynamics, and a lesser compartment of maturation or reproduction (Figure 4.8).
Reserve does not mean storing for a later use, but refers to the whole organism compounds that can be metabolized to fuel metabolic processes. The reserve does not require maintenance. The reserve content depends on food availability, size and energy mobilisation for maintenance, growth, maturation or reproduction. The ingested food by an organism undergoes energy losses related to digestion and faeces production and the remaining energy goes to the reserve.
Structure refers to all fundamental compounds for survival and achievement of basic life functions. The increase of structural biomass is not directly affected by food availability but depends on both energy that can be mobilised from the reserve and previously built structure which implies somatic maintenance costs. The somatic maintenance includes all metabolic processes required to maintain the fish alive and it implies energy costs proportional to structural volume for some and to structural surface area for other (Kooijman, 2010). The energy mobilised from the reserve is first allocated to the somatic maintenance and the rest is used to the growth of structural biomass which involves costs of converting the energy of reserve into structure, as the chemical composition of both compartments are different (Kooijman et al., 2008; Jusup et al., 2011).
Maturation corresponds to physiological complexity of organism and involves all the functions which are not absolutely necessary for survival, such as immune system or gametes development. The increase of the maturity level, i.e. organism complexity, depends on energy that can allocated from the reserve once the maturity maintenance costs paid. These cost are proportional to the level of maturity previously acquired. An organism becomes progressively more complex so as to achieve adult stage, able to reproduce. At this stage, the organism is fully developed and does not mature any more. The energy is then redirected to a reproduction buffer. This latter is a storage compartment of the same composition as the reserve.

Growth in length is only related to the increase of structural biomass, while the weight gain depends on the increase of structural biomass, the energy amount of reserve and the energy stored in reproduction buffer. The energy invested for the maturation does not contribute to the weight, this energy being dissipated in form of heat or metabolites (Kooijman, 2010).

2.1.2 State variables and dynamics of a standard DEB model

According to the conceptualisation of the DEB theory, three states variables can be defined, the energy amount of the reserve, E, the structural length, L_v and the maturity level E_H. The energy stored in the reproduction buffer is quantified by an auxiliary variable E_R whose dynamics is zero in sexually immature individuals. The dynamics of the state variables and the status of the reproduction buffer are controlled by various energy fluxes whose specifications allow to define a DEB model (Figure 4.8 and Table 4.1).

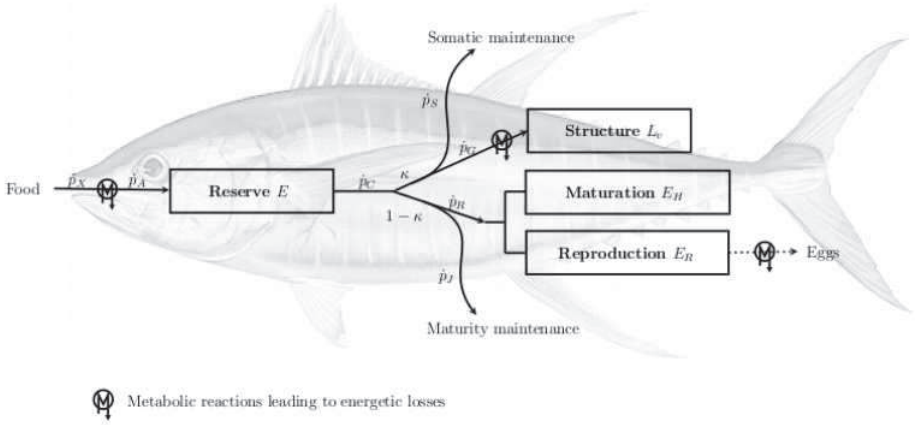

FIGURE 4.8 – Conceptual representation of a Dynamic Energy Budget model for yellowfin tuna

Specifically, fish ingests and assimilates some energy amount into the reserve depending on environmental food availability, its surface-area of assimilation and its conversion efficiency of food. The assimilation process involves energy losses related to digestion and faeces. The energy reserve is then mobilized according to the κ-rule : a fixed fraction κ is allocated to *soma*, i.e. in order of priority, somatic maintenance and growth, and the rest $(1-\kappa)$ is allocated to maturity maintenance and maturation for juvenile. As from puberty, the energy allocated to maturation is redirected to reproduction. In the standard DEB model, κ is constant and does not depend on the energy amount of reserve nor the amount of structure (Kooijman, 2010).

TABLE 4.1 – Energy fluxes ($J.d^{-1}$) used in the yellowfin DEB model ; all parameters are definied in Table 4.2

Metabolic process	Energy flux
Ingestion	$\dot{p}_X = \{\dot{p}_{Xm}\} f L_v^2 = \frac{\{\dot{p}_{Am}\} f L_v^2}{\kappa_X}$
Assimilation	$\dot{p}_A = \frac{\dot{p}_X}{\kappa_X} = \{\dot{p}_{Am}\} f L_v^2$
Mobilisation	$\dot{p}_C = [E_m] L_v^3 \left(\frac{\dot{v}}{L_v} + \dot{k}_M \left(\frac{L_v + L_T}{L_v} \right) \right) \frac{eg}{e+g}$
Somatic maintenance	$\dot{p}_S = \{\dot{p}_T\} L_v^2 + [\dot{p}_M] L_v^3$
Growth	$\dot{p}_G = \frac{\kappa \dot{p}_C - \dot{p}_S}{[E_G]}$
Maturity maintenance	$\dot{p}_J = \dot{k}_J E_H$
Maturation or reproduction	$\dot{p}_R = (1-\kappa)\dot{p}_C - \dot{p}_J$

The standard DEB model deals with an isomorphic organism that keeps the same body shape over its lifespan. Three life stages are considered, embryo, juvenile and adult. An embryo becomes a juvenile at the time of first feeding and a immature juvenile becomes a fully developed adult suited for the reproduction at maturity threshold $E_H = E_H^p$. In this study, we have not considered the embryonic stage.
As the energy dimension is not necessary to estimate the growth and to simplify the model, the reserve can be replaced by the scaled reserve density $e = [E]/[E_m]$, a dimensionless quantity. $[E] = E/L_v^3$ is the reserve density and $[E_m] = \{\dot{p}_{Am}\}/\dot{v}$ represent the maximum reserve density. The dynamics in the standard DEB model are then described by the following differential equation system :

$$\frac{de}{dt} = (f - e)\frac{\dot{v}}{L_v} \tag{4.1}$$

$$\frac{dL_v}{dt} = \frac{\dot{v}}{3(e+g)} \left(e - \frac{L_v + L_T}{L_m} \right) \tag{4.2}$$

$$\frac{dE_H}{dt} = \begin{cases} (1-\kappa) \times \dfrac{\{\dot{p}_{Am}\}}{e+g} \times \left(e \left(g + \dfrac{L_v + L_T}{L_m} \right) \right) \times L_v^2 - \dot{k}_J \times E_H & \text{if } E_H < E_H^p \\ 0 & \text{else} \end{cases} \tag{4.3}$$

$$\frac{dE_R}{dt} = \begin{cases} 0 & \text{if } E_H < E_H^p \\ (1-\kappa) \times \dfrac{\{\dot{p}_{Am}\}}{e+g} \times \left(e \left(g + \dfrac{L_v + L_T}{L_m} \right) \right) \times L_v^2 - \dot{k}_J \times E_H^p & \text{else} \end{cases} \tag{4.4}$$

All parameters are described in Table 4.2. Here is considered the case of an individual after hatching which is defined as the first feeding. Before hatching, the scaled functional response $f = 0$.

2.1.3 Forcing variables

The standard DEB theory considers two environmental variables forcing the metabolic processes and therefore the model outputs, the temperature and the food density.

Temperature. All the metabolic rates are controled by enzymatic processes which activity depend on body temperature. Within the species-specific temperature tolerance range, the Arrhenius (1889) relationship expresses the sensitivity of metabolic rates to changes in temperature :

$$\dot{k}(T) = \dot{k}(T_1) exp\left(\frac{T_A}{T_1} - \frac{T_A}{T}\right) \tag{4.5}$$

T is the body temperature (in Kelvin), T_A is the Arrhenius temperature, T_1 is a chosen reference temperature, $\dot{k}(T)$ is the value of a metabolic rate $\dot{k}$ at a temperature T. All parameters with a time dimension referring to physiological processes, such as $\{\dot{p}_{Am}\}$, $\dot{v}$, $[\dot{p}_M]$, $\{\dot{p}_T\}$ and $\dot{k}_J$, depend on body temperature and must be corrected when this one varies.

Food density. The feeding or ingestion rate depends on environmental food availabilty, or food density X, and fish ability to acquire food. The Holling type II scaled functional response converts the food availability into ingestion. It is a dimensionless quantity definied as :

$$f = \frac{X}{X + X_k} \tag{4.6}$$

X is the environmental food density and X_k is the half-saturation constant that account for the fish ability to uptake food. This function represents the ratio between the food amount available for feeding and the food amount that can be ingested by the fish. For low food density, the fish ingests all the food available with a rate which depends on time spent to foraging, uptake and food processing. A feeling of satiety appears gradually and leads to a progressive decrease in the rate of ingestion depending on the food density. For a strictly monophagous fish, the ingestion rate $\dot{p}_X$ (J.cm^{-1}) can then expressed as :

$$\dot{p}_X = \{\dot{p}_{Xm}\} f L_v^2 \tag{4.7}$$

$\{\dot{p}_{Xm}\}$ is the specific maximum ingestion rate per unit of surface (J.day^{-1}.cm^{-2}) which only depends on maximum abilities of fish to foraging and process food.
The assimilation rate corresponds to the ingestion rate minus the energy losses due to the conversion of food into the energy reserve (digestion) and the energy lost in

faeces. The assimilation efficiency, denoted by κ_X, is considered as independent of the feeding rate. Thus the assimilation rate $\dot{p}_A$ remains proportional to ingestion rate so that the surface-area specific maximum assimilation rate $\{\dot{p}_{Am}\} = \kappa_X\{\dot{p}_{Xm}\}$. The assimilation rate can then be directly linked to the food density through f as follows :

$$\dot{p}_A = \{\dot{p}_{Am}\} f L_v^2 \tag{4.8}$$

Growth under constant environmental conditions. In constant temperature and food density conditions, the scaled functional response f is constant and the energy density in reserve does not vary. Thus, $e = f$ and the standard DEB model predicts a Von Bertalanffy growth (Appendix C). The asymptotic length L_∞ and the growth rate coefficient k_{VB} of Von Bertalanffy can then be expressed from the DEB parameters as follows :

$$L_\infty = \frac{f L_m}{\delta_j} - L_T = \frac{f\kappa\{\dot{p}_{Am}\} - \{\dot{p}_T\}}{\delta_j[\dot{p}_M]} \tag{4.9}$$

$$k_{VB} = \frac{\dot{v}}{3L_m(f+g)} = \frac{\dot{v}[\dot{p}_M]}{3(f\kappa\{\dot{p}_{Am}\} + \dot{v}[E_G]} \tag{4.10}$$

The food density affects both the asymptotic length and the growth rate coefficient while the temperature does not affect the ultimate length achieved by the fish, but only the rate at which this length is reached.

2.1.4 Additional assumptions for yellowfin

A. Additional life stage

The implemented DEB model for yellowfin started to metamorphosis and three life stages were considered, early juvenile, juvenile and adult (Figure 4.6 in section 1.5). The stage transitions occured at defined thresholds of maturity level. Thus, an early juvenile became a juvenile when $E_H = E_H^e$ and a juvenile became a fully developed adult when $E_H = E_H^p$.
The early juvenile yellowfin are unable to raise their body temperature above the seawater temperature. This capacity, linked to the storage of the metabolic heat through vascular heat exchanger systems, appears in the end of early juvenile stage, when the fish size is about 20 cm F_L (Wexler et al., 2011). Raising the body temperature involves costs expressed through the parameter L_T. L_T is interpreted as the reduction of the ultimate structural length that a strictly ectothermic individual could reach due to energy costs of heating. To account for these additional costs, the parameter L_T was fixed to zero until the end of early juvenile of juvenile stage, i.e. as long as $E_H < E_H^e$.

B. Reproduction module

After reaching the puberty, the fish accumulates energy in the reproduction buffer throughout the year according to Eq.4.4, but the standard DEB model does not

describe how an individual uses the energy stored in the buffer. Thus, a reproduction module which defined yellowfin-specific handling rules of the energy stored in the buffer was implemented. Defining the species-specific handling rules is important because the energy stored in the buffer contributes to body mass.
For Indian Ocean yellowfin, the spawning season takes place twice a year, a main season from November to March and a minor period from June to August (Stéquert et al., 2001; Zhu et al., 2008; Zudaire et al., 2013a). During a spawning season, the energy stored in the reproduction buffer is converted to eggs that are released in different batches. Spawning has been shown to occur almost daily (Wexler et al., 2003; Margulies et al., 2007), but no information is available on the batch number spawned per season. In addition, the batch fecundity, i.e. the number of eggs released by batch, increases with the female size and varies strongly from one female to another of the same size (Zudaire et al., 2013a). Thus, to simplify the model, the spawning seasons were triggered cyclically every 6 months once the maturity level at the puberty reached. Thus, a time-dependent sinusoidal function with a period of 182 days was definied :

$$S(t) = sin\left(2\pi\frac{t}{182}\right) \tag{4.11}$$

For adult stage, i.e. when $E_H > E_H^p$, as soon as $S(t) > 0$, the reproduction buffer is fully emptied.

2.1.5 Link between state variables and fishery observations

The state variables of a DEB model correspond to hidden states that are non-directly measurable. Thus, additional assumptions and parameters were defined to connect the state variables with the various available observations that have been used to calibrate and validate the DEB model developped for yellowfin.
The physical length F_L (cm) of fish only provides information on the structural length L_v. F_L is proportional to L_v and both lengths can be connected using a species-specific shape parameter δ_j :

$$F_L = \frac{L_v}{\delta_j} \tag{4.12}$$

The wet weight W_W (g) has contributions from structure W_v, reserve W_E and reproduction buffer W_{E_R} and it expresses as follows :

$$\begin{aligned} W_W &= W_v + W_E + W_{E_R} \\ &= d_v L_v^3 + \frac{E + E_R}{\rho_E} \end{aligned} \tag{4.13}$$

where d_v is the density of the structural volume (g.cm^{-3}) and ρ_E the energy content of 1 g of reserve, the reproduction buffer has the same chemical composition as the reserve.

The absolute fecundity AF, i.e. the total number of eggs released during a spawning period, is calculated as follows :

$$AF = \frac{\kappa_R E_R}{E_0} \tag{4.14}$$

κ_R represents the converting cost of the energy of reproduction buffer in egg. It is fixed to 0.95 as for most species (Kooijman, 2010). E_0 is the energy content of one egg has been evaluated from caloric values known for other scombroid species. Comparing the lipid profiles from eggs of wild Atlantic bluefin tuna (*Thunnus thynnus*) and bonito (*Sarda sarda*), Ortega and Mourente (2010) have shown similar lipid contents for both species which were approximately 20% of the dry mass. According these authors, the lipid content corresponded to 7.953 J.mg^{-1}, i.e. 26.4% of the total caloric value of a freshly spawned egg. From these observations and knowledge of mean dry weight of an egg of captive yellowfin, estimated at 0.043 mg (Margulies et al., 2007), we were able to deduce a value of 1.295 J for E_0 :

$$E_0 = \frac{0.043 \times 7.954}{0.264} \tag{4.15}$$

From AF, the batch fecondity BF is estimated for a batch number N_B :

$$BF = \frac{\kappa_R E_R}{E_0 N_B} \tag{4.16}$$

The estimated BF can then compared to the observed batch fecundity for yellowfin to check the realism of the order of magnitude of the energy allocated to the reproduction buffer and thus the energy balance of the organism.

We also define the reproductive investment IR as the ratio between the weight of reproduction buffer and the wet weight of fish :

$$IR = 100 \times \frac{W_{E_R}}{W_W} = 100 \times \frac{E_R}{d_v \rho_E L_v^3 + E + E_R} \tag{4.17}$$

This latter provides information on the weight losses due to the spawning activity. As it depends on both the growth in weight and the reproduction, it allows for checking the energy balance.

The daily energy intake (J.kg^{-1}.day^{-1}) is use to check the consistency of model outputs in relation with the values of daily caloric consumption found in literature. It can be calculated according to the following relationship :

$$\text{Daily energy intake} = \frac{f\{\dot{p}_{Am}\} L_v^2}{\kappa_X W_W} \tag{4.18}$$

where $\{\dot{p}_{Am}\}$ must be corrected to account for body temperature variations according to Eq.4.5. κ_X is the digestive capacity, i.e. the fraction of energy from ingested food fixed in the reserve ; its value was considered equal to 0.8, a commonly used value when fish are fed with non-processed food [2].

2. http://www.bio.vu.nl/thb/deb/deblab/add_my_pet/Species.html

2.1.6 Parameters

The whole system was characterized by eighteen parameters (Table 4.2) : (i) seven primary parameters, κ, $\{\dot{p}_{Am}\}$, $\dot{v}$, $[\dot{p}_M]$, $\{\dot{p}_T\}$, $[E_G]$ and $\dot{k}_j$, control the system dynamics, (ii) three parameters, E_H^j, E_H^e and E_H^p, control the transition stages, (iii) three parameters, δ_j, d_v and ρ_E, connect the state variables to the observation variables, (iv) two parameters, T_A and X_k, allows to take account of the environnemental conditions, (v) two parameters, E_0 and κ_R, are required to regulate the use of energy stored in the reproduction buffer and (vi) one parameter, κ_X, allowed to link the feeding and assimilation rates.

TABLE 4.2 – List of parameters used in yellowfin DEB model

Definition	Parameter	Unit
Primary parameters		
Fraction of mobilised reserve allocated to soma	κ	-
Surface-area specific maximum assimilation rate	$\{\dot{p}_{Am}\}$	$\mathrm{J.d^{-1}.cm^{-2}}$
Energy conductance	$\dot{v}$	$\mathrm{cm.d^{-1}}$
Volume-specific somatic maintenance rate	$[\dot{p}_M]$	$\mathrm{J.d^{-1}.cm^{-3}}$
Surface area-specific somatic maintenance rate	$\{\dot{p}_T\}$	$\mathrm{J.d^{-1}.cm^{-2}}$
Volume-specific costs of structure	$[E_G]$	$\mathrm{J.cm^{-3}}$
Maturity maintenance rate coefficient	$\dot{k}_J$	$\mathrm{d^{-1}}$
Maturation threshold for metamorphosis	E_H^j	J
Maturation threshold for end of early juvenile stage	E_H^e	J
Maturation threshold for puberty	E_H^p	J
Fraction of food energy fixed in reserve	κ_X	-
Link parameters		
Shape parameter for juvenile and adult stages	δ_j	-
Structural volume density	d_v	$\mathrm{g.cm^{-3}}$
Weight-energy coupler	ρ_E	$\mathrm{J.g^{-1}}$
Arrhenius temperature	T_A	K
Half saturation constant	X_k	$\mathrm{J.cm^{-3}}$
Reproduction module parameters		
Energy costs of one egg	E_0	J
Fraction of reproduction energy fixed in eggs	κ_R	-
Compound parameters		
Scaled functional response	$f = \dfrac{X}{X + X_k}$	-
Energy investment ratio	$g = \dfrac{\dot{v}[E_G]}{\kappa\{\dot{p}_{Am}\}}$	-
Structural heating length	$L_T = \dfrac{\{\dot{p}_T\}}{[\dot{p}_M]}$	cm
Maximum structural length	$L_m = \dfrac{\kappa\{\dot{p}_{Am}\}}{[\dot{p}_M]}$	cm

2.2 Data selection

2.2.1 Wild Indian Ocean yellowfin

A. Length-at-age data

Length and age data were collected during the Regional Tuna Tagging Project (RTTP, Chapter 1, section 1) and the West Sumatra Tuna Tagging Project (WSTTP, section 2). Saggital otoliths were collected from (i) 128 yellowfin caught during 2005-2012 through the RTTP measuring between 43-72 cm F_L at tagging and 47.9-135.4 cm F_L at recapture, (ii) 18 fish caught in 2007 through the WSTTP measuring between 19-29 cm F_L and (iii) 35 fish collected from 2008-2009 at the Indian Ocean Tuna Ltd (IOT) cannery and measuring between 31-147.5 cm F_L.
The ages of the fish were estimated from repeated otolith readings with the model described in Chapter 2 (section). Developed in a hierarchical Bayesian framework, this model includes expert judgment and it explicitly accounts for some process and interpretation errors in otolith readings i.e. (i) bias in accretion rate estimated by the reader, (ii) loss of increments at the nucleus and edge and (iii) error in counting and interpreting missing increments from multiple readings of the same otolith.

B. Length-weight data

Length and weight data corresponded to measurements made on defrosted yellowfin caught in the whole Indian Ocean basin : (i) 5089 fish from the IOT Ltd cannery caught in 2005-2012 measuring 66-165 cm F_L and weighing 5.8-87.5 kg and (ii) 212 collected in 2010-2013 as part of the EMOTION project (Chapter 1, section 4) measuring 29-157.7 cm F_L and weighing 0.4-91 kg.

C. Fecundity data

Data from Zudaire et al. (2013a) were used to investigate the relationship between the fork length and the batch fecundity. Zudaire et al. (2013a) were estimated the number of eggs released per batch estimated by counting the oocytes in the germinal vesicle migration or hydration stages. 40 females from 79 to 146.9 cm F_L collected on board of commercial purse seiners in the western Indian Ocean during 2009-2010 were used. The batch fecundity varied from 0.32 million to 6.91 million eggs with a mean of 3.07 million eggs.

2.2.2 Farmed Pacific yellowfin

In order to calibrate and validate the model, the experimental data described in the publication of Wexler et al. (2003) were used. Regarding Pacifc tuna, these data are part of the few experimental data currently available for this species. These data involved 55 yellowfin (53% females, 46% males) caught in 1996 and in 1998 in the coastal waters of the northwest Panama Bight. Measuring 32.5-81.2 cm F_L and weighing 1.8-10.6 kg at catch, these fish were transferred in a broodstock yellowfin

tank at the Achotines Laboratory in the Republic of Panama.

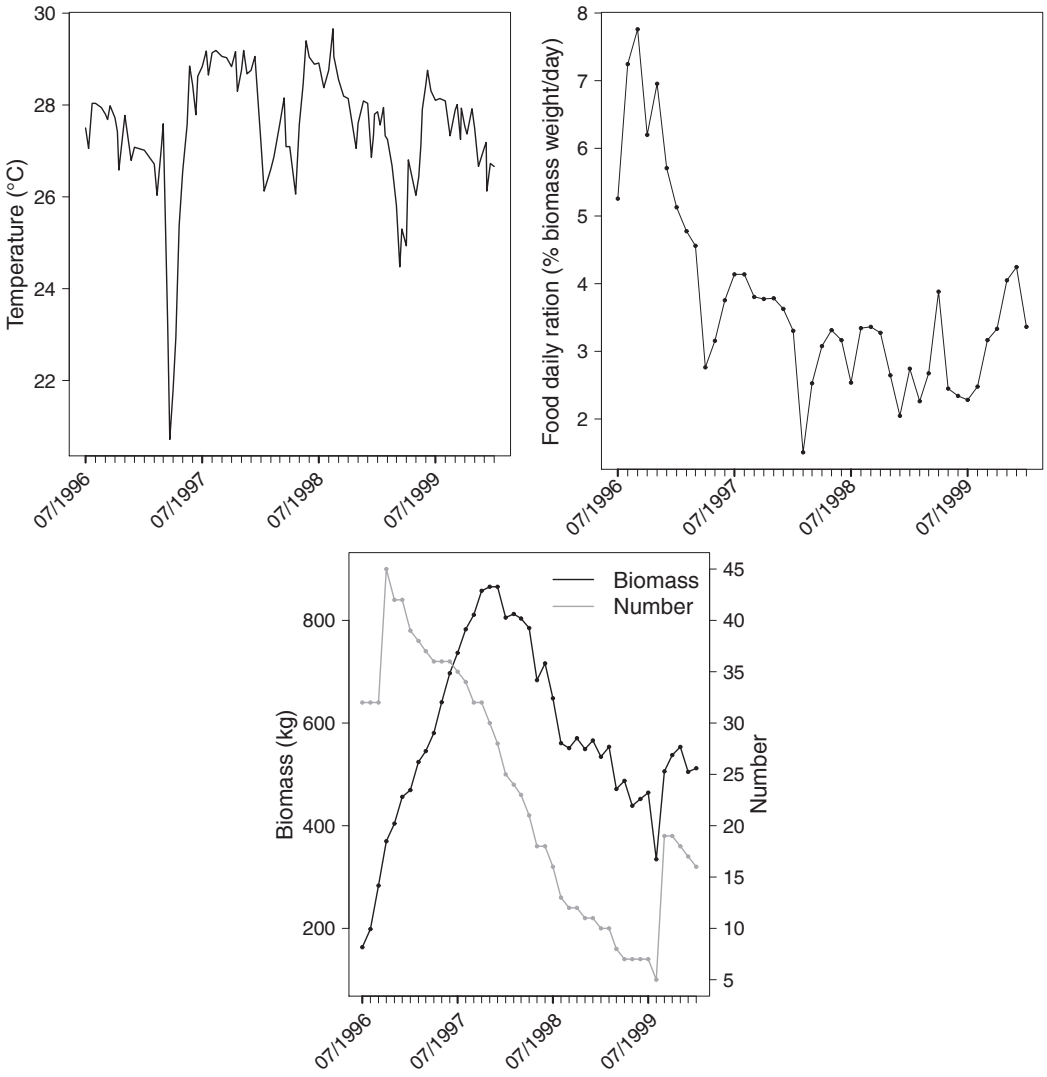

FIGURE 4.9 – Daily temperature, daily food ration and daily estimates of biomass and number of yellowfin in tank from July 1996 to December 1999 from Wexler et al. (2003)

The tank was filled with seawater and semi-open to ocean, thus the temperature and salinity in tank were influenced by the seasonal fluctuations in ocean upwelling and rainfall (Table 4.3). The experiment lasted over 3 years, from June 1996 to December 1999. During the experiment, daily temperatures in tank ranged from 20.1 to 29.7°C with an average of 27.5°C (Figure 4.9). Yellowfin were fed once day with one of five prey species. The caloric values of prey, calculated based on metabolizable energy values of protein (4.23 kcal.g^{-1}) and lipid (8.0 kcal.g^{-1}), were given. The food daily rations (FDR) expressed as a percentage of wet weight biomass per day and the progression of the total biomass and fish number in tank were also given (Figure 4.9).

TABLE 4.3 – Main characteristics of broodstock tank from Wexler et al. (2003)

Diameter × depth (m)	Capacity (m^3)	Temperature (°C)	Salinity (‰)	Dissolved O_2 ($mg.L^{-1}$)	pH	Water exchange rate ($m^3.day^{-1}$)
17 × 6	1362	20.1-29.7	26-36.1	4.23-7.7	7.6-8.3	7

The length and weight of fish were measured at the time of the transfer in the tank and their death and the authors fitted a Von Bertalanffy growth curve from the informations on growth rates between transfer and death. They also fitted a power regression function to the length-weight data (Figure 4.10). A food conversion ratio (FCR) was calculated as the ratio between the wet weight of ingested food on increasing biomass over given times intervals of 12–103 days with a constant yellowfin number.

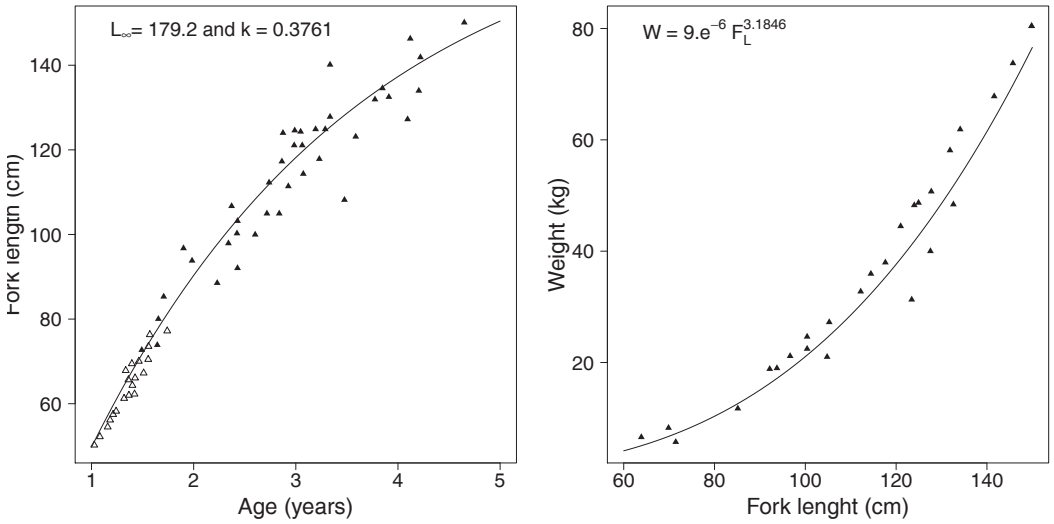

FIGURE 4.10 – Growth in length and length-weight relationship of yellowfin in tank from Wexler et al. (2003) ; △ corresponds to measurements at transfer in tank and ▲ to measurements at death

2.3 Length-weight relationship for wild yellowfin

From the length-weight data from EMOTION project, the length-weight relationship for wild yellowfin was examined with the power function $W = aF_L^b$ conventionally used for tunas (ICCAT, 2013) where W is the wet weight (kg) and F_L the fork length (cm). Given a fish i, the following Bayesian model was implemented :

$$W_i = aF_{L_i}^b + \varepsilon_i \tag{4.19}$$

with the weight measurement errors ε_i assumed to be independent and normally distributed around zero with a common variance σ^2. Gamma distributions defined from the reference values of ICCAT for Atlantic yellowfin were considered as weakly

informative priors for the parameters a and b. Both gamma distribution were caracterised by a 5% coefficient of variation and by a mean of $2.153.10^{-5}$ kg.cm^{-1} and 2.976 for a and b respectively. The standard deviation σ was assigned uninformative inverse gamma distribution.
Posterior distributions of a, b and σ were obtained from Markov Chain Monte Carlo (MCMC) simulations using the Metropolis-within-Gibbs sampling algorithm implemented in *BRugs* package of statistical software R (R Development Core Team, 2010). Three chains starting at contrasting initial values were considered and the convergence of the MCMC to stationary posterior distribution was checked from the second half of MCMC simulation using the Gelman-Rubin diagnostic (Gelman and Rubin, 1992). This diagnostic is based on the ratio of inter-chain variance on intra-chain variance that should be close to 1 for getting convergence.

2.4 Model calibration

In this section, informations found in the literature for Pacific bluefin tuna were used to reproduce using simulations the data described in the experimental study of Wexler et al. (2003). All simulations were performed with the *dde* function, a numerical solver for delay differential equations of the *PBSddesolve* package (Couture-Beil et al., 2010) in R software (R Development Core Team, 2010).

All simulations were performed in constant conditions of food density X (J.cm^{-3}) expressed through a scaled functional response f fixed to the value of 0.925. Indeed, it was possible to evaluate f values consistent with the biology of yellowfin. As against, the food density is a difficult variable to handle and as no information was available for this variable, nor for X_k, the choice of their values was difficult to justify. According the X_k value, a small variation of f may be behind a significant or negligible variation in the food density (Figure 4.11).

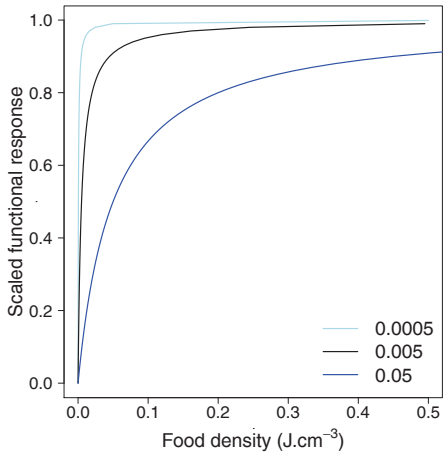

FIGURE 4.11 – Holling type II scaled functional response patterns for different half-saturation constants

2.4.1 Comparison between yellowfin and bluefin tuna

In practice, estimating of complete set of DEB parameters poses persistent difficulties and require extensive datasets regarding the different key biological functions. First, most of parameters correspond to non-directly measurable quantities related to several state variables and they must be jointly estimated. Secondly, the state variables correspond to hidden states and are related to one another. Indeed, although the physical length is only linked to the structural biomass, the body mass depends at once on structural biomass, reserve and energy stored in reproduction buffer.

Based on the metabolic properties leading to differences in ultimate size among phylogenetically related species, *the rule of the body-size scaling relationships* allows to benefit from information on other species for a first parameters estimate. The primary parameters of a DEB model may be classified as intensive or extensive. The first are related to biochemical processes assumed roughly invariant among species of a given taxon, e.g. genus, family or order, while the latter depend on maximum size because they are related to the physical design and vary from one species to another (Kooijman, 2010; Nisbet et al., 2012). Specifically, the surface-area specific maximum assimilation rate, $\{\dot{p}_{Am}\}$, and the maturity thresholds, E_H^j, E_H^e and E_H^p, varying systematically with the maximal structural length L_m. These parameters can be directly adjusted using a zoom factor z defined as the ratio of the maximum structural length of species of interest to that of the reference species.

As datasets available for yellowfin are insufficient to estimate a complete parameters set, we used the rule of the body-size scaling relationships to infer the parameter values of yellowfin from those of adult Pacific bluefin tuna (*Thunnus orientalis*) obtained by Jusup et al. (2011) (Table 4.4). These authors have been developed a model very close to that proposed in this study. To estimate the parameters of their model, they used observations on growth, relationship between weight and length, hatching depending on the temperature and batch fecundity from Pacifc bluefin farmed at at research station on Amami Island in southern Japan.
Let $\{\dot{p}_{Am}\}$, E_H^j, E_H^e and E_H^p the parameters for Pacific bluefin (PBT), the parameters become $z\{\dot{p}_{Am}\}$, $z^3E_H^j$, $z^3E_H^e$ and $z^3E_H^p$ for yellowfin (YFT). The zoom factor $z = L_{m_{\mathrm{YFT}}}/L_{m_{\mathrm{PBT}}}$ was defined for a Pacific bluefin of maximum structural length of 214.7 cm and for a yellowfin of maximum structural length estimated according to Eq.4.9 from a physical asymptotic length fixed to 200 cm F_L. This value was in agreement with the the maximum sizes observed in commercial fishery catches. For both species, the values of maximum structural length were obtained for constant conditions of food density and temperature, i.e. $f = 0.925$ and $T = 298K$.

The growth in length, relationship between length and weight and annual reproductive investment (IR, Eq.4.17) of both tuna species were simulated and compared. The simulations were performed under constant conditions of body temperatures of $298.5K$ and $298K$ for bluefin and yellowfin respectively. The state

of the system at metamorphosis was considered as initial condition (Table 4.5).

TABLE 4.4 – Parameter values of Pacific bluefin tuna at a reference temperature of 25°C from Jusup et al. (2011)

Parameter	Unit	Value
κ	$-$	0.7807
$\{\dot{p}_{Am}\}$	$J.d^{-1}.cm^{-2}$	4783.707
$\dot{v}$	$cm.d^{-1}$	7.056
$[\dot{p}_M]$	$J.d^{-1}.cm^{-3}$	17.39483
$\{\dot{p}_T\}$	$J.d^{-1}.cm^{-2}$	2215.415
$[E_G]$	$J.cm^{-3}$	8563.387
$\dot{k}_j$	d^{-1}	0.06117797
δ_j	$-$	0.2704164
ρ_E	$J.g^{-1}$	7763.975
d_v	$g.cm^{-3}$	1
T_A	K	5298.838
T_1	K	298
E_H^j	J	6902.209
E_H^e	J	969476
E_H^p	J	25484395.636
E_0	J	3.75
κ_R	$-$	0.95
L_m	cm	214.7061

2.4.2 Estimating Arrhenius temperature T_A

The Arrhenius temperature T_A was deduced from the value of van't Hoff coefficient Q_{10} given by Dewar and Graham (1994) for juveniles Pacific yellowfin, i.e. 1.65 at 18-24°C and 1.67 at 24-30°C. The Q_{10} is a correcting factor applied to metabolic rates for every 10°C increase in temperature. For any body temperature T, Q_{10} and T_A are related according to the following relationship :

$$Q_{10} = exp\left(\frac{10T_A}{T(T+10)}\right) \tag{4.20}$$

2.4.3 Estimating link parameters δ_j, d_v and ρ_E

Juveniles do not store energy for reproduction, thus their wet weight W_W receives contributions from both the structure W_v and the reserve W_E and it expresses as follows :

$$W_W = W_v + W_E = d_v L_v^3 + \frac{E}{\rho_E} \tag{4.21}$$

with $L_v = \delta_j F_L$ and $E = [E].L_v^3$, δ_j is the shape parameter, d_v is the structural volume density (g.cm^{-3}) and ρ_E is the weight-energy coupler (J.g^{-1}). Given a fish i

of fork length F_L, the following Bayesian model was then implemented assuming no measurement error on length and weight :

$$W_{w_i} = \left(\delta_j^3 F_{L_i}^3 \left(d_v + \frac{[E]_i}{\rho_E}\right)\right) \times \psi_i \tag{4.22}$$

where ψ_i is the process error.
The model was fitted to 87 immatures yellowfin collected in the Indian Ocean. These fish measured between 29 and 61 cm F_L and weighed between 0.39 and 4.2 kg.
d_v was assigned a normal distribution centered on 1. δ_j was assumed to vary according to a beta prior distribution between 0 and 1. ρ_E was fixed such that the ratio of ρ_E to δ_j was the same as Jusup et al. (2011). The reserve densities $[E]_i$ and the process error ψ_i were assigned uninformative priors through inverse gamma distributions. The estimates of parameters were based on conventional sampling approach of Markov Chain Monte Carlo simulations as implemented in OpenBugs version 3.2.1 (Spiegelhalter et al., 2011). The convergence of the MCMC to the stationary posterior distribution was evaluated by the Gelman-Rubin diagnostic (Gelman and Rubin, 1992) from the second half of MCMC simulation sample.

2.4.4 Adjustment of maturity thresholds E_H^j, E_H^e and E_H^p

Yellowfin have a shorter life expectancy than Pacific bluefin and they reach earlier the end of early juvenile stage and the puberty. Thus, the maturity thresholds E_H^e and E_H^p were reappraised such that the end of early juvenile stage correspond to a size of 20 cm F_L and the puberty to a size close to 75 cm F_L in agreement with available knowledge from literature (Wexler et al., 2011; Zudaire et al., 2013a). In addition, the metamorphosis occurres at approximately 13 mm standard length (S_L) for yellowfin (Kaji et al., 1999) against 16 mm S_L for bluefin (Tanaka et al., 2007) and the maturity threshold E_H^j was also reappraised. As the thermo-conservation ability, marking the end of the early juvenile stage, appears at the same size for both species (Jusup et al., 2011; Wexler et al., 2011), E_H^j was adjusted for tuna such that the ratio E_H^e/E_H^j of bluefin was kept and we verified that the new value for E_H^j led to a size of 13 mm.

2.4.5 Simulating farmed yellowfin data

The final set of parameters obtained in the previous modeling steps was used to simulate the data described in the study of Wexler et al. (2003), i.e. growth in length, length-weight relationship, food daily ration (FDR) and food conversion ratio (FCR). The FDR (% body wet weight / day) was calculated as the ratio between wet weight of ingested food W_X and the wet weight of an individual W_W at each time step t of the simulation, i.e. 1 day.

$$FDR = 100 \times \frac{W_{X_t}}{W_{W_t}} \tag{4.23}$$

The FCR was defined as the ratio between the wet weight of ingested food and increased wet weight of an individual over time interval of 1 day. To be consistent

with the calculation of Wexler et al. (2003), the weight of reproduction has been ignored for the FCR.

$$FCR = \sum_{t=n}^{t=n+1} \frac{W_{X_n}}{(W_{v_{n+1}} + W_{E_{n+1}}) - (W_{v_n} + W_{E_n})} \tag{4.24}$$

The wet weight of ingested food was calculated using the following equation for $dt = 1$ day :

$$W_{X_t} = \frac{f\{\dot{p}_{Am}\} L_{v_t}^2 dt}{\kappa_X \rho_X} \tag{4.25}$$

κ_X is the digestive capacity fixed to 0.8 and ρ_X is the energy content of 1 g of food estimated from the caloric value of preys (Wexler et al., 2003). As the species offered to farmed yellowfin for a given day was not specified, three values illustrating the range of possible levels in terms of energy were used for ρ_X. These values corresponded to the most energetic species (6471.556 J.g^{-1}), the less energetic species (2980.432 J.g^{-1}) and the mean (4910.178 J.g^{-1}).
In accordance with the reproduction pattern of yellowfin, two spawning periods per year were considered and the simulation outputs of reproductive investment (IR, Eq.4.17) and absolute fecundity (AF, Eq.4.14) were examinated. The batch fecundity (BF) was estimated from AF for a variable batch number N_B (Eq.4.16) and compared to the batch fecundity observed for Indian Ocean yellowfin (Zudaire et al., 2013a).

Assuming yellowfin had no need to raise their body temperature for the seawater temperature range of the tank, the body temperatures were considered equivalent to the daily temperature measurements. The parameters $\{\dot{p}_{Am}\}$, $\dot{v}$, $[\dot{p}_M]$, $\{\dot{p}_T\}$ and $\dot{k}_J$ were corrected for temperature changes with Eq.4.5. The age and length at the beginning of the experiment were considered as initial conditions, i.e. an age of 395 days and a length of 53 cm F_L from which we deduced the structural length L_v and the corresponding E_H value (Table 4.5).

Table 4.5 – Initial conditions for Pacific bluefin (PBT) and yellowfin (YFT) for simulations regarding (1) the comparison between bluefin and yellowfin, (2) captive yellowfin and (3) wild yellowfin

State variable	PBT	YFT		
		1	2	3
Scaled reserve density e	0.925	0.925	0.925	0.925
Structural length L_v (cm)	1.525	0.35154	13.52892	0.33267
Maturity level E_H (J)	6902.209	5263.279	2460526	1368.719
Investment in reproduction E_R (J)	0	0	0	0
Age (days)	37	30	395	30

2.5 Investigating mechanisms behind the growth stanzas

In this section, two main assumptions likely to explain the growth stanzas observed for yellowfin were investigated using simulations, (i) a decrease of competition for food resource due to change in schooling behavior, (ii) a food diet change due to habitat change and improvement of some physiological traits. For each situation considered, the growth in length and the length-weight relationship were simulated and compared to data of wild Indian Ocean yellowfin. The seasonal reproductive investment (IR, Eq.4.17) and the daily energy intake (Eq.4.18) were also examined. The simulations were run from metamorphosis to death of fish with a time step of 1 day (Table 4.5) under constant temperature of 27°C.

2.5.1 Competition for food resource

In mixed associated schools, the inter and intra-species competition for food resource is assumed to be strong which could result in lower food intake by young yellowfin as compared to adults. In a DEB model, this is expressed by a lower value of food density modeled through a lower scaled functional response. Thus, two functional responses, f_j and f_p for juvenile and adult stages respectively, were defined such as $f_j < f_p$ and the effect of an abrupt transition from f_j to f_p was investigated. Four values of f_j were tested, 0.8, 0.825, 0.85 and 0.875, for a value of f_p fixed to 0.925. The transition was considered occur at 70 cm F_L which corresponds to the size at which the yellowfin leaves the schools associated with FADs.

2.5.2 Food diet change

Early juveniles and juveniles forage in shallower and warmer waters than adults, they might have access a range of prey which might be not as nutritious as for larger yellowfin. This was expressed in our DEB model through a surface-area specific maximum assimilation rate lower for juveniles than adults. Thus $\{\dot{p}_{Am}\}_j$ and $\{\dot{p}_{Am}\}_p$ were defined such that $\{\dot{p}_{Am}\}_j < \{\dot{p}_{Am}\}_p$. Hence, the effect on growth of an abrupt transition from $\{\dot{p}_{Am}\}_j$ to $\{\dot{p}_{Am}\}_p$ on growth was investigated. We considered two values of $\{\dot{p}_{Am}\}_j$, 3900 and 4000 J.day^{-1}.cm^{-2}, for a value of $\{\dot{p}_{Am}\}_p$ fixed to 4370 J.day^{-1}.cm^{-2}. The transition between these maximum assimilation rates was assumed to occur at 60 cm F_L, i.e; the minimum size of fish exhibiting deep dives (Schaefer et al., 2011). These simulations were performed with a constant functional response of 0.925.

2.6 Changes in body temperature

We also investigated the effect on growth of an increasing ability to maintain a body temperature (T) above the seawater temperature (T_a) due to the enhancement of vascular heat exchanger systems (section 1.1.1). These systems are set up at the end of early juvenile stage and gradually develop until the puberty resulting in a higher deviation between T and T_a. For yellowfin, deviations of more than 5°C were

measured (Cayré, 1989). To take account for the ability of yellowfin to increase heat-regulation, the following correction was implemented :

$$T = T_a + 5 \times \frac{min(max(E_H, E_H^e), E_H^p) - E_H^e}{E_H^p - E_H^e} \begin{cases} T = T_a & \text{if} \quad E_H \leqslant E_H^e \\ T_a < T < T_a + 5°\text{C} & \text{if} \quad E_H^e < E_H < E_H^p \\ T = T_a + 5°\text{C} & \text{if} \quad E_H \geqslant E_H^p \end{cases} \tag{4.26}$$

where T and T_a were expressed in °C. The simulations was performed under constant functional response of 0.925 and constant seawater temperature of 22°C.

3 Results

3.1 Length-weight relationship

The scaling exponent b obtained through the Bayesian fitting of a power-regression model to the length-weight data was 3.039. According the Bayesian 95% credibility interval, this value was significantly higher than 3 (Table 4.6). The joint posterior distribution was considered to be stationary as indicated by a Gelman-Rubin diagnostic of 1.06.

The standard DEB theory deals with an isomorphic individual, i.e. an individual that does not change in shape during the life. An isomorphic individual that does not reproduce should have a wet weight proportional to the cube of the physical length under constant food density conditions. In adult yellowfin, the weight contribution of reproduction buffer is important. Females accumulates energy in the reproduction buffer throughout the years which is released in the form of yolk reserve in eggs over the spawning season and can result in significant weight losses.

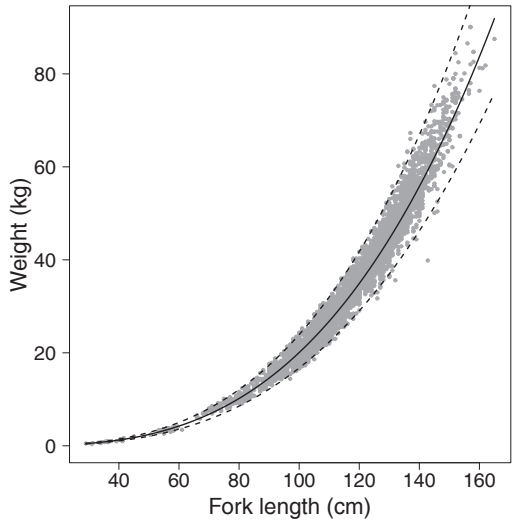

FIGURE 4.12 – Length-weight relationship of yellowfin tuna as estimated by Bayesian procedure ; the solid line representes the mean relationship and the dotted lines represente the limit of the 95% credibility interval

TABLE 4.6 – Mean, standard deviation (Std.dev) and credibility interval for parameters of length-weight relationship

Parameter	Mean	Std.dev	Posterior quantiles	
			2.5%	97.5%
a	$1.673.10^{-5}$	$7.975.10^{-7}$	$1.537.10^{-5}$	$1.844.10^{-5}$
b	3.039	0.0098	3.018	3.056
σ	4.056	0.024	4.012	4.112

3.2 Calibration of a yellowfin DEB model

3.2.1 Primary parameters from Pacific bluefin tuna

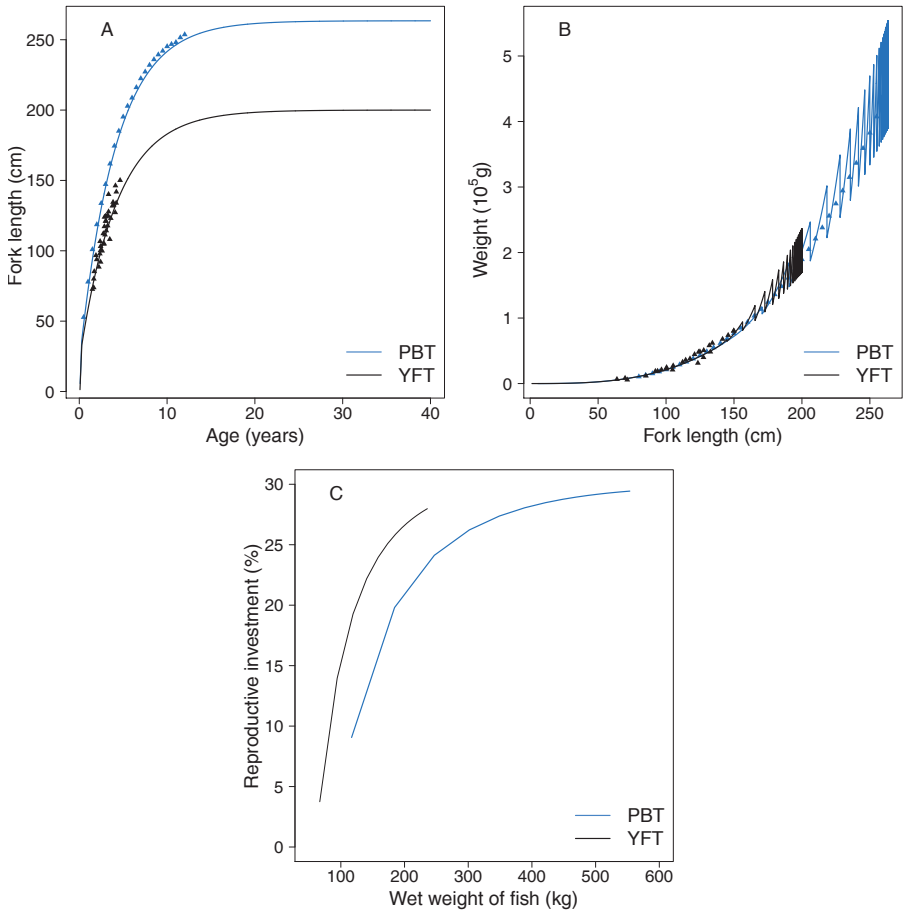

FIGURE 4.13 – Representation of growth in length (A), length-weight relationship (B) and reproductive investment (in % of body wet weight, C) of Pacific bluefin (PBT Jusup et al., 2011) and yellowfin (YFT) ; ▲ represents the captive fish data

Comparing the model predictions with the observation collected from farmed bluefin and yellowfin showed that (i) the model developed in this study was able to reproduce the changes in length and weight of Pacific bluefin and (2) the primary

parameters of yellowfin were inferable from those of Pacific bluefin tuna. The parameters set used is that described in the study of Jusup et al. (2011) for a reference temperature of 293 K (Table 4.4). For the yellowfin, the same parameters values were used, with the exception of $\{\dot{p}_{Am}\}$, E_H^j, E_H^e and E_H^p that were corrected with the zoom factor. The obtained values were thus 3226.6 J.day^{-1}.cm^{-2} for $\{\dot{p}_{Am}\}$, 5,263.3 J for E_H^j, 739,279.9 J for E_H^e and 19,433,126 J for E_H^p.

The difference between the model described in Jusup et al. (2011) and the model developed in this study concerns the ability acquisition of maintain a high body temperature. In both models, this acquisition resulted in an additional energy cost. In the model of Jusup et al. (2011), this additional cost appears to metamorphosis and gradually increases until the end of the early juvenile stage. In our model, this additional cost appears at the end of the early juvenile stage.

The length-weight relationships and the growth in length of bluefin tuna showed a good agreement with the data. For yellowfin, growth in length for larger individuals (> 130 cm) was a bit underestimated (Figure 4.13). The predicted values of length and age at the end of early juvenile stage and at puberty were higher than what has been observed for wild Indian Ocean yellowfin. This indicates that the obtained values for maturity thresholds E_H^e and E_H^p were not appropriate. Thus, the model predicted the end of early juvenile and the puberty at 32.85 cm for 106 days and at 136.45 cm for 4.4 years respectively. In wild yellowfin, the end of early juvenile corresponded to a length of 20 cm and an age between 73-131 days and the puberty was reached at about 75 cm at 2.2-2.5 years.
The reproductive investment, i.e. the energy amount accumulated for reproduction in the buffer, increased with the body mass to reach slightly about 30% of total body wet weight in older fish, i.e. 69.5 kg for a a fish of 235.8 kg (Figure 4.13).

3.2.2 Arrhenius temperature T_A

From the Q_{10} values of Pacific yellowfin found in the literature for juvenile yellowfin, the Arrhenius temperature was estimated at 4622.495 ± 207 K. This value was lower that of bluefin, about 5298 K, determined from (Jusup et al., 2011) from incubation time of egg according different temperatures. This indicated that yellowfin are less sensitive to temperature variations within their temperature tolerance range.

3.2.3 Link parameters δ_j, d_v and ρ_E

The estimates of the shape parameter δ_j, the structural volume density d_v and the weight-energy coupler ρ_E were derived from Bayesian inference of the length-weight relationship for immature yellowfin (Table 4.7). The Gelman–Rubin diagnostic of 1.0 for each parameter indicated the model convergence. The model proved able to reproduce the length-weight data (Figure 4.14). The values for the reserve density $[E]$, varying between 340 and 749 J.cm^{-3} according fish size, were consistent with the values given by the previous model for both bluefin and yellowfin in juvenile stage.

According to the Bayesian credibility interval, d_v was significantly higher of 1. This results was in agreement with the observation that tuna have a density greater than seawater (Magnuson, 1973).

TABLE 4.7 – Mean, standard deviation (Std.dev) and credibility interval of link parameters as estimated by Bayesian inference

Parameter	Mean	Std.dev	Posterior quantiles	
			2.5%	97.5%
δ_j	0.2559	0.0048	0.2455	0.2628
d_v	1.0821	0.0643	1.0013	1.2337
ρ_E	7346.034	136.6962	7046.95	7545.025

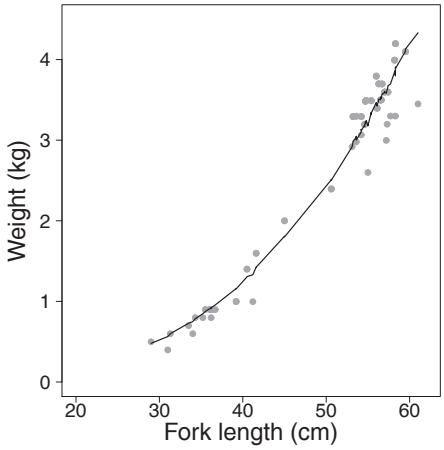

FIGURE 4.14 – Length-weight relationship for immature yellowfin estimated with DEB parameters (solid line) and relationship observed for wild yellowfin (grey circles)

3.3 Model validation using captive yellowfin data

From the model calibrated from the primary parameters of bluefin and the new values estimated for δ_j, d_v, ρ_E and T_A, the maturity thresholds E_H^j, E_H^e and E_H^p have been reappraised and led to the parameters set described in Table 4.8. Simulation outputs based on this latter parameters set were in very good agreement with the features described in the study of Wexler et al. (2003). The model successfully reproduced the growth in length and the length-weight relationship. What is more, the observed values of FDR and FCR were well within the simulated range (Figue 4.15). The puberty was reached at 1.61 years, at a length of 74.77 cm F_L, which was consistent with the observations on wild and farmed yellowfin used in this study (Wexler et al., 2003; Zudaire et al., 2013a).

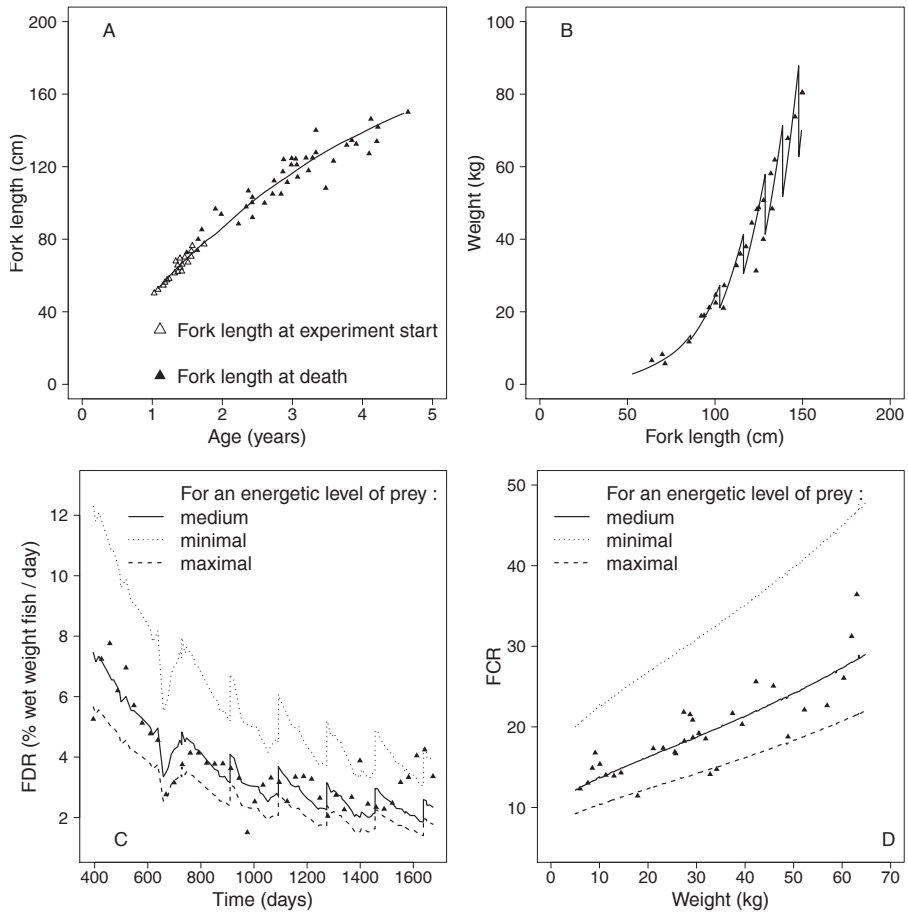

FIGURE 4.15 – Model validation by comparing simulation outputs with captive yellowfin data (▲ Wexler et al., 2003) : growth in length (A), length-weight relationship (B), food daily ration (FDR, C) and food conversion ratio (FCR, D). Simulation was performed with a constant functional response of 0.925 and with daily body temperatures equal to the seawater temperature variations in tank.

From the energy stored in the reproduction buffer at the time of reproduction, the absolute fecundity per spawning season was evaluated. The absolute fecundity was divided by a variable number of egg and compared with the data of batch fecundity per length for Indian Ocean yellowfin. The mean batch number per spawning season was thus visually estimated between 30 and 60, resulting in a spawning duration from 1 to 2 months with one spawn per day (Figure 4.16.A).
The energy stored in the reproduction buffer was also converted in weight to determine the seasonal reproductive investment. This investment increased with fish size and it was estimated at 28.5% of total body wet weight for fish of 87 kg. It varied with the temperature and was higher when the temperature increased (Figure 4.16.B).

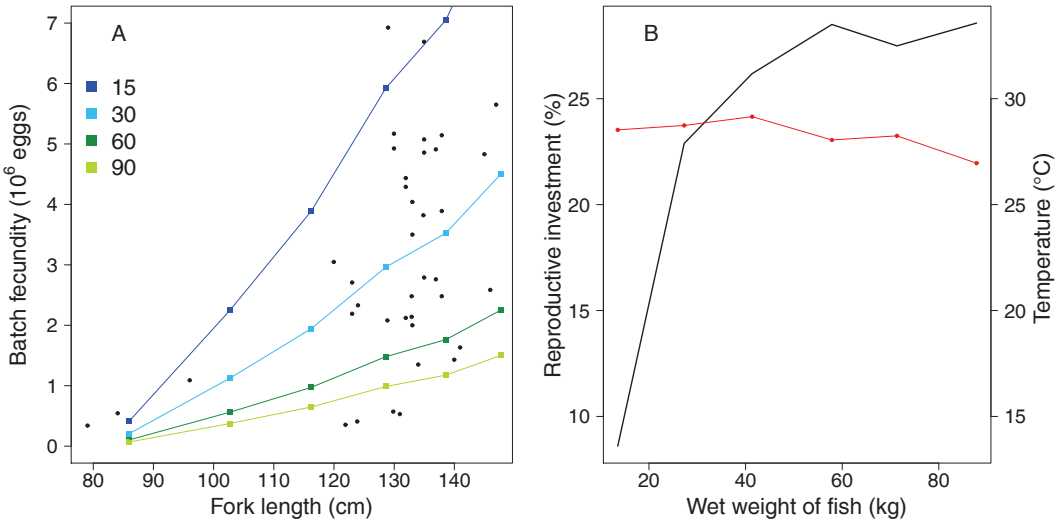

FIGURE 4.16 – Mean batch fecundity for different batch number scenarios compared with batch fecundity of wild yellowfin (A ; Zudaire et al., 2013a) and reproductive investment per spawning season (B, black curve) in relation to ambiant temperature (B, red curve)

TABLE 4.8 – Parameter values estimated for reference model of yellowfin at 25°C

Parameter	Unit	Value
κ	–	0.7807
$\{\dot{p}_{Am}\}$	$J.day^{-1}.cm^{-2}$	4370.394
$\dot{v}$	$cm.day^{-1}$	7.056
$[\dot{p}_M]$	$J.day^{-1}.cm^{-3}$	17.39483
$\{\dot{p}_T\}$	$J.day^{-1}.cm^{-2}$	2215.415
$[E_G]$	$J.cm^{-3}$	8563.387
$\dot{k}_j$	day^{-1}	0.06117797
δ_j	–	0.2559
ρ_E	$J.g^{-1}$	7346.034
d_v	$g.cm^{-3}$	1.0821
T_A	K	4622.495
T_1	K	298
E_H^j	J	1368.719
E_H^e	J	192248.7
E_H^p	J	5053598
E_0	J	1.295
κ_R	–	0.95

3.4 Investigation for a two-stanzas growth

3.4.1 Reference model

Subsequently, the previous model validated with the captive yellowfin data and run with a constant temperature of 27°C and a constant food density expressed by a scaled functional response of 0.925 is called "reference model" (Table 4.8). This model resulted in a Von Bertalanffy type growth which appeared suitable for adult growth but overestimated juvenile growth (Figure 4.17). The puberty, which is determined above all else to the sexual maturity acquisition, was reached at a length of 74.85 cm, which was consistent with the length of 50% maturity observed for wild yellowfin (Zudaire et al., 2013a). However, this length was reached in the model at an age of 1.4 years, which appeared early compared to the 2.2-2.5 years forecasted by the growth curve of Indian Ocean yellowfin (Chapter 3). The evolution of weight relative to length was higher than expected as evidenced by the predicted length-weight relationship exceeding the upper limit of the 95% Bayesian credibility interval estimated from wild yellowfin data (Figure 4.17).

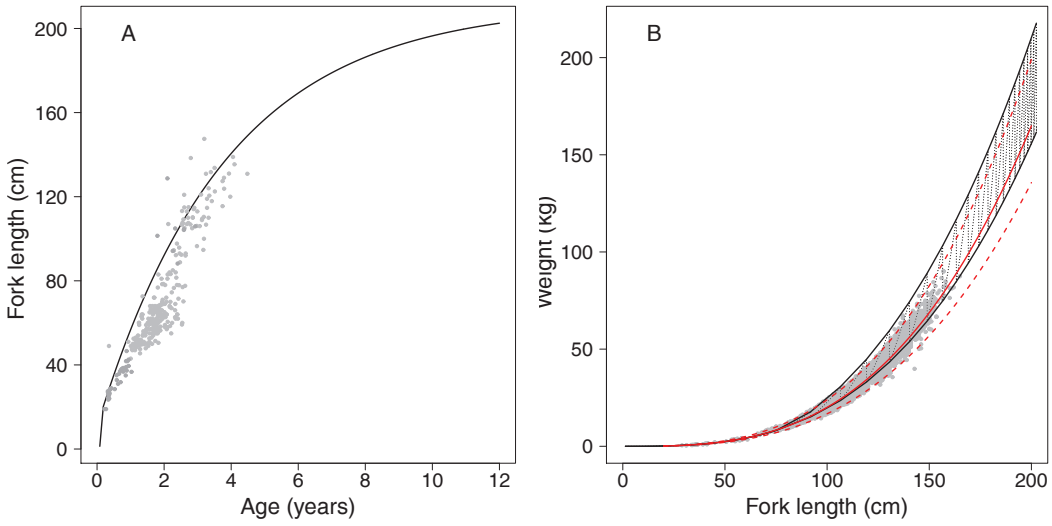

FIGURE 4.17 – Comparaison of growth in length (A) and length-weight relationship (B) as simulated by the reference model in constant condition of temperature (27°C) and food density ($f = 0.925$) with wild yellowfin data •. The solid red line represents the mean length-weight relationship previously estimated and the dotted red lines represent the limits of the 95% Bayesian credibility interval (Figure 3.1)

The seasonal reproductive investment increased with the size up to 27.8 % of body wet weight at 150 cm F_L and then slightly decreased to 25.9% (Figure 4.18.A)
For yellowfin heavier than 10 kg, the reference model predicted a daily energy intake between 69.07 and 213.7 kJ.kg^{-1}.day^{-1}, which is comparable with the values of caloric consumption observed for yellowfin, ranging from 37 to 435 kJ.kg^{-1}.day^{-1} (Figure 4.18.B ; Mourente and Tocher, 2009).

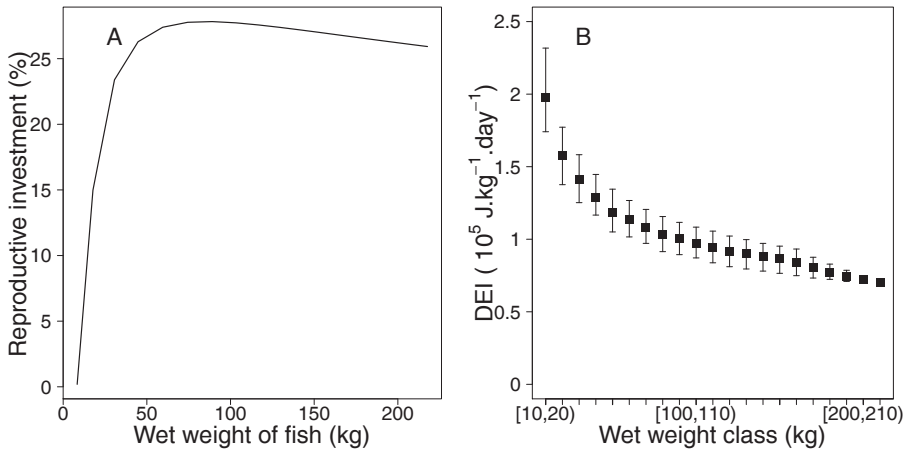

FIGURE 4.18 – Seasonal reproductive investment (A) and daily energy intake (DEI, B) as simulated by the reference model in constant condition of temperature (27°C) and food density ($f = 0.925$). In B, the black squares represent the mean and the vertical lines represent the variability.

3.4.2 Effect of different food density levels

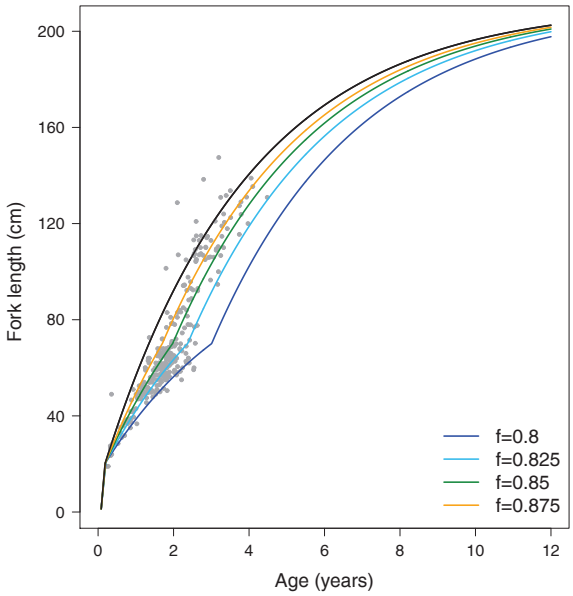

FIGURE 4.19 – Simulation of growth curve under the assumption of a decrease in food availability during the juvenile stage on the growth. The black curve corresponds to the reference model and the grey circles represent the wild yellowfin data

The assumption of a decrease in food availability during the juvenile stage resulted in a stanza growth by reducing the juvenile growth rates. Among the various values of f tested for juveniles, 0.8 led to an underestimation of growth and 0.875 to an overestimation. With a value between 0.825 and 0.85, the model captured the juvenile

growth but underestimated the growth thereafter (Figure 4.19 and Table 4.9). The variation in food availability did not result in a significant change in the length-weight relationship or in the seasonal reproductive investment. The values of daily energy ingestion were comparable to those obtained with the reference model.

TABLE 4.9 – Age and physical length predicted by simulations on food density variations

Value of f_j	End of early juvenile stage		Puberty	
	Age (day)	Fork length (cm)	Age (year)	Fork length (cm)
0.8	75	20.72	3.14	74.97
0.825	74	20.65	2.5	74.89
0.85	72	20.5	2.11	74.9
0.875	71	20.44	1.83	74.89

3.4.3 Effect of a food diet change

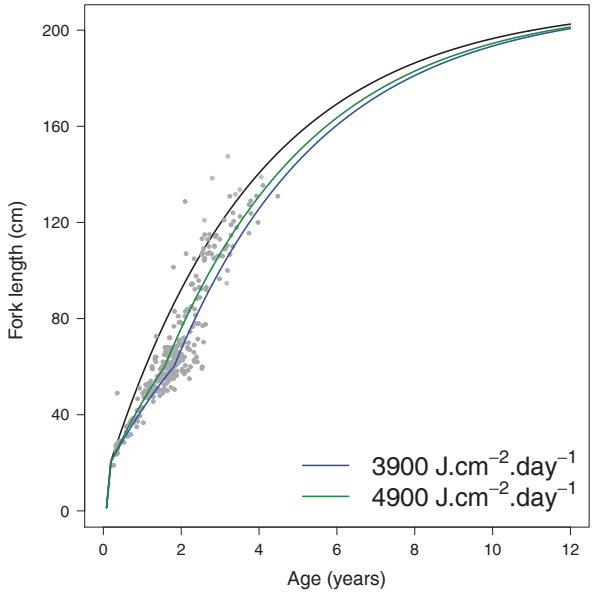

FIGURE 4.20 – Simulation of growth curve under the assumption of a less energetic intake during the juvenile stage on the growth. The black curve corresponds to the reference model and the grey circles represent the wild yellowfin data

The intake of less energetic prey during the juvenile stage could partly explain the two-stanza growth. By reducing the value of $\{\dot{p}_{Am}\}$ for yellowfin smaller than 60 cm F_L, the model was able to capture well juvenile growth, particularly with a value of 3900 J.day^{-1}.cm^{-2}. The model however underestimated the growth above 60 cm (Figure 4.20). The predicted age and fork length at puberty were 2.2 years for 74.79 cm and 1.96 years for 74.77 cm for $\{\dot{p}_{Am}\}_j$ values of 3900 and 4000 J.day^{-1}.cm^{-2}

respectively. The variation of $\{\dot{p}_{Am}\}$ did not result in any change in the length-weight relationship nor in the seasonal reproductive investment. The daily energy intake was close to that of the reference model and within the range of values available from literature.

3.5 Effect of change in body temperature

A gradual decrease in body temperature of 5°C during the juvenile stage led to a slower growth than predicted under constant temperature condition, but it did not generate distinct stanzas (Figure 4.21). No significant change in the length-weight relationship was observed.

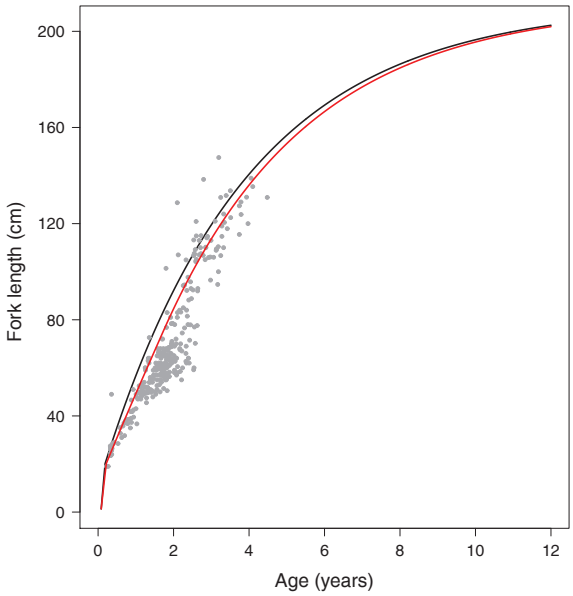

FIGURE 4.21 – Simulation of growth curve under a gradual decrease in body temperature of 5°C during the juvenile stage on the growth (red curve) in relation to a constant body temperature (black curve). The grey circles represent the wild yellowfin data

4 Discussion

Since the early 1960s, yellowfin growth has been the focus of considerable research effort, especially for its importance in the stock assessment process. However, despite increasing evidences for a two-stanza growth (Fonteneau, 1980; Marsac and Lablache, 1985; Gascuel et al., 1992; Lehodey and Leroy, 1999, Eveson et al. *in press*), this growth pattern is still controversial (Driggers et al., 1999; Kolody, 2011). Biases in growth estimation might weaken the scientific advices , by affecting stock status relative to limit reference points, and ultimately the proposed management measures for the sustainable exploitation of yellowfin stocks. A better understanding of the

mechanisms that lie behind the growth stanzas would improve the estimation of yellowfin growth and overall quality of current yellowfin stock assessments. With this idea in mind, using the Dynamic Energy Bugdet (DEB) theory, we investigated the two major assumptions that might explain the existence of two growth stanzas for yellowfin, (i) a low food availability during juvenile stage in relation with high intra and inter-specific competition and (ii) ontogenic changes in food diet characterized by the consumption of more energetic prey in older yellowfin. We also assessed the effect of an enhancement in yellowfin ability to raise their body temperature above the seawater temperature, although we did not considered that this could generate such acceleration in growth.

4.1 Establishment of a bioenergetic yellowfin pattern

Developed in the 1980s, the DEB theory (Kooijman, 1986) has been successfuly used to study the influence of environmental conditions on growth and reproduction patterns in various fish species (Freitas et al., 2010; Pecquerie et al., 2011; Pethybridge et al., 2013). The major advantage of the DEB theory, in relation to traditional bioenergetic approaches, is that it provides a powerful framework to describe the full life cycle of an organism in a variable environment (Nisbet et al., 2012). As the larva stage was not required to meet the aim of this study, in the absence of data for this stage, it was not considered here.

However, it should be kept in mind that estimation of a species-specific set of DEB parameters is very difficult (Kooijman et al., 2008). Theoretically, this would require experiments including simultaneous measurements of ingestion, assimilation, growth, reproduction and respiration in controlled conditions of food and temperature (van der Veer et al., 2006). Regarding yellowfin, the available data sets were insufficient to estimate the DEB parameters and it has proved difficult to infer the parameter values from historical experimental studies.

It was however possible to benefit from the work on Pacific bluefin tuna through the use of the rule of the *body-size scaling relationships*. This rule is based on the properties of primary parameters leading to differences in maximum size among phylogenetically related species. Under this rule, the size difference between yellowfin and bluefin tuna would only result from a lower assimilation capacity for yellowfin, both species having identical metabolic and physiological processes. This assumption may not be quite accurate. Indeed, Blank et al. (2007) showed that Pacific bluefin tuna has higher metabolic rates than a similar sized yellowfin. In addition, bluefin tuna have greater thermoregulation abilities due to more developed vascular heat exchanger systems and a higher relative proportion of red muscles (Blank et al., 2007; Shadwick et al., 2013). As the internal heat production is scaled with the surface, the surface area-specific maintenance costs, $\{\dot{p}_T\}$, are probably lower for yellowfin tuna. In spite of these limits, the calibrated model from primary parameters estimated for Pacific bluefin tuna had successfully reproduced the experiments on captive yellowfin and the model predictions appeared in agreement with the knowledge on species biology.

4.2 Growth under constant environmental conditions

The reference model, which was run for constant and optimal conditions of temperature and food, has proved particularly suitable for reproducing the growth in length and the length-weight relationship of farmed yellowfin (Figure 4.15). This model forecasted particularly fast initial growth until the end of the early juvenile stage and then, as was expected for farmed fish, it complied to a Von Bertalanffy growth implying relatively high growth rates for juveniles and young adults which gradually slowed as asymptotic length approaches (Figure 4.17). Towards the end of the early juvenile stage, the internal warming ability from the metabolic heat retention appears. As heating is associated with an additional somatic maintenance cost, it led to a change in the energy balance resulting in a growth slowdown. The slowdown in growth towards the asymptotic size expressed a trade-off between the increase of structural biomass and the extra costs required for somatic maintenance. Thus the increase in somatic maintenance costs with increasing size resulted in a deficit of the energy available for growth.
Regarding wild yellowfin, the reference model was consistent with the adult growth over 90 cm F_L and overestimated the growth in juvenile and pre-adult stages, as we might expect. Therefore, the puberty was reached at at a length of 74.85 cm F_L cm in compliance with the observations on the length of 50% maturity in the Indian Ocean (Rohit and Rammohan, 2009; Zudaire et al., 2013a), but at 1.4 years, which was too early in relation to the predictions of the growth model of Indian Ocean yellowfin (2.2-2.5 years ; Chapter 3). By contrast, the predicted length-weight relationship was appropriate for juveniles, but the model overestimated the weight gain over 100 cm F_L, suggesting an excessive weight contribution of the reproduction buffer.

4.3 Reproduction pattern

A mean number of 30 to 60 batches per spawning season was estimated (Figure 4.16) resulting in a spawning season lasting from 1 to 2 months consistent with the observations on farmed yellowfin. The spawning period in captivity varies from 1 to 3 months depending on the females, with a near-daily spawning frequency which may be intermittent during the first months (Wexler et al., 2003; Margulies et al., 2007). In the Indian Ocean, the duration of the spawning period for the whole population could vary from 2 to 5 months (Rohit and Rammohan, 2009; Stéquert et al., 2001; Zudaire et al., 2013a).
The seasonal reproductive investment (IR), i.e. the energy allocated to eggs production for a single spawning period, and the absolute fecundity (AF) increased with size (Figure 4.18), in accordance with what is observed for both wild and livestock yellowfin. The maximal IR accounted for 27.8% of body wet weight, i.e. 19 kg of a total of 69.22 kg for fish of 150 cm F_L. Thus, a female could lose up to one-third of its body weight due to spawning activity.
The IR was sensitive to low temperature variations, as shown the simulation of captive yellowfin data. The IR was maximal at 26°C and decreased when the temperature exceeded 28°C (Figure 4.16). This result agrees with the study of Itano (2000)

who has been highlighted a cessation of spawning activity around 28°C from Pacific yellowfin caught at sea.
The energetic cost of maturing a single batch was evaluated at 1.06% of body weight from yellowfin sampled at sea (Schaefer, 1996 in Margulies et al., 2007). According to our estimate of 30 batchs per season, we should get an IR of 31.8% of body weight leading to the same rough weight loss estimate of one-third. The differences in IR values could be explained either by an overestimation of the absolute fecundity and therefore of the batch number, or by a poor handling of energy in reproduction buffer. During the spawning period, females increase their feeding rate in response to greater energy requirements, and thus the energy required to eggs production comes from both the energy stored as fat in the liver and food. In this study, such variations in feeding rate have not been taken into account. In addition, the energy stored for reproduction was released in one shot.

4.4 Behavioral changes behind the two-stanzas growth

The farmed yellowfin considered in this study did not display the acceleration of growth occurring in teenage years for wild fish. This observation supported that the origin of the stanza growth would rather be behavioral than physiological. In captivity, the food rations are adjusted to comply with the nutritional requirements of tunas which do not suffer from competition for food. Thus, the growth stanza would be caused by a behavioral change related to feeding.
Both investigated assumptions, i.e. a low food availability during juvenile stage and the consumption of more energetic prey in pre-adult and adult stages, led to a two-stanza growth close to that of Indian Ocean yellowfin (Figures 4.19 and 4.20). In both cases, the model captured the juveniles growth but the acceleration of growth rate and therefore the growth in the asymptotic part of the curve were underestimated. With a lower food density or a less energetic diet, yellowfin reached puberty at similar size but later than predicted by the reference model, leading to age values consistent with our knowledge. Compared to relative daily energy consumptions under optimal and constant food conditions, the predicted values under both assumptions were only slightly lower and consistent with those assessed for the farmed fish (Mourente and Tocher, 2009). As the increase in food density as well as the food diet change occurred before puberty, no significant change neither in the investment nor in the length-weight relationship was noticed. In the light of these results, greater food availability or consumption of more energetic prey appear as plausible causes for growth rate acceleration observed in the wild, although none of them is sufficient to explain the acceleration magnitude. Thus, it would be relevant to examine the effect on growth of combining both assumptions in future studies.

In this study, we highlighted the credibility of the two assumptions considered as the most relevant. Nonetheless, the veracity of these assumptions remains to be verified. Several lines of evidence support low feeding rates among the young yellowfin huddled in mixed schools associated with drifting objects. In particular, the stomach contents analysis point out a much higher proportion of empty stomachs

for fish caught from associated schools (Potier et al., 2001) which are significantly slimmer than yellowfin caught in free schools (Hallier and Gaertner, 2008).
The assumption of a food diet change is more difficult to verify. From a bioenergetic point of view, a food diet change correspond to a divergence in energy intake. Studies on the diet of yellowfin tuna, as well as stomach contents data, underline conspicuously different stomachal compositions according to fish size (Potier et al., 2004, 2007). Yellowfin is an opportunistic species that feeds on a large number of prey categories. Firstly, young yellowfin feed mainly on planktonic crustaceans and then, from 50 cm F_L, they become essentially piscivorous with a decline in crustaceans consumption around 80 cm and a strong consumption of cepahalopodes between 80-100 cm (Maldeniya, 1996; Potier et al., 2001). The diet of yellowfin, especially in younger stages, is dominated by epipelagic species. Fish about 60 cm include in their diet mesopelagic species, probably due to their ability to forage in deeper waters, but also other tunas such as skipjack and young yellowfin. However, the change in dietary preferences does not necessarily result in an energetic shift. Investigating the relative caloric value of stomach content in various size classes would link these diet changes to changes in energetic term. Unfortunately we had not enough information about the nutritional value of prey for such investigation.

4.5 Rise in body temperature

As a regional endothermic species, yellowfin is able to maintain a high temperature in some tissues, by conservation of the heat produced by metabolism, with temperature differences between tissues. The ability of raising internal temperatures above the seawater temperature gradually increases during juvenile stage. In this study, this ability was not considered as a factor likely to explain a two-stanza growth. Indeed, some evidences suggest that young yellowfin remain in shallow and warmer waters to offset their lower ability to thermoregulate. The improvement of thermoregulation abilities is probably the root of greater depths reached by adult yellowfin. During a deep diving, yellowfin experience major changes of internal temperature over short time periods (Dagorn et al., 2006). Such time periods are too short to be considered in a DEB model. As yellowfin spend most of their time above the mixed surface-layer and less than 15% of their time in diving (Schaefer et al., 2011), we could assume that the daily body temperature was about constant.
In this study, we shown that a gradual rise of the internal temperature from 0 to 5°C in relation to seawater temperature had only led to a slight increase in growth rates, insufficient to generate a growth stanza. However, the increase in growth rates reflected an increasing metabolic activities. This result corroborated the observation on captive yellowfin whose energy needs increased in response to an elevation of surrounding temperature (Wexler et al., 2003). Thus, the thermo-conservation abilities of yellowfin might become a handicap in case of strong elevations of seawater temperatures.

4.6 Enhancement of the yellowfin DEB model

The main contribution of this study is the development of a DEB model for testing assumptions likely to be behind the growth stanza of yellowfin tuna. We also provided a first approximation of a comprehensive set of parameters. Additional data from controlled environment experiments are required to improve our estimates of yellowfin-specific parameters. However, our results, particularly those respecting farmed fish, are promising and emphasize the interest for further research for better understanding of life-history strategies.

The reproductive behavior of yellowfin should be better investigated to define more realistic handling rules of the reproduction buffer. With more adequate handling rules, model would allow to examine the influence of environmental conditions on the reproduction, which is useful for a better assessment of resilience of such species to environmental change and fishing pressure. We can already suggest some improvements.
During the spawning season, the energy stored in the reproduction buffer is converted to eggs released through several batches. As the reproductive capabilities increase with size, the energy required for a single batch E_B, including the energy content of eggs and the energy losses associated with the conversion of the buffer energy in yolk, increases with the structural length. Under the assumption of a constant energy density of one batch $[E_B]$, at a spawning event, the reproduction buffer is emptied of an energy quantity $E_B = [E_B]L^3$ (Pecquerie et al., 2009). As long as the energy content of the reproduction buffer is greater than E_B spawning continues with a daily frequency, otherwise a smaller batch is spawned and the buffer is fully emptied, marking the end of spawning season. Studies on Pacific yellowfin show that spawning activity occures from a surrounding temperature of 24°C and declines above 28°C (Itano, 2000; Margulies et al., 2007). Thus, the spawning season could be triggered according to temperature fluctuation in the Indian Ocean.

The early life stages of yellowfin have been experiencing an increase interest over the last years (Margulies et al., 2007; Wexler et al., 2011), especially for aquaculture purposes (Kaji et al., 1999), and a wealth of information is potentially available. It would then be interesting to implement these stages in future modeling work and consider the full life cycle of yellowfin.
During the larva stage, yellowfin undergoes significant transformations in both physiologically and morphologically including the development of the digestive system, spines and rays or vascular heat exchanger systems. Moreover, the larvae grow exponentially. These changes could be taken into account by adjusting the surface-dependent parameters $\dot{v}$, $\{\dot{p}_{Am}\}$ and $\{\dot{p}_T\}$ defined for juvenile and adult stages using the following function :

$$\frac{max(min(L_v, L_j), L_b)}{L_j} \begin{cases} \frac{L_b}{L_j} & \text{for} \quad L_v < L_b & \text{egg and yolk-sac larva} \\ \frac{L_v}{L_j} & \text{for} \quad L_b \leqslant L_v < L_j & \text{larva} \\ 1 & \text{for} \quad L_v \geqslant L_j & \text{juvenile and adult} \end{cases}$$

wherein L_v, L_b and L_j are the structural lengths to any age, first-feeding and metamorphosis respectively. L_b and L_j are reached at corresponding maturity thresholds E_{H_v}, E_{H_b}, E_{H_j} (Kooijman, 2010; Jusup et al., 2011).

Conclusion générale

1 Démarche de l'étude et principaux résultats

Depuis le début des années 1960, la croissance de l'albacore fait l'objet d'une attention toute particulière tant dans le domaine de la recherche que pour la gestion des pêcheries. Dans l'océan Indien, le suivi et la gestion du stock d'albacore souffrent de nombreuses incertitudes associées à la modélisation de la courbe de croissance actuellement considérée, ce qui fragilise les avis scientifiques sur l'état d'exploitation du stock. En particulier, de nombreuses lacunes subsistent dans notre compréhension des processus biologiques et écologiques élémentaires qui régulent la croissance.

Différentes approches de modélisation ont été mises en œuvre afin de renforcer les connaissances sur la croissance de l'albacore de l'océan Indien nécessaires à une évaluation plus objective de l'état du stock. Dans une premier partie, des modèles d'état stochastique Bayésiens ont été développés afin d'améliorer la courbe de croissance actuellement utilisé dans les évaluations du stock. Les résultats de cette première partie constituent une avancée vers une meilleure compréhension du patron de croissance. Néanmoins, ils n'apportent aucune information sur les processus éco-physiologiques à l'origine des stances de croissance observées. Pour cette raison, une seconde partie de cette étude s'est attachée au développement d'un modèle bio-énergétique fondé sur la théorie des bilans dynamiques d'énergie (DEB ; Kooijman, 2010). Ce dernier a permis de simuler le patron de croissance en fonction des besoins physiologiques de l'albacore sous différentes scénarios de disponibilité en nourriture et de qualité nutritive des proies.

1.1 Prise en compte des incertitudes dans les estimations d'âge par otolithométrie

Dans cette étude, nous proposons une méthode pour l'estimation d'âge qui quantifie explicitement les différentes sources d'incertitudes associées aux lectures de stries d'otolithes. La méthode proposée montre l'intérêt du cadre Bayésien. Son utilisation a permis d'exploiter les connaissances des experts sur les erreurs liées à la préparation et à l'interprétation des stries d'otolithe (par exemple, incertitudes aux niveaux du nucléus et de la partie terminale liées à la perte de certaines stries).
Cette méthode a conduit à une sensible amélioration des estimations d'âge. En particulier, elle a tenu compte d'un biais dans la périodicité du dépôt des stries estimée par le lecteur. Les résultats ont indiqué que le dépôt estimé était significativement différent d'un dépôt quotidien avec un ratio de 0.939 strie par jour. La standardisation du nombre de stries comptée est donc nécessaire pour la conversion en âge.

L'approche par simulation-estimation a montré que le choix de la méthode d'estimation d'âge peut fortement affecter les estimations de croissance. Ceci peut avoir des répercussions importantes sur les matrices de capture par âge utilisées dans les modèles d'évaluation des stocks. Ainsi, la procédure traditionnelle, basée

sur le postulat d'un dépôt journalier des stries, a conduit à une sous-estimation systématique de l'âge réel des poissons ayant pour conséquence une surestimation de la croissance. En revanche, le modèle de croissance couplé à notre modèle d'erreur d'estimation d'âge a estimé une courbe de croissance qui correspondait de très près à la courbe simulée.
De plus, notre modèle a conduit à l'estimation d'importantes incertitudes autour des estimations d'âges découlant de la lecture des otolithes. En propageant ces incertitudes dans l'estimation de la croissance, il nous a permis de mieux évaluer la précision des estimations de croissance et le risque associé à leur utilisation pour la répartition en âge des captures commerciales. La procédure traditionnelle néglige ces incertitudes et tend ainsi à sur-évaluer la fiabilité de l'information portée par les données. En conséquent, l'ajustement du modèle de croissance en découlant s'est révélé sur-confiant au niveau de l'incertitude autour des estimations.

Par ailleurs, nos résultats ont mis en évidence que des différences entre les méthodes d'interprétation des stries d'otolithe peuvent conduire à des précisions d'âge variables. Pour l'albacore, les deux équipes de lecteurs ont abouti à des résultats contradictoires quant à la périodicité du dépôts de stries, avec des ratios de 0.852 et 1.025 stries par jour. Des différences dans les âges estimés par les deux équipes de plus de 300 jours ont ainsi été mises en évidence. Ces différences pourraient en partie être liées à une non-stationnarité des processus de dépôt des stries au cours de la vie des albacores.
Malgré l'utilisation du modèle d'erreur d'estimation d'âge, quantifiant explicitement le biais dans la périodicité du dépôt, ces différences ont entraîné des estimations de croissance significativement différentes. Ces résultats indiquent que, bien que considérées comme les données les plus utiles pour l'estimation de la croissance individuelle, les lectures d'otolithes sont à utiliser avec précaution. La mise en place d'une collection de préparations d'otolithes de référence associées à des exercices d'inter-calibration entre lecteurs et des tests de lectures en routine apparaît indispensable pour standardiser la méthode d'interprétation des stries d'otolithes de thons tropicaux et évaluer la qualité des lectures fournies (précision et biais).
En outre, l'utilisation d'approches intégrant des lectures d'otolithes effectuées par différents lecteurs et issues de plusieurs méthodes d'interprétations, ainsi que d'autres sources d'information sur la croissance est préférable. Dans le cas contraire, les erreurs de lecture aléatoires ne peuvent être détectées. Ainsi, concernant le patudo, les difficultés associées aux lectures d'otolithes ont occasionné des aberrations dans les estimations d'âge réalisées par l'équipe 3 et des contradictions par rapport aux informations fournies par l'équipe 2 ainsi que par les progressions modales. Les lectures d'âge réalisées par l'équipe 3 ont finalement été considérées peu fiables.

1.2 Modélisation de la croissance à partir de différentes sources d'information

Alors que la plupart des études sur la croissance de l'albacore s'appuient sur une seule source de données, cette étude décrit un modèle qui combine (i) des estimations d'âge obtenues par otolithométrie, (ii) des analyses de progression modale et (iii) des informations sur les taux de croissance individuels issus du marquage-recapture. Développé dans un cadre hiérarchique Bayésien, notre modèle tient compte des incertitudes associées aux estimations d'âge, aux mesures de longueur et à l'identification des modes de longueur. De plus, il inclue des avis d'experts sur l'interprétation des stries d'otolithes ainsi que des observations historiques de croissance.

L'adjonction progressive des données d'estimations d'âge, de progressions modales puis de marquage-recapture a permis d'évaluer l'influence de chaque source de données sur l'estimation de la courbe de croissance. Cette estimation variait en fonction de la quantité et de la qualité des informations fournies.
Les ajustements du modèle aux estimations d'âge et aux progressions modales ont abouti à des résultats satisfaisants, cohérents avec les précédentes études sur la croissance de l'albacore. L'ajout des progressions modales a amélioré l'estimation globale des paramètres. Elle a donné lieu à une plus petite longueur asymptotique ainsi qu'à une transition plus marquée entre les deux stances de croissance, liée à des taux de croissance plus élevés pour la seconde stance.
En revanche, le modèle intégrant les trois sources de données a montré des difficultés à estimer conjointement les paramètres de croissance et les âges des individus issus du marquage-recapture. De ce fait, ce dernier a conduit à des estimations singulières. Les estimations des âges au marquage des individus de 70 à 120 cm F_L étaient très proches, ce qui a engendré des taux de croissance très élevés, jusqu'à 6,4 cm.mois^{-1}. De tels taux semblent beaucoup trop élevés. De plus, la longueur asymptotique moyenne a été estimée à 137,9 cm F_L. Cette valeur apparait beaucoup trop faible par rapport aux longueurs maximales historiquement déclarées pour l'albacore de l'océan Indien.
L'absence d'information sur l'âge des poissons est un obstacle limitant l'utilisation des données de marquage-recapture pour l'ajustement de modèles de croissance multi-stances. En effet, la transition entre les différentes phases de croissance dépend de paramètres liés à l'âge et elle ne peut être estimé en l'absence de la connaissance de celui-ci.

L'utilisation de la loi généralisée des valeurs extrême (GEV) a permis d'apporter de l'information supplémentaire sur la longueur asymptotique et a conduit a des estimations cohérentes. Ainsi, la longueur asymptotique moyenne a été estimée à 165,07 cm F_L à partir des estimations d'âge, puis à 155,7 cm F_L après ajout des progressions modales. Ces valeurs sont proches des tailles maximales observées dans les captures des senneurs (160 cm).

Malgré les difficultés d'estimation rencontrées avec le jeu de données de marquage-recapture, l'approche de modélisation mise en œuvre est adaptée à l'étude de la croissance d'albacore de l'océan Indien. Les résultats obtenus confirment l'existence d'un processus de croissance complexe avec deux phases distinctes. Les taux de croissance sont d'abord relativement faibles et diminuent légèrement jusqu'à une taille de 60-65 cm F_L (1,8 ans). Puis ils augmentent de façon importante jusqu'à atteindre un maximum autour de 75-86 cm F_L (2,2-2,5 ans). Ils diminuent ensuite de façon progressive pour atteindre un plateau à l'approche de la taille asymptotique.

1.3 Investigation bio-énergétique des facteurs à l'origine des stances de croissance

Afin de mieux comprendre les facteurs à l'origine des stances de croissance observées chez l'albacore, un modèle bio-énergétique s'appuyant sur les principes de la théorie DEB (Kooijman, 2010) a été mis en œuvre. Les données actuellement disponibles pour l'albacore ne permettant pas l'estimation d'un jeu complet de paramètres, le modèle DEB à été calibré par simulation à partir des paramètres connus pour le thon rouge du Pacifique (*Thunnus orientalis* ; Jusup et al., 2011).

Le modèle de référence, établi pour une température et une densité en nourriture constantes, a reproduit de façon satisfaisante les paramètres de l'étude de Wexler et al. (2003) sur les albacores captifs du Pacifique. De plus, les prédictions de ce modèle étaient en accord avec les connaissances actuelles sur la biologie de l'espèce. Ainsi, la taille à maturité prédite par le modèle, d'environ 75 cm F_L, s'accorde à la fois aux observations faites sur les albacores captifs et sur les albacores sauvages de l'océan Indien (Wexler et al., 2003; Zudaire et al., 2013a).
Ce modèle prédit des taux de croissance très élevés jusqu'à la fin de la première phase juvénile. Celle-ci est marquée par l'apparition de la capacité à conserver la chaleur produite par le métabolisme (20 cm F_L). L'apparition de cette capacité est associée à un coût énergique supplémentaire qui se traduit par un ralentissement de la croissance. Par la suite, le modèle a prédit une croissance de type Von Bertalanffy impliquant des taux de croissance relativement élevés chez les juvéniles et les jeunes adultes qui ralentissent progressivement et se stabilisent à l'approche de la taille asymptotique. Ce ralentissement traduit un compromis entre l'accroissement de la masse et les coûts énergétiques supplémentaires liés cet accroissement.
Concernant les albacores sauvages de l'Indien, ce modèle est adapté pour la croissance des adultes de plus de 90 cm F_L, mais il surestime celle des juvéniles.

À partir des sorties du modèle de référence, un nombre moyen de 30 à 60 événements de ponte par saison a été estimé. Sous l'hypothèse d'une ponte journalière, ce nombre correspond à une période de reproduction de 1 à 2 mois, ce qui est en accord avec les durées de ponte observées chez les albacores captifs. L'investissement reproducteur saisonnier a été estimé à 27,8% de la masse corporelle. Ainsi, une femelle pourrait perdre jusqu'à un tiers de son poids en raison de l'activité de ponte.

Le modèle de référence a ensuite été utilisé pour tester deux hypothèses apparaissant comme les plus pertinentes pour expliquer les stances de croissance : (i) une faible disponibilité alimentaire liée à une forte compétition inter et intra-spécifique chez les jeunes albacores se rassemblant en bancs et (ii) un changement ontogénique du régime alimentaire caractérisé par la consommation de proies plus énergétiques au stade adulte. Les résultats ont montré que ces deux hypothèses sont susceptibles d'expliquer, au moins partiellement, les stances de croissance. Les deux hypothèses ont conduit à des courbes de croissance compatibles avec les données d'estimations d'âge dans la phase juvénile, mais sous-estimant l'amplitude de l'accélération de croissance.
L'examen des niveaux de remplissage stomacal et les mesures d'embonpoint attestent que de faibles taux d'alimentation des juvéniles seraient à l'origine du ralentissement de leur croissance. De plus, ce ralentissement n'est pas observé lorsque la nourriture n'est plus un facteur limitant.
L'hypothèse d'une consommation de proies plus nutritives est quant à elle plus difficile à vérifier et les résultats obtenus sont à considérer avec précaution. Les études des contenus stomacaux indiquent que les préférences alimentaires des albacores évoluent selon leur taille. Toutefois rien ne permet d'affirmer que ces changements ontogénétiques s'accompagnent de changements en terme de quantité d'énergie ingérée. Une recherche plus poussée sur la valeur énergétique des différentes proies consommées par les albacores devra être mise en œuvre.

Notre modèle a prédit une hausse de l'activité métabolique en réponse à une augmentation de la température corporelle. Ceci corrobore les observations de Wexler et al. (2003) mettant en évidence une hausse des besoins énergétiques avec la température. Ainsi, la capacité de l'albacore à réchauffer ses tissus grâce à la conservation de la chaleur métabolique pourrait devenir un handicap en cas de fortes hausses des températures. L'espèce serait alors obligée d'augmenter la fréquence de ses plongées pour refroidir son corps ou migrer vers des zones plus froides.

2 Limites de l'étude

2.1 Informations fournies par les données

Bien que les données utilisées dans cette étude constituent incontestablement la meilleure source d'information pour l'étude de la croissance de l'albacore de l'océan Indien, l'absence de certaines informations ont limité les analyses statistiques.

Les otolithes de thons sont petits et présentent des marques d'accroissement parfois difficilement discernables dont la lecture exige l'interprétation subjective du lecteur. Dans un tel cas, l'expérience du lecteur a une forte influence sur la précision et la justesse des estimations d'âge. L'examen de la précision de chaque lecteur et de la variabilité entre lecteurs sont alors indispensables pour évaluer la performance d'une méthode de lecture. Dans le cadre du RTTP, les préparations et les lectures

d'otolithes ont été réalisées par différents contractuels recrutés de manière successive sur de courtes périodes. Ainsi, aucun exercice initial n'a pu être mis en place pour comparer la précision de chaque lecteur ou de chaque équipe. De plus, l'identité de chaque lecteur au sein d'une même équipe ne pouvant pas toujours être identifiée, de telles comparaisons entre lecteurs n'ont pu être réalisées dans cette étude.

D'autre part, l'absence de plan d'échantillonnage pour l'analyse des otolithes a conduit à des déséquilibres importants dans la structure des données qui ont limité les estimations de croissance basées sur les estimations d'âge. Ainsi, le faible nombre de lectures concernant les patudos de taille supérieure à 70 cm F_L n'a pas permis un ajustement satisfaisant du modèle de croissance VB log-K. Cette expérience devrait servir de modèle au prochain grand programme de marquage de thons qui est actuellement en train de se mettre en place dans l'Atlantique.

Les données d'estimations d'âge provenant de la campagne WSTTP suggèrent des taux de croissance plus rapides que ceux prévus par le modèle VB log-K pour les individus de taille inférieure à 30 cm F_L. Ces individus ont été capturés au large de la côte Indonésienne et leur croissance peut différer de celle des individus provenant du programme RTTP, capturés à l'ouest de l'océan Indien, en raison de conditions environnementales locales différentes, bien qu'un seul stock d'albacore soit actuellement considéré par les pays membres de la CTOI. En effet, les études génétiques n'apportent pas de preuve solide de l'existence d'une structure génétique spatiale (Nishida et al., 2001; Kunal et al., 2014).
Une première stance de croissance rapide a était mise en évidence pour les jeunes albacores du Pacifique. Cette stance se caractérise par des taux de croissance très élevés qui ralentissent par la suite entre 35 cm (Yamanaka, 1990) et 45 cm F_L (Lehodey and Leroy, 1999). D'autres espèces de thons, tels que le thon rouge du sud (Hearn and Polacheck, 2003; Eveson et al., 2004) et le thon rouge du Pacifique (Bayliff, 1991; Jusup et al., 2011) présentent également une première phase de croissance rapide. Pour ces raisons, nous soupçonnions une troisième stance de croissance. Cependant, les données utilisées dans cette étude provenant principalement de la pêche à la senne, le nombre d'individus inférieurs à 35 cm F_L (taille de recrutement de la senne) était insuffisant pour mettre en évidence cette troisième stance de croissance.
Des informations supplémentaires sur la croissance des juvéniles d'albacores permettrait l'ajustement d'un modèle de croissance en trois stances combinant le modèle VB log-K à un modèle logistique. La taille L à un âge A serait alors décrite comme suit :

$$L(A) = \frac{L_d}{1 + exp(-k_0(A - t_0))} + (L_\infty - L_d)\left(1 - exp(-k_2(A - t_d))\left(\frac{1 + exp(-\beta(A - t_0 - \alpha))}{1 + exp(-\beta(td - t_0 - \alpha))}\right)^{\frac{k_1 - k_2}{\beta}}\right)$$

L_d est la taille atteinte à la fin de la première phase de croissance, t_d l'âge correspondant à L_d et k_0 le coefficient de vitesse de croissance initiale. Les autres paramètres de ce modèle sont ceux décrits dans le tableau 3.2 du chapitre 3. Des mesures d'épaisseurs de stries d'otolithes, la croissance somatique pouvant être

estimée à partir de l'accroissement des otolithes (Mugiya and Tanaka, 1992), et des informations collectées dans les fermes aquacoles de l'IATTC devraient permettre l'application de ce modèle.

L'existence d'un dimorphisme sexuel de croissance chez l'albacore est une hypothèse communément admise que nous n'avons pu tester de façon objective dans cette étude. En effet, les estimations d'âge pour les individus sexés étaient insuffisante en nombre et ne concernaient que de grands individus (7 individus de chaque sexe de taille $>$ 137 cm F_L). Aussi, différentes tentatives de modélisation ont été mise en œuvre, seulement, les résultats étant très sensibles aux hypothèses posées, ils ont été considérés comme peu fiables.
Les différents résultats obtenus mettaient cependant en évidence une taille asymptotique plus faible associée à des taux de croissance dans la seconde stance moins élevés pour les femelles que pour les mâles (Figure 5.1). Ces résultats sont en accord avec l'étude de Wild (1986), menée sur l'albacore du Pacifique, qui souligne une croissance plus rapide des mâles à partir de 95 cm F_L.

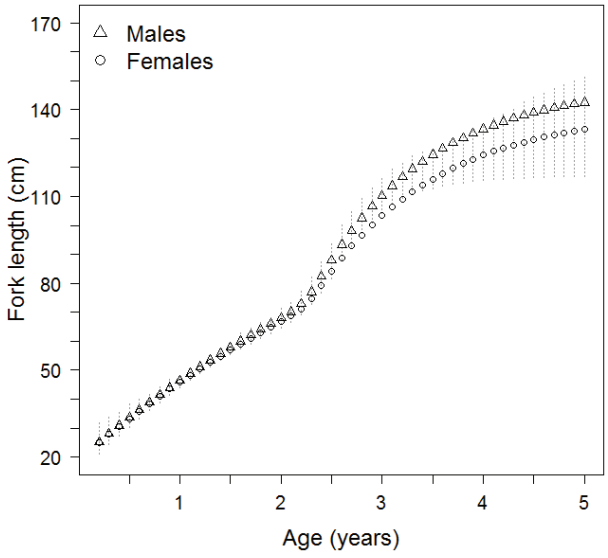

FIGURE 5.1 – Courbes de croissance moyennes des mâles et des femelles albacores de l'océan Indien estimées à partir des données d'estimations d'âge. Les données recueillies à partir des captures de la pêche à la senne commerciale montrant un sex-ratio équilibré jusqu'à 125 cm F_L, une première courbe a été ajustée à partir des estimations d'âge des individus non-sexés. Les données sur les individus sexés ont alors été utilisées pour ré-estimer les coefficients de vitesse de croissance (k_1 et k_2) et la longueur asymptotique (L_∞).

Les données de fréquences de tailles échantillonnées à partir de la pêche à la senne commerciale comportent peu d'individus de taille intermédiaires, i.e. entre 70 et 100 cm F_L. Il s'agit là d'un cas classique lié à la sélectivité de la senne. À partir de 70 cm, les albacores quittent les Dispositifs de Concentration de Poissons (DCP) sous lesquels ils se rassemblent en bancs en association avec de jeunes patudos et des listaos. Il deviennent alors moins vulnérables à la senne en se dispersant sur une plus large aire géographique qui englobe des zones non ciblées par la pêche. De plus, ils pourraient présenter un comportement plutôt solitaire (Fonteneau and Gascuel, 2008). En raison de ce manque d'individus de taille intermédiaire, le suivi de la progression mensuelle des modes de longueur s'est avéré difficile au-delà de 70 cm F_L, ce qui a grandement limité les ajustements d'un modèle de croissance en deux stances ne considérant que ce jeu de données.

2.2 Modélisation statistique de la croissance

L'ajustement du modèle de croissance intégré a révélé des problèmes d'identifiabilité. Deux sortes d'identifiabilité peuvent être distinguées : (i) l'identifiabilité intrinsèque qui est une caractéristique inhérente à la structure du modèle et (ii) l'identifiabilité extrinsèque qui est liée à la qualité et à la quantité des données disponibles (Viallefont et al., 1998; Gimenez et al., 2004). Dans notre cas, le problème d'identifiabilité semble provenir d'un manque d'individus de grande taille dans les jeux de données utilisées (extrinsèque). En effet, les données apportent essentiellement de l'information sur les taux de croissance qui, dans le modèle VB log-K, renseignent à la fois sur la taille asymptotique et sur les coefficients de vitesse de croissance. Ainsi, de fortes corrélations ont été mises en évidence entre la longueur asymptotique et les coefficients de vitesse de croissance, ce qui suggère que ces paramètres ne peuvent pas être estimés séparément.
L'utilisation d'une loi de distribution *a priori* informative pour la longueur asymptotique semble avoir limité ce problème. De fait, les modèles ajustés sur les estimations d'âge et les analyses de progressions modales ont conduit à des estimations cohérentes avec les connaissances issues des précédentes études sur la croissance de l'albacore. En revanche, ce problème d'identifiabilité associé à la non-connaissance des âges au marquage apparaît être à l'origine des mauvaises estimations obtenues avec le modèle intégrant les trois sources de données. Basé sur l'estimation conjointe des paramètres de croissance, des paramètres d'erreur et des âges au marquage des individus, ce denier modèle était sur-paramétré et la composante logistique n'était alors pas identifiable.

Au vu de la complexité de notre modèle, l'identification du nombre de paramètres estimables et les raisons de leur non-identification (intrinsèque ou extrinsèque) auraient du être analysées afin de mieux appréhender les difficultés relatives aux ajustements. Une approche par simulation-estimation serait appropriée pour détecter les redondances intrinsèques et les redondances extrinsèques de notre modèle. Selon la taille et la qualité du jeu de donnée simulé, cette approche

permettrait, par exemple, d'évaluer l'influence de la quantité d'information sur les individus de grande taille sur les estimations finales.
En outre, des analyses de sensibilité auraient été intéressantes pour évaluer l'influence des lois *a priori* utilisées sur les sorties des modèles. Ces analyses auraient notamment permis d'apprécier la quantité d'informations apportée par les données, en particulier en examinant différentes distributions *a priori* pour la longueur asymptotique.

2.3 Approche bio-énergétique

Le choix de la théorie DEB pour la modélisation de la croissance de l'albacore a nécessité certaines approximations et simplifications. La principale difficulté à laquelle nous avons été confronté est l'estimation d'un jeu de paramètres spécifiques à l'albacore.
La théorie DEB propose une vision synthétique des grandes caractéristiques physiologiques communes aux différentes espèces au travers d'un modèle unique. Les disparités entre les espèces sont alors réduites à des différences dans les quantités d'énergie allouées aux différents processus physiologiques (Kooijman, 2010). Il en découle un grand nombre de paramètres dont la plupart correspondent à des grandeurs non directement mesurables. L'estimation des paramètres est alors une étape fastidieuse qui exige de nombreuses informations sur les principaux traits physiologiques, sous diverses conditions de température et nourriture connues (par exemple, ingestion, assimilation, respiration, croissance, reproduction ; van der Meer, 2006; van der Veer et al., 2006; Nisbet et al., 2012). Ces informations peuvent être collectée expérimentalement dans le cas d'espèces élevées pour l'aquaculture (Bourlès et al., 2009; Rosland et al., 2009; Jusup et al., 2011).
Il s'est avéré difficile d'acquérir de l'information sur la physiologie de l'albacore. Bien que des expériences en bassin aient été réalisées, les données ne sont généralement que partiellement disponibles au travers de publications et de rapports scientifiques. De plus, il était délicat d'inférer les valeurs des paramètres à partir de ces dernières. En outre, nous ne pouvions pas extraire suffisamment d'information des données disponibles. En particulier, il n'était pas possible d'obtenir une connaissance précise des conditions environnementales vécues par les individus. Nous avons alors considéré des conditions environnementales stables à partir desquelles nous avons établi un schéma moyen de croissance sans tenir compte de la variabilité inter-individuelle.
D'autre part, les valeurs des paramètres du modèle pour l'albacore ont été définies par simulation à partir des valeurs connues pour le thon rouge du Pacifique (Jusup et al., 2011). Cette approche a nécessité certaines hypothèses que nous savons être inexactes. Nous avons notamment considéré que physiologiquement ces deux espèces ne diffèrent que par leurs capacités d'assimilation, qui sont plus faibles chez l'albacore. Or ces deux espèces divergent sur de nombreux points. En particulier, le thon rouge présente des systèmes vasculaires échangeurs de chaleur plus performants, des coûts métaboliques liés à la nage plus importants, une masse et des rythmes cardiaques plus élevés (Blank et al., 2007).

Des données supplémentaires seront nécessaires à l'obtention de valeurs de paramètres vraiment spécifiques à l'albacore. Cependant, nos résultats, en particulier ceux concernant les albacores captifs, sont prometteurs et ce premier jeu de paramètres devrait contribuer aux futurs travaux d'estimation de paramètres spécifiques à l'albacore.

Par ailleurs, les règles définies pour le module de reproduction manquent de réalisme. Dans l'océan Indien, les albacores peuvent frayer deux fois par an sur une période prolongée (novembre-mars, juin-juillet ; Rohit and Rammohan, 2009; Stéquert et al., 2001; Zudaire et al., 2013a). Cependant, la durée individuelle de frai et la fréquence de ponte sont méconnues en raison du comportement reproductif asynchrone des albacores et de la difficulté inhérente liée à la détermination de sa fécondité, les ovaires ne conservant pas de traces des précédents événements de pontes (Zudaire et al., 2013a). Aussi, dans notre modèle, l'énergie allouée à la reproduction est libérée instantanément tous les 6 mois, sans tenir compte d'une possible ré-allocation de cette énergie (Zudaire et al., 2013b). Cette simplification peut conduire à une surestimation de la perte de poids lié à l'activité reproductrice.

3 Apports méthodologiques et scientifiques

Pour la première fois, la croissance de l'albacore de l'océan Indien a été abordée à l'aide d'un modèle hiérarchique Bayésien qui exploite les diverses sources d'information disponibles, tant au niveau de la population que de l'individu. Les courbes de croissances obtenues à l'aide de ce modèle sont une réelle amélioration de celle actuellement utilisée dans les évaluations du stock. Par ailleurs, dans l'optique de mieux comprendre les processus à l'origine des stances de croissance, nous présentons l'un des premiers essais de développement d'un modèle DEB appliqué à l'albacore. Malgré leur caractère préliminaire, les résultats permettent de mieux appréhender les effets de l'environnement sur la croissance de l'albacore et apportent des éléments de réponse quant à l'origine des stances.

Le développement de modèles de croissance intégrant de multiples sources de données reste un challenge que très peu d'études ont tenté de relever. Sur la base d'un modèle de croissance complexe en deux stances, notre étude propose une approche rigoureuse et robuste permettant d'une part, d'exploiter les sources d'information les plus pertinentes pour l'étude de la croissance et d'autre part, de quantifier explicitement les diverses erreurs associées à chaque ensemble de données ainsi qu'au processus d'estimation.
La quantification des incertitudes entourant les estimations des paramètres biologiques est capitale, à la fois pour les scientifiques, lors de la phase de diagnostic sur l'état du stock, et pour les gestionnaires des pêcheries, afin d'évaluer objectivement les décisions de gestion et les risques subséquents pour la production du stock. À ce titre, l'utilisation du cadre hiérarchique Bayésien est apparue particulièrement adaptée. Il présente l'avantage de prendre en compte séparément les incertitudes

dans les processus d'observation et d'analyse et de fournir une description détaillée de la confiance avec laquelle chaque quantité d'intérêt est identifiée. L'approche fréquentiste, représentant l'incertitude comme un intervalle de confiance ou une variance diffuse autour d'une situation moyenne, ne permet pas une telle précision et masque le caractère conditionnel du risque.
D'autre part, l'utilisation de l'inférence Bayésienne nous a permis de valoriser explicitement les connaissances issues de l'expertise scientifique et les informations sur les traits biologiques des individus. Pour la longueur asymptotique, l'élicitation d'un prior informatif par le biais de la loi GEV a permis de valoriser les informations sur les tailles maximales observées dans les captures de différentes flottilles de pêche. Cette approche originale a conduit à l'obtention de valeurs cohérentes malgré le peu d'individus de grandes tailles dans les jeux de données utilisés.
L'absence d'individus de grandes tailles est un problème récurrent lié à l'utilisation de données issues de la pêche à la senne qui se traduit souvent par une sous-estimation de la longueur asymptotique. Afin de remédier à ce problème, certains auteurs utilisent la relation empirique de Pauly (1985) qui suppose la longueur maximale du jeu de donnée égale à 95% de la longueur asymptotique. Néanmoins, cette relation ne repose sur aucune preuve concrète et fait une hypothèse implicite sur la distribution des tailles observées, indépendamment de l'espèce de poissons considérée. Cette étude propose une solution plus rigoureuse et objective pour palier à ce problème.

Le couplage du modèle de croissance à un modèle d'erreur dans les estimations d'âge par otolithométrie est une démarche innovante permettant d'une part, une amélioration significative des estimations d'âge et des paramètres de croissance en résultant, et d'autre part, une meilleure évaluation de la fiabilité des estimations. La méthode d'estimation d'âge développée peut être adaptée à n'importe quelle structure présentant des marques d'accroissements périodiques et être ainsi appliquée à d'autres groupes taxonomiques pour répondre à divers problèmes écologiques.

Le modèle bio-énergétique développé dans cette étude est une avancée significative pour la compréhension du potentiel de croissance de l'albacore sur l'ensemble des stades juvénile et adulte.
La théorie DEB considère explicitement l'énergie allouée au développement physiologique et fonctionnel de l'organisme. Elle permettrait ainsi de percevoir l'impact potentiel du réchauffement des océans et des changements dans les communauté de proies sur la croissance, mais aussi sur certains traits d'histoire de vie de l'albacore (transition entre différents stades de vie, acquisition de la maturité sexuelle). Notre modèle DEB-albacore constitue une base intéressante sur laquelle de telles études peuvent s'appuyer.
La démarche adoptée a permis de remédier aux difficultés liées au paramétrage d'un modèle DEB et se révèle efficace pour tester l'effet de différents scénarios environnementaux sur les traits d'histoire de vie des poissons. Cette étude propose ainsi un moyen simple pour généraliser l'utilisation de la théorie DEB à un grand nombre d'espèces dont peu d'informations sont disponibles. Ceci s'avère d'un intérêt

majeur pour les espèces de grands pélagiques dont l'élevage en bassin est limité en raison des difficultés à pérenniser leur maintient en milieu artificiel. Ces difficultés résultent principalement d'un méconnaissance de leur biologie et de leur écologie du fait de la complexité à les observer dans leur habitat naturel.

4 Perspectives

4.1 Applications statistiques

L'approche de modélisation statistique élaborée pour l'étude de la croissance de l'albacore devrait être appliquée aux autres thonidés ciblés par la CTOI, i.e. patudo et lisato. Le patudo présentant une croissance semblable à celle de l'albacore, le même modèle de croissance peut être utilisé. De nouvelles lectures d'otolithes doivent cependant être effectuées. En particulier, elle devront apporter de l'information sur la seconde stance de croissance (individus > 70 cm).
En ce qui concerne le listao, le modèle statistique devra être adapté en raison de l'absence de données renseignant sur l'âge des individus. En effet, les listaos possèdent de petits otolithes caractérisés par un taux d'accrétion irrégulier, en particulier chez les individus matures. Ces otolithes sont donc inexploitables pour les estimations d'âge (Sardenne et al. *in press*). En outre, cette espèce opportuniste présente une période de reproduction continue tout au long de l'année et en conséquent, les fréquences de taille des captures de la pêche commerciale n'affichent pas de tailles modales clairement visibles et interprétables.

4.2 Développement de nouveaux modèles de croissance

Par convention, un modèle de croissance décrit l'évolution de la taille d'un individu en fonction de l'âge. Cependant, des modèles de croissance permettant de prédire directement l'âge des individus à partir de leur taille nous apparaissent plus pertinents. En effet, la taille est une variable facilement mesurable tandis que l'âge absolu repose sur des estimations souvent fastidieuses, ne pouvant être effectuées que pour un nombre limité d'individus, et les données nécessaires ne sont pas toujours disponibles. Aussi, dans de nombreuses évaluations des stocks, les modèles de croissance servent à déterminer la structure d'âge des prises de pêche à partir de leur structure de taille systématiquement connue. Or, les modèles de croissance multi-stances utilisés pour les évaluations des stocks d'albacore des océans Indien (VB log-K) et Atlantique (modèle de Gascuel) ne sont pas réversibles.
D'autre part, un tel modèle devrait faciliter l'intégration des données de marquage-recapture. Dans une première composante du modèle, les âges au marquage des individus pourrait être directement estimés à partir des paramètres de croissance obtenus avec les estimations d'âge. Les données de marquage-recapture serait alors utilisées, dans une deuxième composante, pour actualiser les estimations des paramètres de croissance. Ce modèle permettrait l'identification d'un dimorphisme sexuel à partir des données de marquage d'individus de sexe connu.

4.3 Comparaison avec le patudo

Le travail réalisé sur la modélisation bio-énergétique de l'albacore peut servir au développement d'un modèle DEB pour le patudo. La comparaison entre ces espèces permettrait alors de mieux appréhender les processus à l'origine de l'accélération de la croissance.
L'albacore et le patudo de l'océan Indien sont des espèces physiologiquement très proches dont les juvéniles quasi-semblables présentent le même type de comportement. Au stade juvénile, ces deux espèces se regroupent en bancs avec d'autres espèces de thons (listao) sous des objets flottants naturels ou artificiels. Ces deux espèces auraient alors une croissance comparable jusqu'à 60-70 cm F_L, taille à partir de laquelle elles quittent les bancs. Au stade adulte, le patudo présente des taux de croissance plus faibles que l'albacore, probablement liés à des divergences de comportement. À ce stade, les patudos occupent une plus large zone géographique et se rencontrent à de plus grandes profondeurs que les albacores en raison de systèmes échangeurs de chaleur plus performants et de plus hautes tolérances aux faibles concentrations en oxygène (Brill et al., 1994; Graham and Dickson, 2004; Schaefer and Fuller, 2010).

4.4 Acquisition d'informations sur la biologie de l'albacore

L'acquisition de données expérimentales sur les principaux traits physiologiques de l'albacore et de nouvelles observations en milieu naturel sont nécessaires pour l'estimation de paramètres spécifiques à cette espèce et l'amélioration du modèle.

Une collaboration avec le laboratoire Achotines[3] situé au Panama est à envisager. Il est l'un des rares centres de recherche spécifiquement conçu pour l'étude expérimentale des traits d'histoire de vie des thons tropicaux. Ce centre comprend des réservoirs-viviers aménagés pour la reproduction des albacores et des bassins d'élevage des larves et des juvéniles. Il semble donc à même d'être le siège des expérimentations nécessaires pour informer notre modèle DEB.
Par exemple, des mesures de taux respiratoires sous différentes températures seraient utiles pour évaluer l'influence de la température sur les taux métaboliques. Sous différents niveaux d'activités, ces mesures permettraient de mieux appréhender les dépenses énergétiques liées aux processus de maintenance et à diverses activités (nage, digestion). Des mesures d'ingestion, particulières à différents types de proies, en fonction de la masse corporelle des albacores apparaissent pertinentes pour l'estimation du taux d'ingestion maximal. L'ingestion devrait être mesurée pour divers niveaux d'apports alimentaires et sous différentes températures. La quantification des pertes énergétiques associées, à partir des fèces, permettrait alors une première approximation du taux d'assimilation maximal. Enfin, le coupleur poids-énergie ρ_E peut être directement estimé à partir de la masse fraiche du corps et de la quantité d'énergie associée. Cette dernière peut être évaluée pour les œufs, les larves ou les très jeunes individus à partir de leur composition élémentaire (teneur en eau,

3. www.iattc.org/AchotinesLab/AchotinesDefaultENG.htm

protéines, acides gras, hydrates de carbone) ou à l'aide d'une bombe calorimétrique.

D'autre part, la relation entre la température du corps et la température externe doit être mieux comprise pour étudier l'effet des variations de température sur la croissance. La différence entre ces deux températures peut être mesurée à partir de marques archives implantées dans la cavité abdominale ou dans la masse musculaire. Ces marques apportent également d'autres informations sur l'habitat rencontré, telles que la profondeur (Dagorn et al., 2006). Des marquages électroniques de thons, réalisés au cours du programme RTTP, ont cependant échoué pour des raisons qui demeurent mal comprises.

Les études réalisées au sein du laboratoire Achotines se sont principalement intéressées aux premiers stades de vie (larves et jeunes juvéniles) et au comportement reproducteur. Cependant, la littérature sur ces sujets ne se montre pas suffisamment précise pour être pleinement exploitée dans un DEB.
De l'information sur les premiers stades de vie de l'albacore est nécessaire pour la modélisation de l'ensemble du cycle de vie. Un tel modèle serait un outil utile pour l'étude de la dynamique du stock. Il permettrait, par exemple, de mieux identifier les facteurs impliqués dans la variabilité inter-annuelle de recrutement de l'albacore. Le recrutement est conditionné par la croissance et la survie des œufs et des larves. Ces stades de vie sont très sensibles aux conditions physiques de l'environnement. La température, la salinité, et la quantité de nourriture constitueraient les principaux facteurs limitants. Toutefois, les mouvements et le comportement de ces stades restent difficilement observables *in-situ*, de ce fait peu d'études ont pu réellement vérifier l'influence de ces facteurs.

Une meilleure connaissance du comportement reproducteur est indispensable à la définition de règles plus réalistes pour le module de reproduction. En particulier, le nombre de pontes pendant la saison de fraie, la durée individuelle de celle-ci et les facteurs déclencheurs de ponte sont des informations fondamentales pour définir l'activité reproductrice. Il n'est cependant pas possible d'acquérir ces informations à partir d'individus échantillonnés sur le terrain. En effet, chez l'albacore, les ovaires asynchrones se renouvèlent presque entièrement entre chaque ponte et ne conservent donc pas de trace des précédentes pontes. Le suivi *in-vitro* de femelles reproductrices est alors obligatoire pour le dénombrement des pontes et l'étude du rythme de frai. Qui plus est, ces paramètres pourront être mis en relation avec les conditions physiologiques des géniteurs et certaines caractéristiques de l'environnement (température, alimentation ; Margulies et al., 2007).

4.5 Programme de marquage

Les futures opérations de marquage devront se concentrer sur l'étude du comportement et des mouvements des thons (larves, juvéniles et adultes) en relation avec leur habitat. Des mesures d'épaisseurs de stries des otolithes et l'étude de leur composition chimique permettront non seulement de reconstruire la croissance des individus sur l'ensemble du cycle de vie, mais également d'identifier certaines caractéristiques des habitats fréquentés (température, salinité) et de retracer les migrations des thons (Secor et al., 1995; Campana and Thorrold, 2001). À terme, l'objectif est de disposer de modèles mécanistes ayant de meilleures capacités de prédiction que les modèles statistiques actuels afin de fournir aux gestionnaires et décideurs politiques des avis scientifiques fondés sur les principes biologiques fondamentaux qui régissent les populations marines. En effet, de tels modèles permettront de mieux anticiper les risques d'effondrement du stock face à la pêche, aux changements climatiques, à la pollution et la dégradation des habitats.

References

Albaret, J.-P. (1977). La reproduction de l'albacore (*Thunnus albacares*) dans le Golfe de Guiné. *Cahier O.R.S.T.O.M., Série Océanographie*, XV(4) :389–419.

Altringham, J. D. and Block, B. A. (1997). Why do tuna maintain elevated slow muscle temperatures ? Power output of muscle isolated from endothermic and ectothermic fish. *Journal of Experimental Biology*, 200(20) :2617–2627.

Altringham, J. D. and Ellerby, D. J. (1999). Fish swimming : patterns in muscle function. *The Journal of Experimental Biology*, 202 :3397–3403.

Altringham, J. D. and Shadwick, R. E. (2001). Swimming and muscle function. In *Tuna physiology, ecology and evolution*, volume 19 of *Fish physiology series*, pages 314–344. Academic Press.

Amstrup, S., McDonald, T., and Manly, B. (2005). *Handbook of Capture-Recapture Analysis*. Princeton University Press.

Anderson, R. (1988). Growth and migration of juvenile yellowfin tuna (*Thunnus albacares*) in the central Indian Ocean. *IPTP Collective volume of working documents*, 21 :28–39.

Andrade, H. and Kinas, P. (2004). Estimation of birthdates and catch-at-age using length frequency analysis (LFA), with application for skipjack tuna (*Katsuwonus pelamis*) caught in the Southwest Atlantic. *ICES Journal of Marine Science*, 61 :798–811.

Anonymous (1955). Tagged tuna recoveries. *Pan-American Fisherman*, 10(2) :23 p.

Anonymous (2008). West Sumatera Tuna Tagging Project 2006-2007, Final Report. Technical report.

Bagliniére, J., Castanet, J., Conand, F., and Meunier, F. (1992). Terminologie en sclérochronologie chez les vertébrés. In Baglinière, J., Castanet, J., Conand, F., Meunier, F., and Colloque National, Bondy, editors, *Tissus durs et âge individuel des vertébrés*, Colloques Séminaires, Bondy, pages 443–447. ORSTOM, Paris.

Bard, F. (1984). Croissance de l'albacore (*Thunnus albacares*) Atlantique d'aprés les données des marquages. *Collective Volume of Scientific Papers ICCAT*, 20(1) :104–116.

Bard, F., Chabanet, N., and Caouder, N. (1991). Croissance du thon albacore (*Thunnus albacares*) en Océan Atlantique estimées par marquages. *Collection Volume Scientific Paper ICCAT*, 36 :182–204.

Bard, F.-X., Bach, P., and Josse, E. (1998). Habitat, ecophysiologie des thons : quoi de neuf depuis 15 ans ? In Beckett, J. and ICCAT Tuna Symposium 1998, editors, *Proceedings of ICCAT tuna symposium*, volume 50 of *Collective Volume of Scientific Papers*, pages 319–341.

Bayliff, W. (1991). Status of northern bluefin tuna in the Pacific Ocean. *Inter-American Tropical Tuna Commission Bulletin, Special Report*, 7 :29–88.

Bertignac, M. and De Pontual, H. (2007). Consequences of bias in age estimation on assessment of the northern stock of European hake (*Merluccius merluccius*) and on management advice. *ICES Journal of Marine Science*, 64(5) :981–988.

Bertolero, A., Carretero, M., and Lorente, G. (2005). An assessment of the reliability of growth rings counts for age determination in the Hermann's Tortoise Testudo hermanni. *Amphibia-Reptilia*, 26 :17–23.

Bertrand, A., Josse, E., and Massé, J. (1999). In situ acoustic target-strength measurement of bigeye (*Thunnus obesus*) and yellowfin tuna (*Thunnus albacares*) by coupling split-beam echosounder observations and sonic tracking. *ICES Journal of Marine Science : Journal du Conseil*, 56(1) :51–60.

Blank, J. M., Farwell, C. J., Morrissette, J. M., Schallert, R. J., and Block, B. A. (2007). Influence of swimming speed on metabolic rates of juvenile pacific bluefin tuna and yellowfin tuna. *Physiological and Biochemical Zoology*, 80(2) :167–177.

Block, B. A., Dewar, H., Blackwell, S. B., Williams, T. D., Prince, E. D., Farwell, C. J., Boustany, A., Teo, S. L. H., Seitz, A., Walli, A., and Fudge, D. (2001). Migratory Movements, Depth Preferences, and Thermal Biology of Atlantic Bluefin Tuna. *Science*, 293(5533) :1310–1314.

Block, B. A., Finnerty, J. R., Stewart, A. F., and Kidd, J. (1993). Evolution of Endothermy in Fish : Mapping Physiological Traits on a Molecular Phylogeny. *Science, New Series*, 260(5105) :210–214.

Block, B. A., Keen, J. E., Castillo, B., Dewar, H., Freund, E. V., Marcinek, D. J., Brill, R. W., and Farwell, C. (1997). Environmental preferences of yellowfin tuna (*Thunnus albacares*) at the northern extent of its range. *Marine Biology*, 130(1) :119–132.

Booth, A., Alan, J., and Malcolm, J. (2011). Age validation, growth, mortality, and demographic modeling of spotted gully shark (*Triakis megalopterus*) from the southeast coast of South Africa. *Fishery Bulletin*, 109 :101–112.

Borchani, A. (2010). Statistiques des valeurs extrêmes dans le cas de lois discrètes. Technical Report ESSEC Working Paper 10009, ESSEC Business School.

Bourlès, Y., Alunno-Bruscia, M., Pouvreau, S., Tollu, G., Leguay, D., Arnaud, C., Goulletquer, P., and Kooijman, S. A. L. M. (2009). Modelling growth and reproduction of the Pacific oyster *Crassostrea gigas* : Advances in the oyster-DEB model through application to a coastal pond. *Journal of Sea Research*, 62(2–3) :62–71.

Brill, R. W. (1994). A review of temperature and oxygen tolerance studies of tunas pertinent to fisheries oceanography, movement models and stock assessments. *Fisheries Oceanography*, 3(3) :204–216.

Brill, R. W., Bigelow, K. A., Musly, M. K., Fritsches, K. A., and Warrant, E. J. (2005). Bigeye tuna (*Thunnus obesus*) behavior and physiology and their relevance to stock assessments and fishery biology. *Collective Volume of Scientific Papers ICCAT*, 57(2) :142–161.

Brill, R. W., Block, B. A., Boggs, C. H., Bigelow, K. A., Freund, E. V., and Marcinek, D. J. (1999). Horizontal movements and depth distribution of large adult yellowfin tuna (*Thunnus albacares*) near the Hawaiian Islands, recorded using ultrasonic telemetry : implications for the physiological ecology of pelagic fishes. *Marine Biology*, 133 :395–408.

Brill, R. W. and Bushnell, P. G. (2001). The cardiovascular system of tunas. In *Tuna physiology, ecology and evolution*, volume 19 of *Fish physiology series*, pages 79–120. Academic Press.

Brill, R. W., Dewar, H., and Graham, J. B. (1994). Basic concepts relevant to heat transfer in fishes, and their use in measuring the physiological thermoregulatory abilities of tunas. *Environmental Biology of Fishes*, 40(2) :109–124.

Brill, R. W., Lowe, T. E., and Cousins, K. L. (1998). How water temperature really limits the vertical movements of tunas and billfishes - It's the heart stupid. Towson University, Baltimore, MD. American Fisheries Society.

Brill, R. W. and Lutcavage, M. E. (2001). Understanding Environmental Influences on Movements and Depth Distributions of Tunas and Billfishes Can Significantly Improve Population Assessments. *American Fisheries Society Symposium*, 25 :179–198.

Bromhead, D., Foster, J., Attard, R., Findlay, J., and Kalish, J. (2003). *A review of the impact of fish aggregating devices (FADs) on tuna fisheries*. Final report to Fisheries Resources Research Fund. Australia Department of Agriculture, Fisheries and Forestry, Canberra.

Brown, J., Gillooly, J., Allen, A., Savage, V., and West, G. (2004). Toward a metabolic theory of ecology. *Ecology*, 87(7) :1771–1789.

Buratti, C. and Santos, B. (2010). Otolith microstructure and pelagic larval duration in two stocks of the Argentine hake, *Merluccius hubbsi*. *Fisheries Research*, 106 :2–7.

Bushnell, P. G. and Jones, D. R. (1994). Cardiovascular and respiratory physiology of tuna : adaptations for support of exceptionally high metabolic rates. *Environmental Biology of Fishes*, 40 :303–318.

Caillart, B. and Morize, E. (1989). Etude du rythme de dépôt des microstries sur les otolithes d'un Serranidé tropical, *Epinephelus microdon* (Bleeker) àl'aide d'un marqueur fluorescent : l'oxytétracycline. *Aquatic Living Resources*, 2 :255–261.

Cailliet, G., Smith, W., Mollet, H., and Goldman, K. (2006). Age and growth studies of chondrichthyan fishes : the need for consistency in terminology, verification, validation, and growth function fitting. *Environmental Biology of Fishes*, 77 :211–228.

Campana, S. E. (1999). Chemistry and composition of fish otoliths : pathways, mechanisms and applications. *Marine Ecology Progress Series*, 188 :263–297.

Campana, S. E. (2001). Accuracy, precision and quality control in age determination, including a review of the use and abuse of age validation methods. *Journal of Fish Biology*, 59(2) :197–242.

Campana, S. E. and Thorrold, S. R. (2001). Otoliths, increments, and elements : keys to a comprehensive understanding of fish populations ? *Canadian Journal of Fisheries and Aquatic Sciences*, 58 :30–38.

Campana, S. E. and Neilson, J. D. (1985). Microstructure of Fish Otoliths. *Canadian Journal of Fisheries and Aquatic Sciences*, 42(5) :1014–1032.

Campana, S. E. and Thorrold, S. R. (2001). Otoliths, increments, and elements : keys to a comprehensive understanding of fish populations ? *Canadian Journal of Fisheries and Aquatic Sciences*, 58 :30–38.

Carey, F. G., Kanwisher, J. W., and Stevens, E. D. (1984). Bluefin Tuna Warm Their Viscera During Digestion. *Journal of Experimental Biology*, 109(1) :1–20.

Carey, F. G. and Teal, J. M. (1966). Heat Conservation in Tuna Fish Muscle. *Proceedings of the National Academy of Sciences of the United States of America*, 56(5) :1464–1469.

Carey, F. G., Teal, J. M., Kanwisher, J. W., Lawson, K. D., and Beckett, J. S. (1971). Warm-Bodied Fish. *American Zoologist*, 11(1) :137–143.

Castanet, J., Meunier, F., and Francillon-Vieillot, H. (1992). Squelettochronologie á partir des os et des dents chez les vertébrés. In Baglinière, J., Castanet, J., Conand, F., Meunier, F., and Colloque National, Bondy, editors, *Tissus durs et àge individuel des vertébrés*, Colloques et Séminaires, pages 257–280. ORSTOM, Paris.

Cayré, P. (1989). 3. Bases physiologiques de la thermoécologie des thons : 3.1. Physiologie de la thermorégulation des thons. In Le Gall, J., editor, *Télédétection satellitaire et pècheries thonières océaniques*, Document Technique sur les Pèches - FAO, pages 43–47. FAO, Rome.

Chapman, E. W., Jorgensen, C., and Lutcavage, M. (2011). Atlantic bluefin tuna (*Thunnus thynnus*) : a state-dependent energy allocation model for growth, maturation, and reproductive investment. *Canadian Journal of Fisheries and Aquatic Sciences*, 68 :1934–1951.

Chassot, E. (2011). Projet EMOTION - Estimation of Maternal effects On the sustainability of large pelagic populaTIONs.

Chassot, E., Dubroca, L., Bousquet, N., Dortel, E., and Bonhommeau, S. (2012). Two-stanza growth for tropical tunas : myth or reality ?

Chen, Y., Jiao, Y., and Chen, L. (2003). Developing robust frequentist and Bayesian fish stock assessment methods. *Fish and Fisheries*, 4 :105–120.

Clark, J. S. (2005). Why environmental scientists are becoming Bayesians. *Ecology Letters*, 8(1) :2–14.

Collette, B. B., Reeb, C., and Block, B. A. (2001). Systematics of the tunas and mackerels (Scombridae). In *Tuna physiology, ecology and evolution*, volume 19 of *Fish physiology series*, pages 1–33. Academic Press.

Cotter, A., Burt, L., Paxton, C., Fernandez, C., Buckland, S., and Pan, J. (2004). Are stock assessment methods too complicated ? *Fish and Fisheries*, 5 :235–254.

Couture-Beil, A., Schnute, J., and Haigh, R. (2010). PBSddesolve : solver for delay differential equations. rpackage version 1.08.9.

Cressie, N., Calder, C., Clark, J., Ver Hoef, J., and Wikle, C. (2009). Accounting for uncertainty in ecological analysis : the strengths and limitations of hierarchical statistical modeling. *Ecological Applications*, 19(3) :553–570.

Dabin, W. (2006). Odontochronologie : principe et techniques de déterminqtion de l'âge des odontocètes par histologie des tissus dentaires. *Revue Française d'Histotechnologie*, 19(1) :57–69.

Dagorn, L., Bach, P., and Josse, E. (2000). Movement patterns of large bigeye tuna (*Thunnus obesus*) in the open ocean, determined using ultrasonic telemetry. *Marine Biology*, 136(2) :361–371.

Dagorn, L., Holland, K. N., Hallier, J. P., Taquet, M., Moreno, G., Sancho, G., Itano, D. G., Aumeeruddy, R., Girard, C., Million, J., and Fonteneau, A. (2006). Deep diving behavior observed in yellowfin tuna (*Thunnus albacares*). *Aquatic Living Resources*, 19 :85–88.

Davidoff, E. (1963). Size and year class composition of catch, age and growth of yellowfin tuna in the eastern tropical Pacific Ocean. *Inter-American Tropical Tuna Commission Bulletin*, 8(4) :199–251.

De Pontual, H., Groison, A., Piñeiro, C., and Bertignac, M. (2006). Evidence of underestimation of European hake growth in the Bay of Biscay, and its relationship with bias in the agreed method of age estimation. *ICES Journal of Marine Science*, 63 :1674–1681.

Degens, E. T., Deuser, W. G., and Haedrich, R. L. (1969). Molecular structure and composition of fish otoliths. *Marine Biology*, 2(2) :105–113.

Dewar, H. and Graham, J. B. (1994). Studies of tropical tuna swimming performance in a large water tunnel. *The Journal of Experimental Biology*, 192 :13–31.

Diaz, E. (1963). An increment technique for estimating growth parameters of tropical tunas, as applied to yellowfin tuna (*Thunnus albacares*). *Inter-American Tropical Tuna Commission Bulletin*, 8(7) :383–416.

Dickson, K. A. and Graham, J. B. (2004). Evolution and Consequences of Endothermy in Fishes. *Physiological and Biochemical Zoology*, 77(6) :998–1018.

Dizon, A. E. and Brill, R. W. (1979). Thermoregulation in yellowfin tuna, *Thunnus albacares*. *Physiological Zoology*, 52 :581–593.

Dortel, E., Massiot-Granier, F., Rivot, E., Million, J., Hallier, J., Morize, E., Munaron, J., Bousquet, N., and Chassot, E. (2013). Accounting for age uncertainty in growth modeling, the case study of yellowfin tuna *Thunnus albacares* of the Indian Ocean. *PLoS ONE*, 8(4) :1–12.

Dortel, E., Sardenne, F., Bousquet, N., Rivot, E., Million, J., Le Croizier, G., and Chassot, E. (*in submission*). An integrated Bayesian modeling approach for the growth of Indian Ocean yellowfin tuna. *Fisheries Research*.

Dortel, E., Sardenne, F., Le Croizier, G., Million, J., Hallier, J.-P., Morize, E., Munaron, J.-M., Bousquet, N., and Chassot, E. (2012). A hierarchical Bayesian integrated model incorporated direct ageing, mark-recapture and length-frequency data for yellowfin (*Thunnus albacares*) and bigeye (*Thunnus obesus*) of the Indian Ocean. *IOTC Working Party on Tropical Tunas*, 14(24) :38p.

Dotson, R. C. (1976). Minimum swimming speed of albacore, *Thunnus alalunga*. *Fishery Bulletin*, 74(4) :955–960.

Draganik, B. and Pelczarski, W. (1984). Growth and age of bigeye and yellowfin tuna in the central Atlantic as per data gathered by R/V "WIECZNO". *Collection Volume Scientific Paper ICCAT*, 20(1) :96–103.

Driggers, W., Grego, J., and Dean, J. (1999). Age and growth of yellowfin tuna (*Thunnus albacares*) in the western north Atlantic Ocean. *Collective Volume of Scientific Papers ICCAT*, 49(3) :374–383.

Eaton, M. and Link, W. (2011). Estimating age from recapture data : integrating incremental growth measures with ancillary data to infer age-at-length. *Ecological Applications*, 21(7) :2487–2497.

Eltink, A., Newton, A., Morgado, C., Santamaria, M., and Modin, J. (2000). Guidelines and tools for age reading comparisons (PDF document version 1.0 October 2000) Internet : http ://www.efan.no.

Essington, T., Kitchell, J., and Walters, C. (2001). The von Bertalanffy growth function, bioenergetics, and the consumption rates of fish. *Canadian Journal of Fisheries and Aquatic Sciences*, 58 :2129–2138.

Essington, T. E. (2003). Development and Sensitivity Analysis of Bioenergetics Models for Skipjack Tuna and Albacore : A Comparison of Alternative Life Histories. *Transactions of the American Fisheries Society*, 132 :759–770.

Eveson, J. and Million, J. (2008). Estimation of growth parameters for yellowfin, bigeye and skipjack tuna using tag-recapture data. *IOTC Working Party on Tagging Data Analysis*, 7(07) :31p.

Eveson, J. P., Laslett, G. M., and Polacheck, T. (2004). An integrated model for growth incorporating tag-recapture, length-frequency, and direct aging data. *Canadian Journal of Aquatic and Fisheries Sciences*, 61 :292–306.

Eveson, J. P., Million, J., Sardenne, F., and Le Croizier, G. (2012). Updated growth estimates for skipjack, yellowfin and bigeye tuna in the Indian Ocean using the most recent tag-recapture and otolith data. *IOTC Working Party on Tropical Tunas*, 14(23) :57p.

Eveson, J., Million, J., Sardenne, F., and Le Croizier, G. (*in press*). Estimating growth of tropical tunas in the Indian Ocean using tag-recapture data and otolith-based age estimates. *Fisheries Research*.

Fabens, A. (1965). Properties and fitting of the Von Bertalanffy growth curve. *Growth*, 29 :265–289.

Fänge, R. (1983). Gas exchange in fish swim bladder. In *Reviews of Physiology, Biochemistry and Pharmacology, Volume 97*, number 97 in Reviews of Physiology, Biochemistry and Pharmacology, pages 111–158. Springer Berlin Heidelberg.

FAO Fisheries Departement (FAO-FI) (2013). Review of the state of world marine fishery resources 2011. World Global Tuna Fisheries, 2009. FIRMS Reports. In *Fishery Resources Monitoring System (FIRMS)*. FAO, Rome.

Farley, J., Clear, N., Leroy, B., Davis, T., and McPerson, G. (2006). Age, growth and preliminary estimates of maturity of bigeye tuna, *Thunnus obesus*, in the Australian region. *Marine and Freshwater Research*, 57 :713–724.

Farrell, A. P. and Jones, D. R. (1992). 1. The Heart. In W.S. Hoar, D. R. and Farrell, A., editors, *Fish Physiology*, volume Volume 12, Part A of *The Cardiovascular System*, pages 1–88. Academic Press.

Firoozi, A. and Carrara, G. (1992). An analysis of lengh-frequencies of Thunnus albacares in Iranian waters. *IPTP Collective volume of working documents*, 8 :95–102.

Fish, F. (2010). Swimming Strategies for Energy Economy. In Domenici, P. and Kapoor, B., editors, *Fish Locomotion*, pages 90–122. Science Publishers.

Fitzgibbon, Q., Baudinette, R., Musgrove, R., and Seymour, R. (2008). Routine metabolic rate of southern bluefin tuna (*Thunnus maccoyii*). *Comparative Biochemistry and Physiology Part A : Molecular & Integrative Physiology*, 150(2) :231–238.

Fitzgibbon, Q. P., Seymour, R. S., Buchanan, J., Musgrove, R., and Carragher, J. (2010). Effects of hypoxia on oxygen consumption, swimming velocity and gut evacuation in southern bluefin tuna (*Thunnus maccoyii*). *Environmental Biology of Fishes*, 89(1) :59–69.

Floch, L., Delgado de Molina, A., Assan, C., Dewals, P., Areso, J., and Chassot, E. (2012). Statistics of the European purse seine fishing fleet and associated flags targeting tropical tunas in the Indian Ocean (1981-2011). *IOTC Working Party of Tropical Tuna*, 14(22) :32 p.

Fonteneau, A. (1980). Croissance de l'albacore (*Thunnus albacares*) de l'Atlantique Est. *Collective Volume of Scientific Papers ICCAT*, 9(1) :152–168.

Fonteneau, A. (1981). Dynamique de la population d'albacore (*Thunnus albacares*, Bonnaterre 1788) de l'Océan. PhD thesis, Université Pierre et Marie Curie

Fonteneau, A. (2010). *Atlas des pécheries thoniéres de l'Océan Indien = Atlas of Indian Ocean tuna fisheries*. IRD, Marseille.

Fonteneau, A., Ariz, J., Gaertner, D., Nordstrom, V., and Pallares, P. (2000). Observed changes in the species composition of tuna schools in the Gulf of Guinea between 1981 and 1999, in relation with the Fish Aggregating Device fishery. *Aquatic Living Resources*, 13 :253–257.

Fonteneau, A. and Gascuel, D. (2008). Growth rates and apparent growth curves, for yellowfin, skipjack and bigeye tagged and recovered in the Indian Ocean during the IOTTP. *IOTC Working Party of Tagging Data Analysis*, 8 :23p.

Fournier, D., Hampton, J., and Sibert, J. (1998). MULTIFAN-CL : a length-based, age-structured model for fisheries stock assessment, with application to South Pacific albacore, *Thunnus alalunga*. *Canadian Journal of Fisheries and Aquatic Sciences*, 55 :2105–2116.

FranceAgriMer (2011). Le marché mondial du thon, production et échanges, Zoom sur le marché français. Les synthèses de FranceAgriMer, Pêche/Aquaculture 2.

Freitas, V., Cardoso, J. F. M. F., Lika, K., Peck, M. A., Campos, J., Kooijman, S. A. L. M., and van der Veer, H. W. (2010). Temperature tolerance and energetics : a dynamic energy budget-based comparison of North Atlantic marine species. *Philosophical Transactions of the Royal Society B : Biological Sciences*, 365(1557) :3553–3565.

Fréon, P. and Dagorn, L. (2000). Review of fish associative behaviour : Toward a generalisation of the meeting point hypothesis. *Reviews in Fish Biology and Fisheries*, 10(2) :183–207.

Gaertner, D. and Pagavino, M. (1992). Observation sur la croissance de l'albacore (*Thunnus albacares*) dans l'Atlantique Ouest. *Collection Volume Scientific Paper ICCAT*, 36 :479–505.

Gascuel, D. (1994). Une méthode simple d'ajustement des clés taille/âge : application aux captures d'albacores (*Thunnus albacares*) de l'Atlantique Est. *Canadian Journal of Fisheries and Aquatic Sciences*, 51 :723–733.

Gascuel, D., Fonteneau, A., and Capisano, C. (1992). Modélisation d'une croissance en deux stances chez l'albacore (*Thunnus albacares*) de l'Atlantique Est. *Aquatic Living Resources*, 5 :155–172.

Gelman, A., Carlin, J., Stern, H., and Rubin, D. (2004). *Bayesian Data Analysis, Second Edition*. Chapman & Hall/CRC Texts in Statistical Science, CRC press book edition.

Gelman, A. and Rubin, D. (1992). Inference from iterative simulation using multiple sequences. *Statistical Science*, 7(4) :457–511.

Gerritsen, H., McGrath, D., and Lordan, C. (2006). A simple method for comparing age-length keys reveals significant regional differences within a single stock of haddock (*Melanogrammus aeglefinus*). *ICES Journal of Marine Science*, 63 :1096–1100.

Gilman, E., Chaloupka, M., Read, A., Dalzell, P., Holetschek, J., and Curtice, C. (2012). Hawaii longline tuna fishery temporal trends in standardized catch rates and length distributions and effects on pelagic and seamount ecosystems. *Aquatic Conservation : Marine and Freshwater Ecosystems*, page 43p.

Gimenez, O., Viallefont, A., Catchpole, E. A., Choquet, R., and Morgan, B. J. T. (2004). Methods for investigating parameter redundancy. *Animal Biodiversity and Conservation*, 27(1) :561–572.

Graham, J. B. and Dickson, K. A. (2001). Anatomical and physiological specializations for endothermy. In *Tuna physiology, ecology and evolution*, volume 19 of *Fish physiology series*, pages 121–165. Academic Press.

Graham, J. B. and Dickson, K. A. (2004). Tuna comparative physiology. *The Journal of Experimental Biology*, 207 :4015–4024.

Graham, J. B. and Laurs, R. M. (1982). Metabolic rate of the albacore tuna *Thunnus alalunga*. *Marine Biology*, 72(1) :1–6.

Hallier, J. (2008). Status of the Indian Ocean tuna tagging programme - RTTP-IO. *IOTC Working Party of Tagging Data Analysis*, 10 :40p.

Hallier, J. P., Anganuzzi, A., and Sugathadasa, N. (2010). Regional tuna tagging project - indian ocean : It consultant documentation. Final report, Indian Ocean Tuna Commission.

Hallier, J. P. and Gaertner, D. (2008). Drifting fish aggregation devices could act as an ecological trap for tropical tuna species. *Marine Ecology Progress Series*, 353 :255–264.

Hampton, J. (2000). Natural mortality rates in tropical tunas : size really does matter. *Canadian Journal of Fisheries and Aquatic Sciences*, 57 :1002–1010.

Hampton, J. (2008). Effect of purse seine selectivity and individual variability in growth on tag length increments. *IOTC*.

Hampton, J. and Fournier, D. (2001). A spatially-disaggregated, length-based, age-structured population model of yellowfin tuna (*Thunnus albacares*) in the western and central Pacific Ocean. *Marine and Freshwater Research*, 52 :937–963.

Hansen, M., Boisclair, D., Brandt, S., Hewett, S., Kitchell, J., Lucas, M., and Ney, J. (1993). Applications of Bioenergetics Models to Fish Ecology and Management : Where Do We Go from Here ? *Transactions of the American Fisheries Society*, 122 :1019–1030.

Hasselblad, V. (1966). Estimation of parameters for a mixture of normal distributions. *Technometrics*, 8(3) :431–444.

Hayes, E. and Wall, R. (1999). Age-grading adult insects : a review of techniques. *Physiological Entomology*, 24(24) :1–10.

Hearn, W. S. and Polacheck, T. (2003). Estimating long-term growth-rate changes of southern bluefin tuna (*Thunnus maccoyii*) from two periods of tag-return data. *Fishery bulletin*, 101 :58–74.

Hennemuth, R. (1961). Size and year class composition of catch, age and growth of yellowfin tuna in the eastern tropical pacific ocean. *Inter-American Tropical Tuna Commission Bulletin*, 5(1) :1–112.

Herpandi, N. H., Rosma, A., and Wan Nadiah, W. (2011). The Tuna Fishing Industry : A New Outlook on Fish Protein Hydrolysates. *Comprehensive Reviews in Food Science and Food Safety*, 10(4) :195–207.

Herrera, M. and Pierre, L. (2010). Status of IOTC databases for tropical tunas. *IOTC Working Party of Tropical Tuna*, 3 :28p.

Hilborn, R. and Mangel, M. (1997). *The Ecological Detective : Confronting Models with Data*. Princeton University Press.

Huang, C., Sun, L., and Yang, R. (1973). Age, growth and population structure of Indian yellowfin tuna. *Journal of the Fisheries Society of Taiwan*, 2 :16–30.

Huang, C. and Yang, R. (1974). Age and growth of yellowfin tuna in the waters around the southern part of Taiwan. *Journal of the Fisheries Society of Taiwan*, 3(2).

IOTC (2012). Report of the Fourteenth Session of the IOTC Working Party on Tropical Tunas. *IOTC Working Party of Tropical Tuna*, 14 :88p.

Itano, D. G. (2000). The reproductively biology of yellowfin tuna (*Thunnus albacares*) in Hawaiian waters and the Western Tropical Pacific Ocean : Project Summary. *SOEST 00-01, JIMAR Contribution 00-328*.

Jennings, S., Greenstreet, S. P. R., and Reynolds, J. D. (1999). Structural change in an exploited fish community : a consequence of differential fishing effects on species with contrasting life histories. *Journal of Animal Ecology*, 68(3) :617–627.

Jones, F. R. H. (1951). The Swimbladder and the Vertical Movement of Teleostean Fishes I. Physical Factors. *Journal of Experimental Biology*, 28(4) :553–566.

Jusup, M., Klanjscek, T., Matsuda, H., and Kooijman, S. (2011). A full lifecycle bioenergetic model for bluefin tuna. *PLoS ONE*, 6(7) :1–17.

Kaji, T., Tanaka, M., Oka, M., Takeuchi, H., Ohsumi, S., Teruya, K., and Hirokawa, J. (1999). Growth and Morphological Development of Laboratory-Reared Yellowfin Tuna *Thunnus albacares* Larvae and Early Juveniles, with Special Emphasis on the Digestive System. *Fisheries Science*, 65(5) :700–707.

Karkach, A. (2006). Trajectories and models of individual growth. *Demographic Research*, 15(12) :347–40.

Katsanevakis, S. (2006). Modelling fish growth : model selection, multi-model inference and model selection uncertainty. *Fisheries Research*, 81 :229–235.

King, J. and McFarlane, G. (2003). Marine fish life history strategies : applications to fishery management. *Fisheries Management and Ecology*, 10 :249–264.

Kirkwood, T. and Austad, S. (2000). Why do we age ? *Nature*, 408 :233–238.

Kitchell, J. F., Stewart, D., and Weininger, D. (1977). Applications of a bioenergetics model to yellow perch (*Perca flavescens*) and walleye (*Stizostedion vitreum vitreum*). *Journal of the Fisheries Research Board of Canada*, 34 :1922–1935.

Kolody, D. (2011). Can length-based selectivity explain the two stage growth curve observed in indian ocean YFT and BET ? *IOTC Working Party of Tropical Tuna*, 13(33) :5 p.

Kooijman, S. (1986). Energy budgets can explain body size relations. *Journal of Theoretical Biology*, 121 :269–282.

Kooijman, S. (2010). *Dynamic Energy Budget Theory for Metabolic Organisation*. Cambridge Univerty Press, third edition edition.

Kooijman, S., Sousa, T., Pecquerie, L., van der Meer, J., and Jager, T. (2008). From food-dependent statistics to metabolic parameters, a practical guide to the use of dynamic energy budget theory. *Biological Reviews*, 83 :533–552.

Korsmeyer, K. E. and Dewar, H. (2001). Tuna metabolism and energetics. In *Tuna physiology, ecology and evolution*, volume 19 of *Fish physiology series*, pages 35–78. Academic Press.

Korsmeyer, K. E., Lai, N. C., Shadwick, R. E., and Graham, J. B. (1997). Heart rate and stroke volume contributions to cardiac output in swimming yellowfin tuna : response to exercise and temperature. *The Journal of Experimental Biology*, 200 :1975–1986.

Kume, S. and Joseph, J. (1966). Size composition, growth and sexual maturity of bigeye tuna, *Thunnus obesus* (Lowe), from the japanese lon-line fishery in the Eastern Pacific Ocean. *Inter-American Tropical Tuna Commission Bulletin*, 11(2) :47–75.

Kunal, S., Kumar, G., and Menezes, M. (2014). Genetic Variation in Yellowfin Tuna *Thunnus Albacares* (Bonnaterre, 1788) Along Indian Coast Using Pcr-Rflp Analysis of Mitochondrial Dna D-Loop Region. *International Journal of Scientific Research*, 3(1) :25–30.

Langley, A., Herrera, M., and Million, J. (2012). Stock assessment of yellowfin tuna in the Indian Ocean using MULTIFAN-CL. *IOTC Working Party of Tropical Tuna*, 14(38) :72 p.

Laslett, G., Eveson, J., and Polacheck, T. (2002). A flexible maximum likelihood approach for fitting growth curves to tag-recapture data. *Canadian Journal of Fisheries and Aquatic Sciences*, 59 :976–986.

Laslett, G., Eveson, J., and Polacheck, T. (2004). Fitting growth models to length frequency data. *ICES Journal of Marine Science*, 61 :218–230.

Laurec, A. and Le Guen, J.-C. (1981). *Dynamique des populations marines exploitées - Tome 1 Concepts et Modèles*. Number 45 in Rapports scientifiques et techniques. Centre National pour l'Exploitation des Océans.

Law, R. (2000). Fishing, selection, and phenotypic evolution. *ICES Journal of Marine Science*, 57 :659–668.

Le Guen, J. and Sakagawa, G. (1972). Apparent growth of yellowfin tuna from the Eastern Atlantic Ocean. *Fishery Bulletin U.S.*, 71(1) :175–187.

Le Guen, J. and Sakagawa, G. (1973). Apparent growth of yellowfin tuna from the Eastern Atlantic ocean. *Fishery Bulletin*, 71(1) :175–187.

Lehodey, P. and Leroy, B. (1999). Age and growth of yellowfin tuna (*Thunnus albacares*) from the western and central Pacific Ocean as indicated by daily growth increments and tagging data. *12th Meeting of the SCTB, Working Paper YFT-2*, pages 1–21.

Lessa, R. and Duarte-Neto, P. (2004). Age and growth of yellowfin tuna (*Thunnus albacares*) in the western equatorial Atlantic, using dorsal fin spines. *Fisheries Research*, 69 :157–170.

Li, T., Wang, C., and Yeh, Y. (1995). Age and growth of yellowfin tuna influenced by the human exploitation. *ACTA Oceanographica Taiwanica*, 34(4) :43–60.

Longhurst, A. R. and Pauly, D. (1987). Dynamic of Tropical Fish Populations. In *Ecology of Tropical Oceans*, pages 257–370. Academic Press inc., San Diego.

Lucena, F. and O'Brien, C. (2001). Effects of gear selectivity and different calculation methods on estimating growth parameters of bluefish, *Pomatomus saltatrix* (Pisces : Pomatomidae), from southern Brazil. *Fishery Bulletin*, 99 :432–442.

Ludwig, D., Hilborn, R., and Walters, C. (1993). Uncertainty, Resource Exploitation, and Conservation : Lessons from History. *Science*, 260(5104) :17–36.

Lumineau, O. (2002). Study of the growth of Yellowfin tuna (*Thunnus albacares*) in the Western Indian Ocean based on length frequency data. *IOTC Proceedings*, 5 :316–327.

Macdonald, P. and Green, P. (1988). User's guide to program MIX : An interactive program for fitting mixtures of distributions. *Ichthus Data Systems*.

Magnuson, J. (1973). Comparative study of adaptations for continuous swimming and hydrostatic equilibrum of Scombroid and Xiphoid fishes. *Fishery Bulletin*, 71(2) :337–356.

Majkowski, J. (2007). Global fishery resources of tuna and tuna-like species. FAO Fisheries Technical Paper 483, FAO, Rome.

Maldeniya, R. (1996). Food consumption of yellowfin tuna, *Thunnus albacares*, in Sri Lankan waters. *Environmental Biology of Fishes*, 47 :101–107.

Marcille, J. and Stéquert, B. (1976). Croissance des jeunes albacores *Thunnus albacares* et patudo *Thunnus obsesus* de la côte Nord-Ouest de Madagascar. *Cahier O.R.S.T.O.M., Série Océanographie*, XIV(2) :153–162.

Margulies, D., Suter, J. M., Hunt, S. L., Olson, R. J., Scholey, V. P., Wexler, J. B., and Nakazawa, A. (2007). Spawning and early development of captive yellowfin tuna (*Thunnus albacares*). *Fishery Bulletin*, 105 :249–265.

Marriott, R. J. and Mapstone, B. D. (2006). Consequences of inappropriate criteria for accepting age estimates from otoliths, with a case study for a long-lived tropical reef fish. *Canadian Journal of Fisheries and Aquatic Sciences*, 63(10) :2259–2274.

Marsac, F. (1991). Preliminary study of the growth of yellowfin estimated from purse seine data in the Western Indian Ocean. *IPTP Collective volume of working documents*, 6 :35–39.

Marsac, F., Fonteneau, A., and Ménard, F. (2000). Drifting FADs used in tuna fisheries : an ecological trap ? In Le Gall, J., Cayré, P., Taquet, M., and Pêhe Thonière et Dispositifs de Concentration de Poissons : Colloque Caraibe-Martinique, Trois-Ilets (MTK), 1999/10/15-19, editors, *Pêche thonière et dispositifs de concentration de poissons*, number 28 in Actes de Colloques - IFREMER, pages 537–552. IFREMER, Plouzané.

Marsac, F. and Lablache, G. (1985). Preliminary study of the growth of yellowfin estimated from purse seine data in the Western Indian Ocean. *IPTP Collective volume of working documents*, pages 91–110.

Maury, O. and Poggiale, J. (2013). From individuals to populations to communities : A dynamic energy budget model of marine ecosystem size-spectrum including life history diversity. *Journal of Theoretical Biology*, 324 :52–71.

Mcfee, W. E., Schwacke, J. H., Stolen, M. K., Mullin, K. D., and Schwacke, L. H. (2009). Investigation of growth phases for bottlenose dolphins using a bayesian modeling approach. *Marine mammal science*, 26(1) :67–85.

Meyer, R. and Millar, R. (1999). BUGS in Bayesian stock assessments. *Canadian Journal of Fisheries and Aquatic Sciences*, 56 :1078–1086.

Mitchell, N., Dardeau, M., and Schroeder, W. (1993). Colony morphology, age structure, and relative growth of two gorgonian corals, *Leptogorgia hebes* (Verrill) and *Leptogorgia virgulata* (Lamarck), from the northern Gulf of Mexico. *Coral Reefs*, 12 :65–70.

Miyabe, N. (1984). On the growth of yellowfin and bigeye tuna estimated from the tagging results. *ICCAT Rec. Doc. Sci.*, 1 :117–122.

Miyake, M., Guillotreau, P., Sun, C., and Ishimura, G. (2010). *Recent developments in the tuna industry : stocks, fisheries, management, processing, trade and markets.* FAO Fisheries Technical Paper No. 543. Rome, FAO.

Miyake, M., Miyabe, N., and Nakano, H. (2004). *Historical trends of tuna catches in the world*, volume 467 of *FAO Fisheries Technical Paper* No. 467. Rome, FAO.

Mohan, M. and Kunhikoya, K. (1985). Age and growth of *Katsuwonus pelamis* (Linnaeus) and *Thunnus albacares* (Bonnaterre) from Minicoy waters. *Central Marine Fisheries Research Institute*, 36(14) :143–216.

Moore, H. (1951). Estimation of age and growth of yellowfin tuna (*Neothunnus macropterus*) in Hawaiian waters by size frequencies. *U.S. Fish and Wildlife Service, Fishery Bulletin*, 52(65) :132–149.

Morales-Nin, B. (2000). Review of the growth regulation processes of otolith daily increment formation. *Fisheries Research*, 46 :53–67.

Morize, E., Munaron, J.-M., Hallier, J.-P., and Million, J. (2008). Preliminary growth studies of yellowfin and bigeye tuna (*Thunnus albacares* and *T. obesus*) in the Indian Ocean by otolith analysis. *IOTC Working Party on Tropical Tunas*, (30) :1–13.

Morton, R. and Bravington, M. (2008). Comparison of methods for estimating age composition with application to Southern Bluefin Tuna (*Thunnus maccoyii*). *Fisheries Research*, 93 :22–28.

Moura, P., Gaspar, M. B., and Monteiro, C. C. (2009). Age determination and growth rate of a *Callista chione* population from the southwestern coast of Portugal. *AQUATIC BIOLOGY*, 5 :97–106.

Mourente, G. and Tocher, D. R. (2009). Tuna Nutrition and Feeds : Current Status and Future Perspectives. *Reviews in Fisheries Science*, 17(3) :373–390.

Mugiya, Y. and Tanaka, S. (1992). Otolith development, increment formation, and an uncoupling of otolith to somatic growth rates in larval and juvenile Goldfish. *Nippon Suisan Gakkaishi*, 58(5) :845–851.

Natanson, L., Kohler, N., Ardizzone, D., Cailliet, G., Wintner, S., and Mollet, H. (2006). Validated age and growth estimates for the shortfin mako, *Isurus oxyrinchus*, in the North Atlantic Ocean. *Environmental Biology of Fishes*, 77 :367–383.

Nauen, J. C. and Lauder, G. V. (2000). Locomotion in scombrid fishes : morphology and kinematics of the finlets of the chub mackerel *Scomber japonicus*. *Journal of Experimental Biology*, 203(15) :2247–2259.

Neilson, J. (1992). Sources of error in otolith microstructure examination *In* D.K. Stevenson and S.E. Campana, Otolith microstructure examination and analysis. *Canadian Special Publication Fisheries Aquatic Science*, 117 :115–126.

Ney, J. (1993). Bioenergetics Modeling Today : Growing Pains on the Cutting Edge. *Transactions of the American Fisheries Society*, 122 :736–748.

Nisbet, R., Muller, E., Lika, K., and Kooijman, S. (2000). From molecules to ecosystems through dynamic energy budget models. *Journal of Animal Ecology*, 69 :913–926.

Nisbet, R. M., Jusup, M., Klanjscek, T., and Pecquerie, L. (2012). Integrating dynamic energy budget (DEB) theory with traditional bioenergetic models. *The Journal of Experimental Biology*, 215 :892–902.

Nisbet, R. M., Muller, E. B., Brooks, A. J., and Hosseini, P. (1997). Models relating individual and population response to contaminants. *Environmental Modeling & Assessment*, 2(1-2) :7–12.

Nishida, T., Chow, S., Ikame, S., and Kurihara, S. (2001). RFLP analysis on single copy nuclear gene loci in yellowfin tuna (*Thunnus albacares*) to examine the genetic differentiation between the western and eastern samples from the Indian Ocean. *IOTC Proceedings*, 16(4) :437–441.

Nishida, T. and Rademeyer, R. (2011). Stock and risk assessments on bigeye tuna (*Thunnus obesus*) in the Indian Ocean based on AD Model Builder implemented Age-Structured Production Model (ASPM). *IOTC Working Party of Tropical Tuna*, 13(42) :23p.

Nootmorn, P., Yakoh, A., and Kawises, K. (2005). Reproductive biology of yellowfin tuna in the Eastern Indian Ocean. *IOTC Working Party of Tropical Tuna*, 14 :379–385.

Norberg, B., Weltzien, F.-A., Karlsen, O., and Holm, J. C. (2001). Effects of photoperiod on sexual maturation and somatic growth in male Atlantic halibut (*Hippoglossus hippoglossus* L.). *Comparative Biochemistry and Physiology Part B*, 129 :357–365.

Norbis, W., Lorenzo, M., and Torres, G. (1999). Intra-annual growth variations of young-of-the-year hake (*Merluccius hubbsi*) of the Uruguayan continental shelf based on otolith analysis. *Fisheries Research*, 44 :129–137.

Ohta, I. and Kakuma, S. (2005). Periodic behavior and residence time of yellowfin and bigeye tuna associated with fish aggregating devices around Okinawa Islands, as identified with automated listening stations. *Marine Biology*, 146 :581–594.

Ortega, A. and Mourente, G. (2010). Comparison of the lipid profiles from wild caught eggs and unfed larvae of two scombroid fish : northern bluefin tuna (*Thunnus thynnus* L., 1758) and Atlantic bonito (*Sarda sarda* Bloch, 1793). *Fish Physiology and Biochemistry*, 36 :461–471.

Panfili, J., De Pontual, H., Troadec, H., and Wright, P. (2002). *Manuel de sclérochronologie des poissons*. Coédition Ifremer-IRD.

Panfili, J., Tomas, J., and Morales-Nin, B. (2009). Otolith microstructure in tropical fish. In *Tropical fish otoliths : information for assessment, management and ecology*, Methods and Technologies in Fish Biology and Fisheries Volume 11 : 212-248. Green B.S. et al. [Ed.].

Pannella, G. (1971). Fish Otoliths : Daily Growth Layers and Periodical Patterns. *Science*, 173(4002) :1124–1127.

Pauly, D. (1985). Quelques méthodes simples pour l'estimation des stocks de poissons tropicaux. *FAO Document Technique sur les Pêches*, 234 :56p.

Pauly, D. and Morgan, G. (1987). *Length-based methods in fisheries research*. Number 13 in ICLARM Conference Proceedings.

Pecquerie, L., Johnson, L. R., Kooijman, S. A. L. M., and Nisbet, R. M. (2011). Analyzing variations in life-history traits of Pacific salmon in the context of Dynamic Energy Budget (DEB) theory. *Journal of Sea Research*, 66(4) :424–433.

Pecquerie, L., Petitgas, P., and Kooijman, S. A. L. M. (2009). Modeling fish growth and reproduction in the context of the Dynamic Energy Budget theory to predict environmental impact on anchovy spawning duration. *Journal of Sea Research*, 62 :93–105.

Pethybridge, H., Roos, D., Loizeau, V., Pecquerie, L., and Bacher, C. (2013). Responses of European anchovy vital rates and population growth to environmental fluctuations : An individual-based modeling approach. *Ecological Modelling*, 250 :370–383.

Pianet, R. (1999). Évolution du système de collecte et de traitement des données de la pêche thonière des senneurs européens et assimilés de 1981 à 1998. *IOTC Proceedings*, 2 :74–96.

Pillai, G. N. and Satheeshkumar, P. (2012). Biology, Fishery, Conservation and Management of Indian Ocean Tuna Fisheries. *Ocean Science Journal*, 47(4) :411–433.

Popper, A. N., Ramcharitar, J., and Campana, S. E. (2005). Why otoliths ? Insights from inner ear physiology and fisheries biology. *Marine and Freshwater Research*, 56 :497–504.

Potier, M., Marsac, F., Cherel, Y., Lucas, V., Sabatié, R., Maury, O., and Ménard, F. (2007). Forage fauna in the diet of three large pelagic fishes (lancetfish, swordfish and yellowfin tuna) in the western equatorial Indian Ocean. *Fisheries Research*, 83 :60–72.

Potier, M., Marsac, F., Lucas, V., Sabatié, R., Hallier, J. P., and Ménard, F. (2004). Feeding Partitioning among Tuna Taken in Surface and Mid-water Layers : The Case of Yellowfin (*Thunnus albacares*) and Bigeye (*T. obesus*) in the Western Tropical Indian Ocean. *Western Indian Ocean Journal of Marine Science*, 3(1) :51–62.

Potier, M., Sabatié, R., Ménard, F., and Marsac, F. (2001). Preliminary results of tuna diet studies in the west equatorial Indian Ocean. *IOTC Proceedings*, 4 :273–278.

Punt, A. and Hilborn, R. (1997). Fisheries stock assessment and decision analysis : the Bayesian approach. *Reviews in Fish Biology and Fisheries*, 7 :35–63.

Punt, A. E., Smith, D. C., KrusicGolub, K., and Robertson, S. (2008). Quantifying age-reading error for use in fisheries stock assessments, with application to species in Australia's southern and eastern scalefish and shark fishery. *Canadian Journal of Fisheries and Aquatic Sciences*, 65(9) :1991–2005.

R Development Core Team (2010). *R : A Language and Environment for Statistical Computing*. R Foundation for Statistical Computing, Vienna, Austria. ISBN 3-900051-07-0.

Radtke, R. and Fey, D. P. (1996). Environmental effects on primary increment formation in the otoliths of newly-hatched Arctic charr. *Journal of Fish Biology*, 48(6) :1238–1255.

Ren, J. S. and Schiel, D. R. (2008). A dynamic energy budget model : parameterisation and application to the Pacific oyster *Crassostrea gigas* in New Zealand waters. *Journal of Experimental Marine Biology and Ecology*, 361(1) :42–48.

Restrepo, V., Diaz, G., Walter, J., Neilson, J., Campana, S., Secor, D., and Wingate, R. (2010). Updated estimate of the growth curve of Western Atlantic bluefin tuna. *Aquatic Living Resources*, 23 :335–342.

Ricker, W. (1975). *Computation and Interpretation of Biological Statistics of Fish Population*. Number 191 in Bulletin of the Fisheries Research Board of Canada. Department of the Environment, Fisheries and Marine Service, Ottawa.

Roff, D. A. (1983). An Allocation Model of Growth and Reproduction in Fish. *Canadian Journal of Fisheries and Aquatic Sciences*, 40 :1395–1404.

Rohit, P. and Rammohan, K. (2009). Fishery and Biological Aspects of Yellowfin Tuna *Thunnus albacares* along Andhra Coast, India. *Asian Fisheries Science*, 22 :235–244.

Romanov, E. and Korotkova, L. (1988). Age and growth rates of yellowfin tuna *Thunnus albacares* (Bonnaterre 1788) (Pisces, Scombridae) in the north-western part of the Indian Ocean, determined by counting the rings of vertebrae. *FAO/IPTP Collection Volume of Working Documents*, 3 :68–73.

Rosland, R., Strand, O., Alunno-Bruscia, M., Bacher, C., and Strohmeier, T. (2009). Applying Dynamic Energy Budget (DEB) theory to simulate growth and bioenergetics of blue mussels under low seston conditions. *Journal of Sea Research*, 62(2-3) :49–61.

Royer, F., Fromentin, J.-M., and Gaspar, P. (2004). Association between bluefin tuna schools and oceanic features in the western Mediterranean. *Marine Ecology Progress Series*, 269 :249–263.

Saether, S., Kalas, J., and Fiske, P. (1994). Age-determination of breeding shorebirds - quantification of feather wear in the lekking great snipe. *The Condor Volume*, 96(4) :959–972.

Santiago, J. and Arrizabalaga, H. (2005). An integrated growth study for North Atlantic albacore (*Thunnus alalunga* Bonn. 1788). *ICES Journal of Marine Science*, 62(4) :740–749.

Sarà, G., Reid, G. K., Rinaldi, A., Palmeri, V., Troell, M., and Kooijman, S. A. L. M. (2012). Growth and reproductive simulation of candidate shellfish species at fish cages in the Southern Mediterranean : Dynamic Energy Budget (DEB) modelling for integrated multi-trophic aquaculture. *Aquaculture*, 324-325 :259–266.

Sardenne, F., Dortel, E., Le Croizier, G., Million, J., Labonne, M., Leroy, B., Bodin, N., and Chassot, E. (*in press*). Aging tropical tunas from otolith microstructures : Insights from the Indian Ocean Tuna Tagging Program. *Fisheries Research*.

Schaefer, K. M. and Fuller, D. W. (2005). Behavior of bigeye (*Thunnus obesus*) and skipjack (*Katsuwonus pelamis*) tunas within aggregations associated with floating objects in the equatorial eastern Pacific. *Marine Biology*, 146 :781–792.

Schaefer, K. M. and Fuller, D. W. (2010). Vertical movements, behavior, and habitat of bigeye tuna (*Thunnus obesus*) in the equatorial eastern Pacific Ocean, ascertained from archival tag data. *Marine Biology*, 157(12) :2625–2642.

Schaefer, K. M., Fuller, D. W., and Block, B. A. (2011). Movements, behavior, and habitat utilization of yellowfin tuna (*Thunnus albacares*) in the Pacific Ocean off Baja California, Mexico, determined from archival tag data analyses, including unscented Kalman filtering. *Fisheries Research*, 112(1-2) :22–37.

Schnute, J. (1981). A Versatile Growth Model with Statistically Stable Parameters. *Canadian Journal of Fisheries and Aquatic Sciences*, 38 :1128–1140.

Schnute, J. and Fournier, D. (1980). A new approach to length-frequency analysis : growth structure. *Canadian Journal of Fisheries and Aquatic Sciences*, 37(9).

Secor, D., Dean, J., and Laban, E. (1991). Manual for otolith removal and preparation for microstructural examination. *Electric Power Research Institute and the Belle W. Baruch Institute for Marine Biology and Coastal Research*.

Secor, D. H., Henderson-Arzapalo, A., and Piccoli, P. M. (1995). Can otolith microchemistry chart patterns of migration and habitat utilization in anadromous fishes ? *Journal of Experimental Marine Biology and Ecology*, 192(1) :15–33.

Sepulveda, C. and Dickson, K. A. (2000). Maximum sustainable speeds and cost of swimming in juvenile kawakawa tuna (*Euthynnus affinis*) and chub mackerel (*Scomber japonicus*). *Journal of Experimental Biology*, 203(20) :3089–3101.

Shadwick, R. E., Katz, S. L., Korsmeyer, K. E., Knower, T., and Covell, J. W. (1999). Muscle dynamics in skipjack tuna : timing of red muscle shortening in relation to activation and body curvature during steady swimming. *Journal of Experimental Biology*, 202(16) :2139–2150.

Shadwick, R. E., Schiller, L. L., and Fudge, D. S. (2013). Physiology of Swimming and Migration in Tunas. In *Swimming Physiology of Fish*, pages 45–78. Springer edition.

Shadwick, R. E. and Syme, D. A. (2008). Thunniform swimming : muscle dynamics and mechanical power production of aerobic fibres in yellowfin tuna (*Thunnus albacares*). *The Journal of Experimental Biology*, 211 :1603–1611.

Shono, H., Satoh, K., Okamoto, H., and Nishida, T. (2009). Updated stock assessment for bigeye tuna in the Indian Ocean up to 2008 using Stock Synthesis III (SS3). *IOTC Working Party of Tropical Tuna*, 11(20) :9 p.

Shuford, R., Dean, J., Stéquert, B., and Morize, E. (2007). Age and growth of yellowfin tuna in the Atlantic Ocean. *Collection Volume Scientific Paper ICCAT*, 60(1) :330–341.

Sigourney, D., Letcher, B., Obedzinski, M., and Cunjak, R. (2008). Size-independent growth in fishes : patterns, models and metrics. *Journal of Fish Biology*, 72 :2435–2455.

Spiegelhalter, D., Thomas, A., Best, N., and Lunn, D. (2011). OpenBUGS version 3.2.1 user manual.

Stéquert, B. (1995). Détermination de l'âge des thons tropicaux à partir de leurs otolithes : exemple du Yellowfin (*Thunnus albacares*). *Document Technique du Centre ORSTOM de Brest*, 76 :1–31.

Stéquert, B. and Conand, F. (2004). Age and growth of bigeye tuna (*Thunnus obesus*) in the Western Indian Ocean. *Cybium*, 28(2) :163–170.

Stéquert, B. and Marsac, F. (1986). *La pèche de surface des thonidés tropicaux dans l'océan Indien*, volume 282. Food & Agriculture Org.

Stéquert, B., Panfili, J., and Dean, J. (1996). Age and growth of yellowfin tuna, *Thunnus albacares*, from the western indian ocean, based on otolith microstructure. *Fishery Bulletin*, 94 :124–134.

Stéquert, B., Rodriguez, J., Cuisset, B., and Le Menn, F. (2001). Gonadosomatic index and seasonal variations of plasma sex steroids in skipjack tuna (*Katsuwonus pelamis*) and yellowfin tuna (*Thunnus albacares*) from the Western Indian Ocean. *Aquatic Living Resources*, 14 :313–318.

Sun, C.-L., Su, N.-J., and Yeh, S.-Z. (2003). Estimation of growth parameters and age composition for yellowfin tuna, thunnus albacares, in the western pacific using the length-based MULTIFAN method. volume 5, page 15 p., Mooloolaba, Australia.

Sweenarain, S., Cayré, P., and Le Gall, J. (1998). Impact économique des activités thonières industrielles et perspectives de développement dans les pays membres de la Commission de l'océan Indien. In Cayré, P. and Conférence Internationale Thonière de Maurice, Port Louis (MUS), 1996/11/27-29, editors, *Le thon : enjeux et stratégies pour l'océan Indien*, Colloques et Séminaires, pages 209–236. ORSTOM, Paris.

Swimmer, Y., McNaughton, L., Moyes, C., and Brill, R. (2004). Metabolic biochemistry of cardiac muscle in three tuna species (bigeye, *Thunnus obesus* ; yellowfin, *T. albacares* ; and skipjack, *Katsuwonus pelamis*) with divergent ambient temperature and oxygen tolerances. *Fish Physiology and Biochemistry*, 30 :27–35.

Syme, D. A. and Shadwick, R. E. (2002). Effects of longitudinal body position and swimming speed on mechanical power of deep red muscle from skipjack tuna (*Katsuwonus pelamis*). *Journal of Experimental Biology*, 205(2) :189–200.

Syme, D. A. and Shadwick, R. E. (2011). Red muscle function in stiff-bodied swimmers : there and almost back again. *Philosophical Transactions of the Royal Society B*, 366 :1507–1515.

Tamura, Y. and Takagi, T. (2009). Morphological features and functions of bluefin tuna change with growth. *Fisheries Science*, 75(3) :567–575.

Tanaka, Y., Gwak, W.-S., Tanaka, M., Sawada, Y., Okada, T., Miyashita, S., and Kumai, H. (2007). Ontogenetic changes in RNA, DNA and protein contents of laboratory-reared Pacific bluefin tuna *Thunnus orientalis*. *Fisheries Science*, 73(2) :378–384.

Taranger, G., Carrillo, M., Schulz, R., Fontaine, P., Zanuy, S., Felip, A., Weltzien, F.-A., Dufour, S., Karlsen, O., Norberg, B., Andersson, E., and Hansen, T. (2010). Control of puberty in farmed fish. *General and Comparative Endocrinology*, 165 :483–515.

Taylor, G. K., Holbrook, R. I., and Perera, T. B. d. (2010). Fractional rate of change of swim-bladder volume is reliably related to absolute depth during vertical displacements in teleost fish. *Journal of The Royal Society Interface*, 7(50) :1379–1382.

Taylor, N., Walters, C. J., and Martell, S. (2005). A new likelihood for simultaneously estimating von Bertalanffy growth parameters, gear selectivity, and natural and fishing mortality. *Canadian Journal of Fisheries and Aquatic Sciences*, 62 :215–223.

Thorogood, J. (1987). Age and growth rate determination of southern bluefin tuna, *Thunnus maccoyii*, using otolith banding. *Journal of Fish Biology*, 30(1) :7–14.

Timochina, O. and Romanov, E. (1991). Notes on reproductive biology of yellowfin tuna in the Western Indian Ocean. Workshop on stock assessment of yellowfin tuna in the indian ocean, FAO, Colombo (Sri Lanka).

Uchiyama, J. and Struhsaker, P. (1981). Age and growth of skipjack tuna, *Katsuwonus pelamis*, and yellowfin tuna, *Thunnus albacares* as indicated by daily growth increments of sagittae. *Fishery Bulletin*, 79 :151–162.

van der Meer, J. (2006). An introduction to Dynamic Energy Budget (DEB) models with special emphasis on parameter estimation. *Journal of Sea Research*, 56(2) :85–102.

van der Veer, H. W., Cardoso, J. F. M. F., and van der Meer, J. (2006). The estimation of DEB parameters for various Northeast Atlantic bivalve species. *Journal of Sea Research*, 56(2) :107–124.

Viallefont, A., Lebreton, J.-D., Reboulet, A.-M., and Gory, G. (1998). Parameter Identifiability and Model Selection in Capture-Recapture Models : A Numerical Approach. *Biometrical Journal*, 40(3) :313–325.

Viera, A. (2005). Study of the growth of Yellowfin tuna (*Thunnus albacares*) in the Indian Ocean based on length-frequency data from 2000 to 2004. *IOTC Working Party of Tropical Tuna*, 32 :17p.

Von Bertalanffy, L. (1957). Quantitative laws in metabolism and growth. *The Quarterly Review of Biology*, 32(3) :217–231.

Walli, A., Teo, S. L. H., Boustany, A., Farwell, C. J., Williams, T., Dewar, H., Prince, E., and Block, B. A. (2009). Seasonal Movements, Aggregations and Diving Behavior of Atlantic Bluefin Tuna (*Thunnus thynnus*) Revealed with Archival Tags. *PLoS ONE*, 4(7) :18p.

Walters, C. and Essington, T. (2010). Recovery of Bioenergetics Parameters from Information on Growth : Overview of an Approach Based on Statistical Analysis of Tagging and Size-At-Age Data. *The Open Fish Science Journal*, 3 :52–68.

Wang, Y., Thomas, M., and Somers, I. (1995). A maximum likelihood approach for estimating growth from tag-recapture data. *Canadian Journal of Fisheries and Aquatic Sciences*, 52 :252–259.

Wang, Y.-G. (1998a). An improved Fabens method for estimation of growth parameters in the von Bertalanffy model with individual asymptotes. *Canadian Journal of Fisheries and Aquatic Sciences*, 55 :397–400.

Wang, Y.-G. (1998b). Growth curves with explanatory variables and estimation of the effect of tagging. *Australian and New Zealand Journal of Statistics*, 40(3) :299–304.

Wankowski, J. (1981). Estimated growth of surface-schooling skipjack tuna, *Katsuwonus pelamis*, and yellowfin tuna, *Thunnus albacares*, from the Papua New Guinea region. *Fishery Bulletin*, 79(3) :517–545.

Wardle, C., Videler, J., and Altringham, J. (1995). Tuning in to fish swimming waves : body form, swimming mode and muscle function. *Journal of Experimental Biology*, 198(8) :1629–1636.

Wegner, N. C., Sepulveda, C. A., Aalbers, S. A., and Graham, J. B. (2012). Structural Adaptations for Ram Ventilation : Gill Fusions in Scombrids and Billfishes. *Journal of Morphology*, 274(1) :108–200.

Westneat, M. W. and Wainwright, S. A. (2001). Mechanical design of tunas : muscle, tendon, and bone. In *Tuna physiology, ecology and evolution*, volume 19 of *Fish physiology series*, pages 271–311. Academic Press.

Wexler, J. B., Margulies, D., Masuma, S., Tezuka, N., Teruya, K., Oka, M., Kanematsu, M., and Nikaido, H. (2001). Age validation and growth of yellowfin tuna, *Thunnus albacares*, larvae reared in the laboratory. *Inter-American Tropical Tuna Commission Bulletin*, 22(1) :52–71.

Wexler, J. B., Margulies, D., and Scholey, V. P. (2011). Temperature and dissolved oxygen requirements for survival of yellowfin tuna, *Thunnus albacares*, larvae. *Journal of Experimental Marine Biology and Ecology*, 404 :63–72.

Wexler, J. B., Scholey, V. P., Olson, R. J., Margulies, D., Nakazawa, A., and Suter, J. M. (2003). Tank culture of yellowfin tuna, *Thunnus albacares* : developing a spawning population for research purposes. *Aquaculture*, 220 :327–353.

White, T. (1982). The Philippine tuna fishery and aspects of the population dynamics of tunas in Philippine waters. *IPTP Collective Volume of Working Documents*, pages 1–64.

Wild, A. (1986). Growth of yellowfin tuna, *Thunnus albacares*, in the Eastern Pacific Ocean based on otolith increments. *Inter-American Tropical Tuna Commission Bulletin*, 18(6) :423–479.

Wild, A. and Foreman, T. (1980). The relationship between otolith increments and time for yellowfin and skipjack tuna marked with tetracycline. *Inter-American Tropical Tuna Commission Bulletin*, 17(7) :507–560.

Wild, A., Wexler, J., and Foreman, T. (1995). Extended studies of increment deposition rates in otoliths of yellowfin and skipjack tunas. *Bulletin of Marine Science*, 57(2) :555–562.

Williams, A., Leroy, B., Nicol, S., Farley, J., Clear, N., Krusic-Golub, K., and Davies, C. (2013). Comparison of daily- and annual- increment counts in otoliths of bigeye (*Thunnus obesus*), yellowfin (*T. albacares*), southern bluefin (*T. maccoyii*) and albacore (*T. alalunga*) tuna. *ICES Journal of Marine Science*, page 12p.

Yabuta, Y. and Yukinawa, M. (1957). Age and growth of yellowfin tuna (*Neothunnus macropterus*) in Japanese waters by size frequencies. *Report of Nankai Regional Fisheries Research Laboratory*, 5 :127–133.

Yabuta, Y. and Yukinawa, M. (1959). Growth and age of the yellowfin tuna (*Neothunnus macropterus*) in the equatorial Pacific. *Report of Nankai Regional Fisheries Research Laboratory*, 11 :77–87.

Yabuta, Y., Yukinawa, M., and Warashina, Y. (1960). Growth and age of yellowfin tuna 2 : Age determination (scale method). *Report of Nankai Regional Fisheries Research Laboratory*, 12 :63–74.

Yamanaka, K. (1990). Age, growth and spawning of yellowfin tuna in the southern Philippines. *Indo-Pacific Tuna Development and Management Programme Working Paper*, 21 :1–87.

Yang, R., Nose, Y., and Hiyama, Y. (1969). A comparative study on the age and growth of yellowfin tunas from the Pacific and Atlantic Oceans. *Far Seas Fisheries Research Laboratory Bulletin*, 2 :1–21.

Yesaki, M. (1983). Observations on the biology of yellowfin (*Thunnus albacares*) and skipjack (*Katsuwonus pelamis*) tunas in Philippine waters. *IPTP Collective Volume of Working Documents*, pages 1–66.

Yesaki, M. (1987). Synopsis of biological data of longtail tuna, *Thunnus tonggol*. *Indo-Pacific Tuna Development and Management Programme, Working Paper*, 16 :64p.

Zhu, G., Xu, L., Dai, X., and Liu, W. (2011). Growth and mortality rates of yellowfin tuna, *Thunnus albacares* (Perciformes : Scombridae), in the eastern and central Pacific Ocean. *ZOOLOGIA*, 28(2) :199–206.

Zhu, G., Xu, L., Zhou, Y., and Song, L. (2008). Reproductive Biology of Yellowfin Tuna *T. albacares* in the West-Central Indian Ocean. *Journal of Ocean University of China*, 7(3) :327–332.

Zudaire, I., Murua, H., Grande, M., and Bodin, N. (2013a). Reproductive potential of Yellowfi n Tuna (*Thunnus albacares*) in the western Indian Ocean. *Fishery Bulletin*, 111 :252–264.

Zudaire, I., Murua, H., Grande, M., Korta, M., Arrizabalaga, H., Areso, J. J., and Delgado-Molina, A. (2013b). Fecundity regulation strategy of the yellowfin tuna (*Thunnus albacares*) in the Western Indian Ocean. *Fisheries Research*, 138 :80–88.

Appendix A

Extreme value theory for estimating the fish asymptotic length

Fish growth is one of the life history traits the most widely studied owing to its importance for the stocks assessment and the fishery management. The most commonly model used to describe the somatic growth of fish is the von Bertalanffy model (1938) which requires knowledge of three parameter : the age at zero length, the growth rate coefficient and the asymptotic length. This latter parameter is particularly important because it determines the shape of the growth curve. The asymptotic length can be interpreted as maximum length reached by an individual growing throughout it life, i.e. the length of the oldest fish. Unfortunately, the commercial or scientific fishing catches give very little information on the oldest fish, often insufficient to provide a suitable asymptotic length estimate. In order to get around a problem, most authors infer the value of the asymptotic length using the empirical relationship of Pauly (1985) which assumes the largest lenght of the dataset equal to 95% of the asymptotic length. Nevertheless, there is no evidence to validate this assumption can result in obtaining an growth pattern inconsistent with the biology of the species. This study therefore proposes a new estimating method for the asymptotic length through the extreme values theory.

1 Extreme values theory

Extreme value theory (GEV) allows for the estimation of the occurrence probability of extreme events from the greatest values of a random variable by the extrapolation of the behavior of distribution tails (Pickands, 1975; Borchani, 2010). The GEV theory is enjoying an increasing interest in many disciplines, such as finance, insurance (Embrechts et al., 1997), hydrology (Bernier, 1957), climatology (Katz and Brown, 1992), but remains uncommon in the ecology and biology fields.
Two approaches exist for extreme value analysis. The first relies on the limit distribution of a serie of independent and identically distributed random variables generated from the maximas or minimas of a sample and leads to the generalized extreme value distribution (GEV) combining three possible extrama laws.The second, referred to as the "Peaks Over Thresholds" method (POT), is based on extracting of observations exceeding a certain threshold. In this study, we are focused on the first approach.
Let a sequence L_1,...,L_n of n independent and identically distributed random variables with continuous distribution function F. The distribution of the largest values of the n variables $M_n = max(L_1, ..., L_n)$ is :

$$\mathbb{P}(M_n \leqslant x) = \mathbb{P}(L_1 \leqslant x, ..., L_n \leqslant x) = F^n(x)$$

The Fisher–Tippett–Gnedenko theorem provides the attraction domain of $F^n(x)$, i.e. the distribution law to which $F^n(x)$ converges. According this theorem, $F^n(x)$ belongs to the attraction domain of $H_\xi(x)$ if there two normalizing sequences, $a_n > 0$ and $b_n \in \mathbb{R}$ such as :

$$\lim_{x\to\infty} \mathbb{P}\left(\frac{M_n - b_n}{a_n} \leqslant x\right) = F^n(a_n x + b_n) = H_\xi(x) \tag{A.1}$$

$H_\xi(x)$ is the law of extreme values. ξ is the tail index ; depending on its sign, three distribution families are distinguished :

- $\xi > 0$, $F^n(x)$ belongs to attraction domain of Fréchet characterised by a heavy tail with a polynomial decay.

$$\varphi_\xi = \begin{cases} 0 & x \leqslant 0 \\ exp(-x^{-\xi}) & x > 0 \end{cases} \tag{A.2}$$

- $\xi = 0$, $F^n(x)$ belongs to attraction domain of Gumbel defined by an exponential type of the tail

$$\Lambda_\xi = exp(-exp(-x)) \tag{A.3}$$

- $\xi < 0$, $F^n(x)$ belongs to attraction domain of Weibull characterised by a light tail with finite upper bound

$$\psi_\xi = \begin{cases} exp(-(-x^{-\xi})) & x \leqslant 0 \\ 1 & x > 0 \end{cases} \tag{A.4}$$

The Fréchet, Gumbel and Weibull distributions can be combined into the Generalized Extreme Value distribution (GEV) defined as :

$$GEV_{\mu,\sigma,\xi}(x) = exp\left(-\left(1 + \frac{\xi(x-\mu)}{\sigma}\right)^{\frac{-1}{\xi}}\right) \tag{A.5}$$

Where $\mu \in \mathbb{R}$ is a location parameter, $\sigma > 0$ is the scale parameter and $\xi \in \mathbb{R}$ is the shape parameter that governs the tail behaviour of the distribution. $\xi > 0$, $\xi = 0$ and $\xi < 0$ correspond to the Fréchet, Gumbel and Weibull domains respectively (Figure 5.1).

Fréchet
$$GEV_{\mu,\sigma,\xi}(x) = \begin{cases} 0 & x \leqslant \mu \\ exp\left(\left(-\frac{x-\mu}{\sigma}\right)^{-\frac{1}{\xi}}\right) & x > \mu \end{cases} \tag{A.6}$$

(A.7)

Gumbel
$$GEV_{\mu,\sigma,0}(x) = exp\left(-exp\left(-\frac{x-\mu}{\sigma}\right)\right) \tag{A.8}$$

(A.9)

Weibull
$$GEV_{\mu,\sigma,\xi}(x) = \begin{cases} exp\left(-\left(-\frac{x-\mu}{\sigma}\right)^{-\frac{1}{\xi}}\right) & x < \mu \\ 1 & x \geqslant \mu \end{cases} \tag{A.10}$$

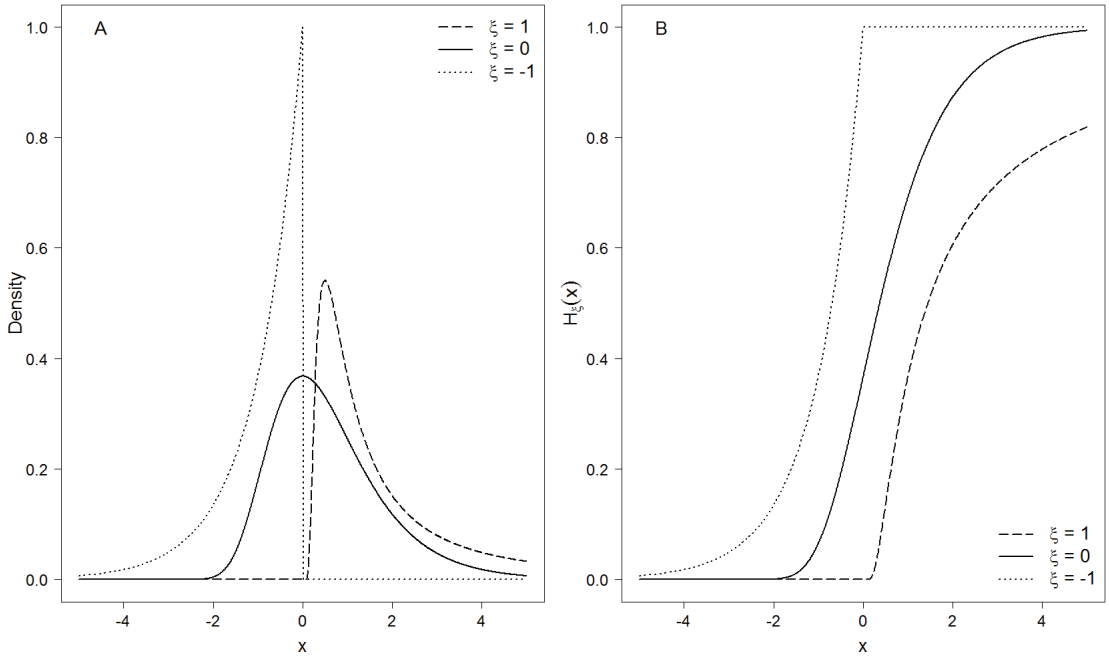

FIGURE 5.1 – Probability density (A) and distribution function (B) for the GEV law for different values of the shape parameter ξ

2 Application to estimating asymptotic length

In order to illustrate the application of the GEV theory in estimating the asymptotic length, this study relied on three tuna species of primary importance for the Indian Ocean tuna industry, yellowfin, bigeye and skipjack (Pillai and Satheeshkumar, 2012).

For each of the three species, a GEV distribution was fit based on length measurement data from fresh fish collected during 1952–2011 from the European and Seychelles purse seine fisheries, Maldivian pole and line vessels, and Taiwanese and Japanese longliners. The length measurements were made either on vessels board or in cannery and correspond to fork lengths, i.e. fish length from the front to the fork in the center of the tail. We extracted the greatest lengths from each measurement platform (on board or in cannery), year, fishery and fleet thus obtained 103 measurements from 150 to 200 cm, 74 measurements from 166 to 206 cm and 72 measurements from 55 to 100 cm for yellowfin, bigeye and skipjack respectively.

We have assumed that the n largest measurements, F_L, followed a GEV distribution as described in Eq. whose density function can be defined as follows :

$$g(F_{L_i}) = \frac{1}{\sigma}\left(1+\frac{\xi(F_{L_i}-\mu)}{\sigma}\right)^{\frac{-1-\xi}{\xi}} exp\left(-\left(1+\frac{\xi(F_{L_i}-\mu)}{\sigma}\right)^{\frac{-1}{\xi}}\right) \qquad \text{(A.11)}$$

The parameters of the GEV distribution were estimated using the maximum likelihood method (Hosking, 1985), i.e. we looked for parameters vector $\theta = \{\mu, \sigma, \xi\}$

maximizing the following likelihood :

$$\mathcal{L} = \prod_{i=1}^{n} g(F_{L_i}) \tag{A.12}$$

The likelihood was maximized with the *fgev* function of the *evd* package (Smith, 1985) of the statistical software R version 2.12.1 (R Development Core Team, 2010) using the quasi-Newton algorithm (Nash, 1990).

3 Results

The mean asymptotic length was estimated to a value of 173.14, 187.62 and 75.63 for yellowfin, bigeye and skipjack respectively (Figure 5.2). The parameters estimates of GEV distribution at the maximum likelihood are presented in Table A.1.

Table A.1 – Parameter estimates of GEV distribution.
Std.dev. : Standard deviation

Parameter	Yellowfin		Bigeye		Skipjack	
	Mean	Std.dev.	Mean	Std.dev.	Mean	Std.dev.
μ	173.141	1.187	187.622	1,186	75,634	0,919
σ	11.067	0.824	9.189	0,856	7,253	0,593
ξ	-0.3474	0.0552	-0.3313	0,0843	-0,1645	0,0512

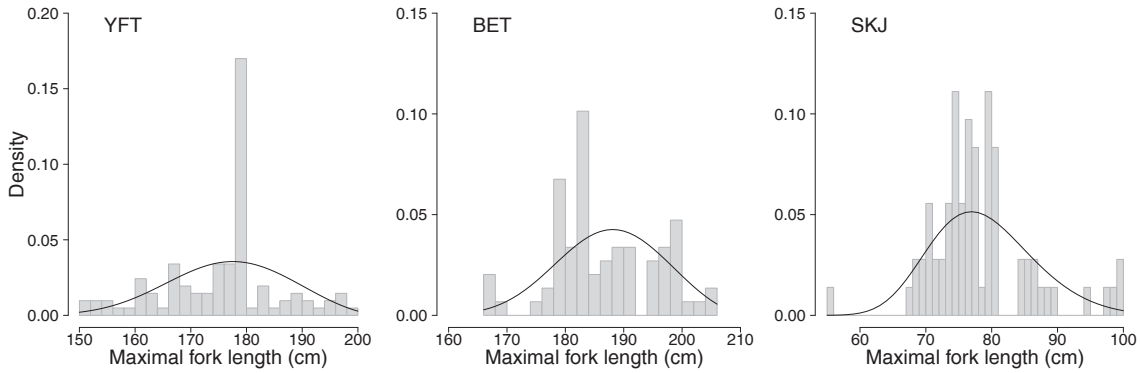

Figure 5.2 – Probability density of GEV distributions for yellowfin (YFT), bigeye (BET) and skipjack (SKJ)

References

Bernier, J. (1957). Sur l'application des diverses lois limites des valeurs extrêmes au problème des débits de crues. *Revue de statistique appliquée*, 5(2) :91–101.

Borchani, A. (2010). Statistiques des valeurs extrêmes dans le cas de lois discrètes. Technical Report ESSEC Working Paper 10009, ESSEC Business School.

Embrechts, P., Klüppelberg, C., and Mikosch, T. (1997). *Modelling Extremal Events : For Insurance and Finance*. Springer.

Hosking, J. (1985). Algorithm AS 215 : Maximum-likelihood estimation of the parameters of the generalized extreme-value distribution. *Journal of Royal Statistical Society*, 34(3) :301–310.

Katz, R. W. and Brown, B. G. (1992). Extreme events in a changing climate : Variability is more important than averages. *Climatic Change*, 21(3) :289–302.

Nash, J. C. (1990). *Compact Numerical Methods for Computers : Linear Algebra and Function Minimisation*. Taylor & Francis, 2 edition edition.

Pauly, D. (1985). Quelques méthodes simples pour l'estimation des stocks de poissons tropicaux. *FAO Document Technique sur les Pêches*, 234 :56p.

Pickands, J. (1975). Statistical inference using extreme order statistics. *The Annals of Statistics*, 3(1) :119–131.

Pillai, G. N. and Satheeshkumar, P. (2012). Biology, Fishery, Conservation and Management of Indian Ocean Tuna Fisheries. *Ocean Science Journal*, 47(4) :411–433.

Smith, R. L. (1985). Maximum likelihood estimation in a class of nonregular cases. *Biometrika*, 72(1) :67–90.

Appendix B

OpenBUGS codes

1 OpenBUGS code of the ageing error model

This code was used to implement the ageing error model developed in Chapter 2. It is designed to run under the OpenBUGS 3.2.1 software.

```
model {

#-------------------------------------------------------------------
### Determining of the deposition periodicity
#-------------------------------------------------------------------
## Prior on increments deposit rate
Rb ~ dbeta(1,1)
R <- 2 * Rb

## Prior on bias at the edge
tauEter <- 1/pow(4,2)
Eter ~ dnorm(0,tauEter)

## Prior on bias at the nucleus
tauEnuc <- 1/pow(3,2)
Enuc ~ dnorm(0,tauEnuc)
# Prior distribution not updated:
Enuc_F <- cut(Enuc)

# Prior on relative percentage of misread otolith increments
p ~ dunif(0,0.5)

## Estimating the deposition periodicity
for (i in 1:n) {
        Im[i] <- R * TL[i] - Eter
        tauIm[i] <- 1/pow((p*Im[i]),2)
        for (l in 1:4) {
                Im_obs[i,l] ~ dnorm(Im[i],tauIm[i]) I(0,)
        }
}

#-------------------------------------------------------------------
### Estimating age from multiple readings
#-------------------------------------------------------------------
# Posterior distributions of R and Eter not updated
R_F <- cut(R)
Eter_F <- cut(Eter)
```

```
## Estimating ages from It with an accurate TL (RTTP)
for (i in 1:n1) {
        It_1[i] ~ dunif(0,3000)
}
for (i in 1:n1) {
        tauIt_1[i] <- 1/pow((p*It_1[i]),2)
        for (l in 1:4) {
                It_obs_1[i,l] ~ dnorm(It_1[i],tauIt_1[i]) I(0,)
        }
}
for (i in 1:n1) {
        Ar_1[i] <- At_1[i] + TL_1[i]
        At_1[i] <- (It_1[i] + Enuc_F)/R_F
}
#-------------------------------------------------------------
## Estimating ages from It with an inaccurate TL (RTTP)
for (i in 1:n2) {
        It_2[i] ~ dunif(0,3000)
        TAL_2[i] ~ dunif(TL_2[i,1],TL_2[i,2])
}
for (i in 1:n2) {
        tauIt_2[i] <- 1/pow((p*It_2[i]),2)
        for (l in 1:4) {
                It_obs_2[i,l] ~ dnorm(It_2[i],tauIt_2[i]) I(0,)
        }
}
for (i in 1:n2) {
        Ar_2[i] <- At_2[i] + TAL_2[i]
        At_2[i] <- (It_2[i] + Enuc_F)/R_F
}
#-------------------------------------------------------------
## Estimating ages from Ir with an accurate TL (RTTP)
for (i in 1:n3) {
        Ir_3[i] ~ dunif(0,3000)
}
for (i in 1:n3) {
        tauIr_3[i] <- 1/pow((p*Ir_3[i]),2)
        for (l in 1:5) {
                Ir_obs_3[i,l] ~ dnorm(Ir_3[i],tauIr_3[i]) I(0,)
        }
}
for (i in 1:n3) {
        At_3[i] <- Ar_3[i] - TL_3[i]
        Ar_3[i] <- (Ir_3[i] + Enuc_F + Eter_F)/R_F
}
```

```
#-------------------------------------------------------------------
## Estimating ages from Ir with an inaccurate TL (RTTP)
for (i in 1:n4) {
        Ir_4[i] ~ dunif(0,3000)
        TAL_4[i] ~ dunif(TL_4[i,1],TL_4[i,2])
}
for (i in 1:n4) {
        tauIr_4[i] <- 1/pow((p*Ir_4[i]),2)
        for (l in 1:5) {
                Ir_obs_4[i,l] ~ dnorm(Ir_4[i],tauIr_4[i]) I(0,)
        }
}
for (i in 1:n4) {
        At_4[i] <- Ar_4[i] - TAL_4[i]
        Ar_4[i]<-(Ir_4[i] + Enuc_F + Eter_F)/R_F
}
#-------------------------------------------------------------------
## Estimating ages from Ir (WSTTP)
for (i in 1:n5) {
        Ir_5[i] ~ dunif(0,3000)
}
for (i in 1:n5) {
        tauIr_5[i] <- 1/pow((p*Ir_5[i]),2)
        for (l in 1:4) {
                Ir_obs_5[i,l] ~ dnorm(Ir_5[i],tauIr_5[i]) I(0,)
        }
}
for (i in 1:n5) {
        Ar_5[i] <- (Ir_5[i] + Enuc_F + Eter_F)/R_F
}

} # End of model
```

2 OpenBUGS code of the integrated growth model

This code was used to implement the integrated growth model developed in Chapter 3. It is designed to run under the OpenBUGS 3.2.1 software.

```
model {

#-------------------------------------------------------------------
### Prior distributions for growth parameters
#-------------------------------------------------------------------
# Asymptotic length
Linf ~ dgev(173.141,11.067,-0.3474)

# Relative age at which the change in growth occurs
rAlpha <- 1/pow(0.5,2)
muAlpha <- 1/(2.901*pow(0.5,2))
alpha ~ dgamma(rAlpha,muAlpha)

# Growth rate coefficient of first stanza
rk1 <- 1/pow(0.6,2)
muk1 <- 1/(0.586*pow(0.6,2))
k1 ~ dgamma(rk1,muk1)

# Growth rate coefficient of second stanza
k2 <- kappa+k1
kappa ~ dunif(0,3)

# Transition rate between k1 and k2
beta ~ dunif(0,30)

# Age of zero fork length
t0 ~ dunif(-2,0)

#-------------------------------------------------------------------
### Prior distributions for errors
#-------------------------------------------------------------------
# Process error for ageing data
tauP ~ dgamma(0.01,0.01)
sigmaP <- 1/sqrt(tauP)

# Process error for length-frequency data
tau_mu ~ dgamma(0.01,0.01)
sigma_mu <- 1/sqrt(tau_mu)
```

```
# Process error for mark-recapture data
tau_r ~ dgamma(0.01,0.01)
sigma_r <- 1/sqrt(tau_r)

# Measurement errors at tagging
tauTAG ~ dgamma(0.01,0.01)
sigmaTAG <- 1/sqrt(tauTAG)

# Measurement errors at tagging due to tunas freezing
tauFROZ ~ dgamma(0.01,0.01)
sigmaFROZ <- 1/sqrt(tauFROZ)

# Measurement errors at recapture
varREC <- pow((sigmaTAG+sigmaFROZ),2)
tauREC <- 1/varREC
sigmaREC <- sqrt(varREC)

#-------------------------------------------------------------
### Estimating length measurement errors
#-------------------------------------------------------------
## At tagging
for (i in 1:nTag) {
        DL[i] ~ dnorm(0,tauTAG)
}

## Due to freezing fish
for (i in 1:nRec) {
        DS[i] ~ dnorm(0,tauFROZ)
}

#-------------------------------------------------------------
### Modeling growth
#-------------------------------------------------------------
# Posterior distributions of length measurement errors not updated
tauT <- cut(tauTAG)
tauR <- cut(tauREC)

#-------------------------------------------------------------
## Ageing data

# Fish caught once
for (i in 1:n1) {
        Log_L1_1[i] <- log(max(Linf*(1-exp(-k2*(A1_1_obs[i]-t0))
        *pow(((1+exp(-beta*(A1_1_obs[i]-t0-alpha)))
        /(1+exp(beta*alpha))),((k1-k2)/beta))),1))
```

```
        L1_1[i] ~ dlnorm(Log_L1_1[i],tauP)
        L1_1_obs[i] ~ dnorm(L1_1[i],tauT)
}

# Fish caught twice
for (i in 1:n2) {

        # At tagging
        Log_L1_2[i] <- log(max(Linf*(1-exp(-k2*(A1_2_obs[i]-t0))
        *pow(((1+exp(-beta*(A1_2_obs[i]-t0-alpha)))/(1+exp(beta*alpha))),
        ((k1-k2)/beta))),1))
        L1_2[i] ~ dlnorm(Log_L1_2[i],tauP)
        L1_2_obs[i] ~ dnorm(L1_2[i],tauT)

        # At recovery
        TaL[i] ~ dunif(TaLmin_obs[i],TaLmax_obs[i])
        A2_2[i] <- A1_2_obs[i] + TaL[i]
        Log_L2_2[i] <- log(max(Linf*(1-exp(-k2*(A2_2[i]-t0))
        *pow(((1+exp(-beta*(A2_2[i]-t0-alpha)))/(1+exp(beta*alpha))),
        ((k1-k2)/beta))),1))
        L2_2[i] ~ dlnorm(Log_L2_2[i],tauP)
        L2_2_obs[i] ~ dnorm(L2_2[i],tauR)
}
#-------------------------------------------------------------
## Length-frequency data

# Prior on the age of the first mode of cohort c
for (c in 1:nC) {
        r_a1[c] <- pow((a1_mean[c]/a1_sd[c]),2)
        mu_a1[c] <- a1_mean[c]/pow(a1_sd[c],2)
        a1[c] ~ dgamma(r_a1[c],mu_a1[c])
}

# Estimating growth
for (c in 1:nC) {
        for (k in 1:nK[c]) {
                # Age of cohort c at month k
                a[c,k] <- (a1[c] + k-1)/12
                Log_mu[c,k] <- log(Linf*(1-exp(-k2*(a[c,k]-t0))
                *pow(((1+exp(-beta*(a[c,k]-t0-alpha)))
                /(1+exp(beta*alpha))),(-(k2-k1)/beta))))
                Log_mu_obs[c,k] ~ dnorm(Log_mu[c,k],tau_mu)
                Log_mu_obs[c,k] <- log(mu_obs[c,k])
        }
}
```

```
#-------------------------------------------------------------------
## Mark-recapture data

# Posterior distributions of alpha and t0 not updated
t0_fix <- cut(t0)
alpha_fix <- cut(alpha)

# Prior to the age-at-tagging (for one size classes)
muT1 <- 1 / (T1_mean * 0.25)
rT1 <- 1 / 0.25
T1 ~ dgamma(rT1,muT1)


# Estimating growth
for (i in 1:n3) {
        t1[i] ~ dgamma(rT1,muT1)
        Log_L2r[i]<-log(max(Linf-(Linf-L1r_obs[i])
        *(exp(-k2*TaLr_obs[i])
        *pow(((1+exp(-beta*(t1[i]+TaLr_obs[i]-t0_fix-alpha_fix)))/
        (1+exp(-beta*(t1[i]-t0_fix-alpha_fix)))),((k1-k2)/beta))),1))
        L2r[i] ~ dlnorm(Log_L2r[i],tau_r)
        L2r_obs[i] ~ dnorm(L2r[i],tauR)
}

} # End of model
```

Appendix C

Link between DEB and Von Bertalanffy parameters

In constant conditions of food density and temperature, the standard DEB model leads to the Von Bertalanffy growth. The physical length L of fish at an age a is then described as :

$$L(a) = L_\infty(1 - e^{-k(a-a_0)}) \tag{C.1}$$

L_∞ is the asymptotic length (cm), i.e. the maximum length that a fish can reach, a_0 is the age of zero fork length (day) and k is the growth rate coefficient of Von Bertalanffy (day^{-1}).

In standard DEB model, the growth of structural length L_v is described by the following differential equation :

$$\begin{aligned} \frac{dL_v}{dt} = & \quad \frac{\dot{v}}{3(e+g)}\left(e - \frac{L_v(t)+L_T}{L_m}\right) \\ \text{with} & \quad g = \frac{\dot{v}[E_G]}{\kappa\{\dot{p}_{Am}\}} \\ \text{and} & \quad L_m = \frac{\kappa\{\dot{p}_{Am}\}}{[\dot{p}_M]} \\ \text{and} & \quad L_T = \frac{\{\dot{p}_T\}}{[\dot{p}_M]} \end{aligned} \tag{C.2}$$

All parameters used in this equation are defined in Table C.1
The Holling type II scaled functional response $f = X/(X + X_k)$ defined for a food density X (J.cm^{-3}) and a half-saturation constant X_k. In constant environment, the reserve density $[E]$, and therefore the scaled reserve density $e = [E]\dot{v}/\{\dot{p}_{Am}\}$, will not vary and $e = f$. Eq.C.2 is then :

$$\frac{dL_v}{dt} = \frac{\dot{v}}{3(f+g)}\left(f - \frac{L_v(t)+L_T}{L_m}\right) \tag{C.3}$$

As $L_v = \delta L$, the growth of physical length L can be described as follows :

$$\begin{aligned} \frac{dL}{dt} = & \quad \frac{1}{\delta}\frac{\dot{v}}{3(f+g)}\left(f - \frac{\delta L(t)+L_T}{L_m}\right) \\ \frac{dL}{dt} = & \quad \frac{\dot{v}}{3L_m(f+g)}\left(\frac{fL_m}{\delta} - L_T - L(t)\right) \end{aligned} \tag{C.4}$$

As all parameters are constants for constant conditions of temperature and food density, Eq.C.4 can be analytically resolved and its integration over a time interval $[t_0, t]$ leads to the following form :

$$L(t) = \left(\frac{fL_m}{\delta} - L_T\right)\left(1 - e^{-\frac{v}{3L_m(f+g)}(t-t_0)}\right) \tag{C.5}$$

By analogy with the Eq.C.1, the DEB parameters can be related with those of the Von Bertalanffy growth model :

$$\begin{aligned} L_\infty &= \frac{fL_m}{\delta} - L_T \\ k &= \frac{\dot{v}}{3L_m(f+g)} \end{aligned} \tag{C.6}$$

Table C.1 – List of DEB parameters

Definition	Parameter	Unit
Fraction of mobilised reserve allocated to soma	κ	-
Surface-area specific maximum assimilation rate	$\{\dot{p}_{Am}\}$	J.d^{-1}.cm^{-2}
Energy conductance	$\dot{v}$	cm.d^{-1}
Volume-specific somatic maintenance rate	$[\dot{p}_M]$	J.d^{-1}.cm^{-3}
Surface area-specific somatic maintenance rate	$\{\dot{p}_T\}$	J.d^{-1}.cm^{-2}
Volume-specific costs of structure	$[E_G]$	J.cm^{-3}
Shape parameter	δ	-
Maximum structural length	L_m	cm
Structural heating length	L_T	cm

Appendix D

List of publications

Accounting for age uncertainty in growth modeling, the case study of yellowfin tuna (*Thunnus albacares*) of the Indian Ocean

E. Dortel[a], F. Massiot-Granier[b], E. Rivot[b], J. Million[c], J.P. Hallier[a], E. Morize[d], J.M. Munaron[d], N. Bousquet[e], E. Chassot[a]

[a] *Institut de Recherche pour le Développement, UMR 212 EME, Avenue Jean Monnet, BP 171, 34 203 Sète cedex, FRANCE*

[b] *Université Européenne de Bretagne, UMR Agrocampus Ouest/INRA Ecologie et Santé des Ecosystèmes, 65 rue de Saint-Brieuc, CS 84215, Rennes cedex, FRANCE*

[c] *Indian Ocean Tuna Commission, PO Box 1011, Victoria, SEYCHELLES*

[d] *Institut de Recherche pour le Dévelopement, UMR 6539 LEMAR, BP70, 29 280 Plouzané, FRANCE*

[e] *EDF Research and Development, Department of Industrial Risk Management,6 quai Watier, 78 401 Chatou, FRANCE*

Abstract : Age estimates, typically determined by counting periodic growth increments in calcified structures of vertebrates, are the basis of population dynamics models used for managing exploited or threatened species. In fisheries research, the use of otolith growth rings as an indicator of fish age has increased considerably in recent decades. However, otolith readings include various sources of uncertainty. Current ageing methods, based on an average increment count, only provide periodic age estimates in which the range of uncertainty is fully ignored. This may have serious implications for the final outcome of the analysis. In this study, we describe a hierarchical model for estimating individual ages from multiple otolith readings. The model was developed within a Bayesian framework to explicitly represent the sources of uncertainty associated with age estimation, to allow for individual variations and to include knowledge on parameters from expertise. Initially, the performance of the proposed model was examined through simulations, and then it was coupled to a two-stanza somatic growth model to evaluate the impact of the age estimation method on the age composition of commercial fisheries catches. We illustrate our approach using the saggital otoliths of yellowfin tuna of the Indian Ocean collected through large-scale mark-recapture experiments. The simulation performance suggested that the ageing error model was able to estimate the ageing biases and provide accurate age estimates, regardless of the age of the fish. Coupled with the growth model, this approach appeared suitable for modeling the growth of Indian Ocean yellowfin and is consistent with findings of previous studies. The simulations showed that the choice of the ageing method can strongly affect growth estimates with subsequent implications for age-structured data used as inputs for population models. Finally, our modeling approach revealed particularly useful to reflect uncertainty around age estimates into the process of growth estimation and it can be applied to any study relying on age estimation.

Keyword : Yellowfin tuna, Hierarchical Bayesian model, Otolith, Tagging, Growth

2013, *PLoS ONE* **8**(4) : 1-12

An integrated Bayesian modeling approach for the growth of Indian Ocean yellowfin tuna

E. Dortel[a], F. Sardenne[a,b,c], N. Bousquet[d], E. Rivot[e], J. Million[b], G. Le Croizier[c], E. Chassot[f]

[a] *Institut de Recherche pour le Développement, UMR 212 EME, Avenue Jean Monnet, BP 171, 34 203 Sète cedex, FRANCE*

[b] *Indian Ocean Tuna Commission, PO Box 1011, Victoria, SEYCHELLES*

[c] *Institut de Recherche pour le Dévelopement, UMR 6539 LEMAR, BP70, 29 280 Plouzané, FRANCE*

[d] *EDF Research and Development, Department of Industrial Risk Management,6 quai Watier, 78 401 Chatou, FRANCE*

[e] *Université Européenne de Bretagne, UMR Agrocampus Ouest/INRA Ecologie et Santé des Ecosystèmes, 65 rue de Saint-Brieuc, CS 84215, Rennes cedex, FRANCE*

[f] *Institut de Recherche pour le Développement, UMR 212 EME, SFA, Fishing Port, BP 570, Victoria, SEYCHELLES*

Abstract : The Indian Ocean Tuna Tagging Program (RTTP-IO) provided a unique opportunity to collect demographic data on the key commercially-targeted tropical tuna species in the Indian Ocean. In this paper, we focused on estimating growth rates for one of these species, yellowfin (*Thunnus albacares*). Whilst most growth studies only draw on one data source, in this study we use a range of data sources : individual growth rates derived from yellowfin that were tagged and recaptured through the RTTP-IO, direct age estimates obtained through otolith readings, and length-frequency data collected from the purse seine fishery between 2000 and 2010. To combine these data sources, we used an integrated Bayesian model that allowed us to account for the process and measurement errors associated with each data set. Our results indicate that the gradual addition of each data type improved the model's parameter estimations. The Bayesian framework was useful, as it allowed us to account for uncertainties associated with age estimates and to provide additional information on some parameters (e.g., asymptotic length). Our results support the existence of a complex growth pattern for Indian Ocean yellowfin, with two distinct growth phases between the immature and mature life stages. Such complex growth patterns, however, require additional information on absolute age of fish and transition rates between growth stanzas. This type of information is not available from the data. We suggest that bioenergetic models may address this current data gap. This modelling approach explicitly considers the allocation of metabolic energy in tuna and may offer a way to understand the underlying mechanisms that drive the observed growth patterns.

Keyword : Fisheries, Otolith, Mark-recapture, Purse seine

In press, *Fisheries Research*

Determining the age of tropical tunas in the Indian Ocean from otolith microstructures

F. Sardenne[a,b], E. Dortel[c], G. Le Croizier[a,b], J. Million[b], M. Labonne[d], B. Leroy[e], N. Bodin[a], E. Chassot[a]

[a] *Institut de Recherche pour le Développement, UMR 212 EME, SFA, Fishing Port, BP 570, Victoria, SEYCHELLES*

[b] *Indian Ocean Tuna Commission, PO Box 1011, Victoria, SEYCHELLES*

[c] *Institut de Recherche pour le Développement, UMR 212 EME, Avenue Jean Monnet, BP 171, 34 203 Sète cedex, FRANCE*

[d] *Institut de Recherche pour le Dévelopement, UMR 6539 LEMAR, BP 70, 29 280 Plouzané, FRANCE*

[e] *Secretariat of the Pacific Community, BP D5, 98 848 Nouméa, NEW CALEDONIA*

Abstract : The Indian Ocean Tuna Tagging Program (IOTTP) provided a unique opportunity to assess the viability of estimating the age of tropical tunas from the micro-structural features of otoliths. Here, we analyzed the length measurements and micro-increment counts collected for 506 sagittal otoliths, of which 343 were chemically marked with oxytetracycline, for bigeye (*Thunnus obesus*), skipjack (*Katsuwonus pelamis*), and yellowfin tuna (*T. albacares*). Our results show that the otoliths of tropical tunas grow more slowly than the rest of the body. Our findings confirm that both yellowfin and juvenile bigeye deposit daily increments in their otoliths, though ages are underestimated for large bigeye (> 100 cm) when derived from micro-increment counts. An apparent non-daily deposition rate (as found for yellowfin) may be due to an interpretation bias associated with reading the micro-increments. Our results also indicate that skipjack otoliths are not suitable for age estimations during the adult phase, as evidenced by the poor agreement between micro-increment counts and days-at-liberty. We hypothesize that the income breeding strategy of skipjack could explain the variability observed in the deposition rates. Due to their complex micro-structural patterns, the reading of tropical tuna otoliths requires a degree of interpretation that can result in poor count precision and large variability in micro-increment counts, both among and within teams of readers. Age estimates were found to vary between readers, a factor which can eventually affect growth estimates and ultimately, impact on fisheries management decisions and outcomes. To address this, we recommend that reference collections of otoliths are developed, with a view to standardizing the reading process. Further, alternative methods, such as annual age estimations (as opposed to daily), and alternative structures, such as dorsal spines for skipjack, should be used to improve the accuracy of age estimations and the speed with which they can be made.

Keyword : Daily age, Micro-increment, Mark-recapture, Oxytetracycline, *Thunnus*

In press, *Fisheries Research*

Croissance de l'albacore (*Thunnus albacares*) de l'océan Indien : de la modélisation statistique à la modélisation bio-énergetique

Résumé : Depuis le début des années 1960, la croissance de l'albacore fait l'objet d'une attention particulière tant dans le domaine de la recherche que pour la gestion des pêcheries. Dans l'océan Indien, la gestion du stock d'albacores, sous la juridiction le Commission Thonière de l'océan Indien (CTOI), souffre de nombreuses incertitudes associées à la courbe de croissance actuellement considérée. En particulier, des lacunes subsistent dans notre connaissance des processus biologiques et écologiques élémentaires régulant la croissance. Leur connaissance est pourtant fondamentale pour comprendre la productivité des stocks et leur capacité de résistance à la pression de pêche et aux changements océanographiques en cours. À travers la modélisation, cette étude se propose d'améliorer les connaissances actuelles sur la croissance de la population d'albacore de l'océan Indien et de renforcer ainsi les avis scientifiques sur l'état du stock. Alors que la plupart des études sur la croissance de l'albacore s'appuient sur une seule source de données, nous avons mis en œuvre un modèle hiérarchique Bayésien qui exploite diverses sources d'informations sur la croissance, i.e. des estimations d'âge obtenues par otolithométrie, des analyses de progressions modales et les taux de croissance individuels issus du marquage-recapture, et intègre explicitement des connaissances d'experts et les incertitudes associées à chaque source de données ainsi qu'au processus de modélisation. En particulier, le modèle de croissance a été couplé un à modèle d'erreurs dans les estimations d'âge par otolithométrie apportant une amélioration significative des estimations d'âge et des paramètres de croissance en résultant et permettant une meilleure évaluation de la fiabilité des estimations. Les courbes de croissances obtenues constituent une avancée majeur dans la représentation du patron de croissance actuellement utilisé dans les évaluations de stock d'albacore. Elles démontrent que l'albacore présente une croissance en phases, caractérisée par une forte accélération en fin de phase juvénile. Cependant, elles n'apportent aucune information sur les mécanismes biologiques et écologiques à l'origine des ces phases de croissance. Afin de mieux comprendre les facteurs impliqués dans l'accélération de la croissance, nous avons mis en œuvre un modèle bio-énergétique s'appuyant sur les principes de la théorie des bilans dynamiques d'énergie (DEB). Deux hypothèses apparaissant comme les plus pertinentes ont été testées : (i) une faible disponibilité alimentaire liée à une forte compétition inter et intra-spécifique chez les jeunes albacores formant des bancs et (ii) un changement dans le régime alimentaire des adultes s'accompagnant de la consommation de proies plus énergétiques. Il apparait que ces deux hypothèses sont susceptibles d'expliquer, au moins partiellement, l'accélération de la croissance.

Mots clés : Croissance, Modélisation hiérarchique Bayésienne, théorie des bilans dynamiques d'énergie, Marquage-recapture, Estimations d'âge

Growth of Indian Ocean yellowfin tuna (*Thunnus albacares*) : statistical to bioenergetic modelling

Abstract : Since the early 1960s, the growth of yellowfin has been enjoyed a particular attention both in the research field and for fisheries management. In the Indian Ocean, the management of yellowfin stock, under the jurisdiction of the Indian Ocean Tuna Commission (IOTC), suffers from much uncertainty associated with the growth curve currently considered. In particular, there remain gaps in our knowledge of basic biological and ecological processes regulating growth. Their knowledge is however vital for understanding the stocks productivity and their resilience abilities to fishing pressure and oceanographic changes underway. Through modelling, this study aims to improve current knowledge on the growth of yellowfin population of the Indian Ocean and thus strengthen the scientific advice on the stock status. Whilst most studies on yellowfin growth only rely on one data source, we implemented a hierarchical Bayesian model that exploits various information sources on growth, i.e. direct age estimates obtained through otolith readings, analyzes of modal progressions and individual growth rates derived from mark-recapture experiments, and takes explicitely into account the expert knowledge and the errors associated with each dataset and the growth modelling process. In particular, the growth model was coupled with an ageing error model from repeated otolith readings which significantly improves the age estimates as well as the resulting growth estimates and allows a better assessment of the estimates reliability. The growth curves obtained constitute a major improvement of the growth pattern currently used in the yellowfin stock assessment. They demonstrates that yellowfin exhibits a two-stanzas growth, characterized by a sharp acceleration at the end of juvenile stage. However, they do not provide information on the biological and ecological mechanisms that lie behind the growth acceleration. For a better understanding of factors involved in the acceleration of growth, we implemented a bioenergetic model relying on the principles of Dynamic Energy Budget theory (DEB). Two major assumptions were investigated : (i) a low food availability during juvenile stage in relation with high intra and inter-specific competition and (ii) changes in food diet characterized by the consumption of more energetic prey in older yellowfin. It appears that these two assumption may partially explain the growth acceleration.

Keywords : Growth, Hierarchic Bayesian modelling, Dynamic Energy Budget theory, Mark-recapture, Age estimates